Investigation into the role of human RAP1 in telomere protection

Liudmyla Lototska

UNIVERSITÉ CÔTE D'AZUR

ÉCOLE DOCTORALE
SCIENCES DE LA VIE ET DE LA SANTÉ

THÈSE DE DOCTORAT

Le rôle de la protéine RAP1 dans la protection des télomères humains

Liudmyla LOTOTSKA

IRCAN – CNRS UMR 7284 – Inserm U1081
Telomere, senescence and cancer

Présentée en vue de l'obtention du grade de docteur en Sciences
De l'Université Côte d'Azur – UFR Sciences
Mention: Interactions moléculaires et cellulaires

Dirigée par le Pr. Eric GILSON
Co-encadrant Dr. Aaron Mendez-Bermudez

Soutenue le 17 Décembre 2018, devant le jury composé de :

Corine BERTOLOTTO	Directrice de Recherche, C3M, Nice	Présidente du Jury, Examinatrice
Paula MARTINEZ	Chargé de recherche, CNIO, Madrid	Rapportrice
Stéphane MARCAND	Directeur de Recherche, CEA, Fontenay-aux-roses	Rapporteur
Eric GILSON	PU-PH, Professeur, IRCAN, Nice	Directeur de thèse

IRCAN Inserm cnrs FONDATION RECHERCHE MÉDICALE SIGNALIFE PhD

UNIVERSITÉ CÔTE D'AZUR

ÉCOLE DOCTORALE
SCIENCES DE LA VIE ET DE LA SANTÉ

PhD THESIS

Investigation into the role of human RAP1 in telomere protection

Liudmyla LOTOTSKA

IRCAN – CNRS UMR 7284 – Inserm U1081
Telomere, senescence and cancer

Presented to obtain the PhD degree
University of Côte d'Azur – UFR Sciences
Specialty: Molecular and Cellular Interactions

Supervised by Prof. Eric GILSON
Co-superviser Dr. Aaron Mendez-Bermudez

Defended on the 17th of December 2018 in front of the committee:

Corine BERTOLOTTO	Director of Research, C3M, Nice	President of the committee, Inspector
Paula MARTINEZ	Staff scientist, CNIO, Madrid	Referee
Stéphane MARCAND	Directeur de Recherche, CEA, Fontenay-aux-roses	Referee
Eric GILSON	PU-PH, Professor, IRCAN, Nice	Director of the thesis

IRCAN Inserm cnrs FONDATION RECHERCHE MÉDICALE SIGNALIFE PhD

Résumé

Les télomères sont des séquences d'ADN, généralement répétées en tandem, localisées à l'extrémité des chromosomes linéaires. Une des fonctions principales des télomères est de différencier l'extrémité des chromosomes des cassures double-brin, et ainsi de prévenir l'activation des voies de réparation de l'ADN. Chez les mammifères, cette fonction est plus spécifiquement assurée par le complexe shelterin. Il s'agit d'un complexe hétérogène composé de six protéines distinctes: TRF1, TRF2, POT1, RAP1, TPP1 et TIN2, qui interagit spécifiquement avec l'ADN télomérique. Au sein de ce complexe, les protéines RAP1 et TRF2 coopèrent afin d'empêcher l'extrémité des chromosomes d'être perçue comme un dommage de l'ADN, ce qui autrement aboutirait à des fusions inter-chromosomiques suite au processus de réparation. La protéine TRF2 se lie directement à la molécule d'ADN dans laquelle elle s'enroule de façon spécifique. Cette propriété est primordiale pour générer une structure d'ADN en forme de boucle, appelée t-loop, et dont le bon fonctionnement des télomères dépend.Les travaux effectués au cours de cette thèse ont mis en évidence deux scenari indépendants dans lesquels la protéine RAP1 assure un rôle critique dans la stabilité des télomères. Premièrement, RAP1 peut prévenir les fusions inter-chromosomiques dans des cellules exprimant une forme altérée de TRF2 incapable de former des t-loops. Deuxièmement, l'inhibition de RAP1 dans des cellules en sénescence réplicative conduit à l'activation des voies de réparation de l'ADN et à la formation de fusions inter-chromosomiques. Ces observations font écho à des résultats précédents obtenus dans des cellules HeLa traitées avec l'inhibiteur de la télomérase BIBR1532, et dont l'expression de la protéine RAP1 était abolie par shRNA. De plus, j'ai montré que les fusions inter-chromosomiques engendrées par la perte de RAP1 sont dépendantes de la ligase IV, qui est un acteur principal de la voie de réparation de l'ADN par recombinaison non-homologue (NHEJ).

Dans l'ensemble, ces travaux démontrent l'importance de la protéine RAP1 dans la stabilité des télomères lorsque la protéine TRF2 est non fonctionnelle, mais aussi dans des situations physiologiques telles que la sénescence réplicative.

Mots-clés: Télomères, RAP1, TRF2, fusions inter-chromosomiques, recombinaison non-homologue (NHEJ), sénescence réplicative

Abstract

In mammals, the shelterin complex is the guardian of telomere stability. It operates through a set of six proteins (TRF1, TRF2, POT1, RAP1, TPP1 and TIN2) that binds telomeric DNA and protects it from being recognized as DNA double-strand breaks and therefore control DNA repair and DNA damage response pathways.

Among them, RAP1 and TRF2 cooperate and together protect chromosome extremities from end-to-end fusions. TRF2 is seen as a major factor to control telomere DNA topology by wrapping DNA around itself in a right handed manner. This property of TRF2 is required to promote the formation of t-loops, special DNA structures at telomeres that are considered as protective barriers to DNA damage response and fusion.

Here we demonstrate two independent situations where RAP1 dysfunction is critical for telomere protection. First, in cells expressing a wrapping-deficient TRF2 allele that cannot form t-loops, RAP1 appears as a backup anti-fusion mechanism. Second, RAP1 downregulation in replicative senescent cells leads to telomere fusions and DNA damage response activation. This is consistent with similar observations in HeLa cells treated with the telomerase inhibitor BIBR1532, and in which RAP1 expression was abolished by an inducible shRNA system. In addition, we show that fusions triggered by RAP1 loss are dependent upon ligase IV, which is a key player of the classical non-homologous end-joining (c-NHEJ) repair pathway.

Altogether, these results indicate that RAP1 takes over telomere protection when TRF2 cannot properly function or in the normal physiological situation, such as replicative senescence.

Key words: telomeres, RAP1, TRF2, chromosome fusions, NHEJ, replicative senescence.

“Somewhere, something incredible is waiting to be known.”

Sharon Begley

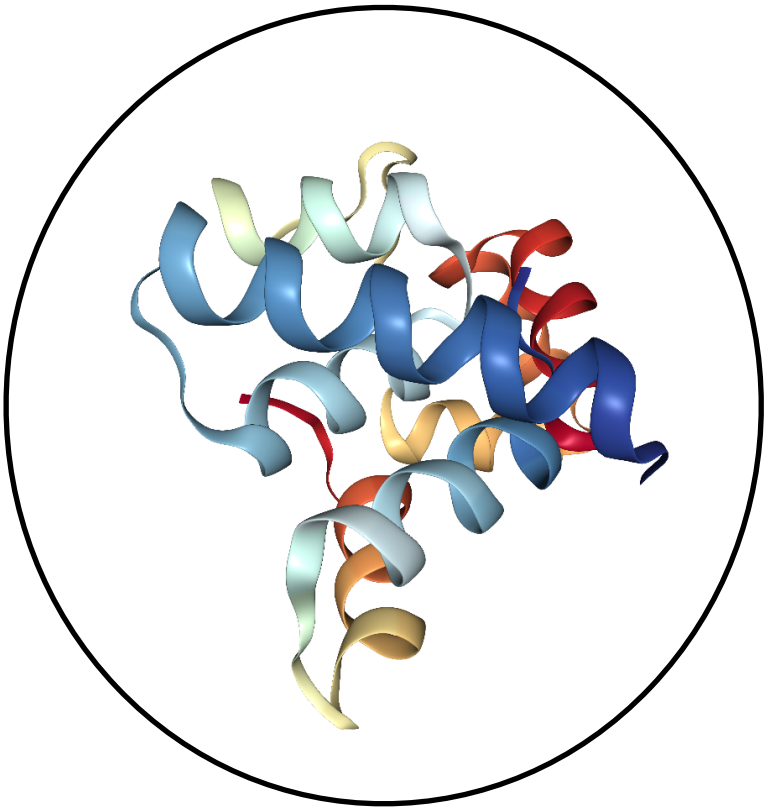

Acknowledgements

First of all, I would like to thank the members of my Thesis committee, Dr. Corine Bertolotto, Dr. Paula Martinez and Dr. Stéphane Marcand, for their courage to accept my invitation and willingness to evaluate my thesis thoroughly. I greatly appreciate your efforts and time spent on my work.

Then I would like to extend my gratitude to my PhD supervisor Pr. Eric Gilson. It was a rare luck and privilege to hit the jackpot twice: being granted a Signalife PhD fellowship and being accepted into your team after project rotations. Thank you very much for allowing me to work on RAP1 and senescence and even more, thank you for believing in my work despite all the project ups and downs we faced together throughout the PhD.

My very special thanks go to my co-supervisor Dr. Aaron Mendez-Bermudez. I thank you enormously for being always by my side during this extreme but surely unforgettable PhD journey. I always admire your optimism and hard work, and I owe you a lot in terms of professional and personal skills I acquired while working with you. I must admit I always felt very privileged and happy to work with you. Thank you for all the amazing discussions and team work, and I'm looking forward to seeing our work published any time soon.

Many many thanks to my lab colleagues, past and present, for welcoming me in the team and providing unbelievable care and support during my PhD. Specifically, I thank Rita for sharing so many memorable moments together, for your helping hand with literally everything, for being my elder sister even though I don't have a real one. Sabrina, my dear "mommy" friend, thank you for taking care of me in very difficult times and for your very big heart. Delphine, thanks a lot for always supporting and encouraging me, especially during my last year. Marie-Jo, I thank you for teaching me a hardcore biochemistry, such as EMSA and overhang assay. Nadir, thank you for being very patient with my orders and thanks a lot for always willing to help. Julien, I would like to thank you for being always a witty and positive person and I learned a lot from you about cancer and immunology. Alex, thanks for reminding me to buy some groceries and for your fantastic lemon cakes, which I will definitely miss in the future. Many thanks to our PhD crew, Alice, Martin, Sol, Charlene, for many great and sometimes crazy moments in the lab and not only. Alice, thanks for your interesting talks about corals, Martin, I learned from you a few cool methods to work with neurons, Sol, you're my autophagy expert, Charlene, you are the one

who knows all the challenges to work with senescent cells. I also thank Claire, Melanie, Serge and many others for contributing to a good atmosphere in the team. I would like to mention also the contribution of Mounir and Marta during my first year of PhD.

I would like to express my gratitude also to our “floor-mates”, teams Liti and Cristofari. Thank you for being amazing neighbours and for sharing with me reagents when I needed the most. Special thanks go to my “stay-late-in-the-lab” mates, Arpita and Ben, for their presence during sometimes late working hours. Arpita, I will never forget our iconic trip to Berlin together with Rita. Ben, I am very grateful for your kind help with a lot of issues I had, no matter whether it’s personal or professional. Thank you also for providing me with an excellent French language expertise.

Many thanks go also to Ludo from the cytometry platform and Sabine for taking care of my radioactivity orders and being so supporting and cheerful person.

I would like to thank my high school teachers, Kavetska Tamara Borysivna and Vasyliuk Tetiana Ivanivna for always believing in me and being my real motivation to study biology and always stay curious. Thanks a lot to all my NaUKMA University teachers, for absolutely intense and fruitful 6 years of studies. Many thanks to Doan Svitlana Ivanivna and Kondratov Oleksandr, my Bachelor and Master thesis supervisors, who motivated me to pursue scientific career.

I absolutely thankful to all my friends who supported me during my PhD and not only. Special thanks to Natalia and Maksym, as well as Daria. I will never forget our trips and the 10th Nice-Cannes marathon in which we participated, they are among the best memories I had during my PhD. Many thanks to Sergii and Tania, for their enthusiasm in cheering me up always when I needed the most.

I am grateful to all the Signalife Labex community that became my second family. Among many people I met thanks to this amazing PhD Program, I would like to acknowledge Dr. Konstanze Beck and Anna Bliznyuk. I greatly appreciate your help with all the administrative procedures and for making me integrate into new culture and country smoothly. Many thanks to Lenka, Ramona and Nikita for many wonderful moments we shared and for your presence in the most difficult times. I feel very blessed to have you as my friends. My very warm wishes and special thanks go also to my Signalife buddy and flatmate Denisa. Words are not enough to express my gratitude to you. Hope we will all cross our paths in the future.

Oleksiy, among many things I am grateful to you, I would like to thank you especially for always believing in me and being my motivation to apply for PhD grants. I wouldn't be here writing these acknowledgements without your love and support. I admire your scientific approach in our daily life, and I am very grateful to all the wonderful moments we spent together and looking forward to many more to come.

Last, but not least, I would like to thank my family. Specifically, my mom and dad, I absolutely adore you for being so loving and caring parents, for so much support I got from you during all my life and especially during my PhD.

Дякую усім, хто підтримував мене протягом моєї роботи над дисертацією, і особлива подяка моїй сім'ї, батькам, за любов і підтримку.

Table of contents

List of abbreviations

ALT	alternative lengthening of telomeres
a-NHEJ	alternative non-homologous end-joining
ATM	ataxia-telangiectasia mutated
ATR	ATM- and Rad3-Related
BFB cycle	breakage-fusion-bridge cycle
BLM	Bloom helicase
BRCA 1/2	Breast-Cancer 1/2
c-NHEJ	classical/canonical non-homologous end-joining
DDR	DNA damage response
dHJ	double Holiday junction
DNA-PK	DNA-dependent protein kinase
DNA-PK cs	DNA-dependent protein kinase, catalytic subunit
DSB	double-strand break
dsDNA	double-strand DNA
EXO1	Exonuclease 1
HHR	homologous reombination repair
lncRNA	Long non-coding RNA
MHEJ	microhomologous end-joining
NHEJ	non-homologous end-joining
POT1	Protection of telomeres 1
PARP1	Poly (ADP-ribose) polymerase
RAP1	Repressor Activator Protein1
RPA	Replication protein A
ssDNA	single-strand DNA
SSA	single-strand annealing
TIN2	TERF1-interacting nuclear factor 2
TRF1/2	Telomeric repeat binding factor 1/2
TERC	telomerase RNA component
TERT	telomerase reverse transcriptase

Introduction

Over the course of evolution, mammalian telomeres developed the shelterin complex, a very elegant way to protect chromosome extremities from various DNA damaging insults. This complex is comprised of six proteins that can employ and control different interactors with one final goal: keep the telomeres functional.

One of highly dangerous events in the life of telomeres is chromosome fusion. Chromosome fusions usually occur when two chromosomes fuse end-to-end forming dicentric or ring chromosomes. Fusion can be executed by several different DNA repair pathways with or without telomere loss as an outcome. Non-homologous end-joining repair (NHEJ) and homologous recombination repair (HRR) are two common DNA repair pathways that promote telomere fusions.

In human, there are two key telomeric proteins that inhibit chromosome fusions: TRF2 and RAP1. TRF2 recruits RAP1 to telomeres and thus is considered as the master regulator of telomere protection, whereas the role of RAP1 at mammalian telomeres has been debatable for a long time.

Therefore, this Thesis manuscript sheds light on human RAP1 and its role in telomere protection.

In Chapter 1, the literature overview is a resume of the most recent and relevant findings in the field of DNA repair and DNA damage in connection to telomere fusion.

Chapter 2 represents the actual results of the thesis project. It is grouped into two articles. Article 1 is the published manuscript, which focuses mainly on how TRF2 protects telomeres in the context of DNA topology. We demonstrate that TRF2 can wrap DNA around its homodimerization domain (TRFH). The TRFH-dysfunctional mutant of TRF2 (called Top-less) is not able to wrap telomeric DNA, has decreased ability to promote t-loop formation and does not protect against DNA damage response (DDR), whereas it was able to rescue chromosome fusions. As part of the PhD project, we show that Top-less was not able to protect chromosomes from NHEJ upon RAP1 dysfunction. The latter result was an inspiration for Article 2, where we focus solely on the RAP1 role in telomere protection in the context of replicative senescence. Specifically, we found that in senescent cells RAP1 becomes essential to protect telomeres from DDR checkpoint and NHEJ repair. In Article 2 (the manuscript in preparation for publication) the main findings of my PhD work are described.

Chapter 3 is the final chapter of this dissertation. It discusses the main findings and suggests future work that would be important to better understand the mechanism of RAP1-dependent telomere protection in senescent cells.

During my PhD training, I have contributed to another research project on the role of TRF2 in pericentromere function. The results were recently published. Since this is not my main research project, the results are not discussed in this manuscript, but the article is attached in Appendix I. Article 3.

Chapter 1

Telomere fusion: control, mechanisms and consequences

1. Telomere basic: structure and replication

Our understanding of telomere functions somehow started 80 years ago by the work of Herman Muller and Barbara McClintock. Muller was studying chromosome damage in *Drosophila melanogaster* upon ionizing radiation. He was the first to introduce the name "telomere", which originates from the Greek words *telos* (end) and *meros* (part), and he used this term to describe the end parts of chromosomes [Muller HJ., 1938]. Simultaneously, McClintock highlighted the importance of telomeres during her studies of plant chromosomes in corn cells. She noted that the loss of natural chromosome ends (telomeres) destabilizes cellular genomes, causing chromosomes to become "sticky" and undergo adhesion and fusion at their ends, with consequent formation of dicentric chromosomes. She also demonstrated that the ends could be restored if chromosomes acquired a new telomere [McClintock B., 1939; McClintock B., 1941].

When the Watson-Crick double helical structure of DNA was resolved in 1953, it immediately suggested a mechanism of its replication – each strand in the duplex acts as a template to guide the synthesis of its complement. However, understanding the mechanism of the semi-conservative DNA replication [Meselson M. and Stahl FW., 1958] identified the "end replication problem", consisting of the inability of cells to completely replicate the linear ends of DNA [Gilson E. and Ségal-Bendirdjian, E., 2010]. The first formulation of the end replication problem was focused on the lagging strand synthesis process where the gap generated by removal of the RNA primer at the 5'-end cannot be filled at the end of the chromosomal DNA, resulting in shortening of the newly synthesized strands with each round of DNA replication. This lagging strand problem was revisited later on by Cech and colleagues on the basis of the structure of the parental telomere extremity that corresponds to a 3'-overhang: the lagging chromatid is expected to somehow reproduce the 3' overhang while the leading chromatid ends as a blunt DNA if the DNA polymerase synthesizes until the last nucleotide and by a 5'-overhang if the polymerase stop before, but

in any case the genetic information of the 3' overhang of the parental DNA is lost. Thus, it was postulated that the end replication is more a leading strand than a lagging strand problem [Lingner J. et al., 1995]. Watson also predicted the existence of a protective mechanism to prevent the chromosomal shortening [Watson JD. et al., 1972]. For Olovnikov, the terminal replication problem was the cause of a progressive telomere shortening, which also acted as an internal clock to determine the number of divisions that a cell can undergo during its lifespan. Therefore, telomere shortening could not only control the process of ageing but also acts as a molecular clock that counts the number of cycles that the cell can support [Olovnikov AM., 1973]. This is also consistent with the "Hayflick limit", an observation made in the early sixties showing that cultured primary fibroblasts have a limited number of divisions [Hayflick L, 1965].

Structure and length of telomeres vary greatly among different species. The basic units of telomeres are tandem repeats, for instance, T2AG3 in mammals. Telomeric DNA is double-stranded with a short 3'-tail (150-300 kb) in the very end of the chromosome. However, plants can have blunt-ended telomeres [Kazda A. et al., 2012]. In species with relatively long telomeres the 3'-overhang can fold backwards and invade the double-stranded telomere DNA forming t-loops (Figure 1). Interestingly, t-loops have been discovered among different species. For example, *Trypanosoma* form very tiny t-loops, less than 1 kb in length, whereas field pea harbours extremely large t-loops, up to 50 kb in size [de Lange T., 2004]. T-loops are considered as structural barriers that protect telomeric DNA from being recognized by DDR machinery [Van Ly D. et al., 2018].

Both G-rich and C-rich telomeric strands may form additional complex DNA structures. For example, the G-rich strand can adopt a four-stranded G-quadruplex structure involving planar G-tetrads of guanine, while the C-rich strand can form the so-called i-motif with intercalated C·C+ base pairs (Figure 1). Different G-quadruplex structures exist, and they may be important to protect 3'-tails [Phan AT. et al., 2002].

Chromosomal DNA extremities can be recognized as accidental double strand breaks (DSBs) and treated as such by the cell leading to cell cycle arrest (DDR checkpoint) and recombination (DDR repair) [Shay JW., 2004]. Therefore, the natural ends of chromosome must be protected both from DDR checkpoint and repair.

Altogether, telomeres have to deal with two major problems: end replication and end protection. It turns out, they can do so with a help from different proteins that are described in the next section.

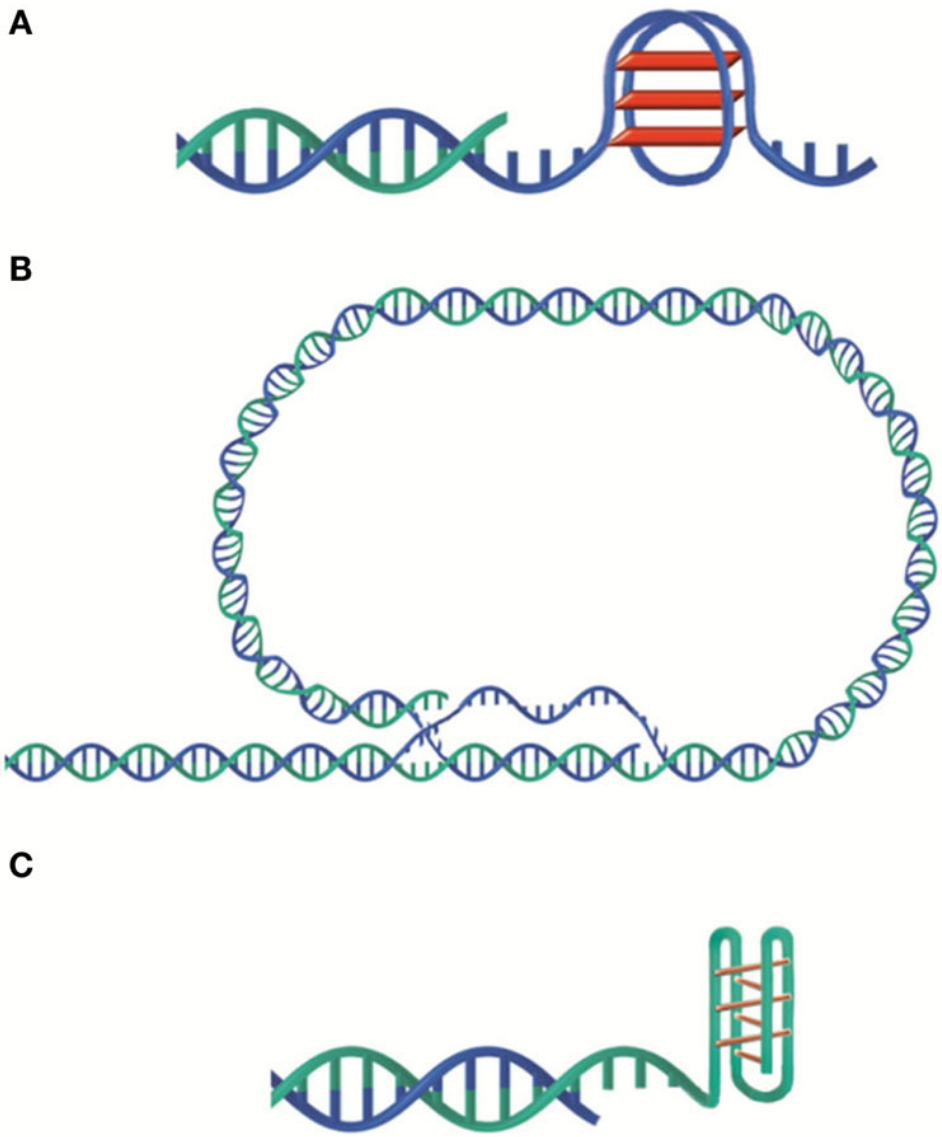

Figure 1. Different telomere structures. *A. G-quadruplex. B. t-loop. C. i-motif. Illustration from [Giraud-Panis MJ. et al., 2013].*

2. Factors that maintain and protect telomeres

To overcome the end protection problem, cells developed a few strategies to keep the equilibrium of the telomere length, such as telomerase and alternative lengthening. At the same time, end protection problem can be effectively solved by means of the capping proteins.

Telomerase was discovered in *Tetrahymena thermophila* by Greider and Blackburn[Greider CW. and Blackburn EH., 1985]. This protein is composed of two essential components: TERT (telomerase reverse transcriptase) and TERC (telomerase RNA component). TERC binds to the 3'-tail and serves as a template for TERT, which elongates telomeres (Figure 2) [Schmidt JC. and Cech TR., 2015].

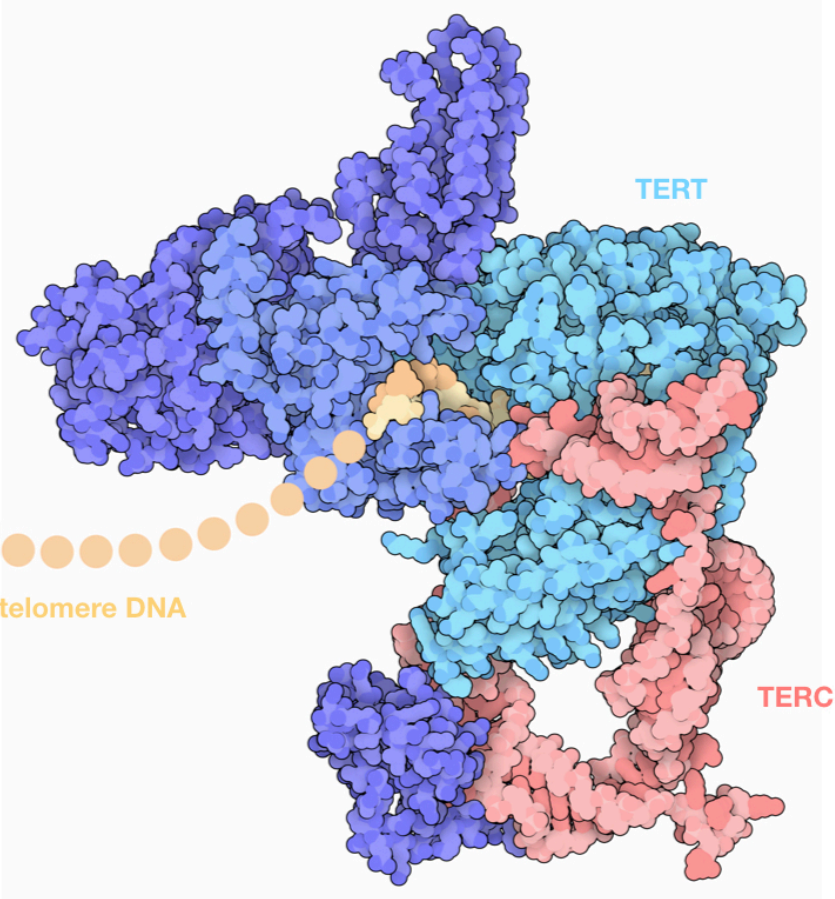

Figure 2. Structure of the telomerase holoenzyme. *This structure includes a reverse transcriptase (TERT) and associated proteins, an RNA template (TERC), and a short piece of the telomere DNA [Illustration from Protein Data Bank, http://pdb101.rcsb.org/motm/227].*

Interestingly, in human and several other vertebrate species, but not all, TERT expression and telomerase activity are severely shut down in somatic tissues at the end of embryogenesis with the exception of progenitor or stem cells but to a level insufficient to fully replenish telomeric DNA ends at each round of cell division [Cong YS. et al., 2002].

An alternative way to counteract telomere attrition is based on homologous recombination and is called alternative lengthening of telomeres (ALT) pathway. Whereas approximately 85-90% of tumours utilize telomerase to elongate their telomeres [Kim NW. et al., 1994], some cancers (notably tumours of mesenchymal origin) use the ALT pathway that relies on homologous recombination[Apte MS. and Cooper JP., 2017].

Several telomere capping proteins, protecting telomeres from unwanted DDR activation, exist among different organisms. The prototypes of telomere capping protein complexes were identified in budding yeast, consisting mainly in two complexes: shelterin and CST (Cdc13-Stn1-Ten1). Shelterin is restricted to the RAP1 protein, which specifically binds telomeric DNA repeats to protect telomere DNA from fusion, while CST plays a key role against telomeric DNA degradation, checkpoint activation and telomere replication [Giraud-Panis MJ. et al., 2010].

The equivalents of the shelterin and CST complexes are found in many (if not all) eukaryotic organisms but with a great diversity of protein composition (Figure 3) [Giraud-Panis MJ. et al., 2013]. In mammals, shelterin is comprised of six proteins: TRF1 and TRF2 that through a Myb-like domain named Telobox bind to double-stranded DNA (dsDNA), TPP1 binding to POT1, which binds to the 3'-overhangs, TIN2 making a protein bridge between TRF1/TRF2 and TPP1 and finally RAP1 that, in contrast to budding yeast, binds indirectly to telomeric DNA via a direct interaction with TRF2 (Figure 3) [de Lange T., 2005; Giraud-Panis MJ. et al., 2013].

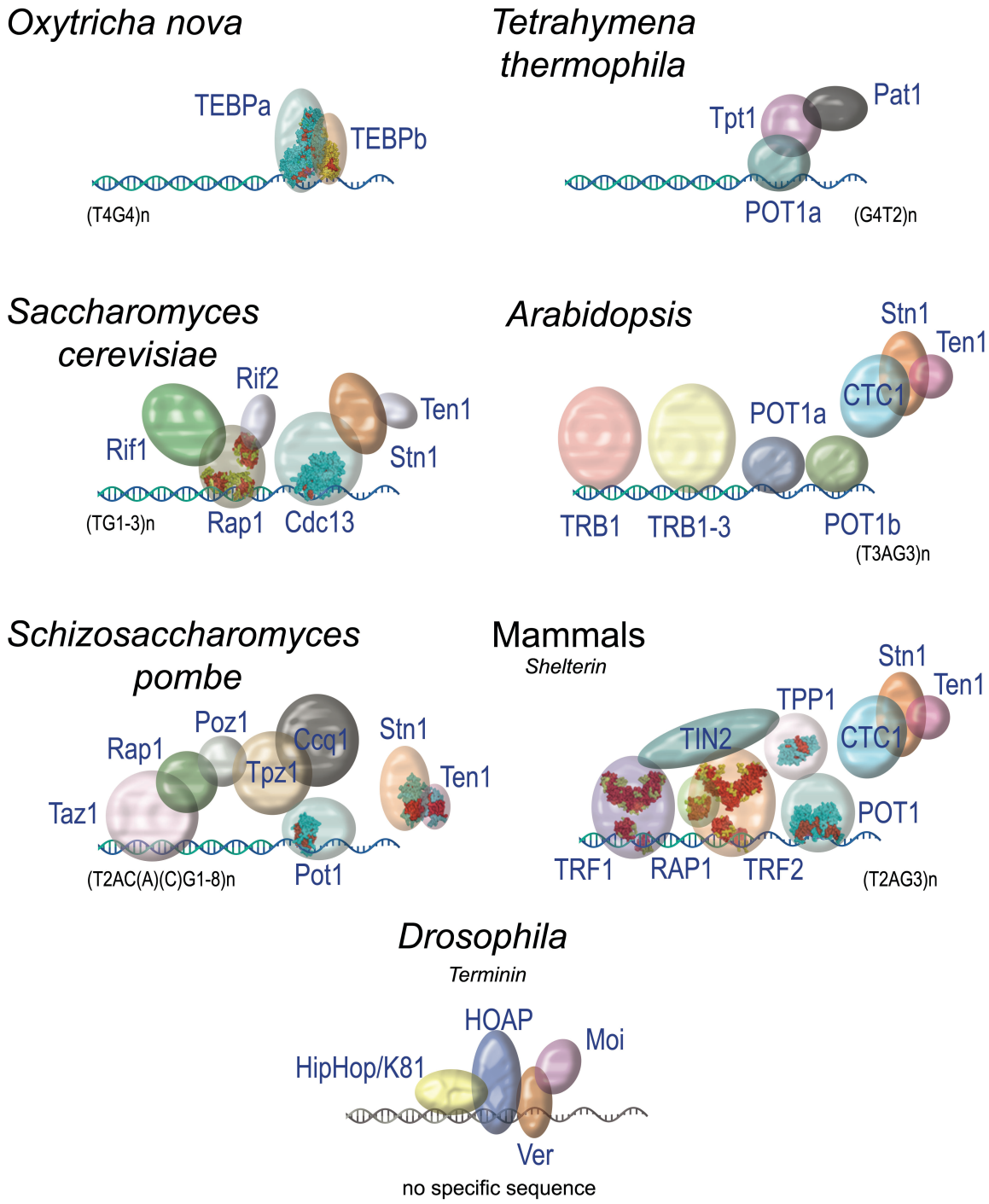

Figure 3. Telomere-associated proteins among different species. *Modified from [Giraud-Panis MJ. et al., 2013].*

3. Chromosome fusions and DNA repair

3.1. The “good” and the “bad” of fused chromosomes: lessons from evolution

Over the years, eukaryotic chromosomes acquired certain differences in their shape, size, composition, and number. These features made species distinguishable among each other, therefore, they appear to be important targets of evolution.

Simply, two ways of chromosome number evolution exist: fusion and fission, which lead to two different consequences for the genome: either reduction or amplification in the number of the existing genetic material [Schubert I., 2007].

In terms of evolution, there is a large body of evidence that end-to-end fusions lead to reduction in the total number of chromosomes. For example, fusion of two ancestral primate chromosomes created human chromosome 2 [Ijdo W. et al., 1991]. Fusions were also a common cause of reduced chromosome number among ant species *Mycetophylax conformis* and *Mycetophylax morschi* [Cardoso DC. et al., 2014], and plant *Arabidopsis thaliana* [Lysak MA. et al., 2006]. Evolution of the budding yeast genome is characterized by the whole-genome duplication (from n=8 to n=16 chromosomes). However, it has been observed that in some other yeast species, such as *Zygosaccharomyces, Kluyveromyces, Lachancea*, and *Ashbya*, the number of chromosomes varies from 6 to 8. The most common event in reducing chromosome number among those yeast is telomere end-to-end fusions [Gordon JL. et al., 2011]. Recently, two independent groups created *Saccharomyces cerevisiae* strains with dramatically reduced number of chromosomes [reviewed in Liti G., 2018]. Luo et al. engineered yeast with n=2 chromosomes, and Shao and colleagues fused all the chromosomes into a single chromosome in a functional yeast [Shao Y. et al., 2018; Luo J., 2018]. Both studies concluded that reduced chromosome number causes no major growth defects when cells are grown under various conditions and stresses. The groups showed that the n = 1 and n = 2 strains can undergo sexual reproduction, albeit with reduced efficiency compared with wild-type yeast, and produce spores that are slightly less viable. Therefore, these engineered yeast strains constitute powerful resources for studying fundamental concepts in chromosome biology [Liti G., 2018].

Probably the most impressive example of natural chromosome reduction is the Indian muntjac (*Muntiacus muntjak*), whose females only have 6 chromosomes, and its males only 7

[Wurster DH. and Benirschke K., 1970]. By means of comparative mapping and sequencing approach, Tsipouri and colleagues characterized the sites of ancestral chromosomal fusions in the Indian muntjac genome [Tsipouri V. et al., 2008]. Specifically, they screened an Indian muntjac bacterial artificial chromosome library with a telomere repeat-specific probe. They found that all seven Indian muntjac sequences, that were analyzed, contained centromeric satellite I repeat sequences immediately adjacent to the telomeric-repeat block [Tsipouri V. et al., 2008]. Furthermore, high frequency of tandem fusions, which arise from telomere and centromere repetitive elements, has been proposed as the main mechanism of stasipatric (rapid) speciation that is common among muntjacs [Wang W. and Lan H., 2000].

Presence of telomere and centromere or pericentromere repeats and their duplication at the fusion site is a proof of DNA damage repair by non-homologous end-joining. This type of repair is usually error-prone and can give rise to certain types of genetic instability through initiation of 'breakage-fusion-bridge' (BFB) cycles, first discovered by McClintock in *Zea mays* [McClintock B.,1939; McClintock, 1941]. Such cycles start with the loss of telomeres at the ends of the chromosomes (Figure 4). Then DNA is replicated, and sister chromatids with fused ends are formed. During anaphase, centromeres of those sister chromatids are pulled in the opposite directions forming bridges as the ends are fused. While pulling centromeres apart from each other, a break of the bridge occurs at any point in a way that a daughter cell receives an uneven chromosome without telomeres. Telomeres can be restored by telomerase, but if the chromosome still lacks telomeres at the ends, the BFB cycle will continue during the next cell division.

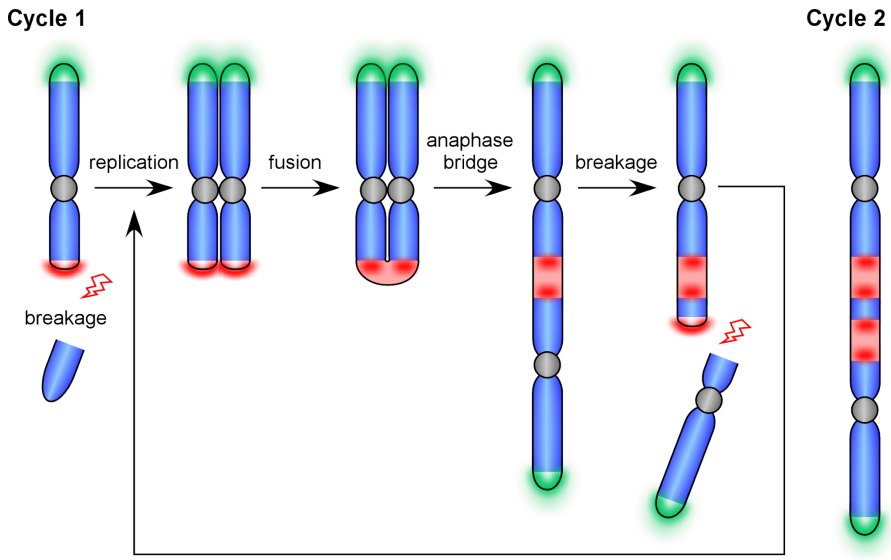

Figure 4. Breakage-fusion-bridge cycles.

BFB cycles cause duplications, deletions, inversions as secondary rearrangements in the chromosomes. Genetic instability that occurs becomes a driving force of evolution. As described above, it can lead to appearance of new species (which can be considered as "good"). On the other hand, it can be a cause of establishing and promoting different malignancies (which for a normal cell and the whole organism is usually considered as "bad") [Selvarajah S. et al., 2006; Kwei KA. et al., 2010; Martínez P. and Blasco MA., 2017; Maciejowski J. and de Lange T., 2017]. Therefore, detailed studies of the mechanisms that lay behind genetic instability are needed to better understand how the switch between “good” and “bad” occurs.

The next part of this manuscript is focused on DNA repair mechanisms that are in connection to telomere fusion.

3.2. The DNA double-strand break repair mechanisms promoting chromosome fusions

In normally functioning cells, chromosome fusion must be prevented in order to maintain genome stability. In this regard, cells developed several mechanisms that inhibit fusion at natural chromosome ends. This is one of the main function accomplished by telomeres. Among the telomere strategies to prevent fusion, one can cite peculiar DNA structures (t-loops, 3'-overhangs), shelterin and other associated telomere factors.

In the absence of a proper anti-fusion activity, chromosome extremities can fuse by different recombinational repair mechanisms: homologous recombination repair as well as classical and alternative non-homologous end-joining (Figure 5).

In the next section of this manuscript, the mentioned pathways will be presented in detail with a focus on their relationship to chromosome fusions.

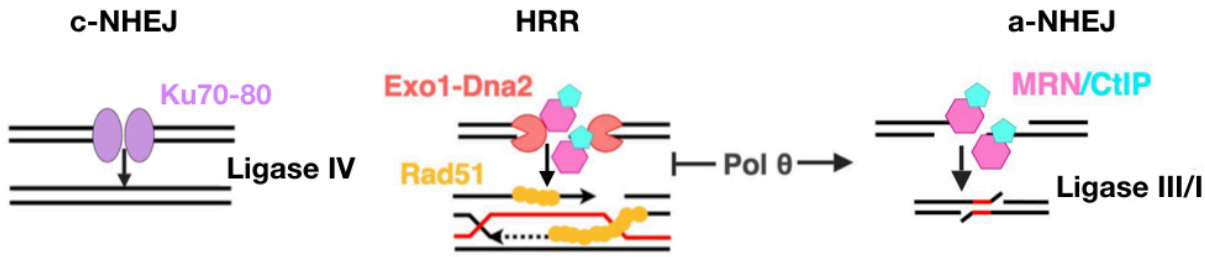

Figure 5. Multiple pathways to repair a DNA double-strand break.

3.2.1. Homologous recombination repair. Homologous recombination repair (HRR) or homology-directed repair (HDR) is a high-fidelity pathway of DSB repair. Although many different proteins and some of the non-coding RNAs are implicated in HRR, and several different mechanisms exist, the basic principles are conserved among prokaryotes and eukaryotes. This type of repair relies on homologous recombination, where a homologous DNA template is used to repair and restore the sequence around the break. DSB repair by HRR in mitotic cells favours the use of the sister chromosome over the homologous chromosome as a template donor [Kadyk LC. and Hartwell LH., 1992]. Notably, repair of DSBs by means of HRR can lead to two different consequences: crossover and non-crossover. For example, crossover occurs during meiosis and can be also used to generate genetic diversity [Baudat F. and de Massy B., 2007; Heyer WD. et al., 2010]. However, the primary mechanism of HRR, gene conversion, does not result in the crossover, which makes it a faithful DNA repair process. Also, synthesis-dependent strand annealing pathway (SDSA) does not result in crossovers and is important to preserve genomic integrity [Verma P. and Greenberg RA., 2016]. When DSBs cannot be processed by the conventional mechanism of HRR, cells decide between SDSA, double-strand break repair (DSBR), break-induced replication (BIR), or single-strand annealing (SSA) (Figure 6) [Chapman JR. et al., 2012; Verma P. and Greenberg RA., 2016; Wright WD. et al., 2018].

Regardless of which choice has been made, initial steps of HRR share the same principles. First, after a DSB occurs, broken DNA ends undergo nucleolytic end resection to generate 3'-ssDNA overhangs. Generation of 3'-overhangs can be characterised by a two-step mechanism. First, in higher eukaryotes, an immediate recruitment of Mre11-Rad50-Nbs1 (MRN) along with CtIP complex occurs at the sites of DSB [Lamarche BJ. et al., 2010; Langerak P. et al., 2011]. MRN-CtIP removes small oligonucleotides to generate a short protruding end [Muraki K. and Murnane P., 2018]. Next, several other enzymes are recruited to produce long single-stranded overhangs by resection, for instance, Exonuclease 1 (EXO1), DNA replication helicase/nuclease 2 (DNA2) [Mimitou EP. and Symington LS., 2009; Jasin M. and Rothstein R., 2013]. Furthermore, Bloom helicase (BLM) can be important for long-range resection of DNA ends [Nimonkar AV. et al., 2011], as well as Werner helicase (WRN). The latter can substitute BLM in DNA2-mediated resection [Sturzenegger A. et al., 2014]. Therefore, BLM and WRN act epistatically and ensure the single-strand 3'-overhang formation on both strands of the break.

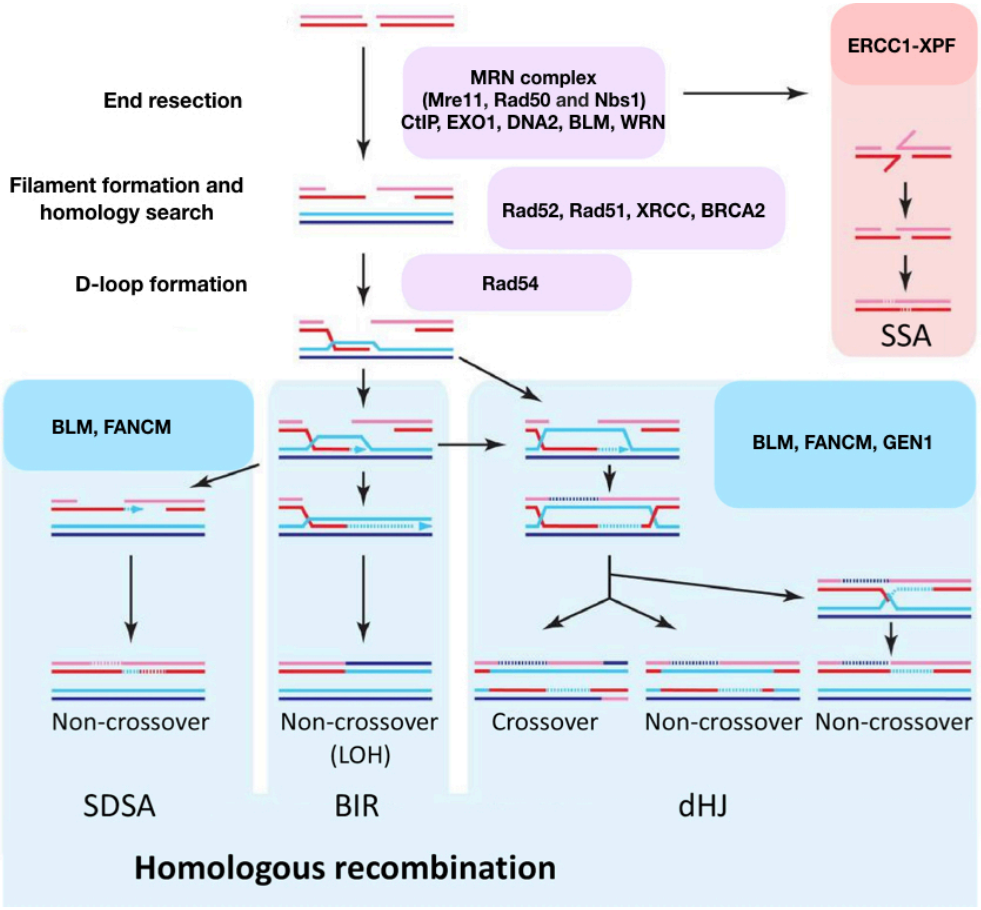

Figure 6. Different pathways of homologous recombination repair in human. *Modified from [Heyer WD. et al., 2010].*

Moreover, breast cancer suppressor BRCA1 can also take part in the initial steps of HRR, since it has been shown to interact with MRN [Zhong Q. et al., 1999] and CtIP [Yu X. et al., 1998] and promote HRR [Moynahan ME. et al. 1999; Stark JM. et al. 2004], as does CtIP [Sartori AA. et al. 2007; Bennardo N. et al. 2008]. Interestingly, BRCA1 may control the CtIP-dependent recruitment of DNA2 to DNA damage sites for subsequent DSB resection [Hoa NN. et al., 2015]. It has been demonstrated that BRCA1-A complex comprised of ubiquitin interacting motif (UIM) containing protein RAP80, adapter protein Abraxas, MERIT40 (mediator of RAP80 interactions and targeting 40 kDa, also known as NBA1), BRCC45, and deubiquitinylating enzyme BRCC36 guides BRCA1 to the sites of DSB through interaction with UIMs of RAP80 [reviewed in Greenberg RA., 2008; Daley JM. et al., 2014; Her J. et al., 2016]. Also, a proper recruitment of BRCA1 to the DSB sites is controlled by lncRNA DDSR1 [Sharma V. et al., 2015].

After 3'-overhangs are generated, they are immediately covered by ssDNA-binding replication protein A (RPA). This binding prevents the formation of unwanted secondary structures on ssDNA [Chen H. et al., 2013]. The next step is to load Rad51 on 3'-overhangs. In humans, several proteins can be important to replace RPA with Rad51. Among them, Rad52 appears to be essential to physically replace RPA with Rad51 and promote, therefore, formation of the nucleoprotein filament [Sugiyama T. and Kowalczykowski SC., 2002; Plate I. et al., 2008]. Notably, it has been also shown that BRCA2 interacts directly with Rad51 and recruits it to the RPA-coated ssDNA at the DSB site [Her J. et al., 2016]. Therefore, several mechanisms exist for the proper functioning of initial steps of HRR.

When the filament is formed, Rad51 initiates the search for a homologous template followed by the donor DNA strand invasion, formation of a D-loop and subsequent DNA synthesis mediated mainly by DNA polymerase δ in eukaryotes [Maloisel L. et al., 2008; McVey M. et al., 2016]. Strand invasion and formation of the D-loop is mediated by Rad54 (a protein that belongs to the SNF2/SW12 family in humans), which removes Rad51 from the filament [Kanaar R. et al., 1996; Li X. and Heyer WD., 2009; Mazin AV. et al., 2010].

To complete HRR, three different scenarios are possible (Figure 6). First, if the second DNA end is present, mitotic cells mainly follow the SDSA pathway [Andersen SL. and Sekelsky J., 2016]. Therefore, either of 3'-overhangs or even both of them can invade the donor template. The invading strand is further displaced during the D-loop migration and the newly formed DNA strand anneals back to the ssDNA overhang of the second end, resulting in a non-crossover product [Heyer WD. et al., 2010]. However, a second possibility is the creation of a double Holiday junction (dHJ), which can result either in the crossover or non-crossover outcome depending on the proteins involved in the processing. For example, BLM together with topoisomerase 3 alpha (Top3A) process dHJs in a way that crossover does not occur [Wu L. and Hickson ID., 2003].

BIR takes place when there is only one accessible DNA end. The available 3'-overhang invades the homologous DNA and then extends to the end of the chromosome. In higher eukaryotes, BIR is an important mechanism to repair and restart broken replication forks, as well as it can contribute to the alternative lengthening of telomeres [reviewed in Verma P. and Greenberg RA., 2016].

SSA is another type of DSB repair, which can be considered as an alternative pathway of HDR [Verma P. and Greenberg RA., 2016]. SSA is initiated when DSB occurs between homologous direct repeats. These repeats first are resected bidirectionally, then nucleases cleave off unpaired 3'-overhangs. The final step is annealing and ligation of the DSB. Remarkably, SSA does not require Rad51 filament, therefore, is Rad51-independent. Because the nuclease cleavage can result in deletion of repeats, SSA is a mutagenic process [Verma P. and Greenberg RA., 2016; Bhargava R. et al., 2016].

In summary, homologous recombination repair is represented by several pathways. All these pathways are conserved among different organisms, and some of them are redundant. However, given how complex is the interaction among different proteins within one pathway, new approaches emerge in order to better dissect the mechanism of HRR. One of these approaches relies on super-resolution microscopy methods to study the process at single-molecule resolution [Kaniecki K. et al., 2018].

If HRR is not properly executed, this can lead to rapid telomere resection and loss followed by appearance of telomere-free ends and massive telomere-free chromosome fusions. Since HDR relies on the presence of homologous DNA template, it favours formation of sister chromatid fusions and can promote unequal sister chromatid exchange that will create fragile chromosomes [Rudd MK. et al., 2007].

3.2.2. Non-homologous end-joining repair. Non-homologous end-joining is a second type of repair that cells employ on a regular basis. Described as a “willy-nilly” end-joining [Deriano L. and Roth DB., 2013], it relies on joining damaged DNA strands together. It can be either very robust and precise if the ends do no miss nucleotides or do not require further processing; otherwise, it can lead to certain genetic instability or diversity [Lieber MR., 2010; Chang HHY. et al., 2017]. For example, V(D)J recombination in immune cells absolutely requires NHEJ and is considered as a normal physiological process [Malu S. et al., 2012], whereas incongruous NHEJ may promote cancer formation [Sishc BL. and Davis AJ., 2017]. The latter is due to formation of dicentric chromosomes that initiate BFB cycles or chromotrypsis [Maciejowski J. and de Lange T., 2017]. If NHEJ acts between two telomeres, it fuses chromosomes as an immediate outcome [Marcand S., 2014]. Therefore, NHEJ is the prime mechanism to create both intra- and inter-chromosome fusions.

Nowadays many different proteins involved in classical or canonical NHEJ have been characterized (which is often referred to as c-NHEJ), however, the basic principles on how

this pathway is executed are the same among various species. In general, the c-NHEJ can be divided into three very general steps: DSB recognition, processing, and ligation (Figure 7) [Lieber MR., 2010; Yang K. et al., 2016].

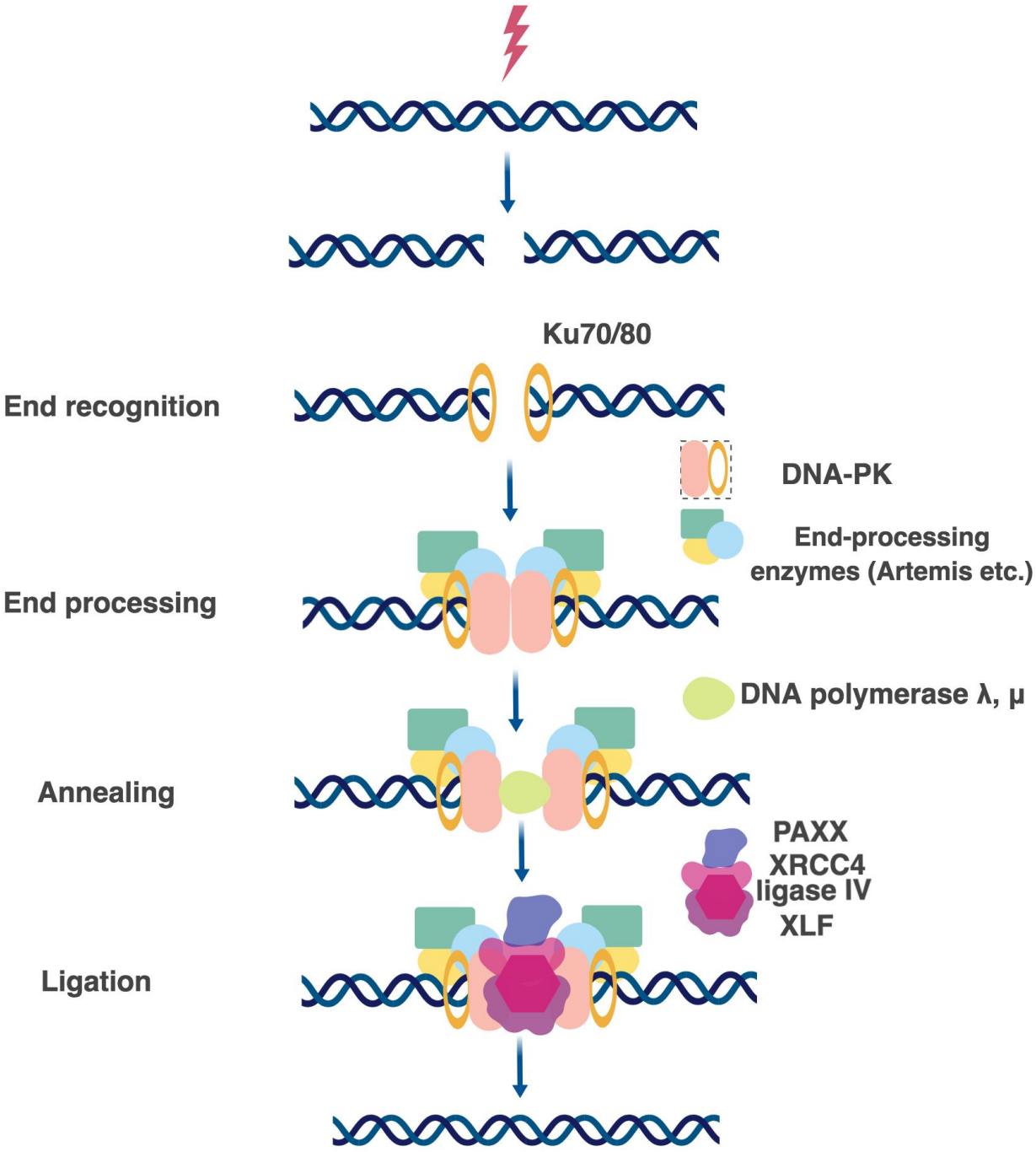

Figure 7. Non-homologous end-joining repair in human.

There are two essential components to make NHEJ work: DNA-PK and the ligase IV complex [Waters CA. et al., 2016]. However, presence of those two complexes can be enough only if the DSB forms blunt ends and do not require further processing. If the DSB is followed by incompatible DNA ends, direct ligation cannot be performed, and therefore several end-processing and annealing proteins are on call before the ligation can occur [Chang HH. et al. 2016; Chang HHY. et al., 2017].

DSB recognition. The first protein, which is recruited within seconds to the sites of DSB, is Ku. In human, Ku is very abundant (500 000 molecules per cell) and demonstrates the strong affinity for DNA binding [Fell VL. and Shild-Poulter C., 2015]. Nevertheless, both *in vitro* and *in vivo* studies show that just two molecules of Ku are enough to cover the sites in the vicinity of the damaged DNA, presumably, each one covering the broken ends [Roberts SA. and Ramsden DA., 2007; Britton S. et al., 2013]. In eukaryotes, Ku is present as a heterodimer, which is called Ku70/80. After being recruited to the sites of damage, Ku70/80 promotes sequestration of several other NHEJ factors for the appropriate repair (nucleases, polymerases, ligases), thus, Ku acts as a hub or scaffold protein [Fell VL. and Shild-Poulter C., 2015]. In yeast, there are Yku70/80 orthologs for mammalian Ku proteins. Strikingly, Yku is not an essential protein in yeast, whereas loss of human Ku86 leads to massive telomere loss and cell death [Wang Y. et al., 2009].

Ku forms the DNA-PK complex together with the DNA-dependent protein kinase catalytic subunit (DNA-PKcs) [Spagnolo L. et al., 2006]. DNA-PKcs has been discovered only in higher eukaryotes so far. Recently, the cryo-EM structure of human DNA-PK has been solved. Two research groups independently demonstrated that DNA-PKcs and Ku70/80 together form a DNA-binding bridge or tunnel. DNA-PKcs is relatively proximal, and Ku70/80 is distal, to the free DNA end. DNA-PKcs and Ku70/80 both wrap around one and a half turn of the DNA duplex with the blocked DNA end flanking outside of the complex [Yin X. et al., 2017; Sharif H. et al., 2017]. Notably, DNA-PKcs alone barely binds to DNA but strongly binds to DNA in the presence of Ku70/80 [Yin X. et al., 2017]. DNA-PKcs can be autophosphorylated or trans-phosphorylated by ATM. These two states of phosphorylation regulate the switch between recruitment of Artemis or ligase reaction [Uematsu N. et al., 2007; Jiang W. et al., 2015].

DSB processing. Components of the DNA-PK complex can recruit to the sites of DSB DNA end-processing factors such as Artemis [Riballo E. et al., 2004], Werner [Chen L. et al., 2003; Shamanna RA. et al., 2016], polynucleotide kinase-phosphatase (PNKP) [Shimada M.

et al., 2015], APTX–polynucleotide kinase-phosphatase-like factor 1 (APLF) [Macrae CJ. et al., 2008; Grundy GJ. et al., 2013], DNA polymerases Pol λ and Pol μ [Capp JP et al., 2006; Chayot R. et al., 2012], terminal deoxynucleotidyl transferase (TdT) [Boubakour-Azzouz I. et al., 2012]. Depending on how complex is the DSB, the mentioned factors can be required for the accurate DNA end cleavage and annealing in order to facilitate further ligation [Yang K. et al., 2016]. Interestingly, mammalian DNA-PKcs and the rest of the mentioned processing factors (except DNA polymerases) do not have orthologs in budding yeast *S.cerevisiae* [Dudásová, Z. et al., 2004]. Instead, MRX complex becomes of outstanding importance to execute NHEJ [Emerson CH. and Bertuch AA., 2016]. Regarding the DNA polymerases in yeast, Pol4 is a Pol X family polymerase (related to mammalian polymerases λ and μ). Moreover, yeast employs also Pol3 (mammalian Polδ) [Ramsden D., 2011].

DSB ligation. Importantly, c-NHEJ is distinct in this regard, because it relies on the ligase IV function [Wang H. et al., 2001]. In mammals, ligase IV forms a complex with XRCC4 and XLF [Ahnesorg P. et al., 2006]. XRCC4 and XLF are particularly important for bridging DNA molecules and therefore promoting ligase IV activity [Andres SN. et al., 2012].

PAXX (XRCC4 paralogs) is a regulator of XRCC4 [Xing M. et al., 2015]. Besides XRCC4-ligase IV complex, it interacts with Ku70 directly and promotes Ku accumulation at the break [Ochi T. et al., 2015; Liu X. et al., 2017]. An emerging view is that PAXX is an additional protein recruited to hard-to-repair DSBs [Tadi SK. et al., 2016], where it can promote DNA polymerase λ activity [Craxton A. et al., 2018].

In yeast, ligation occurs due to the activity of DNA ligase IV or Dnl4 in *S. cerevisiae*. Dnl4 is strongly associated with Lif1. If Lif1 is dysfunctional, Dnl4 becomes unstable [Herrmann G. et al., 1998]. Mrx and Yku were reported to promote association of the Dnl4-Lif1 complex to the DSB, as well as Nej [Emerson CH. and Bertuch AA., 2016].

3.2.3. Alternative non-homologous end-joining pathway. It has been reported that critically short telomeres tend to fuse end-to-end via non-canonical end-joining that requires microhomology [Letsolo BT. et al., 2010].

Alternative NHEJ (a-NHEJ) in certain literature reviews can also be referred to as alternative end-joining (a-EJ). An early evidence for the existence of alternative end-joining pathways came from studies in Ku-deficient budding yeast [Boulton SJ. and Jackson SP., 1996]. In mammals, similar observations were made in p53 knockout mice lacking the

components of the NHEJ machinery, but yet supporting insertions, deletions and microhomology [Zhu C. et al., 2002].

A-NHEJ is distinct from c-NHEJ and HRR on several counts. First, it does not necessarily require homology to function as HRR does. However, certain types of fusions that occur through a-NHEJ can use microhomology, which makes it similar to the SSA pathway [Verma P. and Greenberg R., 2016; Sallmyr A. and Tomkinson AE., 2018]. The latter pathway is called MMEJ or MHEJ (microhomology-mediated repair). In contrast to SSA, MMEJ relies on very short homologies, less than 20 bp [Pannunzio NR. et al., 2014; Mladenov E. et al., 2016]. The final step in the repair is ligation of DNA, but in comparison with c-NHEJ it is ligase IV independent process, which is executed via either ligase III or I [Wang H. et al., 2005; Simsek D. et al., 2011; Masani S. et al., 2016].

The distinct characteristics of a-NHEJ are the key players involved in the pathway: poly(ADP-ribose) polymerase1 (PARP1), DNA polymerase θ (POLQ), and Ligase III/I [Chang HHY. et al., 2017] (Figure 8). The main role of PARP1 is to catalyse the polymerization of ADP-ribose units — derived from the ADP donor NAD+ — resulting in the attachment of either linear or branched PAR polymers to itself or other target proteins. PARP1 is therefore believed to be a sensor of DNA damage [Ray Chaudhuri A. and Nussenzweig A., 2017]. By means of several biochemical and super-resolution microscopy approaches, it has been demonstrated that PARP1 competes with KU for DNA DSB repair. KU can be removed from the sites of DSBs by PARylation that is performed by PARP1 [Wang M. et al., 2006; Yang G. et al., 2018]. Furthermore, PARP1 recruits MRN complex to the repair centre (Figure 8) [Haince JF. et al., 2008]. In analogy to HRR, MRN together with CtIP may be necessary for end processing and removal/recruitment of other proteins [Lamarche BJ. et al., 2010]. Contrary to HRR, MMEJ does not require γ-H2AX, neither BLM nor EXO1 for end processing [Truong LN. et al., 2013].

After DNA is recognized and processed, DNA polymerase θ is needed for a stable annealing of DNA strands. Polθ uses short microhomology (2-6 bp) for annealing. Notably, if this microhomology is not present, due to its transferase activity, Polθ can add several nucleotides to create microhomology at the site of the break [Kent T. et al., 2015]. Remarkably, polymerase θ was found to promote a-NHEJ at dysfunctional telomeres in cooperation with PARP1 [Mateos-Gomez PA. et al., 2015]. Recently, another DNA polymerase β was reported to participate in a-NHEJ [Ray S. et al., 2018].

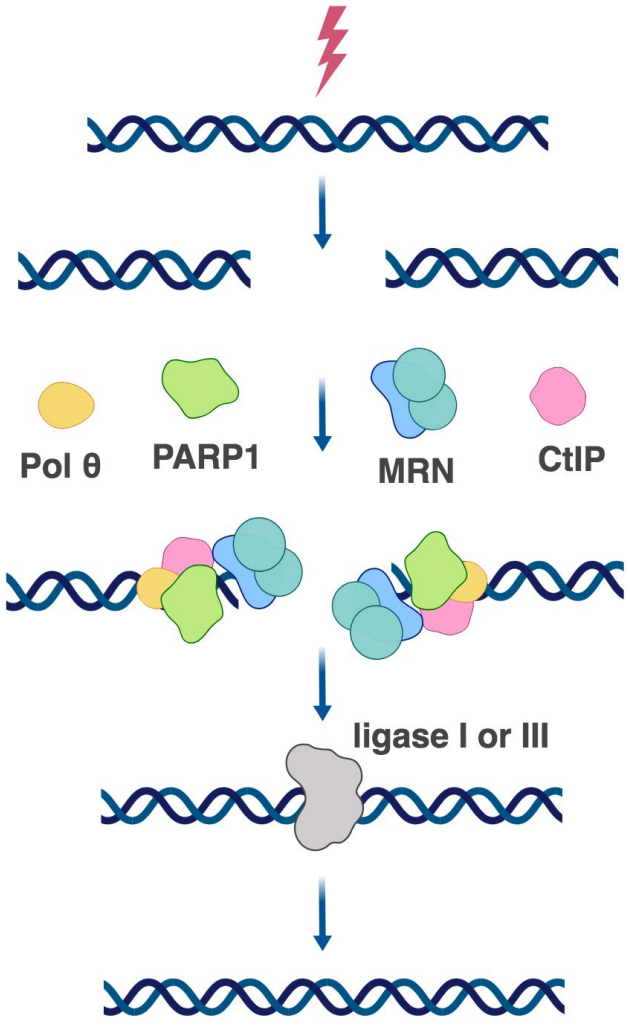

Figure 8. Alternative NHEJ in human.

The final step of a-NHEJ is ligation of the annealed DNA. End ligation is ligase IV-independent and relies on the activity of either ligase III or I. Ligase III seems more efficient in comparison to Ligase I [Lu G., 2016]. Ligase III can form a complex with XRCC1, which was found to co-exist with MRN in a-NHEJ [Caldecott KW. et al., 1994; Della-Maria J. et al., 2011].

Whether this pathway is a backup of the main c-NHEJ or acts independently, there is a body of evidence that a-NHEJ is employed by the cell to create genetic diversity [Ottaviani D. et al., 2014]. Nevertheless, there are still many outstanding questions that have to be explored for better understanding how a-NHEJ works and what is the prime importance of this pathway.

3.3. DNA damage response at the sites of double-strand break

In eukaryotes, DNA damage response (DDR) is a cascade of signalling events within the cell as a response to DNA damage. Like a classical signal transduction pathway, it is comprised of signal sensors, transducers, mediators and effectors. One of the peculiarities of this signalling pathway is that instead of ligand-receptor interactions, DDR machinery upstream events rely on the direct recognition and further processing of damaged DNA molecules. The sensors of this pathway are the proteins that directly recognize damaged DNA and activate upstream DDR kinases. Then the signal is amplified through the activation of different mediator kinases, and the final effectors spread the signal that will determine the fate of the cell.

DNA repair and DDR pathway are tightly connected with each other. MRN complex is essential in this regard because it appears to be in the front line, where different repair choices and DNA damage sensing merge [Williams RS. et al., 2007]. In the context of DDR, MRN is believed to play a role as a sensor of the damage. It is activated immediately at the damaged sites and directly binds dsDNA. Also, MRN acts as the main factor required for the rapid localization of ATM (ataxia-telangiectasia mutated) to DSBs [Lee JH. and Paull TT., 2005]. It is important to mention that ATM and ATR (ATM- and Rad3-Related) pathways are distinct from each other. ATM responds to DSBs, whereas ATR - to both ssDSBs and dsDSBs with a greater preference to ssDSBs, and is particularly important to repair the DNA lesions that occur during replication [Maréchal A. and Zou L., 2013].

At the sites of DSBs, ATM is a transducer protein kinase, which becomes activated by phosphorylation of its serine residue Ser1981 in human [Bakkenist CJ. and Kastan MB., 2003]. It has been shown that ATM activation is impaired in cells with MRN deficiencies [Uziel T. et al., 2003]. Furthermore, the carboxyl terminus of Nbs1 (a protein of the MRN complex) is known to interact with ATM [Falck J. et al., 2005]. Moreover, recently it was demonstrated that several proteins can enhance ATM signalling via direct interaction with the MRN complex. For instance, a signalling mediator, p53-binding protein 1 (53BP1) through it BRCT domain binds to MRN complex directly and regulate ATM phosphorylation of its substrates [Lee JH. et al, 2010]. Rad17, a replication checkpoint protein, also binds directly to MRN and is required for the early recruitment of the MRN complex to the DSB site, and it contributes to ATM activation [Wang Q. et al., 2014]. Smad7 interacts with Nbs1

and enhances the interaction between ATM and Nbs1 upon DNA damage response, leading to phosphorylation of downstream substrates [Park S. et al., 2015].

Among substrates that are phosphorylated by ATM are BRCA1, Chk2, p53, H2AX, MDC1. The latter two act in cooperation. It has been described that H2AX phosphorylation is performed by ATM as one of the upstream events of DDR activation. The phosphorylated histone is called γH2AX. γH2AX, in turn, acts as a hub for nuclear foci formation, the DDR centres where many DNA repair proteins and chromatin remodelling factors are accumulated [Iijima K. et al., 2008; Clouaire T. et al., 2017; Podhorecka M. et al., 2010].

Formation of γH2AX foci is one of the key steps in DDR signalling and repair in the context of chromatin. MDC1 was found to directly interact with γH2AX and therefore contribute to the γH2AX foci formation. At the same time, MDC1 interacts with ATM. Thus, it acts as a mediator between ATM and γH2AX and helps spread phosphorylation of γH2AX by ATM over long chromosome distances[Stewart GS. et al., 2003; Lee JH. et al., 2005; Stucki M. et al., 2005].

Although there is no doubt that phosphorylation of H2AX is essential for the DDR pathway, it has been documented that many other chromatin modifications occur, such as DNA methylation, different histone modifications etc., which require specific chromatin remodelling factors [reviewed in Polo SE. and Jackson SP., 2011]. Notably, γH2AX triggers cascades that rely on ubiquitylation and SUMOylation in order to recruit BRCA1 and 53BP1 to the damaged sites [reviewed in Daley JM. and Sung P., 2014; Muraki K. and Murnane JP., 2017].

In heterochromatin repair, ATM through its substrate Chk2 phosphorylates KAP1 and also stimulates further dissociation of heterochromatin protein HP1-β from H3K9me3 around DSBs [Goodarzi AA. et al., 2008; Bolderson E. et al., 2012]. Also, cells that do not form 53BP1 foci, fail to form phosphorylated KAP1 foci [Noon AT. et al., 2010]. Interestingly, changes in the chromatin structure upon DDR activation have been reported to increase chromosome mobility [reviewed in Hauer MH. and Gasser SM., 2017; Smith MJ. and Rothstein R., 2017; Marnef A. and Legube G., 2017]. This phenomenon is believed to be common in yeast, where damaged DNA becomes highly mobile and moves within the nucleus to the repair centres [Lisby M. et al., 2003]. Notably, DSBs that are unable to be repaired move to the yeast nuclear periphery [Nagai S. et al., 2008]. In higher eukaryotes, chromosome mobility is relatively weaker compared to yeast, however, it does occur. For

example, increased chromosome movement of uncapped telomeres in mouse cells has recently been associated with the 53BP1 repair protein and LINC-domain complex [Dimitrova N. et al., 2008; Lottersberger F. et al., 2015].

As mentioned before, a second transducer kinase pathway can be activated as a response to DNA damage. This pathway relies on ATR. In the DSB repair, ATR is activated when the resection of DNA ends takes place, and therefore ssDNA overhangs of certain length are present [Shiotani B. and Zou L., 2009]. In this process, RPA that coats ssDNA, is required for the recruitment of the ATR-ATRIP complex to the sites of DNA damage [Zou L. and Elledge SJ., 2003]. In order to be activated at the site of ssDNA, ATR-ATRIP interacts with several other proteins. For example, TopBP1 is one of the best characterized proteins that contains an ATR-activation domain to promote ATR kinase activity through interaction with both ATR and ATRIP [Kumagai A. et al., 2006; Mordes DA. et al., 2008]. Interestingly, TopBP1 can be activated through phosphorylation by ATM [Yoo HY. et al., 2007]. Apart from that, ATM may also promote the recruitment of of TopBP1 to sites of DNA damage through γH2AX and Mdc1 [Wang J. et al., 2011].

It turned out that the MRN complex (through its subunit Nbs1) is important for activation of ATR [Shiotani B. et al., 2013]. In line with this, MRN can also recruit TopBP1 to ssDNA-to-dsDNA junctions [Duursma AM et al., 2013]. Recently another TopBP1-independent way to activate ATR was described. Human RPA-binding protein ETAA1 can directly bind to RPA and propagate ATR signalling [Haahr P., et al., 2016; Lee YC. et al., 2016]. Last but not least, ATR can be activated via autophosphorylation [Liu S. et al., 2011].

Altogether, activation and recruitment of ATR-ATRIP complex to the sites of DSBs involves several factors and yet more to be discovered. The key substrate in the ATR pathway is Chk1. Activation of Chk1 triggers important pathways in cell homeostasis, such as response to replication stress, apoptosis and many others [Flynn RL. and Zou L., 2011; Blackford AN. and Jackson SP., 2017].

3.4. Anti-fusion mechanisms at telomeres

3.4.1. Telomere factors controlling fusions. In budding yeast, several different mechanisms to prevent fusions have been described. One of them relies on the protein Rap1 (Repressor Activator Protein 1). In 1985, this protein was initially identified as a DNA binding factor which interacts specifically with the 5'-upstream region of three yeast genes, TEF1, TEF2 and RP51A, whose products are part of the translation apparatus [Huet J. et al., 1985]. At that time, this DNA binding factor was temporarily called TUF, for translational upstream factor [Huet J. et al., 1985]. Although there was no known connection at that time, another study identified this factor to bind telomeric repeats directly [Berman J. et al., 1986]. The link between the two has been established later when Shore and Nasmyth purified the same protein than TUF and described it as a transcriptional regulator that can play a role in either repression or activation of transcription, and therefore dubbed it Rap1 [Shore D. and Nasmyth K., 1987]. Important discoveries were then to show that Rap1 is localized on telomeric DNA in budding yeasts [Conrad MN. et al., 1990; Klein F. et al., 1992], covers the entire length of telomeric DNA [Gilson E. et al., 1993] and regulates telomere length [Lustig AJ. et al., 1990]. Many more outstanding findings were observed later on, which broaden the spectrum of yeast Rap1 functions in heterochromatin formation, telomerase regulation and senescence [Moretti P. et al., 1994; Hecht A. et al., 1995; Marcand S. et al.,1996; Maillet L. et al., 1996; Marcand S. et al., 1997; Platt JM. et al., 2013].

Rap1 is a key protein to protect against c-NHEJ in yeast [Pardo B. and Marcand S., 2005]. It can do so either directly through its RCT domain or via recruitment of two other proteins, Sir4 and Rif1 [Marcand S. et al., 2008]. In addition to Rap1, Nej1 in a complex with Lif1 and Dnl4 prevent telomere fusions due to telomerase dysfunction [Liti G. and Louis EJ, 2003]. Notably, yeast Ku heterodimer (Yku) rapidly associates with the DNA at the damaged sites and prevents resection of DNA through inhibition of MRX complex, which as a consequence prevents fusions [Bertuch AA. and Lundblad V., 2003; Celli GB. et al., 2006].

Finally, higher order telomeric chromatin conformation could play a role in budding yeast to prevent fusion. Although it was not possible to detect conventional t-loops, it was reported that yeast telomeres can form fold-back structures through Rif2-mediated Rpd3L recruitment to telomeres [Poschke H. et al., 2012].

The identification of human RAP1 was obtained thanks to a yeast two-hybrid screen of HeLa cells with TRF2 as a bait [Li B. et al., 2000]. Comparison of RAP1 structure within

different species (*H.sapiens, S.cerevisiae, K.lactis*) revealed a high degree of domain conservation; however, the sequence similarities are surprisingly low [Li B. et al., 2000]. Importantly, in contrast to budding yeast, mammalian RAP1 does not bind telomeric DNA directly but through its direct interaction with TRF2 [Li B. et al., 2000]. Some of the yeast Rap1 functions were confirmed in mice and humans. For instance, it was demonstrated that both mouse and human RAP1 binds to telomeric and extra-telomeric sites and regulates the transcription of its target genes, specifically those involved in the metabolism control [Martinez P. et al., 2010; Yang D. et al., 2011; Yeung F. et al., 2013; Martinez P. et al., 2013]. Interestingly, a cytoplasmic fraction of RAP1 was found to regulate NF-κB signalling pathway [Teo H. et al., 2010]. Some early studies also reported that RAP1 can negatively regulate the telomere length [Li B. and de Lange T., 2003; O'Connor MS. et al., 2004], although, this was not confirmed by means of TALEN RAP1 knockout [Kabir S. et al., 2014]. Since different cell lines were used to measure the length of telomeres upon RAP1 downregulation, this may suggest that RAP1 controls the length in cell type-dependent fashion.

Although yeast RAP1 is a key anti-fusion protein, conflicting results regarding its role as an anti-fusion factor in mammals were reported. Indeed, mouse telomeres lacking RAP1 did not develop DNA damage response activation [Sfeir A. et al., 2010; Kabir S. et al., 2014] but can lead to telomere recombination by HDR [Sfeir A. et al., 2010]. As an outcome, this can trigger telomere resection and fusion [Rai R. et al., 2016]. *In vitro*, human RAP1 has been shown to protect against NHEJ either in cooperation with TRF2 or upon tethering to the telomeric DNA when TRF2 is removed [Bae NS. and Baumann P., 2007; Sarthy J. et al., 2009; Bombarde O. t al., 2010]. However, none of the studies in mice revealed RAP1 role as anti-NHEJ factor [Martinez P. et al., 2010; Sfeir A. et al., 2010] except one observation where upon telomerase dysfunction, RAP1-defficient mice are characterized by progressive telomere shortening, telomere end-to-end fusions and telomere loss [Martinez P. et al., 2016].

In this regard, Rai and co-workers identified that BRCT and Myb domains of RAP1 are important to prevent telomere-free fusions and signal-free ends [Rai R. et al., 2016]. They showed that RAP1 in cooperation with TRF2 are required to fully repress PARP1 and SLX4 localization at telomeres and further t-loop resolution and telomere loss due to circle-mediated excision [Rai R. et al., 2016].

Importantly, the anti-fusion properties of yeast Rap1 are expected to depend on its interacting partner TRF2. Interestingly, in addition to be the RAP1 recruiter at telomeres,

TRF2 exhibits potent anti-fusion activities independently of RAP1. TRF2 dysfunction leads to massive end-to-end-fusions, which are ligase IV-dependent [van Steensel B. et al., 1998; Smogorzewska A. et al., 2002].

What is the mechanism of telomere protection that depends on TRF2?

One mechanism relies on t-loops, which are the terminal loops that results from invasion of the 3' overhang into the duplex part of telomeric DNA forming a lasso-like structure [Doksani Y. et al., 2013; Benarroch-Popivker D. et al., 2016]. TRF2 promotes the formation and stabilization of t-loops and protects them from cleavage by resolvases [Poulet A. et al., 2009; Doksani Y. et al., 2013; Schmutz I. et al., 2017]. It does so through either basic N-terminal domain [Saint-Leger A. et al., 2014] or by means of homodimerization domain (TRFH) [Benarroch-Popivker D. et al., 2016, presented in this manuscript].

TRF2 also interacts with other proteins to prevent NHEJ, like Ku, in order to repress initial steps of NHEJ [Ribes-Zamora A. et al., 2013]. TRF2 also cooperates with Apollo to protect from fusions and aberrant telomere recombination [Lenain C. et al., 2006; van Overbeek M. and de Lange T., 2006; Lam YC. et al., 2010]. Apollo is a Artemis-like nuclease that has 5′ to 3′ exonuclease activity, which can be regulated by TRF2 [Ye J. et al., 2010]. Topoisomerase III alpha was shown to influence chromosome stability in cooperation with BLM and TRF2 because its dysfunction results in formation of anaphase bridges and degradation of the 3'-overhangs [Temime-Smaali N. et al., 2008]. Additionally, ERCC1/XPF complex interacts with TRF2 and is important for the maintenance of the 3'-overhang, which per se is sufficient to prevent telomere fusion, even when TRF2 is inhibited [Zhu XD. et al., 2003].

Outside mammals, Taz1, a functional homolog of TRF2 in fission yeast [Deng W. et al., 2015], interact with a RAP1 homolog to prevent telomere fusion [Miller KM. et al., 2005].
It has been reported that a-NHEJ is activated in cells lacking Ku and is enhanced by further TPP1-POT1 and TRF2 removal [Sfeir A. and de Lange T., 2012]. In addition, DNA-PK inhibits a-NHEJ *in vitro* [Bombarde O. et al., 2010].

3.4.2. How cell cycle controls telomere fusion. DDR at telomeres is controlled by several shelterin factors. TRF2 has been shown to prevent ATM activation, whereas TPP1-POT and TRF1 - ATR [Guo X. et al., 2007; Denchi EL. and de Lange T., 2007; Sfeir A. et al., 2009]. Besides excessive DNA damage, TRF1 dysfunction is characterized by multiple telomere

signals that lead to chromosome fragility and sister fusions as a result of aberrant telomere recombination [Martinez P. et al., 2009; Sfeir A. et al., 2009].

It is noteworthy that DDR at telomeres is coupled with cell cycle and number of divisions. Thus, a body of evidence indicates that different DDR proteins accumulate at telomeres in the cell cycle-dependent manner [Verdun RE. et al., 2005]. Numerous studies show that DDR and DNA repair proteins compete with each other and with shelterin for binding to telomeric DNA, and this guides the choice of DNA repair pathway [Deng Y. et al., 2009; Dimitrova N. and de Lange T., 2009; Rai R. et al., 2017; Muraki K. and Murnane JP., 2018]. In line with this, the main competition occurs between HRR and c-NHEJ (Figure 9). It is now known that c-NHEJ, as well as a-NHEJ, can be active throughout the cell cycle. However, HRR outcompetes c-NHEJ in S/G2 phases, whereas NHEJ is a preferred choice in G1, and both HRR and c-NHEJ inhibit a-NHEJ pathway throughout the cell cycle [Daley JM. and Sung P., 2014]. Interestingly, during mitosis cells tend to keep any repair activities shut down, and therefore repair the accumulated damage later in interphase because repair during mitosis can be highly deleterious [Orthwein A. et al., 2015].

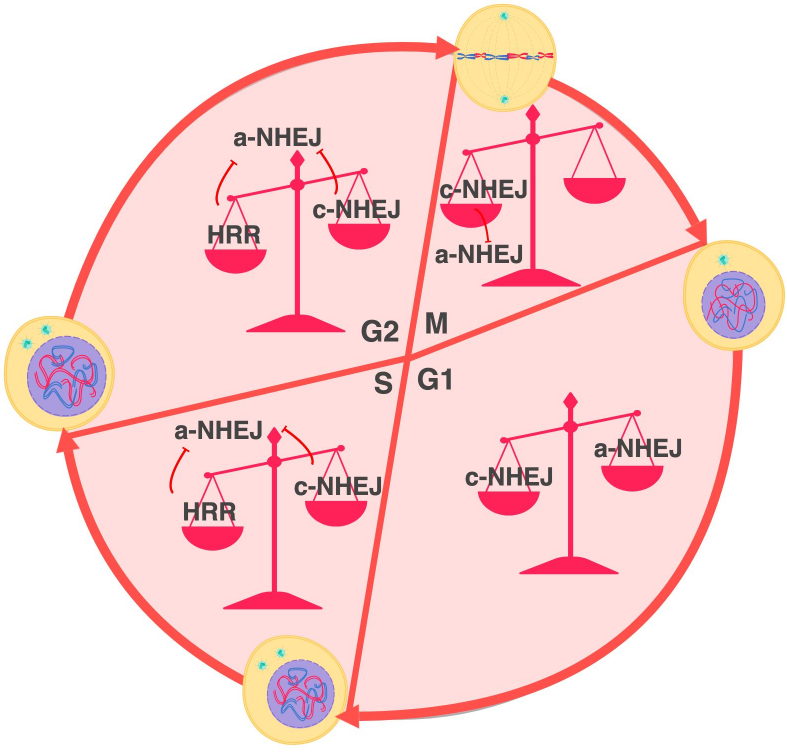

Figure 9. Cell-cycle control of DSB repair.

The choice between NHEJ and HRR depends on competition between 53BP1 and MRN/BRCA1 (Figure 10) [Dimitrova N. and de Lange T., 2009; Zimmermann M. and de Lange T., 2014]. c-NHEJ at telomeres depends on 53BP1. At functional telomeres, TRF2 keeps the ends blocked for DDR, whereas removal of TRF2 leads to the occupation of telomeres by phosphorylated 53BP1. In G1, Rif1 and PTIP are recruited to 53BP1 to mediate exclusion of BRCA1 and MRN/CtIP and prevent therefore 5'-resection (Figure 10). In S/G2, CtIP becomes phosphorylated by CDK and forms a complex with MRN and BRCA1. This complex replaces 53BP1 at telomeres and initiates resection [Zimmermann M. and de Lange T., 2014; Daley JM. and Sung P., 2014]. Recent work also revealed that phosphorylation/dephosphorylation of Nbs1 (MRN subunit) and its association with TRF2 acts as a switch between all three repair pathways [Rai R. et al., 2017]. Moreover, through modulation of de-ubiquitination, TRF2 can also control the recruitment of RNF168, which in turn recruits 53BP1 [Okamoto K. et al., 2013].

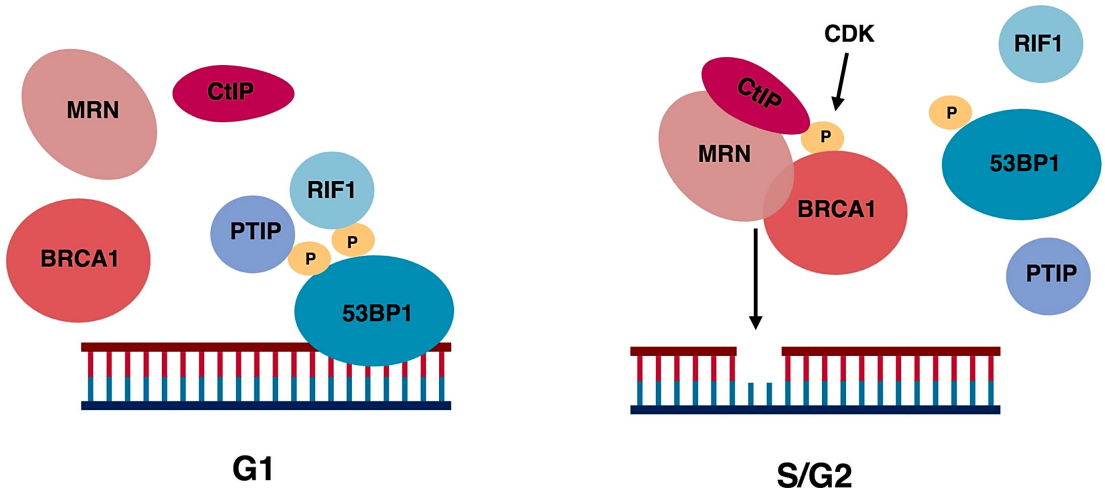

Figure 10. DSB occupancy in G1 and S/G2 phases of cell cycle.

In primary cells, accumulation of DDR at telomeres increases with the number of cell divisions and is passed through generations [Cesare AJ. et al., 2013]. Therefore, telomere becomes a target of persistent and irreparable damage [Hewitt J. et al., 2012; Suzuki M. et al., 2012; Fumagalli M. et al., 2014]. Together with telomere shortening that occurs through divisions, DDR may lead to ceased divisions and replicative senescence or apoptosis if the cell

cannot survive damage anymore [Arnoult N. and Karlseder J., 2015]. Interestingly, only five dysfunctional telomeres are enough to trigger senescence [Kaul Z. et al., 2011].

Many other proteins and protein modifications that are not described here, has been shown to control DDR and DNA damage at telomeres and therefore, control chromosome fusions. A recent work shows evidence that in mammals besides huge protein network, DDR at deprotected telomeres is mediated by telomeric lncRNAs, which are called DDRNAs [Rossiello F. et al., 2017].

Altogether, telomere fusions can occur through different DSB repair pathways which are controlled by comprehensive protein and RNA networks.

Chapter 2

Research project

1. Objectives of the study

In the begin of the research project (2015), there was no clear vision about RAP1 role in telomere protection. The RAP1 paradox emerged based on several observations. In yeast, it has been shown to be among the main factors to protect telomeres from fusions [Pardo B. and Marcand S., 2005; Marcand S., 2014]. However, in mammals its role at telomeres was questionable due to the fact that mouse and human RAP1 knockout cells do not display telomere-dysfunction phenotypes, and RAP1-deficient mice are alive and fertile with no chromosome fusions over generations [Sfeir A. et al., 2010; Martinez P. et al., 2010; Kabir S. et al., 2014]. On the other hand, *in vitro* artificially tethered to telomeres, RAP1 was able to rescue fusions upon TRF2 dysfunction [Sarthy J. et al., 2009]. Thus, it was tempting to speculate that RAP1 role in telomere protection could be masked by the immense effect of TRF2 at telomeres.

Therefore, we aimed to decipher how RAP1 controls NHEJ in human. For this reason, we set the next objectives:

1. To study the contribution of RAP1 in the control of telomere fusions upon TRF2 dysfunction. To do so, we used a topology-deficient mutant of TRF2 (Top-less). The results are discussed in section 2. Article1.

2. To reveal whether RAP1 has any role in telomere protection of replicative senescent cells. The results of this part are discussed in section 3. Article 2.

Article

Molecular Cell

TRF2-Mediated Control of Telomere DNA Topology as a Mechanism for Chromosome-End Protection

Graphical Abstract

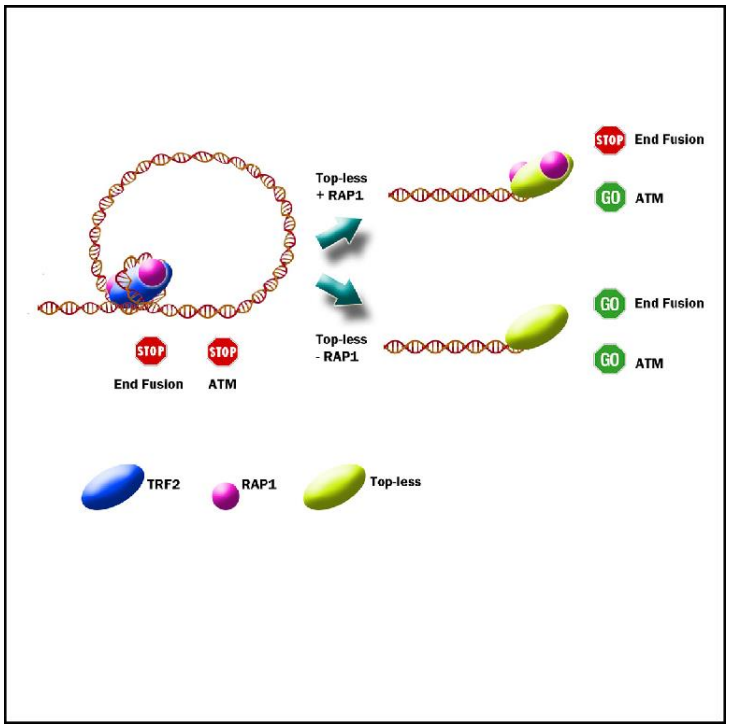

Authors

Delphine Benarroch-Popivker,
Sabrina Pisano,
Aaron Mendez-Bermudez, ...,
Hong Wang, Eric Gilson,
Marie-Jose` phe Giraud-Panis

Correspondence

eric.gilson@unice.fr (E.G.),
giraud-panis@unice.fr (M.-J.G.-P.)

In Brief

Benarroch-Popivker et al. show that TRF2 wraps DNA around its TRFH domain, thereby controlling telomeric DNA topology, t-loop formation, and ATM inhibition. In TRF2 wrapping-deficient cells, protection of telomeres against fusion relies on the recruitment of RAP1.

Highlights

- TRF2 modifies DNA topology by wrapping 90 base pairs of DNA around its TRFH domain
- A mutant deficient in DNA wrapping, Top-less, causes relaxation of telomeric DNA
- Top-less telomeres are deprotected and harbor fewer t-loops but are not fused by NHEJ
- RAP1 protects Top-less telomeres against fusions

Benarroch-Popivker et al., 2016, Molecular Cell 61, 274–286
January 21, 2016
http://dx.doi.org/10.1016/j.molcel.2015.12.009

Molecular Cell
Article

TRF2-Mediated Control of Telomere DNA Topology as a Mechanism for Chromosome-End Protection

Delphine Benarroch-Popivker,[1,9] Sabrina Pisano,[1,9] Aaron Mendez-Bermudez,[1,2] Liudmyla Lototska,[1] Parminder Kaur,[3] Serge Bauwens,[1] Nadir Djerbi,[1] Chrysa M. Latrick,[1,12] Vincent Fraisier,[4] Bei Pei,[1] Alexandre Gay,[1,11] Emilie Jaune,[1] Kevin Foucher,[1] Julien Cherfils-Vicini,[1] Eric Aeby,[5,14,15] Simona Miron,[6,13] Arturo Londoño-Vallejo,[7] Jing Ye,[2] Marie-Hélène Le Du,[6] Hong Wang,[3] Eric Gilson,[1,2,8,10,*] and Marie-Josèphe Giraud-Panis[1,10,*]

[1]Institute for Research on Cancer and Aging, Nice (IRCAN), Faculty of Medicine, CNRS UMR7284, INSERM U1081, University of Nice Sophia Antipolis, Nice, France

[2]International Laboratory in Hematology and Cancer, Shanghai Jiao Tong University School of Medicine/Ruijin Hospital/CNRS/INSERM/Nice University, Pôle Sino-Français de Recherche en Sciences du Vivant et Génomique, Shanghai Ruijin Hospital, Huangpu, Shanghai 200025, P.R. China

[3]Physics Department, North Carolina State University at Raleigh, Raleigh, NC 27695, USA

[4]Cell and Tissue Imaging Platform (PICT-IBiSA), Nikon Imaging Centre, UMR 144 CNRS Institut Curie, 75248 Paris Cedex 05, France

[5]Swiss Institute for Experimental Cancer Research (ISREC), School of Life Sciences, Ecole Polytechnique Fédérale de Lausanne (EPFL), 1015 Lausanne, Switzerland

[6]Institute for Integrative Biology of the Cell (I2BC), CEA, CNRS, Université Paris-Sud, Bâtiment 144, CEA Saclay, Gif-sur-Yvette F-91191, France

[7]UMR3244, Telomeres and Cancer Laboratory, Institut Curie, Paris 75248, France

[8]Department of Genetics, CHU Nice, Nice 06202, France

[9]Co-first author

[10]Co-senior author

[11]Present address: INSERM UMR944, CNRS UMR7212, University of Paris Diderot, Sorbonne Paris Cité, Hôpital St. Louis, 1 Avenue Claude Vellefaux, 75475 Paris Cedex 10, France

[12]Present address: Département de Génomique Fonctionnelle et Cancer, Institut de Génétique et Biologie Moléculaire et Cellulaire (IGBMC), Université de Strasbourg, CNRS, INSERM, 1 rue Laurent Fries, B.P.10142, 67404 Illkirch Cedex, France

[13]Present address: Institute of Biochemistry, Splaiul Independenței 296, 060031 Bucharest 17, Romania

[14]Present Address: Department of Molecular Biology, Massachusetts General Hospital, Boston, MA 02114, USA

[15]Present address: Department of Genetics, Harvard Medical School, Boston, MA 02115 USA

*Correspondence: eric.gilson@unice.fr (E.G.), giraud-panis@unice.fr (M.-J.G.-P.)

http://dx.doi.org/10.1016/j.molcel.2015.12.009

SUMMARY

The shelterin proteins protect telomeres against activation of the DNA damage checkpoints and recombinational repair. We show here that a dimer of the shelterin subunit TRF2 wraps 90 bp of DNA through several lysine and arginine residues localized around its homodimerization domain. The expression of a wrapping-deficient TRF2 mutant, named Top-less, alters telomeric DNA topology, decreases the number of terminal loops (t-loops), and triggers the ATM checkpoint, while still protecting telomeres against non-homologous end joining (NHEJ). In Top-less cells, the protection against NHEJ is alleviated if the expression of the TRF2-interacting protein RAP1 is reduced. We conclude that a distinctive topological state of telomeric DNA, controlled by the TRF2-dependent DNA wrapping and linked to t-loop formation, inhibits both ATM activation and NHEJ. The presence of RAP1 at telomeres appears as a backup mechanism to prevent NHEJ when topology-mediated telomere protection is impaired.

INTRODUCTION

Telomeres have evolved in eukaryotes from the need to protect chromosome ends and provide genome stability. Their maintenance requires protection against the DNA damage response (DDR) that would otherwise stop cell division by checkpoint activation and lead to end-to-end fusion by non-homologous end joining (NHEJ). In humans, telomeres consist of a repetitive DNA ending with a single-stranded 3′ overhang and organized in a peculiar chromatin structure involving the shelterin protein complex and the noncoding RNA TERRA (Giraud-Panis et al., 2013). Their main function is to protect chromosome ends against DNA damage checkpoints and recombinational repair as well as to assist terminal DNA replication and processing (de Lange, 2005; Gilson and Géli, 2007).

TRF2, one of the shelterin subunits, inhibits NHEJ and the ataxia telangiectasia mutated (ATM)-dependent DDR pathway (Celli and de Lange, 2005; Denchi and de Lange, 2007; Okamoto et al., 2013; van Steensel et al., 1998). TRF2 also protects telomeric sequences against replicative DNA damage, particularly those due to topological stress (Muraki et al., 2011; Saint-Léger et al., 2014; Ye et al., 2010). In order to achieve these functions, TRF2 exhibits numerous activities (Feuerhahn et al., 2015). At its N terminus, a basic domain (B domain) interacts with branched

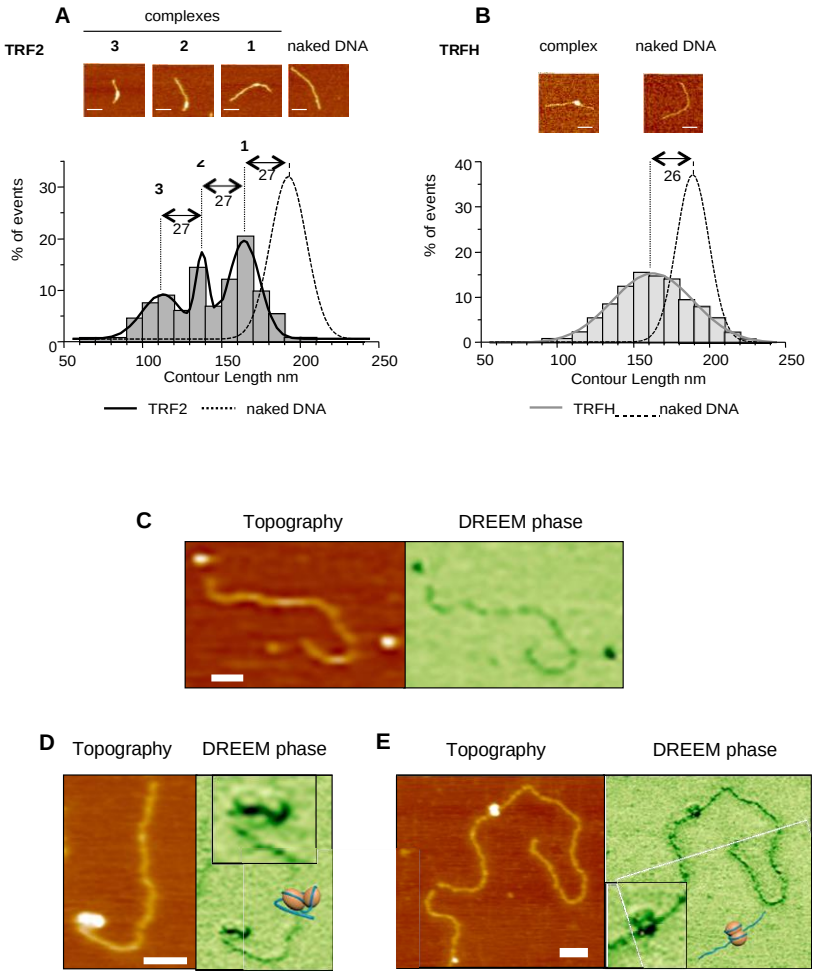

Figure 1. TRFH Domain of TRF2 Condenses 90 bp of DNA

(A) AFM experiments show a decrease in the contour length (CL) of a 650 bp telomeric DNA fragment due to TRF2 binding. (Top) Representative AFM images; scale bars, 50 nm; (bottom) graph representing CL distribution for free and bound DNA (n = 133 for TRF2, n = 304 for DNA). Histograms correspond to raw data and curves to the sum of a Gaussian multipeak fitting.

(B) Same experiment as in (A) using the TRFH domain (n = 130 for TRFH, n = 154 for DNA).

(C) Topographic AFM (left panel) and DREEM phase (right panel) images of free TRFH protein molecules and DNA.

(D and E) Representative topographic AFM (left panels) and DREEM phase (right panels) images of TRFH-DNA complexes with telomeric sequences (D, 135 TTAGGG repeats) or a nontelomeric fragment (E, 3.8 kb).

The XY scale bars, 50 nm. Boxed regions in (D) and (E) are zoomed DREEM images from main figures. The TRFH-DNA models are as follows: orange spheres for TRFH dimers and dark blue lines for DNA.

DNA structures and protects them against resolution (Fouché et al., 2006; Poulet et al., 2009). The homodimerization domain that forms a horseshoe structure in its dimeric form (TRFH for TRF homology domain) (Chen et al., 2008; Fairall et al., 2001) has been shown to suppress ATM activation (Okamoto et al., 2013) and to control TERRA transcription (Porro et al., 2014a, 2014b). This domain also acts as a binding hub for various repair proteins, such as Apollo, SLX4, or RTEL1 (Chen et al., 2008; Kim et al., 2009; Sarek et al., 2015; Wan et al., 2013; Wilson et al., 2013). The hinge domain harbors sites for other protein interactions such as the shelterin subunits RAP1 and TIN2 and also inhibits ATM signaling (Okamoto et al., 2013). Finally, at the C terminus a Myb/SANT domain (Telobox) is responsible for sequence-specific telomeric DNA binding (Bilaud et al., 1996, 1997; Court et al., 2005). TRF2 is also capable of folding telomeric DNA into a lasso-like structure called the t-loop (Griffith et al., 1999; Stansel et al., 2001). This higher-order telomeric DNA structure is believed to play a key role in telomere protection (Doksani et al., 2013) and has been proposed to be linked to the ability of TRF2 to stimulate invasion of duplex telomeric DNA by a homologous single strand (Amiard et al., 2007; Baker et al., 2009, 2011; Poulet et al., 2012; Verdun and Karlseder, 2006).

In this report, we show that 90 base pairs (bp) of DNA is wrapped around a TRFH homodimer. This wrapping involves lysines and arginines located on a DNA path, whose mutation compromises TRF2 capacity to induce DNA wrapping in vitro. In human cells, expression of this mutant, named Top-less, causes changes in telomeric DNA topology, a decrease in the amount of t-loops, and defects in telomere protection against DDR. However, chromosome ends are still protected against NHEJ. A reduced expression of RAP1 alleviates this protection. These findings reveal that a distinctive topological state of telomeric DNA, controlled by TRF2-mediated DNA wrapping and linked to t-loop formation, inhibits both ATM activation and NHEJ. The presence of RAP1 at telomeres appears as a backup mechanism to prevent NHEJ when topology-mediated telomere protection is impaired.

RESULTS

TRF2 Condenses 90 bp of DNA through the TRFH Domain

TRF2-mediated DNA condensation can be observed by measuring the length of DNA molecules (DNA contour length, CL) in TRF2-DNA complexes using atomic force microscopy (AFM). As seen in Figure 1A, TRF2 causes a large decrease in CL. Fitting the CL distribution with a multi-Gaussian curve reveals the presence of three types of complexes (CLs of 165 ± 10, 138 ± 4, and 111 ± 13 nm). Notably, these CL values and that of the naked DNA (192 ± 11 nm) all differ by multiples of

27 nm. Deconvoluted volumes of TRF2-DNA complexes (Figure S1A, available online) also showed a three-peaks distribution. Since the sum of the volumes of one TRFH dimer and two Telobox domains corresponds to 66 nm^3, the mean deconvoluted volume of complexes in peak 1 (90 ±34 nm^3) is compatible with that of a dimer of the protein (Figure S1A). By inference, the two other types of complexes should correspond to two and three dimers bound to DNA. These analyses revealed that TRF2 dimers can form complexes with DNA, each condensing DNA by 27 nm (90 bp).

Since TRF2 ability to condense DNA depends on the TRFH domain (Amiard et al., 2007; Poulet et al., 2012), we explored whether this domain is sufficient. Purified TRFH binds DNA, albeit with low affinity (Figures S1B and S1C), and leads to a DNA condensation similar to that of full-length TRF2 (Figure 1B). In agreement, the preferred length of DNA bound by this domain is 92 bp (Figures S1D and S1E). We also obtained a multipeak distribution for the deconvoluted volumes compatible with dimers and multimers (Figure S1F). As for the full-length protein, larger TRFH-DNA complexes show smaller contour lengths, and vice versa (Figure S1G). Hence, the Gaussian aspect of the TRFH CL distribution (Figure 1B) is probably a consequence of variations in condensation for the different TRFH complexes, likely due to the weak affinity of TRFH for DNA. Alternatively, other domains such as the N-terminal B domain or the C-terminal Myb/SANT domain of TRF2 may stabilize the wrapped structure and be accessory to this TRFH-driven reaction.

We found a good correspondence between circumference and DNA shortening of TRF2-DNA complexes (Figure S1H). Furthermore, the value of nearly 1 in the slope of the linear fit curve suggests that circumference and DNA shortening increase at the same rate. Thus, dimensions of TRF2-DNA complexes can be described by multiples of 27 nm that correspond to both the length of condensed DNA and the circumference of the complexes.

This number is similar to the circumference of 25 nm calculated from the 3D structure of the TRFH domain (PDB 1H6O and 3BUA) (Chen et al., 2008; Fairall et al., 2001). This suggested that the circumference of the TRFH/DNA complexes should be similar to that of the full-length protein, and, indeed, we obtained 26 ±9 nm for the smallest TRFH/DNA complex and multiples of 27 nm for multimeric complexes (Figure S1I).

Overall, these results strongly suggest that the TRFH domain is encircled by 90 bp of DNA. In order to confirm this wrapping, we used a recently developed AFM imaging technique called dual resonance frequency enhanced electrostatic force microscopy (DREEM). In recent studies, DREEM was successfully used to observe DNA wrapping around histone proteins in chromatin, DNA passing through the hMutSa repair protein, and higher-order DNA looping at the edge of multiprotein full-length TRF2-DNA complexes (K.P., D. Wu, J. Lin, P. Countryman, R. Riehn, P.L. Opresko, and H. Wang, unpublished data; Wu et al., 2016). We chose to analyze TRFH-DNA complexes rather than those formed with the full-length protein since the other domains of TRF2 may impede the visualization of the wrapping around TRFH. In DREEM imaging, both free proteins and DNA show a decrease in phase, but proteins show a greater contrast than DNA, thus allowing distinction of both molecules in a complex (Figure 1C). TRFH-telomeric DNA complexes in DREEM phase images show dark regions consistent with protein, and regions with decreased signal consistent with DNA (Figure 1D). The regions with decreased intensities show DNA paths on the TRFH consistent with the wrapping of DNA around this domain. We could also observe wrapping when using a nontelomeric linear DNA fragment (Figure 1E), showing that the DNA wrapping around TRFH is not telomeric DNA-sequence specific.

TRFH Contacts DNA through a Set of Lysine Residues

To identify the TRFH residues in contact with DNA, we performed protein footprinting using in vitro acetylation by sulfosuccinimidyl acetate (Figure S2A). This compound specifically acetylates lysines exposed to the solvent, which can be mapped using mass spectrometry (Mendoza and Vachet, 2009). We used lysine acetylation profiles to calculate probabilities of their acetylation (Figure S2B; Experimental Procedures). Physical contact of the protein with another molecule modifies lysine acetylation. Comparing acetylation profiles for unbound and bound TRF2 on a 650 bp of telomeric DNA, we determined the percentage of DNA-dependent protection for each acetylable lysine (Figure 2A). Lysines not present in the unbound protein profile due to lack of acetylation or partial coverage in mass spectrometry were not analyzed (K140, K495, and K180). TRF2 contains 44 lysines distributed along the sequence, with the exception of the N-terminal basic domain. Binding of the DNA causes variations in acetylation to different degrees. Lysines closer to the DNA in the Telobox structure (Court et al., 2005) are more protected from acetylation, validating this approach (Figure S2C). The acetylation of some lysines in the hinge domain is also modulated upon DNA binding, perhaps due to conformational changes in this domain or to DNA binding. Importantly, marked changes in acetylation were observed in three regions of the TRFH centered on K158, K176, and K242. When positioned on the 3D structure, these lysines could be aligned along a DNA path encircling this domain (Figure 2B). Interestingly, K173, K176, and K179 are located in front for one monomer and in the back for the other monomer, thus introducing chirality in the path around the dimer and forcing DNA strands to cross (Figure S2D).

TRF2 Wraps DNA around Its TRFH Domain

To go further, we constructed a set of TRF2 mutants containing lysine-to-alanine replacement. We focused on the lysines exhibiting highest signals in footprinting (K158, K176, and K242) and their surrounding lysines. Mutants with different numbers of mutated lysines were constructed (Figures S3A and S3B): K241, K242, and K245 in mutant 3K; K158, K173, K176, and K179 in mutant 4K; and all seven of them in mutant 7K. We analyzed the capacity of these mutants to bind and wrap DNA by EMSA and by monitoring their topological activity on a plasmid using the Topoisomerase I relaxation assay (Amiard et al., 2007; Poulet et al., 2012; Figures S3C and 3A; numbers below gels). All mutants were active to different degrees. We concluded that, if these lysines contributed to wrapping, other residues must be involved.

The TRF1 TRFH is also capable of condensing DNA, but in TRF1, this capacity is inhibited by the presence of an acidic N-terminal domain. This suggests that the residues involved in

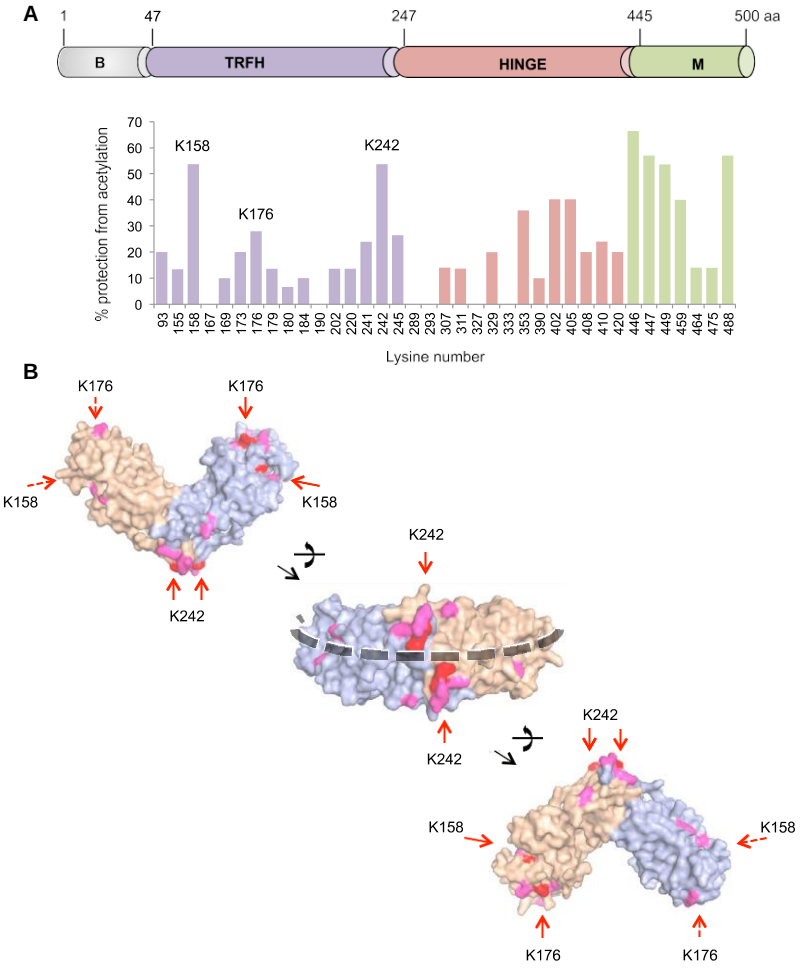

Figure 2. Lysines Involved in DNA Binding Define a "DNA Path" around the TRFH Domain

(A) (Top) Schematic view of TRF2 domains. (Bottom) Footprinting graph showing the percentage of DNA-dependent protection from acetylation for acetylable lysines (Figure S2).

(B) Positions of protected lysines on the 3D structure of the TRFH domain (PDB: 3BUA). Lysines in red show protection above 20%, and those in pink show protection between 10% and 20%. Lysines on the back of the structures are indicated by dashed arrows. The black dashed line marks the identified DNA path.

DNA wrapping might be conserved between TRF1 and TRF2. Indeed, lysines giving a strong signal in the footprinting assay are either conserved, replaced by an arginine, or only slightly shifted (Figure S3D). Two conserved arginines are located on the putative DNA path (R69 and R99 for TRF2; R91 and R121 in TRF1), and their symmetrical location strongly resembles that of the conserved lysines K245. We mutated these two arginines to alanines in combination with the seven lysines, giving the 7K2R mutant (Figure S3A). This mutant showed reduced topological activity (Figure 3A) and wrapping efficiency (Figure 3B). Similarly, the capacity of 7K2R to stimulate single-strand invasion into a telomeric double helix was strongly impaired (Figures 3C and 3D). These reduced activities did not originate from changes in affinities for telomeric DNA (Figures 3E and 3F) and were not due to the sole mutations of the two arginines since the 2K2R mutant (mutations of K158, K242, and the two arginines) was topologically active (Figure S3E). Overall, we conclude that a set of lysine and arginine residues located on the outer surface of the TRFH domain is required to wrap DNA around it and to confer the topological properties of TRF2. Thus, the 7K2R mutant was dubbed Top-less.

In order to characterize Top-less, we compared its biochemical properties to those of the wild-type protein (Figures S3F–S3K). Circular dichroism experiments showed that mutations in Top-less did not modify the overall folding of the protein (Figure S3G). We also showed that Top-less could bind RAP1 in vitro (Figure S3H). As expected, Top-less mutations caused a marked decrease in the affinity of the TRFH for DNA (Figures S3I and S3J). The capacity of TRF2 to promote formation of Holliday junctions and to inhibit their migration, a property a priori unrelated to DNA topology, was unaffected (Figure S3K). We also explored whether Top-less could bind telomeric DNA in vivo. For this purpose, we used a HeLa cell line where TRF2 expression could be severely decreased by expression of a doxycycline (DOX)-inducible shRNA directed against *TERF2* (Grolimund et al., 2013). Cells treated with DOX were transduced with lentiviral vectors expressing either wild-type or Top-less Myc-tagged forms of TRF2 (resistant to the inducible shRNA). Ectopic expression of both wild-type TRF2 and Top-less restored a level of protein that exceeded the endogenous amount observed in cells not treated with DOX (Figure S4A). Binding to telomeres was examined using chromatin immunoprecipitation (ChIP) using either an anti-TRF2 or an anti-Myc antibody (Figures S4B and S4C, respectively). No obvious difference was observed between wild-type and Top-less. Finally, we checked that Top-less modified neither the expression of the other shelterin subunits nor the association of RAP1 and TIN2 at telomeres (Figures S4D–S4G).

Overall, these data show that Top-less is a valuable separation-of-function mutant of TRF2 and is deficient for DNA wrapping activity, but it still exhibits several of the known properties of this protein.

TRF2 Controls Telomeric DNA Topology in Human Cells

Next, we investigated whether DNA wrapping plays a role in the control of telomere DNA topology in human cells. To monitor

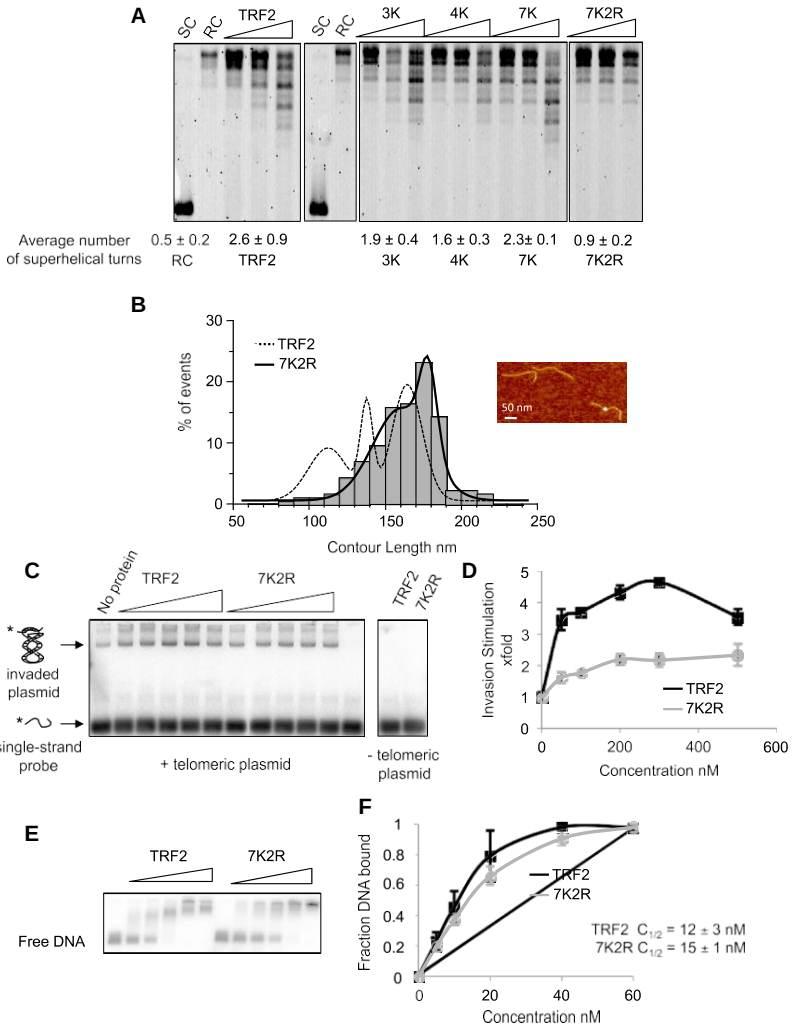

Figure 3. Biochemical Characterization of a Topology-Deficient TRF2 Mutant

(A) Topoisomerase I assay showing the topological activity of TRF2 and of lysine/arginine to alanine mutants. Protein concentrations used were 100, 250, and 500 nM. Average number of helical turns was calculated at 500 nM for at least 3 experiments. SC stands for supercoiled, and RC stands for relaxed circular.

(B) AFM experiments showing the decreased wrapping activity of 7K2R. The graph represents CL distribution for the TRF2- and 7K2R-bound DNA (n = 133 for TRF2, n = 190 for 7K2R). Histograms correspond to raw data and curves to the sum of Gaussian curves fitting the raw data.

(C) Invasion assay showing the decrease in invasion caused by 7K2R mutations. Concentrations used were 50, 100, 200, 300, and 500 nM for both proteins.

(D) Quantitative analysis of (C). Error bars correspond to standard deviation from three experiments.

(E) EMSA using ds106Telo and either TRF2 or 7K2R. Concentrations used were 5, 10, 20, 40, and 60 nM of proteins.

(F) Quantitative analysis of (E). Error bars represent SD from three experiments.

changes in the DNA topological state, we used the capacity of Trioxsalen (4,5′,8-trimethylpsoralen) to bind preferentially to unwound genomic regions and to crosslink DNA strands when exposed to UV. To validate this approach, we performed experiments on cells treated with ICRF-193, a catalytic inhibitor of Topoisomerases 2 (Chen et al., 2015; d'Alcontres et al., 2014; Hsieh et al., 2015; Ye et al., 2010). HeLa cells were incubated with Trioxsalen for 5 min and immediately exposed to UV before recovery of the cells. Hence, the binding profile of Trioxsalen provides a snapshot of the topological state of DNA. As controls, cells were treated with Trioxsalen but not exposed to UV, or vice versa. Trioxsalen DNA crosslinking was quantified on sonicated genomic DNA after denaturation of DNA fragments by glyoxal and separation of crosslinked species (double stranded) and noncrosslinked species (single stranded) by electrophoresis (Kouzine et al., 2013). We verified that fragments were of equivalent length (between 210 and 230 bp) using a Bioanalyzer (an example is given in Figure S5A). After migration, gels were stained with SYBR green II following a denaturing step to remove Trioxsalen. The SYBR green II image obtained thus reflected genome-wide binding of Trioxsalen. To quantify the crosslinked (double stranded) material, we used a 0.6 kb threshold because it corresponded to an inflection point in the telomeric DNA profiles (Figure S5B). We analyzed telomeric DNA by hybridization of the membrane obtained by Southern blot of the SYBR gel with a telomeric probe (Figure S5D). Under our conditions, 20% of genomic DNA was crosslinked (1 Trioxsalen every kilobase). Interestingly, ICRF-193 treatment causes a detectable increase in Trioxsalen crosslinking of telomeric DNA but not of bulk DNA, indicative of a telomere-specific effect on DNA topology (Figure S5E). It may appear counterintuitive to observe an increase in Trioxsalen binding when inhibiting an enzyme that removes DNA-positive supercoils, but this could be due to topology-driven regression of replication forks (Yeeles et al., 2013) or replication/transcription forks stalling, resulting in the accumulation of unwound regions.

Next, HeLa cells were treated with DOX and transduced with either the empty, TRF2, or Top-less lentiviral vectors as above. The binding of Trioxsalen to global genomic DNA does not depend on TRF2 (Figures 4A and 4C), as expected. However, a nearly 2-fold increase in crosslinked telomeric species is observed when treating HeLa cells with DOX. This topological change is rescued by the expression of wild-type TRF2. In contrast, the expression of Top-less fails to rescue topological changes triggered by TRF2 downregulation (Figures 4B and 4C).

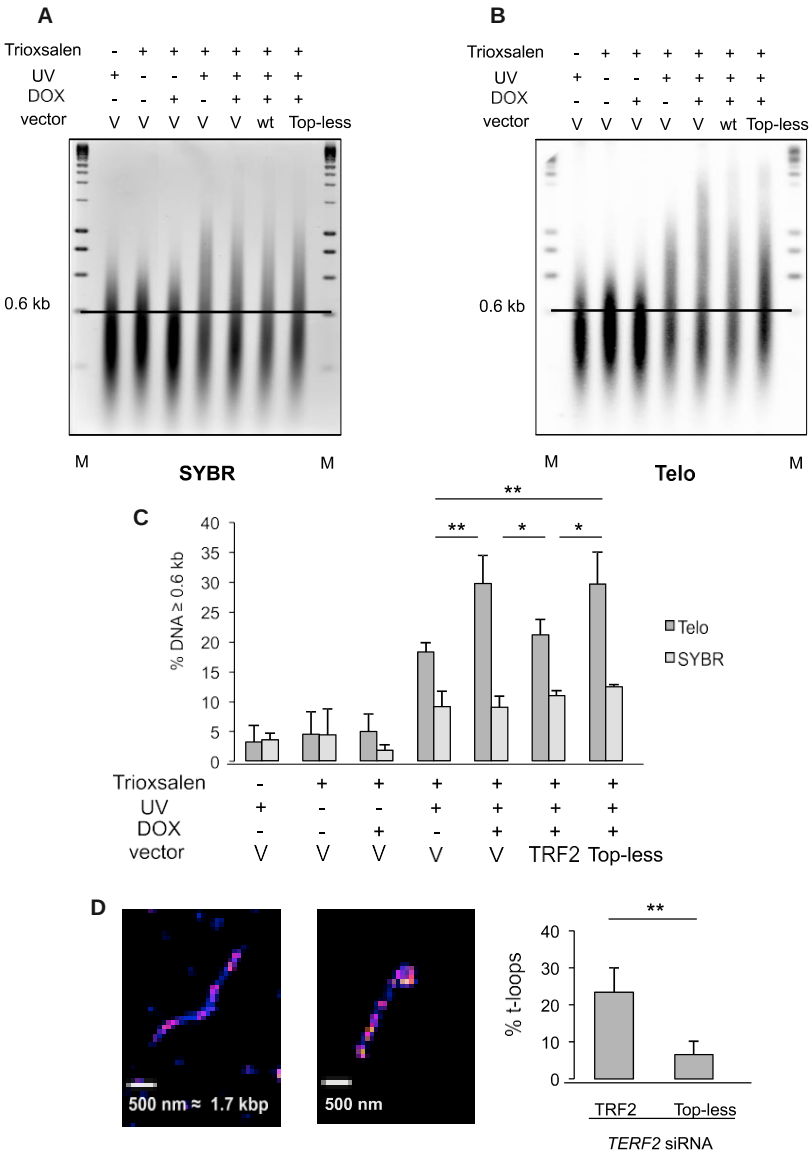

Figure 4. The TRFH-Wrapping Domain of TRF2 Controls Telomeric DNA Topology and t-Loops

(A) SYBRII-stained glyoxal gel. M stands for molecular weight markers, V stands for empty vector, wt stands for wild type TRF2, and the dotted line marks the 0.6 kb threshold used for analysis. Of note, a nonrelevant lane was removed from the image, and glyoxal in the samples slows migration compared to the markers.

(B) Southern blot of the glyoxal gel hybridized using a telomeric probe (Telo). As above, a nonrelevant lane was removed from the image.

(C) Quantitative analysis of (B). The relative amount of DNA material above the 0.6 kb mark was measured for each condition. SYBR indicates the values obtained for the SYBRII stained gels, and Telo for the Southern blots. Error bars correspond to standard errors between three replicates. p values were calculated using the Mann-Whitney test (**p <0.01, *p <0.05; absence of mark indicates no significance).

(D) Representative images of linear (left) DNA and t-loop (right) obtained on spread chromatin of HT1080 super Telomerase cells by STORM and quantification of the percentage of t-loops in TRF2- (437 objects counted) or Top-less (634 objects counted)-expressing cells. Quantification of *TERF2* transcripts was performed by RT-qPCR and corresponded to a 77% knockdown of the endogenous *TERF2* transcript, while in TRF2 and Top-less conditions the ectopic mRNA was 9.5-fold and 6.5-fold more expressed, respectively, than in the endogenous *TERF2* mRNA in the si-Control condition. Data represent the means ± SE. p values were calculated using the Mann-Whitney test (**p <0.01).

It is unlikely that the effect of TRF2 knockdown on telomere DNA topology is related to a decrease in nucleosome occupancy, since we rather observe more H3 binding in this condition than when TRF2 is ectopically expressed (Figure S4C), in agreement with previous reports (Benetti et al., 2008; Galati et al., 2012), showing that Top-less is not impaired in at least some of the chromatin-remodeling properties of TRF2.

The topological change due to TRF2 dysfunction could be due to the increase in telomere transcription that was previously observed upon TRF2 depletion (Porro et al., 2014a, 2014b). However, Top-less fully rescues the increased TERRA expression observed in TRF2-compromised cells (Figures S5F and S5G).

These results demonstrate a functional link between the intrinsic ability of TRF2 to wrap DNA and the in vivo control of telomere DNA topology.

TRF2-Mediated DNA Wrapping Controls t-Loops

Two facts suggested that Top-less could lead to variations in the t-loop content in cells: (1) the reduced capacity of this mutant to stimulate single-strand invasion in vitro (Figure 3C), a property thought to be involved in t-loop formation; (2) the telomere topological change caused by this mutant that could be linked to a loss of constraining structures such as t-loops. In order to investigate this, we performed direct stochastic optical reconstruction microscopy (STORM) imaging as described by Doksani et al. (2013). In order to increase our chances to observe t-loops, we used HT1080 cells overexpressing telomerase which can harbor telomeres of more than 20 kb (Cristofari and Lingner, 2006). Endogenous TRF2 expression was reduced by transfection of a siRNA directed against TRF2, and wild-type TRF2 or Top-less was ectopically expressed. As seen in Figure 4D, the amount of t-loops is

markedly decreased in Top-less cells as compared to wild-type TRF2 cells.

TRF2-Mediated DNA Wrapping Inhibits ATM Signaling

Next, we investigated DDR activation in the HeLa cell-line system used for Trioxsalen experiments (DOX-inducible expression of sh*TERF2*, lentiviral expression of TRF2, or Top-less). We scored telomere dysfunction-induced foci (TIFs) observed through the recruitment of 53BP1 on telomeres. As expected, knockdown of TRF2 significantly increased TIFs (Takai et al., 2003; Figure 5A). This telomere deprotection is rescued by exogenous expression of TRF2, but not of Top-less. Monitoring phosphorylated ATM (pATM) gave similar results, showing that Top-less is impaired in ATM inhibition (Figure S6A). In agreement, the CHK2 phosphorylation triggered by TRF2 down-regulation is not fully rescued by Top-less expression (Figure S6B). Of note, in the time frame of our experiment, we could not detect modifications of the cell cycle (Figure S6C) ruling out an indirect effect of Top-less on cell proliferation. DDR activation was also observed in other Top-less-expressing cells (HT1080 super-telomerase cells used for t-loops measurements, BJ-HELT cells and HT1080 cells; Figures S6D, S6E, and S6F, respectively). We also observed an increased level of TIFs in cells expressing ADB, a TRF2 mutant also compromised for DNA wrapping but through addition of the TRF1 acidic domain and not through TRFH mutations (as in Top-less) (Poulet et al., 2012).

We also analyzed this response in HT1080 cells by monitoring the colocalization of TRF1 and phosphorylated histone H2AX (gH2AX). Again, we obtained a similar response for the Top-less mutant (Figure 5B). Of note, the expression of the 7K and 2R mutants in this setting rescued the telomere uncapping triggered by TRF2 inhibition. We concluded that the strong DDR activation at telomeres triggered by Top-less stems from the combination of both the 7K and 2R mutation sets.

We also explored whether Top-less could alter telomere length and cause formation of t-circles by 2D gel analysis. We did not observe overt production of t-circles and found no difference in mean telomere length upon TRF2 or Top-less expression (Figures S6G and S6H), suggesting that the decrease in t-loop number that we observed does not originate from t-loop excision. Finally, we measured the amount of the 3^0 overhang using an in-gel assay. As expected, TRF2 knockdown decreases the amount of 3^0 overhang, an effect rescued by both TRF2 and Top-less expression (Figure S6I), indicating that the decrease in t-loop formation is not caused by a decreased length of the 3^0 overhang.

In summary, the DNA-wrapping activity of TRF2 is required for telomere protection against ATM activation but is involved neither in telomere length regulation nor in 3^0 overhang formation.

TRF2-Mediated DNA Wrapping Inhibits NHEJ in RAP1-Compromised Cells

Then, we tested the ability of Top-less to prevent NHEJ by scoring telomere fusions in metaphase chromosomes. Upon TRF2 knockdown in HeLa cells, more than 20% of telomeres were fused (Figures 6A and 6B). This effect was rescued by both TRF2 and Top-less expression. Since RAP1 was previously shown to inhibit NHEJ independently of TRF2 (Bae and Baumann, 2007; Sarthy et al., 2009), we analyzed the effect of Top-less in RAP1-compromised cells. In agreement with previous reports showing that RAP1 is dispensable for NHEJ protection in mammalian cells (Kabir et al., 2014), reducing its expression did not increase fusions in wild-type TRF2-expressing cells (Figures 6C and 6D). However, a 10-fold increase in the percentage of chromosome fusions was observed in Top-less cells upon RAP1 inhibition. This effect was rescued by an ectopic expression of RAP1, excluding an off-target effect of the RAP1 shRNA. These results indicate that TRF2-mediated DNA wrapping is involved in NHEJ inhibition independently of RAP1. Moreover, they reveal the anti-NHEJ activity of RAP1 as a backup mechanism for telomere protection in Top-less cells.

DISCUSSION

Although control of DNA topology is crucial for chromosomal integrity (Vos et al., 2011), our understanding of its role at telomeres is limited. Theoretically, the free DNA ends of telomeres should allow dissipation of torsional strain. The fact that we (Biroccio et al., 2011; Chen et al., 2015; Leonetti et al., 2008; Temime-Smaali et al., 2008; Ye et al., 2010) and others (d'Alcontres et al., 2014; Germe et al., 2009; Hsieh et al., 2015) have found that telomere integrity is particularly sensitive to topological stress suggests that telomeres may form topologically constrained chromatin entities. In agreement with this idea, telomeres harbor t-loop structures that may constitute topological barriers. In this report, we unveil that telomeres are topological objects that rely on a particular DNA-wrapping activity of TRF2 to be protected against ATM activation and NHEJ.

By combining AFM, DREEM, protein footprinting, and topology assays, we demonstrate that 90 bp of DNA wrap around the TRFH domain of TRF2 through an interaction with a set of lysines and arginines located on the surface of this domain. Interestingly, the localization of these residues on the TRFH domain imposes a chirality in the DNA–TRF2 complex (Figure S2D).

The identification of TRFH residues contacting DNA allowed us to design a mutant largely deficient in wrapping activity and therefore named Top-less. Top-less behaves as a valuable separation-of-function mutant to study the role of DNA topology at telomeres since, on one hand, it alters the topological state of telomeric DNA in vitro and in vivo, while on another hand, it conserves many TRF2 properties, including (1) proper folding according to CD analysis, (2) specific binding to telomeric DNA both in vitro and in vivo, (3) TIN2 and RAP1 recruitment at telomeres, (4) facilitation of Holliday junction formation and inhibition of their migration, and (5) unaltered expression of the other shelterin subunits.

Top-less causes a marked ATM activation at telomeres showing a loss of function for ATM inhibition. Of note, the parental mutants 7K and 2K, which bear separately the seven mutated lysines (7K) or the two arginines (2R) mutated in Top-less, fully protect against ATM activation. Moreover, the wrapping-deficient ADB mutant, bearing a wild-type TRFH domain, behaves similarly to Top-less in vivo. Overall, the behavior of these mutants indicates that Top-less-mediated telomere deprotection is not due to alterations in unidentified TRFH binding sites for cellular factors. Of note, Top-less cells not only recruit

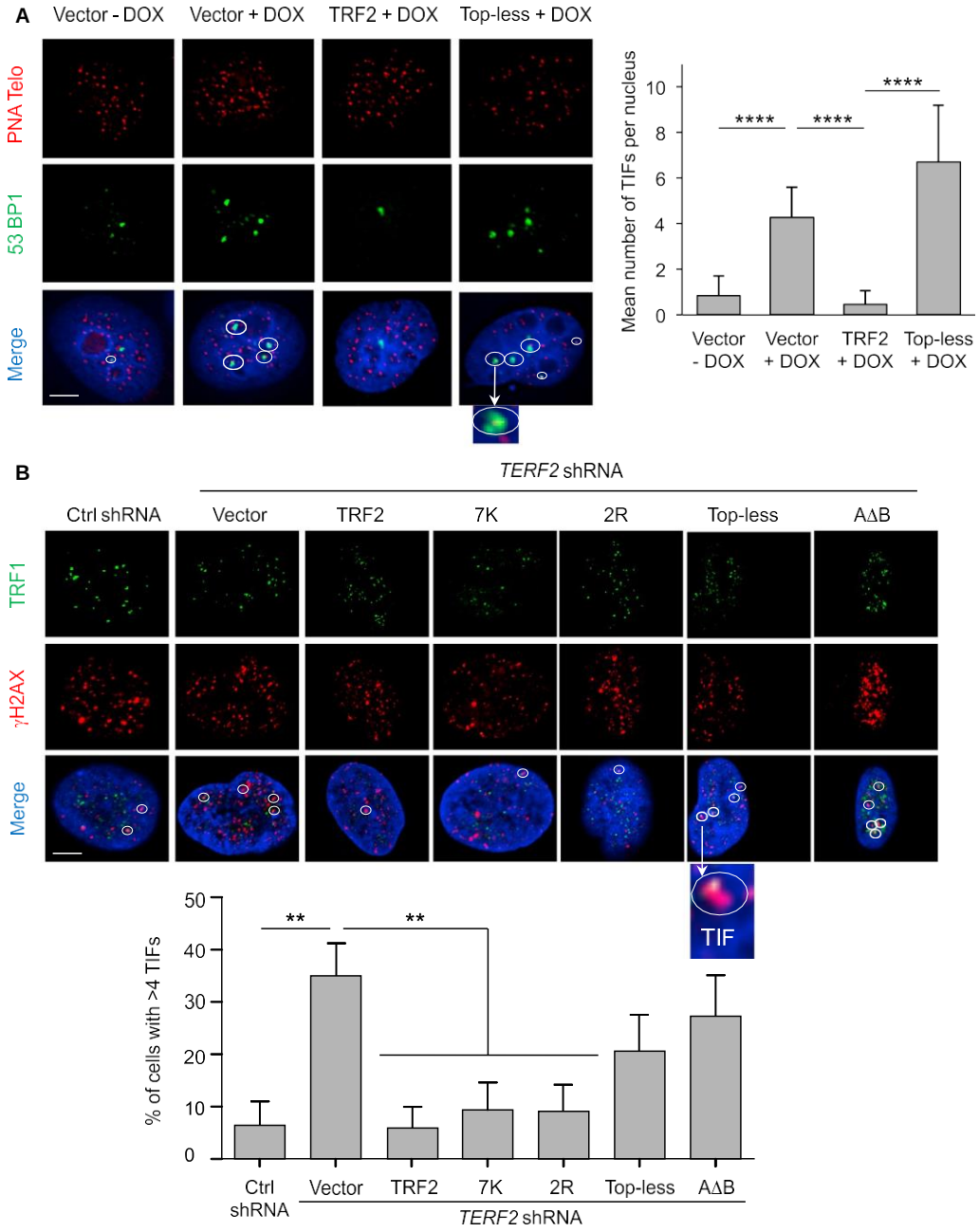

Figure 5. Top-less Does Not Protect against DDR Activation

(A) (Left) Representative section images of detection of 53BP1 by IF (green), telomeric DNA (red), and the merge with DAPI (blue) under the indicated conditions. TIFs are marked with a circle. Scale bar, 5 mm.

(Right) TIFs per nucleus were quantified. Data represent the means ± SE. p values were calculated using the Mann-Whitney test (****$p < 0.0001$).

(B) (Top) Representative section images of detection of TRF1 by IF (green), g-H2AX by IF (red), and the merge with DAPI (blue) under the indicated conditions using HT1080 cells. TIFs are marked circles. Scale bar, 5 mm.

(Bottom) The percentage of cells showing more than four TIFs was quantified. Data represent the means ± SE. p values were calculated using the Mann-Whitney test (**$p < 0.01$; absence of mark indicates no significance). The quantification of *TERF2* transcript level for the different conditions (control scramble shRNA with expression of empty vector, *TERF2* shRNA with expression of either empty vector or TRF2, 7K, 2R, Top-less, or AΔB) was done by RT-qPCR and is, respectively, 1, 0.65, 20, 42, 76,41.

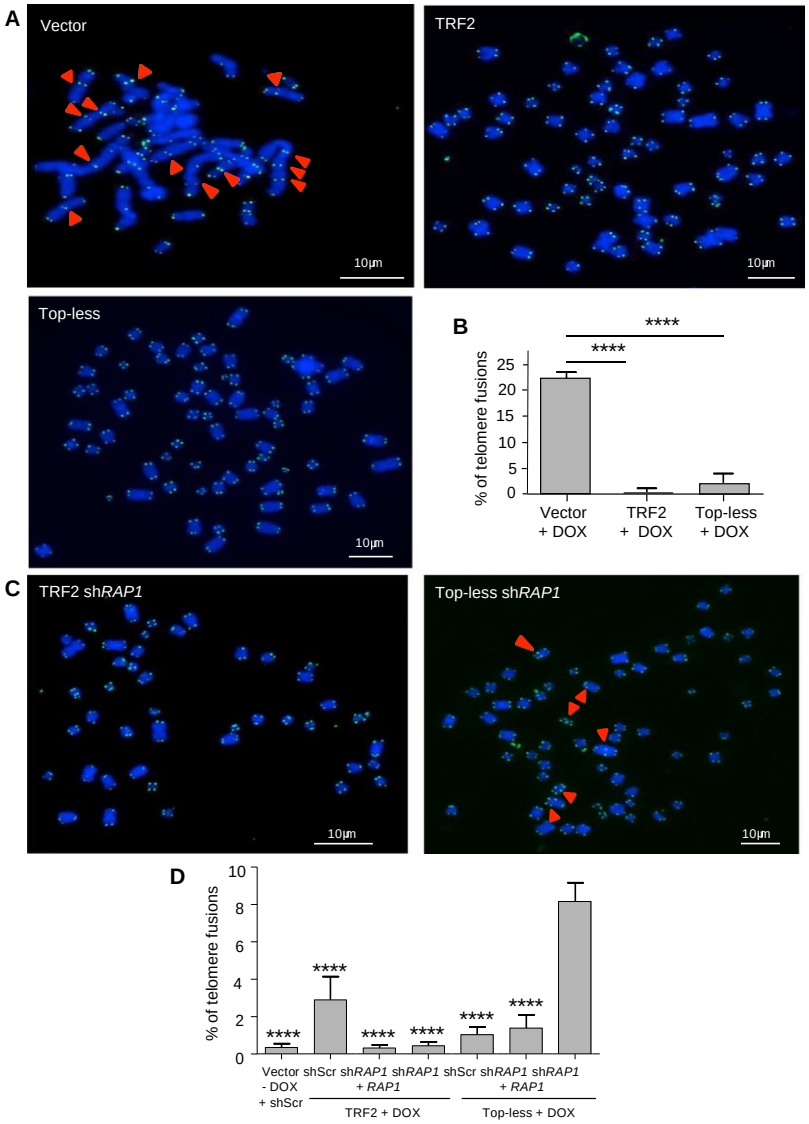

Figure 6. TRF2-Mediated DNA Wrapping Inhibits NHEJ in RAP1-Compromised Cells

(A) Metaphase chromosome spreads of HeLa cells transduced with either empty vector, TRF2, or Top-less viruses upon TRF2 knockdown using doxycycline (DOX). Chromosomes were stained for telomeric DNA (green) and with DAPI (blue). The red arrows show examples of telomere fusions.

(B) Graph showing the percentage of fusions counted on 2,000 chromosomes. Data represent the means ± SE, and p values were calculated using Student's t test (****p <0.0001; absence of a mark indicates no significance).

(C) Metaphase chromosome spreads of HeLa cells transduced with TRF2 or Top-less viruses upon TRF2 knockdown using doxycycline (DOX) and knockdown of RAP1 by shRNA.

(D) Graph showing the percentage of fusions counted on 2,000 chromosomes for each condition. p value was calculated using a one-way ANOVA (****p <0.0001). Downregulation of *RAP1* was quantified by RT-qPCR and corresponded to a knockdown of 83%.

phosphorylated ATM and g-H2AX at telomeres but also recruit 53BP1. Together with an increased amount of phosphorylated CHK2, these results show that Top-less telomeres are impaired in the inhibition of both the initiation and the propagation of ATM signaling. This might appear at odds with the preservation in Top-less of a small region of the hinged domain (iDDR domain, aa 407–431), which has been shown to inhibit the recruitment of 53BP1 (Okamoto et al., 2013). One explanation to reconcile these results could be that the iDDR domain fuction is somehow altered by the Top-less mutations. In agreement, the iDDR domain lies in a region where the lysine acetylation profile changes upon DNA binding (Figure 2A).

An important result of this study is that Top-less cells exhibit a decreased number of t-loops, indicating that TRF2-wrapping activity is required for t-loop folding. This is in agreement with the fact that Top-less is unable to facilitate strand invasion, a key mechanism in t-loop formation (Griffith et al., 1999). As an explanation, DNA wrapping around the TRFH domain could be involved in strand invasion and t-loop folding through the unwinding of DNA outside TRF2 binding sites as we suggested earlier (Amiard et al., 2007). The efficient protection against telomere fusion in Top-less cells seems contradictory to the previously proposed protective role of t-loops against NHEJ (Doksani et al., 2013). Since mammalian RAP1 was shown to protect against NHEJ in a TRF2-independent manner (Bae and Baumann, 2007; Sarthy et al., 2009) and Top-less can still recruit RAP1 at telomeres, RAP1 could provide a backup anti-NHEJ mechanism in Top-less cells (Figure 6E). Indeed, a reduced expression of RAP1 triggers a marked increase in telomere fusions in Top-less. These results show that TRF2 can protect against NHEJ through different mechanisms, including the recruitment at telomeres of RAP1 and its capacity to wrap DNA around its TRFH domain.

Our results show that one of the mechanisms by which telomeres control their DNA topology and protect against ATM activation and NHEJ stems from the right-handed wrapping of telomeric DNA around the TRFH domain of TRF2. Three independent findings support this conclusion: (1) TRF2 wraps DNA in a right-handed manner, (2) TRF2 controls telomere DNA topology in human cells, and (3) the expression of TRF2 mutants specifically impaired in this wrapping activity fails to control telomere DNA topology and uncaps telomeres. Several nonexclusive mechanisms can be envisaged

to link the topological properties of TRF2 to ATM signaling and NHEJ. One is suggested by the decreased amount of t-loops in Top-less cells. This is in agreement with the view that t-loops prevent ATM activation and constitute a poor substrate for NHEJ. Another, nonexclusive possibility is that TRF2 acts as a torsional strain sensor to orchestrate various activities required to resolve topological problems that may arise during DNA processing (replication, transcription, and repair).

In RAP1-proficient cells, Top-less uncouples ATM inhibition from the anti-NHEJ activity of TRF2. Interestingly, this partially uncapped telomere phenotype of Top-less cells is reminiscent of the phenotype of cells either exhibiting spontaneous DDR activation at telomeres (Cesare et al., 2009; Kaul et al., 2012; Thanasoula et al., 2010), either with a reduced expression of TRF2 (Cesare et al., 2013), either upon prolonged mitotic arrest (Hayashi et al., 2012) or upon deletion of the *TIN2* gene (Takai et al., 2011). This phenotype is described as an ''intermediate state'' of telomere protection and was proposed to occur when telomeres of primary human cells become too short to efficiently protect against DDR activation and to lead to cell senescence (Cesare and Karlseder, 2012). A topology switch at telomeres may thus constitute a common mechanism leading to the appearance of such intermediate state telomeres. In this hypothesis, our results predict that RAP1 may be critical to protect telomeres of senescent cells from NHEJ.

This study reveals that telomeres directly use positively superhelical strain to escape from inappropriate activation of DDR. Such a functional link between telomere DNA topology and DDR control is reminiscent of the transcription of nuclear pore-associated genes in yeast (Bermejo et al., 2011). The involvement of mechanisms that control DNA topology in telomeric functions appears conserved during evolution since bacteria and yeast telomeres also rely on topoisomerase to maintain their integrity (Bankhead et al., 2006; Bao and Cohen, 2004; Chaconas and Kobryn, 2010; Germe et al., 2009; Mirabella and Gartenberg, 1997; Tsai et al., 2011). Thus, we propose that the folding of telomeres into topologically constrained superstructures is a universal feature of telomeres that may have been used as a mechanism for end protection during chromosome evolution.

EXPERIMENTAL PROCEDURES

Only specific techniques used in this study are presented in this section. Published protocols have been used for several experiments and are detailed in the Supplemental Information.

Proteins

All proteins were obtained using the plasmid pTrcHisB (Invitrogen), bearing an N-terminal His-tag fusion, and were produced from DH5a bacteria, as described (Poulet et al., 2012). The TRF2 protein used corresponds to a 500 aa peptide.

Cell Lines and Reagents

HT1080 cells were grown in DMEM supplemented with 10% fetal calf serum, penicillin (100 IU/ml), and streptomycin (100 mg/ml) at 37C. sh*TERF2*-inducible HeLa cells were a gift from Joachim Lingner and were used as described previously (Grolimund et al., 2013).

The sequence of *TERF2* shRNA used in HT1080 cells was 5′-CCGGCATTGGAATGATGACTCTGAACTCGAGTTCAGAGTCATCATTCCAATGTTTTT-3′. Lentivirus production was performed by transient cotransfection of 293T cells with the specified lentiviral-expression vector and two packaging plasmids, p8.91 and pVSVg, by calcium-phosphate precipitation. Viral supernatants were collected 24 hr after transfection. The transduction efficiency was determined for the pWPIR-GFP vectors (pWPIR-GFP, pWPIR-GFP-TRF2, pWPIR-GFP-7K, pWPIR-GFP-2R, pWPIR-GFP-Top-less, and pWPIR-GFP-ADB) by flow-cytometry analysis of GFP-positive cells 3 days after infection and for the pLKO-shRNA plasmids (pLKO-shScramble and pLKO-sh*TERF2*) by counting the number of clones after 1 week of selection with puromycin (1 mg/ml).

DREEM Imaging

Topographic signals are collected through mechanically driving cantilevers near its resonance frequency. Simultaneously, electrostatic signals are collected through applying AC and DC biases to a highly doped silicon cantilever with the frequency of the AC bias centered on cantilever's first overtone. Importantly, there are no significant cross-talks between topographic and DREEM channels. The DNA substrates were a mixture of DNA (T135 DNA) fragments from digestion of the pSXneo 135 (T2AG3) plasmid DNA (a gift from Dr. Peter Lansdorp at the University of British Columbia) using XbaI and BglII restriction enzymes (NEB). The two fragments resulted from digestion and have distinct DNA contour lengths, which enable us to differentiate telomeric (263 nm) and plasmidic (1,150 nm) DNA fragments. The TRFH domain was diluted to a final concentration of 445 nM in 5 mM HEPES, 150 mM KCl (pH 7.5) and incubated with the T135 DNA fragments (2 nM) for 20 min at room temperature. The incubated samples were diluted 20-fold in 5 mM HEPES, 150 mM KCl, 10 mM Mg(OAc)2 (pH 7.5) and deposited onto freshly cleaved mica surface (SPI Supply). DREEM images were collected using a MFP-3D-Bio AFM (Asylum Research) and highly doped Pointprobe PPP-FMR probes (Nanosensors; results for force constant were as follows: 2.8 N/m; results for resonant frequency were as follows: f1 = 80 kHz; and results for first overtone were as follows: f2 500 kHz). Detailed description of DREEM imaging technique is described in two studies (K.P., D.Wu, J. Lin, P. Countryman, R. Riehn, P.L. Opresko, and H. Wang, unpublished data; Wu et al., 2016). Briefly, AFM cantilevers were scraped with tweezers to remove the oxidized layer, and the top surface was coated with a thin layer of colloidal liquid silver (Ted Pella Inc.). A function generator (Sanford Research System, model DS335) and lock-in amplifier (Sanford Research System, model SR844 RF) were used to generate the AC and DC biases and monitor changes in vibration amplitude and phase signals near the first overtone frequency as a function of sample positions. While the AC and DC biases are applied to AFM tips, the mica substrate is grounded. To optimize DREEM signals, AC and DC biases were adjusted from 0 to 20 V and 1.5 to 1.5 V, respectively.

Protein Footprinting

In total, 8 pmol of TRF2 protein were incubated for 20 min at 25C with or without 16 pmol of a linearized DNA plasmid containing 650 bp of telomeric sequences in 10 mM Tris-HCl (pH 8), 150 mM NaCl, 0.5 mM DTT, and 5% glycerol. Acetylation of lysines was performed by adding 0.5 mM of sulfosuccinimidyl acetate (Thermo scientific) for 30 min at 30C. The reaction was stopped by adding 1% trifluoroacetic acid (Sigma). The samples were resuspended in Laemmli loading buffer and boiled for 5 min. Proteins were resolved by SDS-PAGE and submitted to trypsin proteolysis, and profiles of lysine acetylation were analyzed using mass spectrometry. We determined the probability of lysine acetylation and the probability of disappearance of lysine acetylation upon DNA interaction. The percentage of protection from acetylation presented in Figure 2 was calculated as follows: probability of disappearance of lysine acetylation upon DNA interaction 3 probability of lysine acetylation of the TRF2 protein. Data shown are the results of five independent experiments.

Trioxsalen Experiments

In total, two million HeLa cells were treated with or without doxycycline (1 mg/ml for 5 days) and ICRF-193 (3 mg/ml final concentration for 24 hr)

and transduced by the Empty, TRF2, or Top-less expressing vectors. Treatment was performed in a 10 cm Petri dish in PBS with 280 ml of a saturated 0.9 mg/ml solution of 4,5′,8-trimethylpsoralen (Trioxsalen) for 4 min at 37C in aluminum foil. Crosslinking was performed on a BioSun (Vilber Lourmat) at 350 nm at 0.36 J/cm2. Then, trioxsalen was removed and cells were washed, trypsinized, and pelleted. After classical extraction, DNA was resuspended in 75 ml of TE and sonicated using a Bioruptor (Diagenode) until fragments were around 200 bp in length. This length was checked using a Bioanalyzer (Agilent). A total of 8 mg of DNA was dried using a speed vac, resuspended in 10 ml of Glyoxal buffer (1 M Glyoxal, 50% DMSO), and incubated at 55 C for 90 min. Orange dye loading buffer was added, and samples were loaded on a 3% agarose 10 mM Na phosphate buffer (pH 7) gel. Migration was performed for 14 hr in 10 mM Na phosphate buffer (pH 7) at 2.5 V/cm. After migration, the gel was incubated for 3 hr at 65 C in 0.5 N NaOH and 1.5 M NaCl. After several washes in water, the gel was incubated 3 times for 20 min in 13 TBE, and 40 ml of SYBR Green II (life Technologies) was added to 200 ml of 13 TBE for staining. After rinsing with water, the gel was scanned using a Typhoon FLA 9500 (GE Healthcare). DNA in the gel was then transferred to a N+ Hybond membrane (Southern blotting), telomeric DNA was revealed using a telomeric radiolabeled probe, and the membrane was analyzed as for EMSA gels.

SUPPLEMENTAL INFORMATION

Supplemental Information includes Supplemental Experimental Procedures and six figures and can be found with this article online at http://dx.doi.org/10.1016/j.molcel.2015.12.009.

AUTHOR CONTRIBUTIONS

D.B.-P. performed cell biology and microscopy experiments with the help of E.J., K.F., S.B., N.D., C.M.L., S.P., A.M.-B., and J.Y.; S.P. performed AFM and STORM with the assistance of V.F., A.L.-V., and S.B.; D.B.-P., A.M.-B., L.L., and M.-J.G.-P. did the biochemical analysis of biological samples; D.B.-P., B.P., A.G., and M.-J.G.-P. performed in vitro biochemical experiments; S.M. and M.-H.L. conducted CD. E.A. constructed the HeLa cell line. P.K. and H.W. performed DREEM experiments. J.C.-V. assisted for data analysis. D.B.-P. and S.P. were involved in the writing of the manuscript. E.G. and M.-J.G.-P. coordinated the study and wrote the manuscript.

ACKNOWLEDGMENTS

We greatly thank Joachim Lingner for the HeLa cell line used in this study. This work was performed using the genomic, PICMI (supported by ARC and the Conseil General 06 de la Région Provence Alpes-Côte d'Azur), and CYTOMED (supported by FEDER, le Ministère de l'Enseignement Supérieur, la région Provence Alpes-Côte d'Azur, and l'INSERM) facilities of IRCAN; we are very grateful for the help they provided. We are also indebted to Isabelle Zanella-Cléon for mass spectrometry analysis (Centre Commun de Micro-analyse des Protéines, IBCP Lyon). We acknowledge the PICT-IBiSA platform of the Institut Curie, member of the French National Research Infrastructure France-BioImaging (ANR-10-INSB-04). We are grateful to Matteo de Chiara and Silvia Bottini for the script of 2D probability density map on R. The AFM facility of PICMI was supported by the ARC and Conseil General 06 de la Région Provence Alpes-Côte d'Azur. This work was supported by grants from the Fondation ARC, Ligue Contre le Cancer (EG Equipe labellisée), ANR ("Teloloop" ANR-1582-30020690), Institut Nationale du Cancer (INCa) (TELOCHROM), "Investments for the Future" LABEX SIGNALIFE (reference ANR-11-LABX-0028-01), and an NIH grant for DREEM experiments (NIH R01GM107559).

Received: June 8, 2015
Revised: October 14, 2015
Accepted: November 30, 2015
Published: January 7, 2016

REFERENCES

Amiard, S., Doudeau, M., Pinte, S., Poulet, A., Lenain, C., Faivre-Moskalenko, C., Angelov, D., Hug, N., Vindigni, A., Bouvet, P., et al. (2007). A topological mechanism for TRF2-enhanced strand invasion. Nat. Struct. Mol. Biol. *14*, 147–154.

Bae, N.S., and Baumann, P. (2007). A RAP1/TRF2 complex inhibits nonhomologous end-joining at human telomeric DNA ends. Mol. Cell *26*, 323–334.

Baker, A.M., Fu, Q., Hayward, W., Lindsay, S.M., and Fletcher, T.M. (2009). The Myb/SANT domain of the telomere-binding protein TRF2 alters chromatin structure. Nucleic Acids Res. *37*, 5019–5031.

Baker, A.M., Fu, Q., Hayward, W., Victoria, S., Pedroso, I.M., Lindsay, S.M., and Fletcher, T.M. (2011). The telomere binding protein TRF2 induces chromatin compaction. PLoS ONE *6*, e19124.

Bankhead, T., Kobryn, K., and Chaconas, G. (2006). Unexpected twist: harnessing the energy in positive supercoils to control telomere resolution. Mol. Microbiol. *62*, 895–905.

Bao, K., and Cohen, S.N. (2004). Reverse transcriptase activity innate to DNA polymerase I and DNA topoisomerase I proteins of Streptomyces telomere complex. Proc. Natl. Acad. Sci. USA *101*, 14361–14366.

Benetti, R., Schoeftner, S., Muñoz, P., and Blasco, M.A. (2008). Role of TRF2 in the assembly of telomeric chromatin. Cell Cycle *7*, 3461–3468.

Bermejo, R., Capra, T., Jossen, R., Colosio, A., Frattini, C., Carotenuto, W., Cocito, A., Doksani, Y., Klein, H., Gómez-González, B., et al. (2011). The replication checkpoint protects fork stability by releasing transcribed genes from nuclear pores. Cell *146*, 233–246.

Bilaud, T., Koering, C.E., Binet-Brasselet, E., Ancelin, K., Pollice, A., Gasser, S.M., and Gilson, E. (1996). The telobox, a Myb-related telomeric DNA binding motif found in proteins from yeast, plants and human. Nucleic Acids Res. *24*, 1294–1303.

Bilaud, T., Brun, C., Ancelin, K., Koering, C.E., Laroche, T., and Gilson, E. (1997). Telomeric localization of TRF2, a novel human telobox protein. Nat. Genet. *17*, 236–239.

Biroccio, A., Porru, M., Rizzo, A., Salvati, E., D'Angelo, C., Orlandi, A., Passeri, D., Franceschin, M., Stevens, M.F., Gilson, E., et al. (2011). DNA damage persistence as determinant of tumor sensitivity to the combination of Topo I inhibitors and telomere-targeting agents. Clin Cancer Res *17*, 2227–2236.

Celli, G.B., and de Lange, T. (2005). DNA processing is not required for ATM-mediated telomere damage response after TRF2 deletion. Nat. Cell Biol. *7*, 712–718.

Cesare, A.J., and Karlseder, J. (2012). A three-state model of telomere control over human proliferative boundaries. Curr. Opin. Cell Biol. *24*, 731–738.

Cesare, A.J., Kaul, Z., Cohen, S.B., Napier, C.E., Pickett, H.A., Neumann, A.A., and Reddel, R.R. (2009). Spontaneous occurrence of telomeric DNA damage response in the absence of chromosome fusions. Nat. Struct. Mol. Biol. *16*, 1244–1251.

Cesare, A.J., Hayashi, M.T., Crabbe, L., and Karlseder, J. (2013). The telomere deprotection response is functionally distinct from the genomic DNA damage response. Mol. Cell *51*, 141–155.

Chaconas, G., and Kobryn, K. (2010). Structure, function, and evolution of linear replicons in Borrelia. Annu. Rev. Microbiol. *64*, 185–202.

Chen, Y., Yang, Y., van Overbeek, M., Donigian, J.R., Baciu, P., de Lange, T., and Lei, M. (2008). A shared docking motif in TRF1 and TRF2 used for differential recruitment of telomeric proteins. Science *319*, 1092–1096.

Chen, L., Zhu, X., Zou, Y., Xing, J., Gilson, E., Lu, Y., and Ye, J. (2015). The topoisomerase II catalytic inhibitor ICRF-193 preferentially targets telomeres that are capped by TRF2. Am. J. Physiol. Cell Physiol. *308*, C372–C377.

Court, R., Chapman, L., Fairall, L., and Rhodes, D. (2005). How the human telomeric proteins TRF1 and TRF2 recognize telomeric DNA: a view from high-resolution crystal structures. EMBO Rep. *6*, 39–45.

Cristofari, G., and Lingner, J. (2006). Telomere length homeostasis requires that telomerase levels are limiting. EMBO J. *25*, 565–574.

d'Alcontres, M.S., Palacios, J.A., Mejias, D., and Blasco, M.A. (2014). Topolla prevents telomere fragility and formation of ultra thin DNA bridges during mitosis through TRF1-dependent binding to telomeres. Cell Cycle *13*, 1463–1481.

deLange, T. (2005). Shelterin: the protein complex that shapes and safeguards human telomeres. Genes Dev. *19*, 2100–2110.

Denchi, E.L., and de Lange, T. (2007). Protection of telomeres through independent control of ATM and ATR by TRF2 and POT1. Nature *448*, 1068–1071.

Doksani, Y., Wu, J.Y., de Lange, T., and Zhuang, X. (2013). Super-resolution fluorescence imaging of telomeres reveals TRF2-dependent T-loop formation. Cell *155*, 345–356.

Fairall, L., Chapman, L., Moss, H., de Lange, T., and Rhodes, D. (2001). Structure of the TRFH dimerization domain of the human telomeric proteins TRF1 and TRF2. Mol. Cell *8*, 351–361.

Feuerhahn, S., Chen, L.Y., Luke, B., and Porro, A. (2015). No DDRama at chromosome ends: TRF2 takes centre stage. Trends Biochem. Sci. *40*, 275–285.

Fouché, N., Cesare, A.J., Willcox, S., Ozgür, S., Compton, S.A., and Griffith, J.D. (2006). The basic domain of TRF2 directs binding to DNA junctions irrespective of the presence of TTAGGG repeats. J. Biol. Chem. *281*, 37486–37495.

Galati, A., Magdinier, F., Colasanti, V., Bauwens, S., Pinte, S., Ricordy, R., Giraud-Panis, M.J., Pusch, M.C., Savino, M., Cacchione, S., and Gilson, E. (2012). TRF2 controls telomeric nucleosome organization in a cell cycle phase-dependent manner. PLoS ONE *7*, e34386.

Germe, T., Miller, K., and Cooper, J.P. (2009). A non-canonical function of topoisomerase II in disentangling dysfunctional telomeres. EMBO J. *28*, 2803–2811.

Gilson, E., and Géli, V. (2007). How telomeres are replicated. Nat. Rev. Mol. Cell Biol. *8*, 825–838.

Giraud-Panis, M.J., Pisano, S., Benarroch-Popivker, D., Pei, B., Le Du, M.H., and Gilson, E. (2013). One identity or more for telomeres? Front. Oncol. *3*, 48.

Griffith, J.D., Comeau, L., Rosenfield, S., Stansel, R.M., Bianchi, A., Moss, H., and de Lange, T. (1999). Mammalian telomeres end in a large duplex loop. Cell *97*, 503–514.

Grolimund, L., Aeby, E., Hamelin, R., Armand, F., Chiappe, D., Moniatte, M., and Lingner, J. (2013). A quantitative telomeric chromatin isolation protocol identifies different telomeric states. Nat. Commun. *4*, 2848–2859.

Hayashi, M.T., Cesare, A.J., Fitzpatrick, J.A., Lazzerini-Denchi, E., and Karlseder, J. (2012). A telomere-dependent DNA damage checkpoint induced by prolonged mitotic arrest. Nat. Struct. Mol. Biol. *19*, 387–394.

Hsieh, M.H., Tsai, C.H., Lin, C.C., Li, T.K., Hung, T.W., Chang, L.T., Hsin, L.W., and Teng, S.C. (2015). Topoisomerase II inhibition suppresses the proliferation of telomerase-negative cancers. Cell. Mol. Life Sci. *72*, 1825–1837.

Kabir, S., Hockemeyer, D., and de Lange, T. (2014). TALEN gene knockouts reveal no requirement for the conserved human shelterin protein Rap1 in telomere protection and length regulation. Cell Rep. *9*, 1273–1280.

Kaul, Z., Cesare, A.J., Huschtscha, L.I., Neumann, A.A., and Reddel, R.R. (2012). Five dysfunctional telomeres predict onset of senescence in human cells. EMBO Rep. *13*, 52–59.

Kim, H., Lee, O.H., Xin, H., Chen, L.Y., Qin, J., Chae, H.K., Lin, S.Y., Safari, A., Liu, D., and Songyang, Z. (2009). TRF2 functions as a protein hub and regulates telomere maintenance by recognizing specific peptide motifs. Nat. Struct. Mol. Biol. *16*, 372–379.

Kouzine, F., Gupta, A., Baranello, L., Wojtowicz, D., Ben-Aissa, K., Liu, J., Przytycka, T.M., and Levens, D. (2013). Transcription-dependent dynamic supercoiling is a short-range genomic force. Nat. Struct. Mol. Biol. *20*, 396–403.

Leonetti, C., Scarsella, M., Riggio, G., Rizzo, A., Salvati, E., D'Incalci, M., Staszewsky, L., Frapolli, R., Stevens, M.F., Stoppacciaro, A., et al. (2008). G-quadruplex ligand RHPS4 potentiates the antitumor activity of camptothecins in preclinical models of solid tumors. Clin Cancer Res *14*, 7284–7291.

Mendoza, V.L., and Vachet, R.W. (2009). Probing protein structure by amino acid-specific covalent labeling and mass spectrometry. Mass Spectrom. Rev. *28*, 785–815.

Mirabella, A., and Gartenberg, M.R. (1997). Yeast telomeric sequences function as chromosomal anchorage points in vivo. EMBOJ. *16*, 523–533.

Muraki, K., Nabetani, A., Nishiyama, A., and Ishikawa, F. (2011). Essential roles of Xenopus TRF2 in telomere end protection and replication. Genes Cells *16*, 728–739.

Okamoto, K., Bartocci, C., Ouzounov, I., Diedrich, J.K., Yates, J.R., 3rd, and Denchi, E.L. (2013). A two-step mechanism for TRF2-mediated chromosome-end protection. Nature *494*, 502–505.

Porro, A., Feuerhahn, S., Delafontaine, J., Riethman, H., Rougemont, J., and Lingner, J. (2014a). Functional characterization of the TERRA transcriptome at damaged telomeres. Nat. Commun. *5*, 5379–5391.

Porro, A., Feuerhahn, S., and Lingner, J. (2014b). TERRA-reinforced association of LSD1 with MRE11 promotes processing of uncapped telomeres. Cell Rep. *6*, 765–776.

Poulet, A., Buisson, R., Faivre-Moskalenko, C., Koelblen, M., Amiard, S., Montel, F., Cuesta-Lopez, S., Bornet, O., Guerlesquin, F., Godet, T., et al. (2009). TRF2 promotes, remodels and protects telomeric Holliday junctions. EMBO J. *28*, 641–651.

Poulet, A., Pisano, S., Faivre-Moskalenko, C., Pei, B., Tauran, Y., Haftek-Terreau, Z., Brunet, F., Le Bihan, Y.V., Ledu, M.H., Montel, F., et al. (2012). The N-terminal domains of TRF1 and TRF2 regulate their ability to condense telomeric DNA. Nucleic Acids Res. *40*, 2566–2576.

Saint-Léger, A., Koelblen, M., Civitelli, L., Bah, A., Djerbi, N., Giraud-Panis, M.J., Londoño-Vallejo, A., Ascenzioni, F., and Gilson, E. (2014). The basic N-terminal domain of TRF2 limits recombination endonuclease action at human telomeres. Cell Cycle *13*, 2469–2474.

Sarek, G., Vannier, J.B., Panier, S., Petrini, J.H., and Boulton, S.J. (2015). TRF2 recruits RTEL1 to telomeres in S phase to promote t-loop unwinding. Mol. Cell *57*, 622–635.

Sarthy, J., Bae, N.S., Scrafford, J., and Baumann, P. (2009). Human RAP1 inhibits non-homologous end joining at telomeres. EMBOJ. *28*, 3390–3399.

Stansel, R.M., de Lange, T., and Griffith, J.D. (2001). T-loop assembly in vitro involves binding of TRF2 near the 3′ telomeric overhang. EMBOJ. *20*, 5532–5540.

Takai, H., Smogorzewska, A., and de Lange, T. (2003). DNA damage foci at dysfunctional telomeres. Curr. Biol. *13*, 1549–1556.

Takai, K.K., Kibe, T., Donigian, J.R., Frescas, D., and de Lange, T. (2011). Telomere protection by TPP1/POT1 requires tethering to TIN2. Mol. Cell *44*, 647–659.

Temime-Smaali, N., Guittat, L., Wenner, T., Bayart, E., Douarre, C., Gomez, D., Giraud-Panis, M.J., Londono-Vallejo, A., Gilson, E., Amor-Guéret, M., and Riou, J.F. (2008). Topoisomerase IIIalpha is required for normal proliferation and telomere stability in alternative lengthening of telomeres. EMBOJ. *27*, 1513–1524.

Thanasoula, M., Escandell, J.M., Martinez, P., Badie, S., Muñoz, P., Blasco, M.A., and Tarsounas, M. (2010). p53 prevents entry into mitosis with uncapped telomeres. Curr. Biol. *20*, 521–526.

Tsai, H.H., Huang, C.H., Tessmer, I., Erie, D.A., and Chen, C.W. (2011). Linear Streptomyces plasmids form superhelical circles through interactions between their terminal proteins. Nucleic Acids Res. *39*, 2165–2174.

van Steensel, B., Smogorzewska, A., and de Lange, T. (1998). TRF2 protects human telomeres from end-to-end fusions. Cell *92*, 401–413.

Verdun, R.E., and Karlseder, J. (2006). The DNA damage machinery and homologous recombination pathway act consecutively to protect human telomeres. Cell *127*, 709–720.

Vos, S.M., Tretter, E.M., Schmidt, B.H., and Berger, J.M. (2011). All tangled up: how cells direct, manage and exploit topoisomerase function. Nat. Rev. Mol. Cell Biol. *12*, 827–841.

Wan, B., Yin, J., Horvath, K., Sarkar, J., Chen, Y., Wu, J., Wan, K., Lu, J., Gu, P., Yu, E.Y., et al. (2013). SLX4 assembles a telomere maintenance toolkit by bridging multiple endonucleases with telomeres. Cell Rep. *4*, 861–869.

Wilson, J.S., Tejera, A.M., Castor, D., Toth, R., Blasco, M.A., and Rouse, J. (2013). Localization-dependent and -independent roles of SLX4 in regulating telomeres. Cell Rep. *4*, 853–860.

Wu, D., Kaur, P., Wang, H., and Erie, D.A. (2016). Visualizing the path of DNA through proteins using DREEM imaging. Mol. Cell *61*, this issue, 315–323.

Ye, J., Lenain, C., Bauwens, S., Rizzo, A., Saint-Léger, A., Poulet, A., Benarroch, D., Magdinier, F., Morere, J., Amiard, S., et al. (2010). TRF2 and apollo cooperate with topoisomerase 2alpha to protect human telomeres from replicative damage. Cell *142*, 230–242.

Yeeles, J.T., Poli, J., Marians, K.J., and Pasero, P. (2013). Rescuing stalled or damaged replication forks. Cold Spring Harb. Perspect. Biol. *5*, a012815.

Molecular Cell

Supplemental Information

TRF2-Mediated Control of Telomere DNA Topology as a Mechanism for Chromosome-End Protection

Delphine Benarroch-Popivker, Sabrina Pisano, Aaron Mendez-Bermudez, Liudmyla Lototska, Parminder Kaur, Serge Bauwens, Nadir Djerbi, Chrysa M. Latrick, Vincent Fraisier, Bei Pei, Alexandre Gay, Emilie Jaune, Kevin Foucher, Julien Cherfils-Vicini, Eric Aeby, Simona Miron, Arturo Londoño-Vallejo, Jing Ye, Marie-Hélène Le Du, Hong Wang, Eric Gilson, and Marie-Josèphe Giraud-Panis

Figure S1

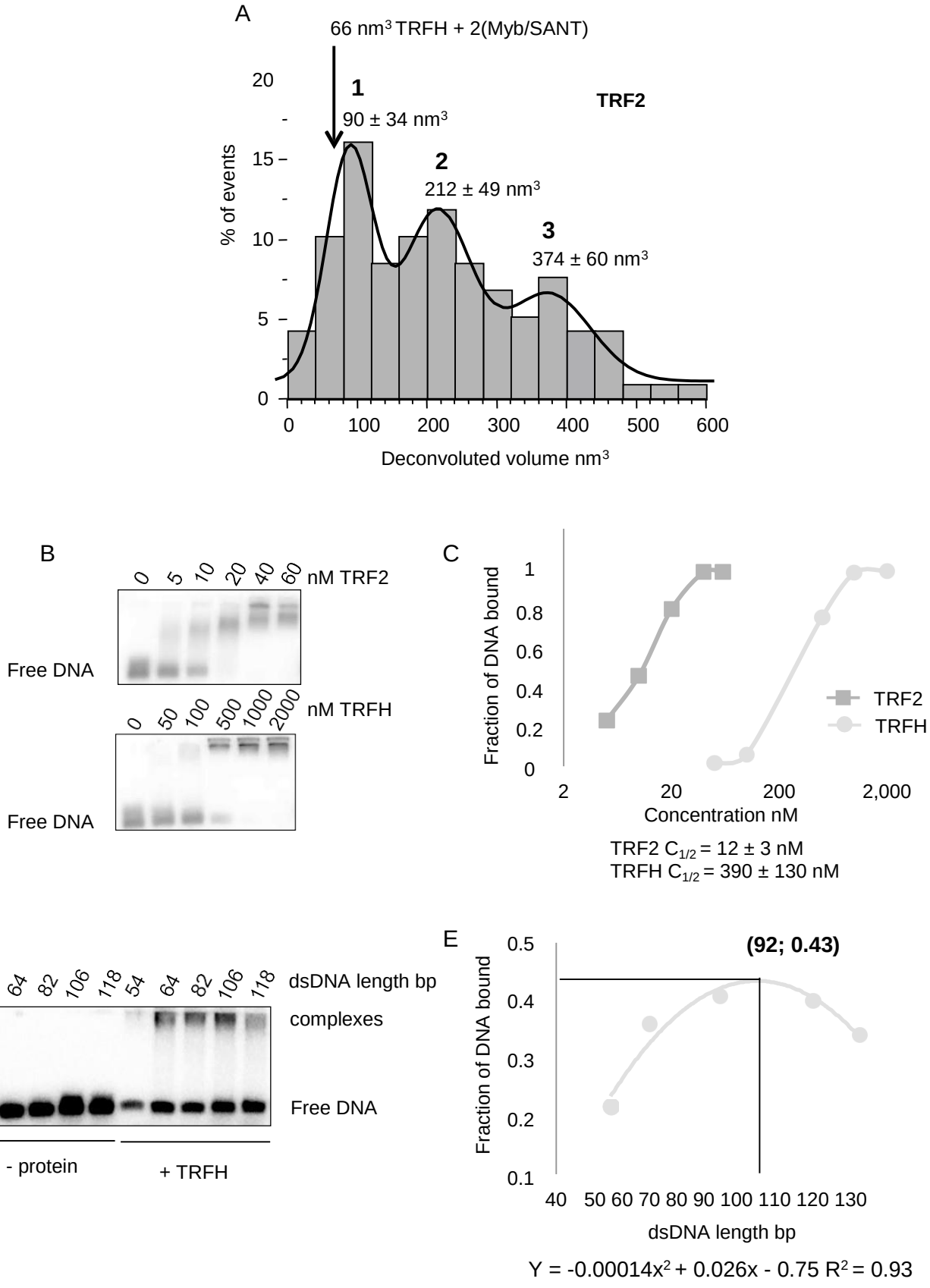
A
66 nm³ TRFH + 2(Myb/SANT)
1
90 ± 34 nm³
2
212 ± 49 nm³
3
374 ± 60 nm³
TRF2
% of events
Deconvoluted volume nm³
B
0 5 10 20 40 60 nM TRF2
Free DNA
0 50 100 500 1000 2000 nM TRFH
Free DNA
C
Fraction of DNA bound
Concentration nM
TRF2
TRFH
TRF2 C1/2 = 12 ± 3 nM
TRFH C1/2 = 390 ± 130 nM
D
54 64 82 106 118 54 64 82 106 118 dsDNA length bp
complexes
Free DNA
- protein
+ TRFH
E
(92; 0.43)
Fraction of DNA bound
dsDNA length bp
Y = -0.00014x² + 0.026x - 0.75 R² = 0.93

Figure **S1**

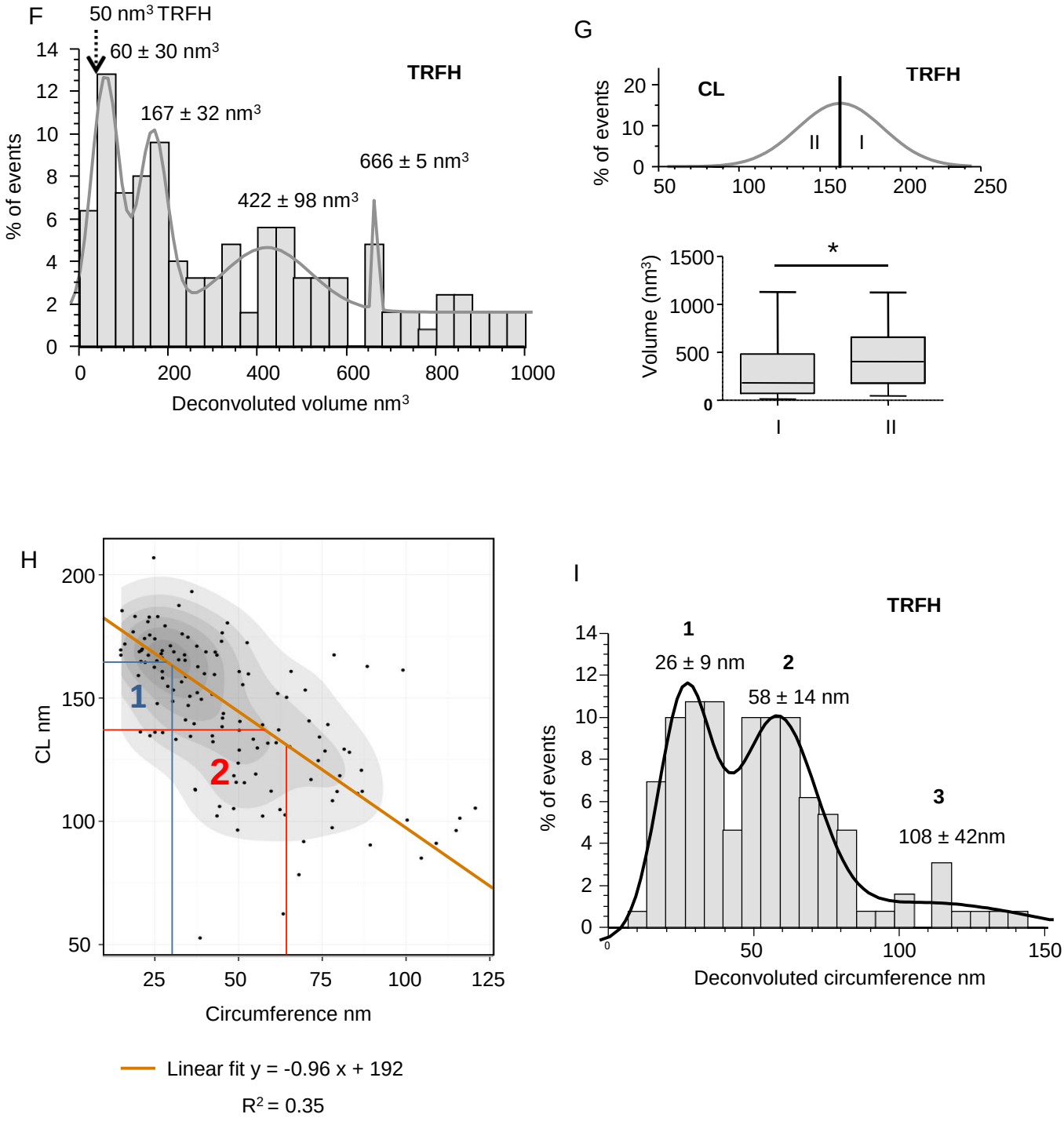
F
50 nm³ TRFH
60 ± 30 nm³
TRFH
167 ± 32 nm³
666 ± 5 nm³
422 ± 98 nm³
% of events
Deconvoluted volume nm³
G
CL
TRFH
% of events
II
I
Volume (nm³)
*
H
CL nm
Circumference nm
1
2
Linear fit y = -0.96 x + 192
R² = 0.35
I
TRFH
1
26 ± 9 nm
2
58 ± 14 nm
3
108 ± 42nm
% of events
Deconvoluted circumference nm

Figure S2

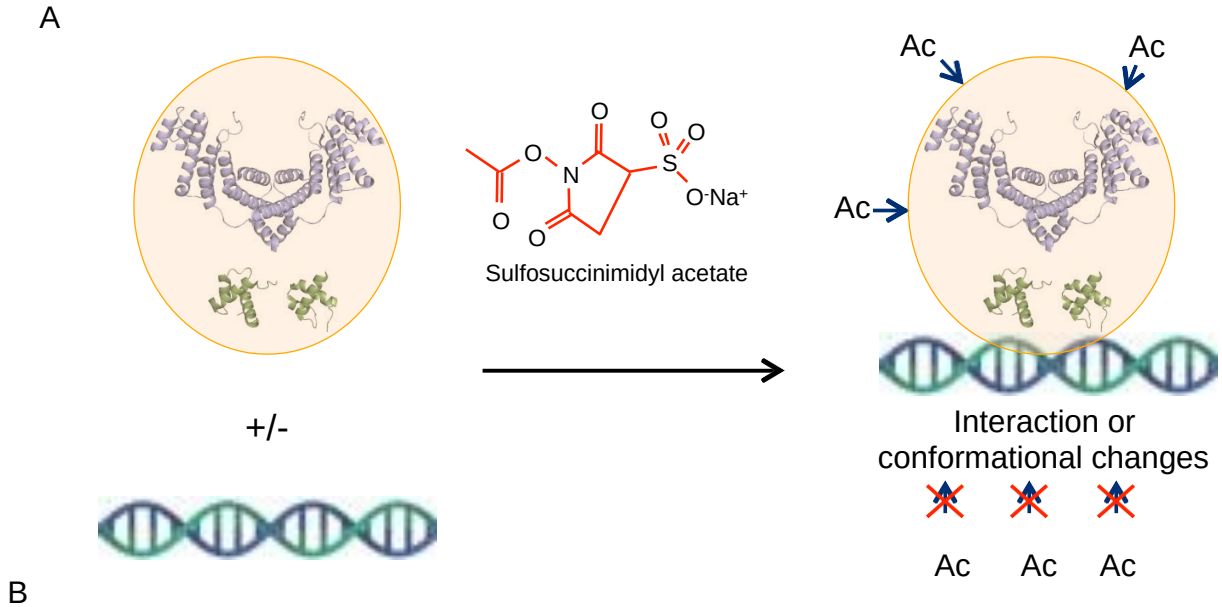
A
Ac
Ac
Ac
Sulfosuccinimidyl acetate
+/-
Interaction or
conformational changes
Ac
Ac
Ac

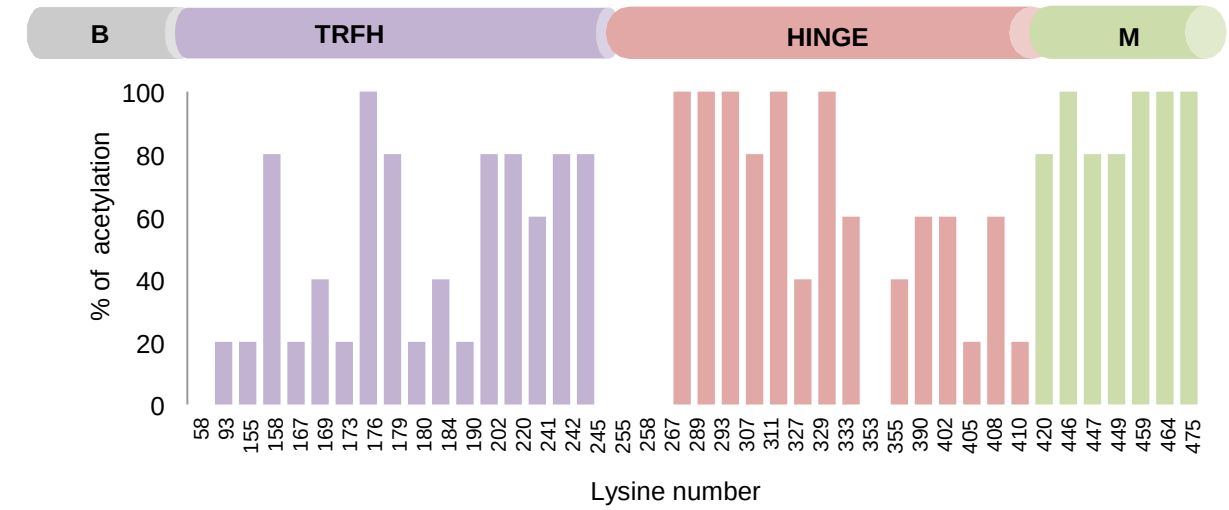
B
B
TRFH
HINGE
M
% of acetylation
100
80
60
40
20
0
58
93
155
158
167
169
173
176
179
180
184
190
202
220
241
242
245
255
258
267
289
293
307
311
327
329
333
353
355
390
402
405
408
410
420
446
447
449
459
464
475
Lysine number

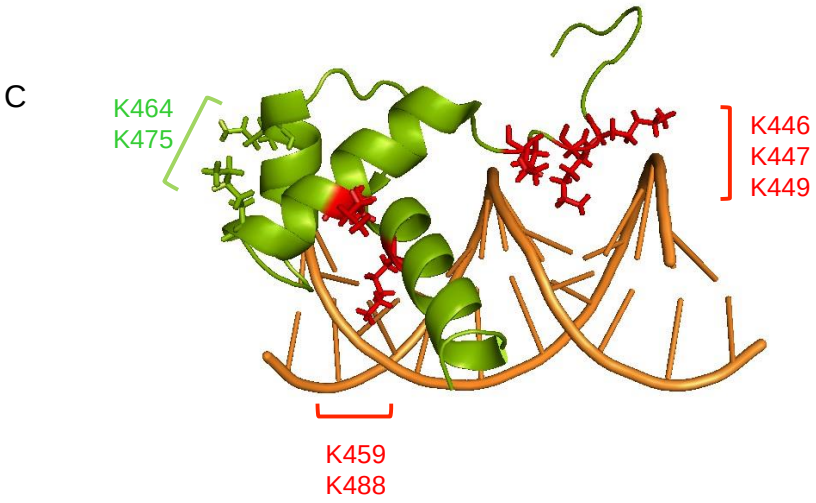
C
K464
K475
K446
K447
K449
K459
K488

D

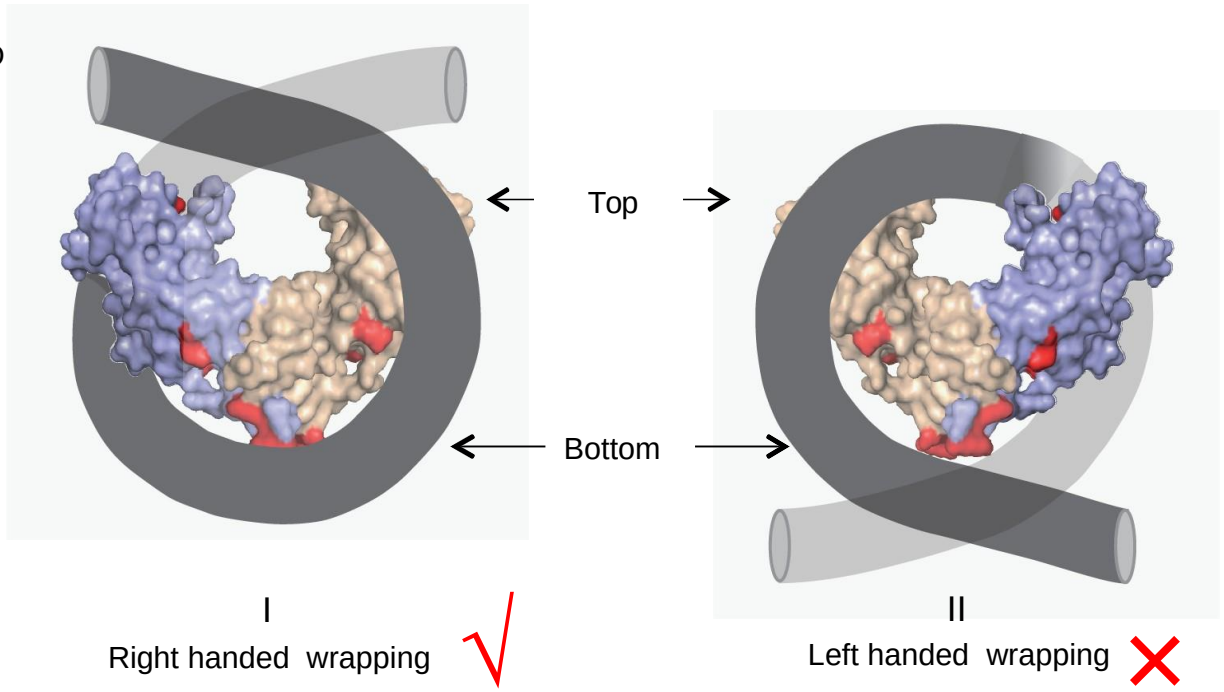

Figure S3

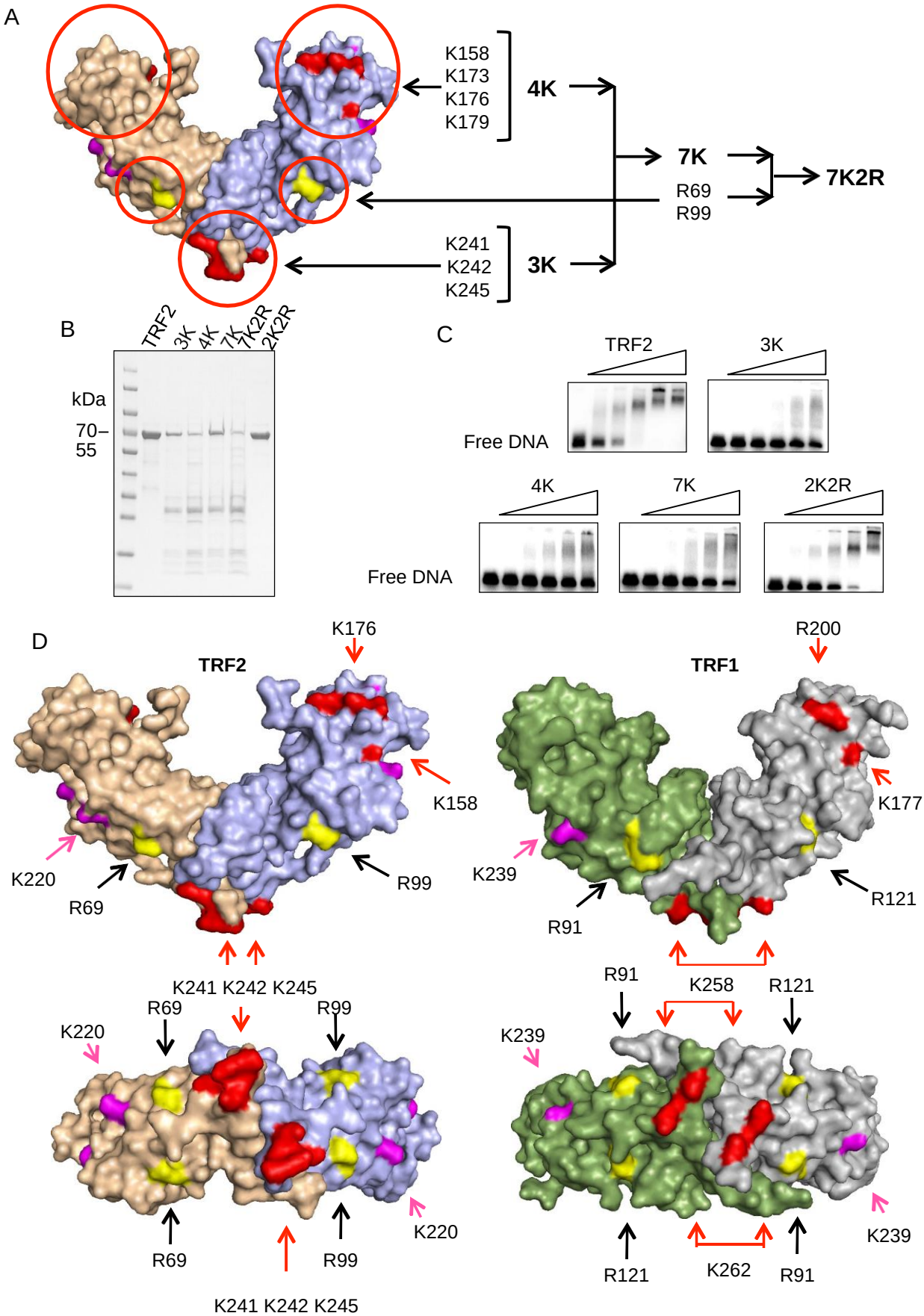
A
K158
K173
K176
K179
4K
7K
R69
R99
7K2R
K241
K242
K245
3K
B
TRF2
3K
4K
7K
7K2R
2K2R
kDa
70–
55
C
TRF2
3K
Free DNA
4K
7K
2K2R
Free DNA
D
TRF2
K176
K158
K220
R69
R99
K241 K242 K245
TRF1
R200
K177
K239
R91
R121
R91
K258
R121
K239
K220
R69
R99
K241 K242 K245
R121
K262
R91
K239

Figure S3

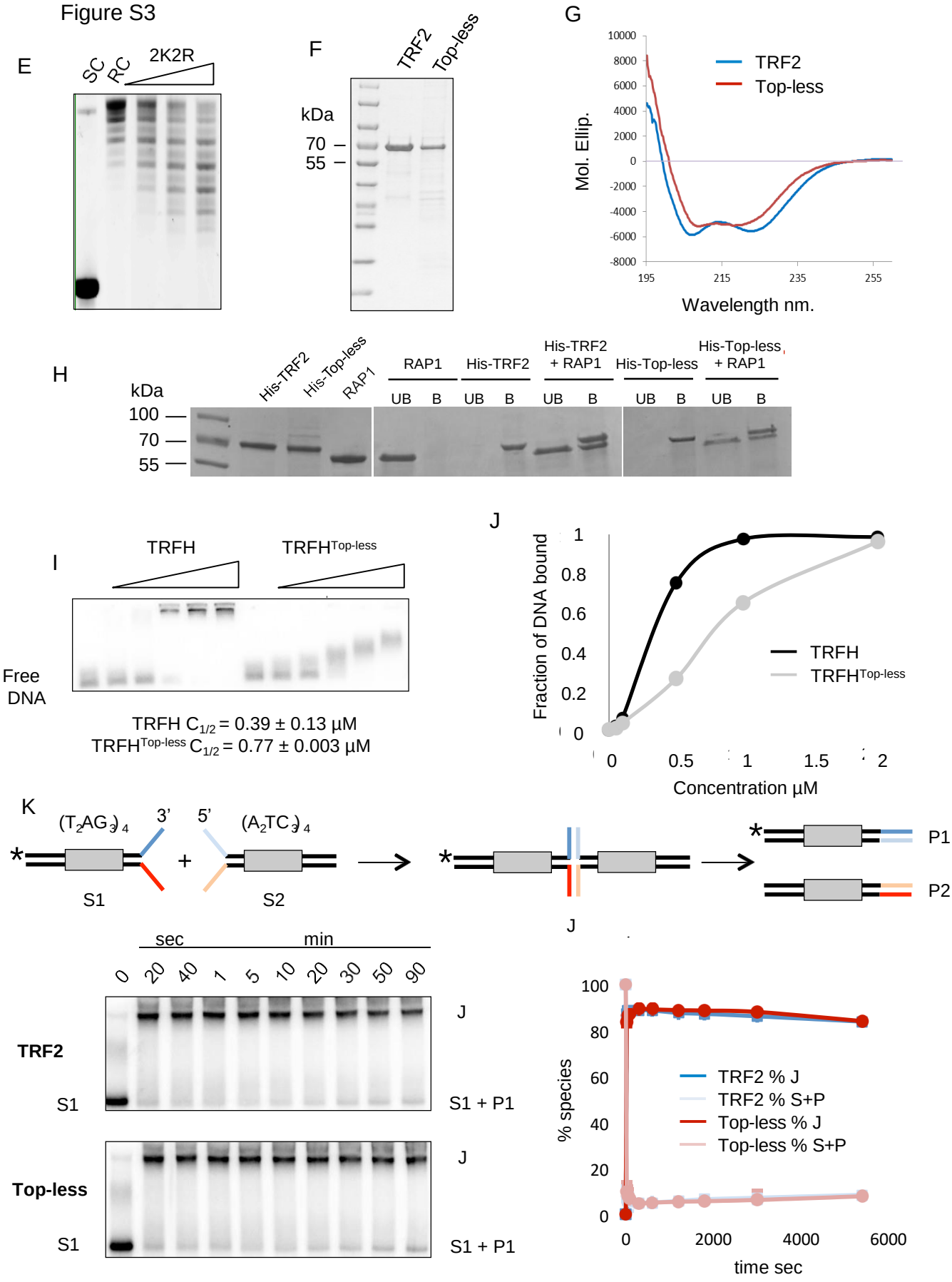
E
SC
RC
2K2R
F
TRF2
Top-less
kDa
70
55
G
TRF2
Top-less
Mol. Ellip.
Wavelength nm.
H
His-TRF2
His-Top-less
RAP1
RAP1
His-TRF2
His-TRF2 + RAP1
His-Top-less
His-Top-less + RAP1
UB
B
kDa
100
70
55
I
TRFH
TRFH^Top-less
Free DNA
TRFH C1/2 = 0.39 ± 0.13 µM
TRFH^Top-less C1/2 = 0.77 ± 0.003 µM
J
Fraction of DNA bound
TRFH
TRFH^Top-less
Concentration µM
K
(T2AG3)4
3'
5'
(A2TC3)4
S1
S2
P1
P2
sec
min
0
20
40
1
5
10
20
30
50
90
TRF2
Top-less
S1
S1 + P1
J
% species
TRF2 % J
TRF2 % S+P
Top-less % J
Top-less % S+P
time sec

Figure S4

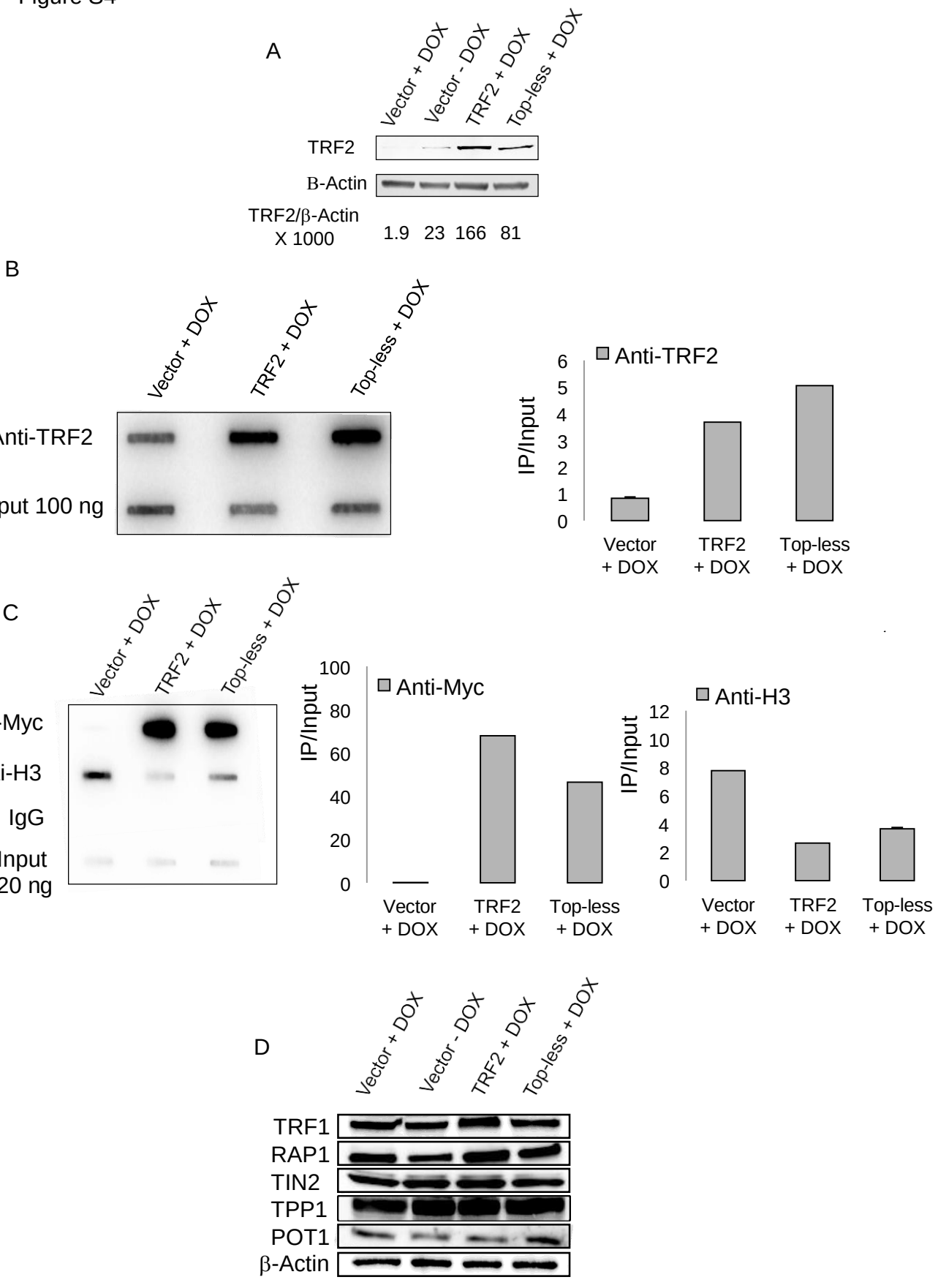
A
Vector + DOX
Vector - DOX
TRF2 + DOX
Top-less + DOX
TRF2
B-Actin
TRF2/β-Actin
X 1000
1.9 23 166 81
B
Vector + DOX
TRF2 + DOX
Top-less + DOX
Anti-TRF2
Input 100 ng
Anti-TRF2
IP/Input
Vector + DOX
TRF2 + DOX
Top-less + DOX
C
Vector + DOX
TRF2 + DOX
Top-less + DOX
Anti-Myc
Anti-H3
IgG
Input 20 ng
Anti-Myc
IP/Input
Anti-H3
IP/Input
Vector + DOX
TRF2 + DOX
Top-less + DOX
D
Vector + DOX
Vector - DOX
TRF2 + DOX
Top-less + DOX
TRF1
RAP1
TIN2
TPP1
POT1
β-Actin

Figure S4

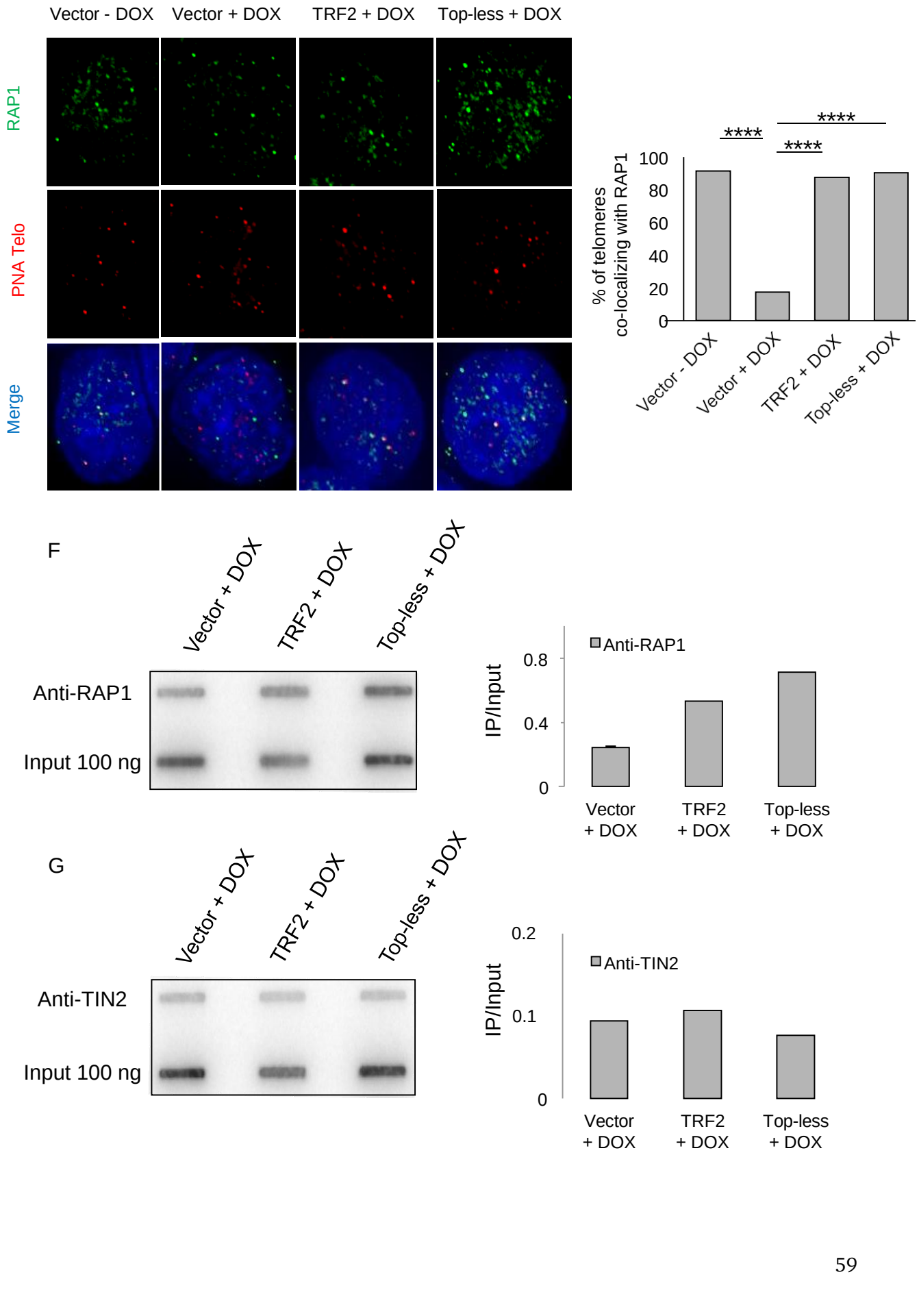
E
Vector - DOX
Vector + DOX
TRF2 + DOX
Top-less + DOX
RAP1
PNA Telo
Merge
% of telomeres co-localizing with RAP1
100
80
60
40
20
0
****
****
****
Vector - DOX
Vector + DOX
TRF2 + DOX
Top-less + DOX
F
Vector + DOX
TRF2 + DOX
Top-less + DOX
Anti-RAP1
Input 100 ng
IP/Input
0.8
0.4
0
Anti-RAP1
Vector + DOX
TRF2 + DOX
Top-less + DOX
G
Vector + DOX
TRF2 + DOX
Top-less + DOX
Anti-TIN2
Input 100 ng
IP/Input
0.2
0.1
0
Anti-TIN2
Vector + DOX
TRF2 + DOX
Top-less + DOX

Figure S5

A

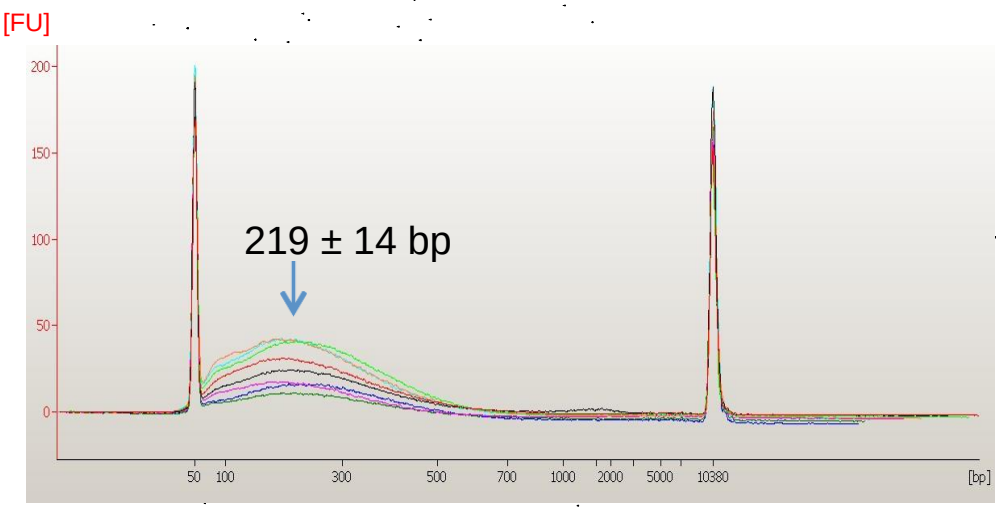
[FU]
200
150
100
50
0
219 ± 14 bp
50
100
300
500
700
1000
2000
5000
10380
[bp]

B

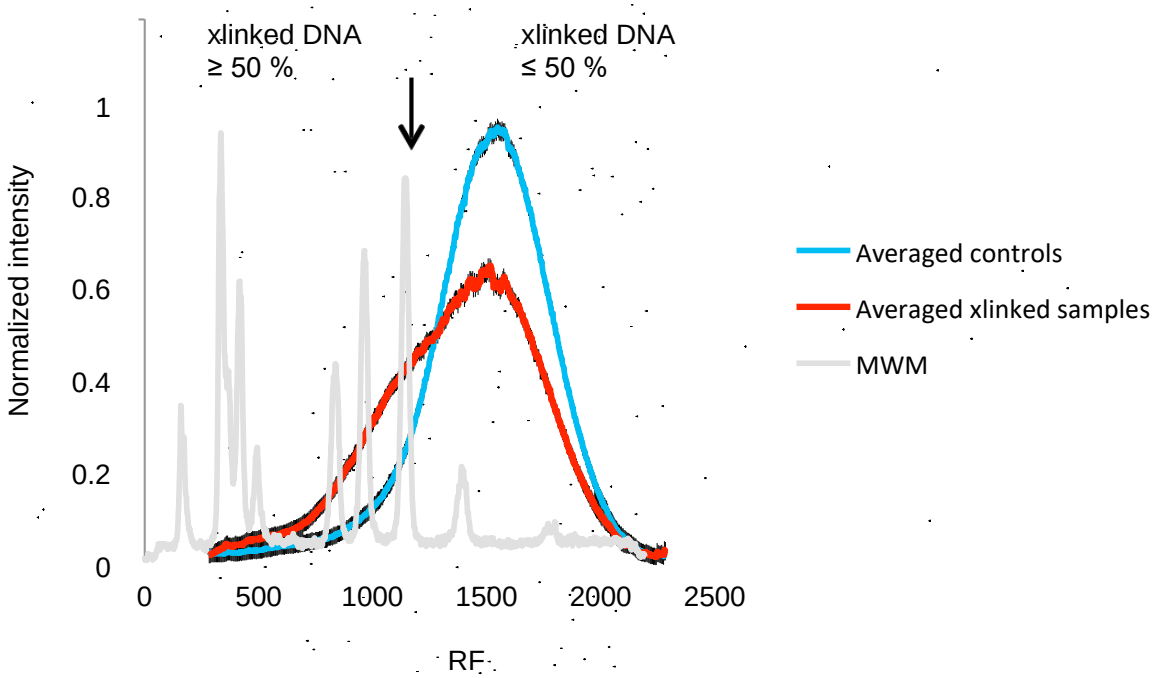
xlinked DNA
≥ 50 %
xlinked DNA
≤ 50 %
Normalized intensity
1
0.8
0.6
0.4
0.2
0
0
500
1000
1500
2000
2500
RF
Averaged controls
Averaged xlinked samples
MWM

Figure S5

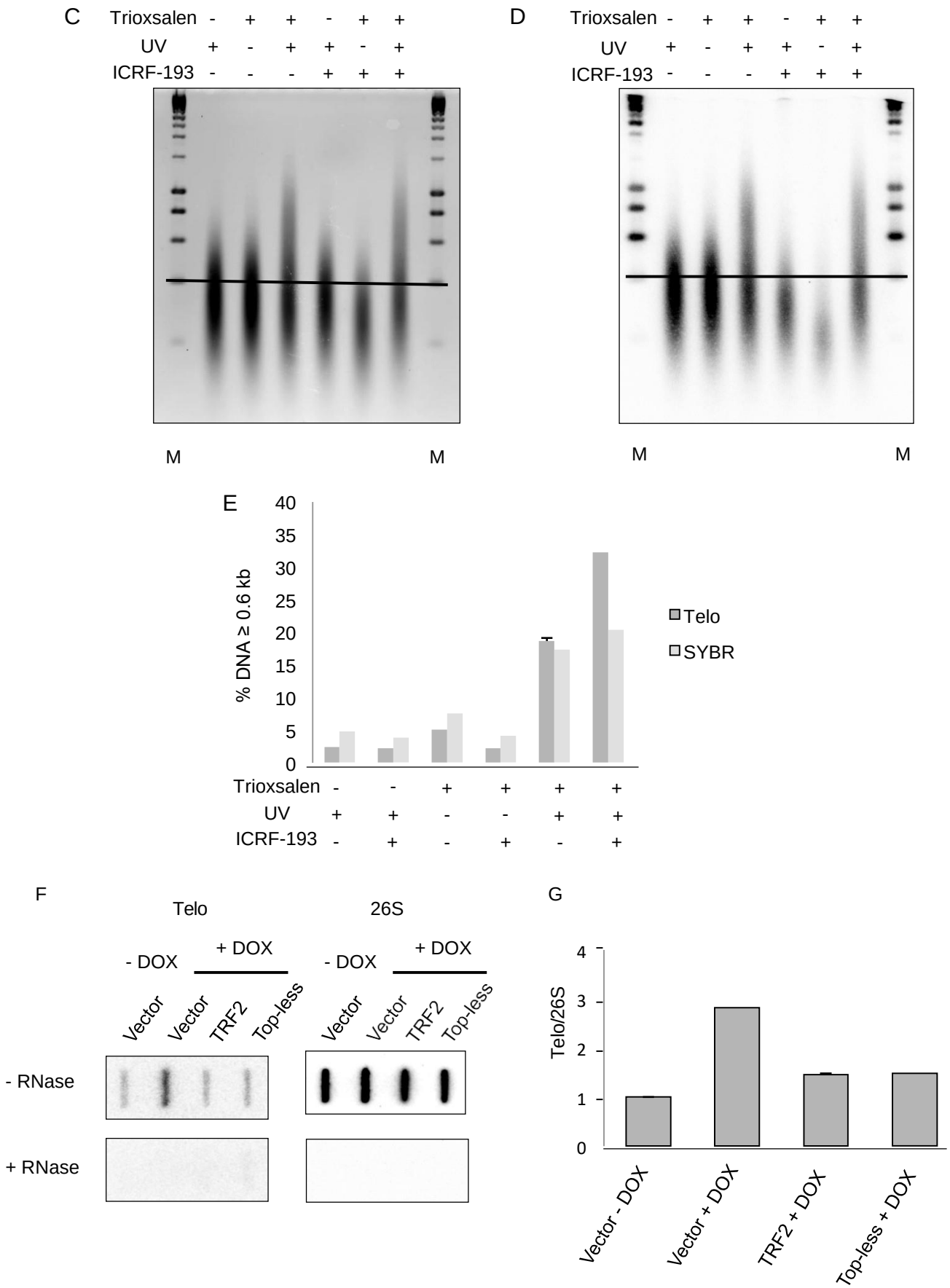
C
Trioxsalen - + + - + +
UV + - + + - +
ICRF-193 - - - + + +
M
M
D
Trioxsalen - + + - + +
UV + - + + - +
ICRF-193 - - - + + +
M
M
E
% DNA ≥ 0.6 kb
40
35
30
25
20
15
10
5
0
Telo
SYBR
Trioxsalen - - + + + +
UV + + - - + +
ICRF-193 - + - + - +
F
Telo
26S
- DOX
+ DOX
- DOX
+ DOX
Vector
Vector
TRF2
Top-less
Vector
Vector
TRF2
Top-less
- RNase
+ RNase
G
Telo/26S
4
3
2
1
0
Vector - DOX
Vector + DOX
TRF2 + DOX
Top-less + DOX

Figure S6

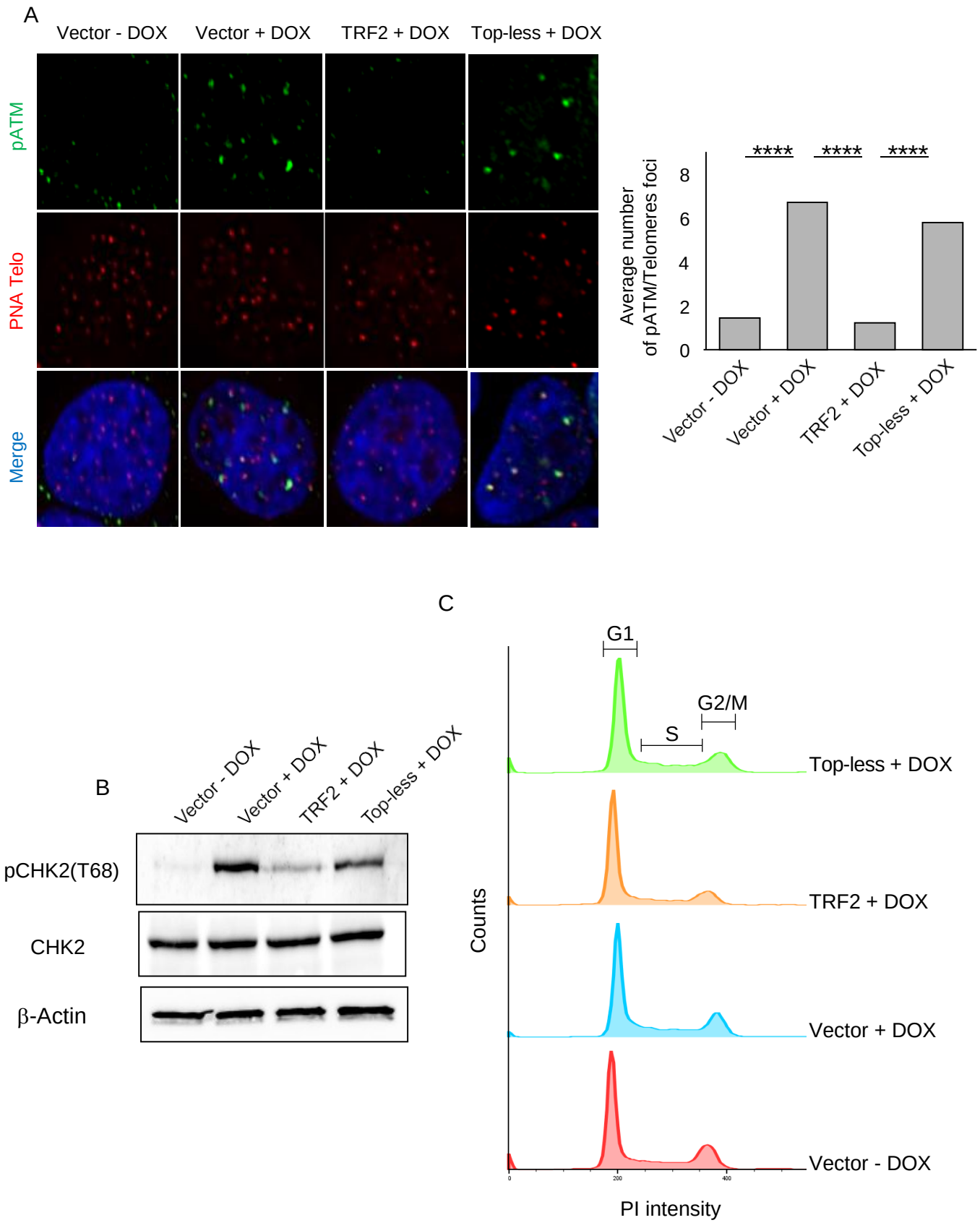
A
Vector - DOX
Vector + DOX
TRF2 + DOX
Top-less + DOX
pATM
PNA Telo
Merge
Average number of pATM/Telomeres foci
****
****
****
0
2
4
6
8
Vector - DOX
Vector + DOX
TRF2 + DOX
Top-less + DOX
B
Vector - DOX
Vector + DOX
TRF2 + DOX
Top-less + DOX
pCHK2(T68)
CHK2
β-Actin
C
G1
S
G2/M
Top-less + DOX
TRF2 + DOX
Vector + DOX
Vector - DOX
Counts
PI intensity

Figure S6

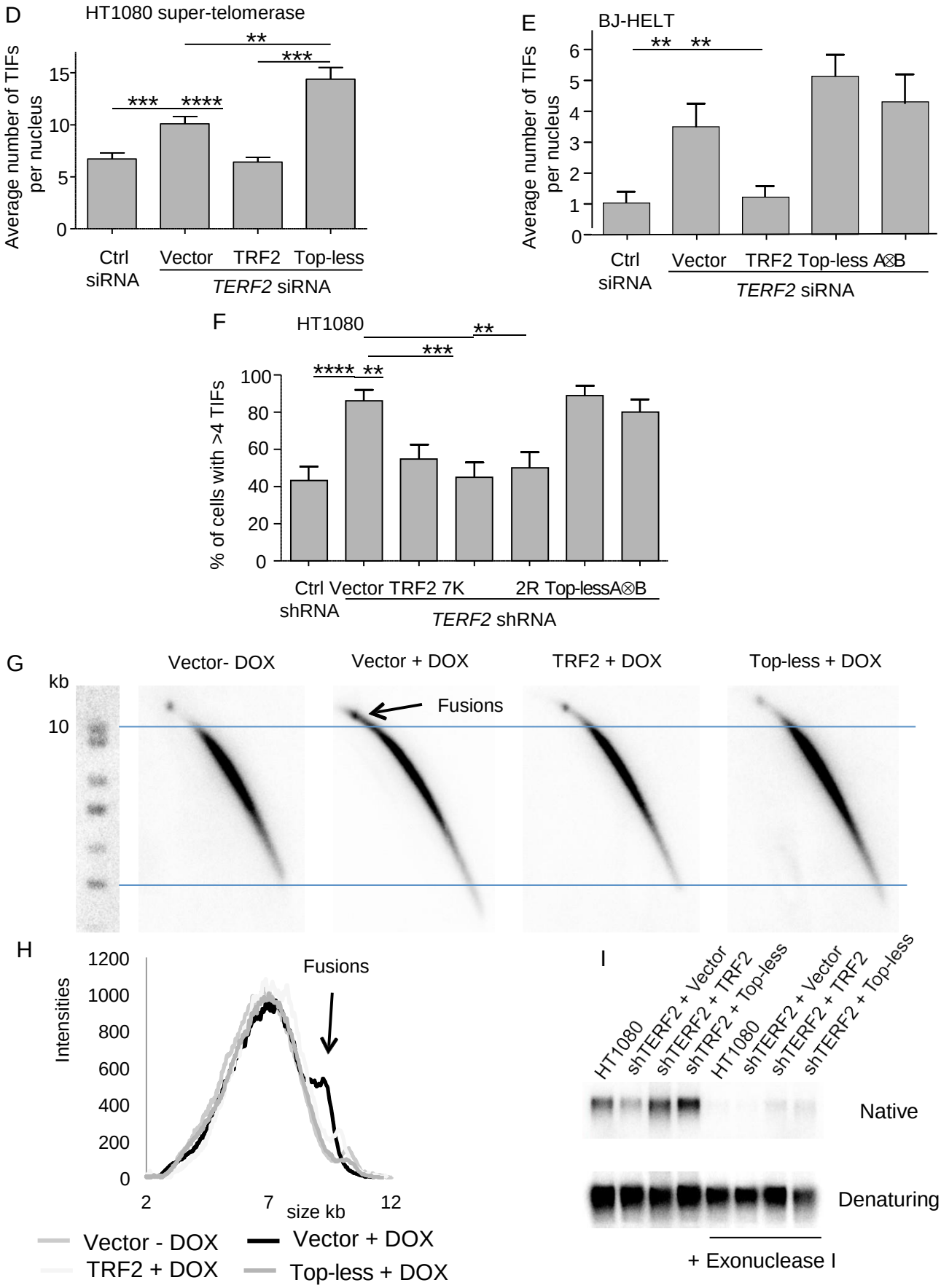
D
HT1080 super-telomerase
Average number of TIFs per nucleus
Ctrl siRNA
Vector
TRF2
Top-less
TERF2 siRNA
E
BJ-HELT
Average number of TIFs per nucleus
Ctrl siRNA
Vector
TRF2
Top-less A⊗B
TERF2 siRNA
F
HT1080
% of cells with >4 TIFs
Ctrl shRNA
Vector
TRF2 7K
2R Top-lessA⊗B
TERF2 shRNA
G
Vector- DOX
Vector + DOX
TRF2 + DOX
Top-less + DOX
kb
10
Fusions
H
Intensities
Fusions
size kb
Vector - DOX
Vector + DOX
TRF2 + DOX
Top-less + DOX
I
HT1080
shTERF2 + Vector
shTERF2 + TRF2
shTRF2 + Top-less
Native
Denaturing
+ Exonuclease I

Supplementary Information

Supplementary figures legends

Figure S1. Volume and circumference distributions of DNA complexes in AFM experiments and DNA binding properties of the TRFH domain. Related to Figure 1.

(A) Distribution of deconvoluted volumes corresponding to the same set of TRF2/DNA complexes shown in Figure 1A. Histograms, expressed as percentage of events and corresponding to the raw data, were fitted with individual populations applying a Gaussian multi-peak fitting. The solid line corresponds to the sum of the multi-fitting. Note that the volume corresponding to the mean value of the first peak is bigger than the calculate volume of the TRFH + 2 Myb domains calculated from the 3D X-ray crystallography data (pdb 3BUA and 1VFC respectively) using the CRYSOL software. Peak 1 is thus compatible with the volume of a dimer.

(B) EMSA using labeled dsTelo106 as DNA probe and either TRF2 or TRFH.

(C) Quantitative analysis of EMSAs. Error bars represent standard deviations from three experiments.

(D) EMSA showing the binding of the TRFH domain at 250 nM on double stranded DNA probes of different lengths (54, 64, 82, 106, 118 bp) and containing 44, 54, 72, 96 and 108 bp of TTAGGG repeats respectively.

(E) Quantitative analysis of EMSAs. Error bars represent standard deviations from three experiments.

(F) Distribution of deconvoluted volumes for TRFH/DNA complexes calculated from AFM data shown in Figure 1B. Histograms correspond to raw data and curves to the sum of a Gaussian multi-peak fitting. Note that the value corresponding to the main volume of the first peak is very close to the volume of the TRFH domain calculated from the 3D X-ray cristallography data (pdb

3BUA) using the CRYSOL software. Peak 1 therefore corresponds to the binding of one dimeric TRFH domain.

(G) Top: Gaussian curve fitting the raw data for the CL distribution of TRFH/DNA complexes shown in Figure 1B. The distribution has been divided in two groups depending on their CL (CL > 163 nm and CL < 163 nm, group I and II respectively). Bottom: The volume distributions corresponding to the two CL groups were analyzed and represented in a box and whiskers graph. A p value < 0.05 was calculated for the difference between the medians of the 2 volume distributions, attesting that, as for TRF2, bigger complexes have smaller CL and *vice-versa*.

(H) 2D-probability density map of contour length (CL) and circumference obtained for the TRF2/DNA complexes representing the probability to find a protein/DNA complex with a given DNA contour length and the corresponding circumference. Note the slope close to 1 of the linear fit.

(I) Distribution of the calculated circumference for TRFH/DNA complexes obtained from the deconvoluted AFM data set shown in Figure 1B.

Figure S2. The acetylation footprinting method: principle and validation. Related to Figure 2.

(A) Schematics of the acetylation protocol. Purified TRF2 is acetylated *in vitro* by sulfosuccinimidyl acetate in the presence or absence of telomeric DNA. This compound only acetylates lysines accessible to solvent. Lysines protected either by DNA or through structural modifications caused by DNA cannot be acetylated. Mass spectrometry analysis gives acetylation profiles of the protein and thus allows the determination of protected lysines on the surface of the protein.

(B) Probability of acetylation (in %) for lysines in TRF2 reflecting their accessibility to solvent. Lysines 140 and 495 are not in the graph since their corresponding peptide were missing in the mass spectrometry profiles.

(C) NMR 3D structure ("PDB: 1VFC") of TRF2 Myb/SANT domain bound to DNA. Lysines in red are located close to DNA, lysines in green are farther away. Note the nice correlation between proximity of DNA and protection shown in Figure 2.

(D) Positions of the protected lysines in the TRFH domain infer chirality in the interaction, thus forcing strands to cross. From earlier work (Amiard et al., 2007) we know that TRF2 introduces positive supercoils in a relaxed circular substrate. Two models can be drawn:

In I, DNA strands are crossing at the top of the TRFH structure giving a right handed wrapping. This would explain the positive supercoils caused by TRF2 in DNA.

In II, DNA strands are crossing at the bottom of the TRFH structure. In this case the wrapping is left handed. This does not fit with the positive supercoils reported.

Figure S3. Top-less: a mutant allowing separation between topology-related and unrelated functions of TRF2. Related to Figure 3.

(A) Positions of lysines and arginines mutated to alanine in the TRFH domain of TRF2. The dotted circle signals residues located at the back of the structure.

(B) Coomassie stained SDS-PAGE of mutants used in the activity (Topoisomerase I assay and EMSA) screening.

(C) EMSAs using the wild type and mutated proteins and the dsTelo106 probe. Protein concentrations were 5, 10, 20, 40 and 60 nM.

(D) Positions of mutated lysines and arginines in the TRFH domain of TRF2 and their corresponding residues in the TRFH of TRF1. Left: positions in TRF2 of lysines giving strong

signals in the footprint assay (red and pink) and of TRF1-conserved arginines (yellow); Right: TRF2-conserved lysines in TRF1 with the same color code than their corresponding residues in TRF2.

(E) Topoisomerase I assay for 2K2R. Protein concentrations used were 100, 250, 500 nM. Several non-relevant lanes were removed from the image. SC stands for supercoiled and RC relaxed circular DNA.

(F) Coomassie stained SDS-PAGE of purified TRF2 and Top-less proteins.

(G) Circular dichroism experiment performed with TRF2 and Top-less proteins.

(H) Coomassie stained SDS-PAGE showing recombinant His-tagged TRF2, His-tagged Top-less and untagged RAP1 proteins purified in E. coli. Recombinant RAP1 (15 µg) was pulled-down with 10 µg of recombinant TRF2 or Top-less proteins bound on cobalt-based magnetic beads. Unbound (UB) and bound (B) fractions were analyzed. Note the similar profile between wild type and mutated proteins showing a similar behavior for RAP1 *in vitro* binding.

(I) EMSA showing the binding of TRFH and $TRFH^{Top\text{-}less}$ on dsTelo106. Protein concentrations used were 50, 100, 500, 1000 and 2000 nM. We noticed a qualitative difference in the nature of the complexes between both TRFH complexes. The wild type domain yielded complexes that did not run in 1% agarose, probably due to extensive distortion of DNA, while the mutated domain yielded complexes that resembled progressive binding of several proteins on less distorted DNA.

(J) Quantitative analysis of EMSAs. Error bars correspond to standard errors between three experiments.

(K) Formation and migration of a telomeric Holliday junction. Top panel: Schematics of the reaction. Two substrates (S1 and S2, S1 is ^{32}P labeled on the top strand) containing four human telomeric repeats and S1 to S2 compatible flapping ends were mixed together in the presence or absence of TRF2 or Top-less. Aliquots of the reaction were taken at different time points and the

nature of the species studied by migration in an acrylamide gel. One can observe the appearance of the slowly migrating four stranded Holliday junction (J). Since substrate (S) and product (P) were undistinguishable, quantification was done on the sum of the two species. Left panel: acrylamide electrophoretic analysis of aliquots at different time point. Right panel: quantitative analysis of the % of Holliday junction (% J) and % of the other species (% S+P) through time. Error bars correspond to standard deviation between three experiments. Note the identical behavior for both proteins.

Figure S4. Top-less binds telomeres in HeLa cells, does not modify shelterins expression and recruits RAP1 and TIN2 to telomeres as well as the wild type protein. Related to Figure 3.

(A) Immuno-blot using an anti-TRF2 antibody showing the expression of wild type or mutant TRF2 in HeLa cells treated or not with doxycycline (DOX) to induce TRF2 knock-down and transduced either with empty vector, TRF2 or Top-less expressing lentiviruses. Numbers below represent quantification of the membrane using the signal from β-Actin for normalization.

(B) ChIP experiment performed on TRF2 knocked down HeLa cells and transduced with viruses either containing an empty vector or expressing TRF2 or Top-less. ChIP was performed using an anti-TRF2 antibody. Membranes were hybridized using a telomeric probe (Telo). Quantification performed on two replicates is shown next. Error bars represent standard deviation.

(C) Same experiment as above using either an anti-Myc antibody, an anti-H3 antibody or an isotype IgG.

(D) Immuno-blots showing the expression of all other shelterin subunits in HeLa cells treated or not by doxycycline (DOX) to induce TRF2 knock-down and transduced either with empty vector, TRF2 or Top-less expressing lentiviruses.

(E) Co-localization of RAP1 (in green) with telomeres (in red) by PNA-FISH IF in the same cells as above. Nuclei were stained with DAPI. Quantification of the percentage of telomeres co-localizing with a RAP1 signal is shown below. Data represent the means ± SE. P values were calculated using the Mann-Whitney test (**** $P < 0.0001$ and an absence of mark indicates no significance).

(F) ChIP experiment performed on TRF2 knocked down HeLa cells and transduced with viruses either containing an empty vector or expressing TRF2 or Top-less. ChIP was performed using an anti-RAP1 antibody. Membranes were hybridized using a telomeric probe (Telo). Quantification performed on two replicates is shown next. Error bars represent standard deviation.

(G) Same experiment as above using an anti-TIN2 antibody.

Figure S5. TRF2 controls telomeric DNA topology. Related to Figure 4.

(A) Bioanalyzer migration profiles of samples. A representative example is shown corresponding to the gel shown in Figure 4. An average size of 219 ± 14 bp was measured.

(B) Normalized profiles from all Southern blots of crosslinked (xlinked samples) DNA or non-crosslinked DNA (controls). Data from all experiments were averaged and plotted with the profile of Molecular Weight Markers (MWM). At the position corresponding to 0.6 kb the quantity of crosslinked and non-crosslinked material were equal in the crosslinked samples. Thus above this threshold DNA will be mainly crosslinked and below mainly un-crosslinked.

(C) Trioxsalen experiment performed with ICRF-193 treated cells. SYBRII stained glyoxal gel. M stands for molecular weight markers and the dotted line marks the 0.6 kb threshold used for analysis.

(D) Southern blot of the glyoxal gel hybridized by a telomeric probe (Telo).

(E) Quantitative analysis of glyoxal gels. The relative amount of DNA material above the 0.6 kb threshold was measured for each condition. SYBR indicates the values obtained for the SYBRII stained gels and Telo for the Southern blots. Error bars represent standard deviation from 4 experiments.

(F) Northern slot blot showing the amount of TERRA RNA in HeLa cells compromised for TRF2 (+ DOX) and transduced with viruses expressing either TRF2 or Top-less. The membrane was hybridized using either the 4C3 telomeric DNA probe (Telo) or a 26S probe (Vincent et al., 1993).

(G) Quantitative analysis of two northern slot blot experiments. The ratio between Telo and 26S signals was calculated for each slot in two experiments. Error bars represent min and max values of 2 replicates.

Figure S6. DDR activation in Top-less expressing cells. Related to Figure 5.

(A) Recruitment of the phosphorylated form of ATM (pATM) on Top-less telomeres. Co-localization of pATM (in green) with telomeres (in red) was analyzed by PNA-FISH and IF in HeLa cells treated or not with doxycycline (DOX) to induce TRF2 knock-down and transduced either with empty vector, TRF2 or Top-less expressing lentiviruses. Quantification of the number of foci colocolizing pATM and telomeres is shown next. Data represent the means ± SE. P values were calculated using the Mann-Whitney test (**** $P < 0.0001$).

(B) Immuno-blots showing the presence of T68 phosphorylated CHK2 in HeLa cells knocked-down for TRF2 (+ DOX) and expressing the Top-less mutant compared to control or wild-type TRF2 expressing cells.

(C) Cell cycle analysis performed on the cells above using propidium iodine staining and analysis by Flow Cytometry.

(D) Co-localization of 53BP1 IF with a PNA-Telomeric probe revealing telomere dysfunction-induced foci (TIFs) in HT1080 super-telomerase cells transduced as indicated. Data show the mean ± SE and P values were calculated using the Mann-Whitney test (** $P < 0.01$, *** $P < 0.001$, **** $P < 0.0001$). The quantification of *TERF2* transcript level for the different conditions of TRF2 expression (control siRNA with expression of empty vector, *TERF2* siRNA with expression of either empty vector or TRF2 or Top-less) was done by RT-qPCR and is respectively of 1.1, 0.2, 9.5, 6.5 fold of enrichment. These cells were used to measure the number of t-loops by STORM.

(E) Recruitment of 53BP1 on telomeres (TIFs) of BJ fibroblasts down-regulated for *TERF2* by siRNA and expressing either TRF2, Top-less or the AΔB protein. Data show the mean ± SE and P values were calculated using the Mann-Whitney test (** $P < 0.01$ and an absence of mark indicates no significance). The quantification of *TERF2* transcript level for the different conditions of TRF2 expression (control scramble siRNA with expression of empty vector, *TERF2* siRNA with expression of either empty vector or TRF2 or Top-less or AΔB) was done by RT-qPCR and is respectively of 1, 0.13, 0.90, 0.79 and 0.97 fold of enrichment.

(F) Recruitment of 53BP1 on telomeres (TIFs) of HT1080 cells down-regulated for *TERF2* by shRNA and expressing either TRF2, and the 7K, 2R, Top-less and AΔB mutants. Data show the mean ± SE and P values were calculated using the Mann-Whitney test (** $P < 0.01$, *** $P <$

0.001, **** P < 0.0001 and an absence of mark indicates no significance). The quantification of *TERF2* transcript level for the different conditions of TRF2 expression (control scramble shRNA with expression of empty vector, *TERF2* shRNA with expression of either empty vector or TRF2 or 7K or 2R or Top-less or AΔB) was done by RT-qPCR and is respectively and 1, 0.7, 55, 65, 106, 16 and 68 fold of enrichment.

(G) 2D gels of genomic DNA from HeLa cells compromised for TRF2 (+ DOX) and infected with viruses expressing either the empty vector, TRF2 or Top-less. The horizontal lines mark the 10 kb and 3 kb sizes. Note the presence of slowly migrating species for the Vector + DOX sample indicating the presence of fusions.

(H) Migration profiles were obtained for each 2D gel and the corresponding intensities reported as a function of the sizes thanks to size markers run beside each sample. Note the shoulder on the Vector + DOX curve corresponding to the fusions.

(I) In-gel 3' overhang experiment, performed with and without Exonuclease I treatment, showing the amount of telomeric single strand overhang (Native) and total telomeric DNA (Denaturing) in HT1080 cells compromised for TRF2 (sh*TERF2*) and transduced with viruses either containing an empty vector or expressing TRF2 or Top-less. Note the expected decrease in overhang due to the presence of the sh*TERF2* and the rescue by both the wild type and mutant proteins.

Material and Methods

AFM imaging

Complexes deposition:

10 µl of a solution of DNA and proteins in 5 mM HEPES pH 7.4, 150 mM KCl and 1 mM $MgCl_2$ was incubated 20 min at 25°C. The protein/DNA molar ratios used were the following: (2.5/10) nM for TRF2, (1100/7) nM for TRFH, (5/10) nM for Top-less. After incubation, samples

were crosslinked with glutaraldehyde (0.1% final concentration) for 30 min on ice. Before applying the sample on freshly cleaved mica, the concentration of $MgCl_2$ was increased to 10 mM. After 2 min on mica the sample was washed with 1 ml of deionized water and dried under a gentle N_2 flow. Imaging was performed on a Multimode 8 equipped with E-scanner controlled by a Nanoscope V (Bruker AXS, Santa. Barbara, CA), in air under Tapping Mode using silicon tips (RTESP, 300kHz). Images were recorded at 1.5–2.0 Hz over 1 μm wide scan area (512×512 pixels). Raw images were flattened using the manufacturer's software (Nanoscope Analysis 1.40) and converted into TIF files.

Contour Length and volume measurements:

Contour lengths (CLs) for each molecule were manually traced and measured using Image J software (http://imagej.nih.gov/ij/). For DNA-protein complexes the read-through DNA length method was used. Measurements of the naked DNA were performed using the naked molecules found in the images corresponding to the different binding experiments.

Although, the expected contour length for a B-DNA molecule of 650 bp is 221 nm (650 bp* 0.34 nm/bp), the measured mean values obtained for each naked DNA is shorter (192 ± 11 nm, 189 ± 9 nm and 188 ± 9 nm for TRF2, TRFH and Top-less binding experiment respectively). This discrepancy is related to a DNA shortening possibly due to a partial B- to A-form transition induced by the drying step (Rivetti and Codeluppi, 2001). The mean helical rise corresponding to the three different naked DNA mean CLs is then 0.29 nm/bp, that gives rise to 93 bp of DNA wrapping (27nm/0.29 nm/bp).

Volumes were calculated as ellipsoids using the formula:

$V=4/3 *\pi *(D/2*d/2*h)$

where D, d and h correspond to major diameter, minor diameter and height respectively.

These parameters were measured using Image SXM software (www.liv.ac.uk/~sdb/ImageSXM). At least 130 objects were scored for each condition.

Volume deconvolution:

The dimensions of an object imaged by AFM are affected by the broadening effect due to the tip-sample convolution radius. The relationship between the experimental width of the sample in the image, W, the radius of curvature of the tip, Rc, and the radius of curvature of the sample, Rm, is given by the equation (Bustamante et al., 1993):

$W=4Rc\ Rm^{1/2}$

If two objects are measured with the same probe the ratio between them is the following:

$W1/W2 = (R1/R2)^{1/2}$

The double-stranded DNA width (2 nm), involved in the protein complex, can be used as an internal reference for size. This allows us to obtain the real diameters for the protein complex (Nettikadan et al., 1996).

$R1= (W1/W2)^{2}* R2$

Where R1 and R2 are the real dimensions of the protein complex and the DNA respectively, while W1 and W2 are their measured dimensions.

Using the deconvoluted values corresponding to the protein diameters, it is possible to calculate the deconvoluted volumes.

Circumference estimation :

Once the deconvoluted values for the minor d and major D diameters are obtained, using the Ramanujan approximation it is possible to calculate the deconvoluted circumference of the ellipsoid using the following formula:

$C \approx \pi *(3*(d+D)-((3d+D)*(d+3D))^{1/2})$

Plots and statistics :

All the histograms represent the distribution of a measured or calculated parameter expressed in percentage of events. To obtain the mean value corresponding to each subpopulation emerging from multimodal distributions, a multi-Gaussian fitting has been applied using the QtiPlot data analysis and scientific visualization (http://soft.proindependent.com/qtiplot.html). All the parameters obtained by the Gaussian fitting are expressed in the text as mean ± FWHM (Full width at half maximum). The 2D-probability density map of contour length (CL) and circumference measured by AFM for the complexes TRF2/DNA is obtained using R open source software (http://www.R-project.org). The software was used to calculate the bivariate kernel density estimation. The resulting 2D map represents the probability to find a protein/DNA complex with a given DNA contour length and the corresponding protein circumference. The darker the region in which the data fall, the higher is their probability density.

The linear fit applied to the scatter plot corresponding to the correlation graph of CLs as a function of circumferences for TRF2/DNA complexes was performed imposing a y-intercept of 192 nm (mean value of the corresponding naked DNA) and calculated using the QtiPlot software. The analysis of the TRFH/DNA volume distributions as a function of TRFH/DNA CL distribution was performed using GraphPad Prism v 5.03. The results are shown as a box and whiskers plot. To the two volume populations the Wilcoxon matched-pairs signed rank test was applied giving a p value < 0.05.

Strand invasion assay, topology assays, EMSAs, and Holliday junction migration assays

Strand invasion assays were performed as described previously (Poulet et al., 2012). Topology assays were also performed as described previously (Amiard et al., 2007; Poulet et al., 2012), but using pLTelo, a pLEU500-Tc (Chen et al., 1992) -based plasmid containing 650 bp of human telomeric repeats between *Bst*API and *Bam*HI sites. EMSAs were performed using a 106-bp DNA probe containing 16 TTAGGG repeats flanked by a 5-bp (CAGCC) sequence at the 5’

and a 5 bp (CCTTG) sequence at the 3' end. A total of 5 nM of 5' labeled probe was incubated in a total volume of 10 µl in 20 mM HEPES pH 8, 100 mM NaCl, and 500 ng/µl of acetylated BSA on ice for 15 min. Ficoll was added to a final concentration of 3% and the samples loaded on a 1% agarose gel with 0.5× TBE under 7 V/cm. Migration was performed at the same voltage for 30 min. The gels were then dried and analyzed using phosphorimager screens. Analysis was performed on a Typhoon FLA 9500 (GE Healthcare) using the Image Quant software (GE Healthcare). Holliday junction migration assays were performed as described previously (Poulet et al., 2009).

Circular dichroism (CD)

Far-UV CD spectra (between 195 nm and 260 nm) were recorded using a Jasco J-815 spectropolarimeter equipped with a Peltier temperature control unit. The spectra were acquired as an average of five scans with a scan speed of 100 nm/min and a response time of 2 s. CD measurements were performed at 20°C, using 1-mm quartz cells. TRF2 and Top-less samples were at 4.6 µM in 10 mM Tris buffer, pH 8.0, 60 mM NaCl, 10% glycerol, and 0.2 mM DTT.

Pull-down assay

A total of 10 µg of purified His-fusion TRF2 or His-fusion Top-less proteins were incubated with cobalt-based magnetic beads (Dynabeads, Lifetechnologies) at 4°C for 30 min in 50 mM sodium phosphate pH 8, 300 mM NaCl, and 0.01% Tween 20. After two washes using the same buffer, 15 µg of purified Rap1 were added at 4°C for 90 min. The supernatant (unbound fraction, UB) was precipitated with cold acetone and resuspended in Laemmli loading buffer. After two washes, the magnetic beads containing the His-tagged proteins and associated Rap1 protein (bound fraction, B) were resuspended in Laemmli loading buffer and analyzed by SDS-PAGE.

Direct Stochastic Optical Reconstruction Microscopy (STORM) experiments

Preparation of nuclei, psoralen crosslinking and chromatin spreading :

Samples were prepared using the protocol described in Doksani et al (Doksani et al., 2013) with minor modification: 5×10^6 nuclei (HT1080 super-telomerase cells with down-regulation of endogenous *TERF2* by siRNA and ectopic expression of TRF2 or Top-less) were isolated as described in Pipkin and Lichtenheld, 2006 (Pipkin and Lichtenheld, 2006), resuspended in 1 ml of NWB (10 mM Tris-HCl pH 7.4, 15 mM NaCl, 60 mM KCl, 5 mM EDTA, 300 mM sucrose), and incubated in a 3.5 cm dish, on ice, in the dark, while stirring for 5 min with 100 µg/ml Trioxsalen (SIGMA). Nuclei were exposed to 365 nm UV light at 2 cm from the light source (model UVL-56, UVP) for 30 min, while stirring on ice. After crosslinking, nuclei were collected, washed once with ice-cold NWB, and resuspended in 250 µl of NWB. For spreading, nuclei were diluted 1:10 in spreading buffer (10 mM Tris-HCl 7.4, 10 mM EDTA, 0.05% SDS, 1 M NaCl, pre-warmed at 37°C) and 100 µl of the suspension was immediately spread on a 18 mm diameter 1.5H coverslip (Marienfeld) using a Shandon Cytospin 3 (600 rpm, 1 min, medium acceleration). Samples were fixed in methanol at −20°C for 10 min followed by 1 min in acetone at −20°C. The coverslips were washed in PBS 1x and dehydrated through a 70%, 95%, 100% ethanol series before performing FISH.

Fluorescence in situ hybridization

The PNA probe [CCCTAA]3, conjugated with Alexa Fluor 647 fluorophore (PNA Bio INC.), was resuspended in water at a stock concentration of 20 µM and diluted 1:100 in the hybridization buffer solution (70% formamide, 10 mM Tris-HCl pH 7.2, 1:10 blocking buffer) before FISH labeling. 10 µl of this solution was put on a glass slide and ethanol-dried samples on coverslips were then put on top of the drop. The slide-coverslip "sandwich" was placed at 80ºC for 10 min on heat block, with the slide-side facing the block, to allow DNA denaturation.

Then the samples were put overnight in the dark at room temperature in a humidified box in order to let the hybridation reaction to occur. The coverslip was then removed from the slide and washed twice for 15 min with 70% formamide; 10 mM Tris-HCl pH 7.2 and 3 times for 5 min with 0.1 M Tris-HCl pH 7.2, 0.15 M NaCl, 0.08% Tween-20, at room temperature and finally with PBS 1x. YOYO-1 (1:20000 in PBS1x) was dropped on samples and immediately washed with PBS 1x. Coverslips were then covered with PBS1x and directly used for imaging.

dSTORM imaging and analysis

The stained coverslips were imaged the same day at room temperature in a closed chamber (Ludin Chamber, Life Imaging Services) mounted on an inverted motorized microscope (Nikon TI-E) equipped with a 100x 1.49 NA PL-APO objective and a Perfect Focus System (Nikon), allowing long acquisition in oblique illumination mode. Imaging was performed in an extracellular solution containing reducing agents and oxygen scavengers. For dSTORM, Alexa-647 was first converted into dark state using a 642 nm laser (Coherent) at 30–50 kw/cm2 intensity. Once the ensemble fluorescence was converted into the desired density of single molecules per frame, the laser power was reduced to 7–15 kw/cm2 and imaged continuously at 10 fps for 5,000 frames. The level of single molecules per frame was controlled by using a 405 nm laser (Omicron). The laser powers were adjusted to keep an optimal level of stochastically activated molecules during the acquisition. Single molecule fluorescence was collected by a TIRF-Quad filter set 405/488/561/640 (F66-04TN from AHF analysentechnik AG). The fluorescence was collected using a 512x512 EMCCD (Evolve, Photometrics). The acquisition and localization sequences were driven by MetaMorph 7.8.3 and Wavetracer 1.5 software (Molecular Devices) in streaming mode at 10 frames per second (100 ms exposure time) using the full chip of the camera. Single molecule localization and re-construction were performed offline using Wavetracer and GPU acceleration. The reconstructed images where analyzed by

Image-J software (Rasband, W.S., ImageJ, U. S. National Institutes of Health, Bethesda, Maryland, USA, http://imagej.nih.gov/ij/, 1997-2014) taking into account only the objects having a length ≥ 1500 μm (corresponding to 5000 bp). Molecules having gaps longer than 0.5 μm and kinked, knobbed-like or branched molecules were not scored as in Doksani et al. (Doksani et al., 2013).

Western blots

A total of 30 μg of total extract was loaded on a 4-20% acrylamide gradient SDS gel in Laemmli buffer. After separation, proteins were transferred on an Immobilon-FL PVDF membrane (Millipore) and TRF2 was revealed using an anti-TRF2 primary antibody from mouse (Imgenex IMG-124A) and an IRdye-labeled goat anti-mouse antibody (Li-Cor) under the conditions recommended by the supplier. Bands were revealed using the Odyssey apparatus and corresponding software (Li-Cor). For shelterin proteins, the following antibodies were used: Rabbit Polyclonal anti-TRF1 (Santa Cruz Biotechnology, Inc., sc-6165-R); Rabbit Polyclonal anti-POT1 (Novus Biologicals, NB100-56429); Rabbit Polyclonal anti-TPP1 (Bethyl Laboratories, Inc., A303-069A): Rabbit Polyclonal anti-TIN2 (Abcam, ab64386); Rabbit Polyclonal anti-RAP1 (Bethyl Laboratories, Inc., A300-306A); Rabbit Monoclonal anti-CHK2 (phospho T68), Abcam ab32148); Mouse Monoclonal anti-CHK2 (BD Biosciences, 611571).

Chromatin immunoprecipitation

Anti-Myc ChIP was performed as described previously (Simonet et al., 2011) with minor modifications. Briefly, HeLa cells were cross-linked for 12 min with 1% formaldehyde and washed with cold PBS. Cells were centrifuged and the pellet was resuspended in cell lysis buffer (5 mM PIPES pH8, 85 mM KCl, 0.5% NP40 and protease inhibitors). The cells were disrupted with a dounce homogenizer and centrifuged at 4°C. The pellet was resuspended in nucleus lysis

buffer (50 mM Tris-HCL pH 8, 10 mM EDTA, 1% SDS, protease inhibitors) and cells were sonicated using a Bioruptor to obtain an average fragment size of 400 bp. IPs were set up with 40 µg of DNA, and Myc-Tag (9B11 Cell Signaling, mouse) and H3 (1791 abcam, rabbit polyclonal) antibodies were incubated overnight. Magnetic beads (Dynabeads, Life Technologies) were added for 2 hours. The beads were washed with a low salt buffer (150 mM NaCl, 1% Triton X-100, 0.1% SDS) and a high salt buffer (500 mM NaCl, 1% Triton X-100, 0.1% SDS), followed by a lithium salt buffer (0.25 M LiCl, 1% NP40, 1% deoxycholic acid). Chromatin was eluted with 1% SDS and 0.1 M $NaHCO_3$ solution, and the cross-link was reversed at 65°C overnight. The DNA was treated with RNase for 20 min, proteinase K for 1 hour at 50°C, prior to phenol-chloroform purification, and ethanol precipitation. DNA samples were dissolved in TE buffer, blotted onto a N+ Hybond membrane (GE Healthcare) using a slot blot apparatus, and hybridized with the same probe as used for the trioxsalen experiments. Membranes analysis was performed as described for trioxsalen experiments. For TRF2, RAP1 and TIN2 ChIP the following antibodies were used: Rabbit polyclonal anti-RAP1 from Bethyl (A300-306A); Rabbit polyclonal anti-TIN2 from Abcam (ab64386); Rabbit polyclonal anti-TRF2 from Novus Biologicals (NB110-57130).

TERRA slot blot

RNA was extracted from 5 million HeLa cells treated (or not) with doxycycline as described above and transduced by the Empty, TRF2, or Top-less expressing vectors (see below for transduction conditions) using the RNAeasy kit from Qiagen. RNA (20 µg) from each condition was digested with 2 units of RNase free DNaseI (New englend Biolabs) at 37°C for 10 min and heated at 75°C for 10 min. From these, 10 µg were digested with 1 µg of RNase (Life Technologies) at 37°C for 10 min. A total of 5 µl of 5× loading buffer (80 mM MOPS, 6 mM

EDTA, 2.6% formaldehyde, 30% formamide, 20 mM sodium acetate) was added and the samples were heated at 75°C for 10 min before slot blotting using a N+ Hybond membrane (GE Healthcare). Before and after slot blotting, wells were washed with 200 µl of 10x SSC. After UV crosslinking of the membrane and baking at 80°C during 15 min, bands were revealed by sequential hybridization in Church buffer with a telomeric probe (the same used for Trioxsalen experiments) and a probe obtained from a 500-bp fragment corresponding to the sequence of the human 26S RNA (precursor of 18S RNA (Vincent et al., 1993)). Membranes analysis was performed as described for trioxsalen experiments.

Immunofluorescence detection of telomere dysfunction-induced foci

Slides were fixed with 4% formaldehyde in PBS at room temperature for 10 min, and then incubated for 90 min with blocking buffer (PBS, 1% Triton X-100, 1% BSA and 5% Donkey serum), followed by incubation overnight at 4°C with anti-TRF1 (sc-6165; Santa Cruz Biotechnology) and anti-γH2AX (05-636; Upstate) antibodies. Cells were then washed with PBS and incubated with anti-rabbit Alexa488 (A21206; Molecular probes) and anti-mouse Alexa555 (A31570; Molecular probes) antibodies. After washing with PBS, the nucleus was labeled with DAPI (VECTASHIELD mounting medium with DAPI, Vector Laboratories). For IF-PNA FISH labelling, slides were first treated as above using a rabbit anti-53BP1 antibody (NB100-305; Novus Biological) followed by a goat anti-rabbit Alexa 488 antibody (111-545-144; Jackson ImmunoResearch) then fixed again with 4% formaldehyde in PBS at room temperature for 2 min, de-hydrated by successive incubation in 50%, 75% and 100% ethanol for three min. Hybridization was performed at 80°C in70% Formamide, 10 mM Tris pH 7.2 for three min followed by an incubation overnight at room temperature. Slides were washed first in the Formamide, Tris solution above, then in a 150 mM NaCl, 50 mM Tris pH 7.5 solution and finally PBS. Mounting was performed as above.

IF images were produced using a Zeiss LSM 5 Exciter confocal laser scanning microscope (Zeiss, Jena, Germany) and analyzed using the ZEN software. PNAFISH/IF images were obtained on a DeltaVision Elite microscope (GE Healthcare).

Metaphase spreads analysis

For chromosome analysis, cells were arrested in metaphase for 3 hours at 37ºC with 50 ng/ml of colcemid (KaryoMAX, Invitrogen). Cells were incubated for 15 min at 37ºC in hypotonic solution (75 mM KCl), fixed in methanol:acetic acid (3:1), and spread on cold, wet, ethanol-cleaned slides. Slides were fixed in 4% formaldehyde in PBS for 2 min, washed in PBS, digested with pepsin (0.5 mg/ml, 0.01 N HCl) for 10 min at 37ºC, washed in PBS, fixed in 4% formaldehyde in PBS for 2 min, washed in PBS, dehydrated in increasing concentrations of ethanol, and air-dried. Hybridization was then performed using FITC-conjugated $(CCCTAA)_3$ PNA probe (Panagene) diluted at 50 nM in 70% formamide, 10 mM Tris-HCl (pH7.2), and 1% blocking reagent (Roche). Slides were denatured at 80ºC for 3 min at room temperature, and hybridization was performed at room temperature in a moist chamber in the dark for 2 hours. Slides were washed twice for 15 min in 70% formamide and 10 mM Tris-HCl (pH 7.2) and three times for 5 min in 50 mM Tris-HCl pH 7.5, 150 mM NaCl, and 0.05% Tween-20 at room temperature. Slides were washed in PBS and mounted in VECTASHIELD with DAPI (Vector laboratories).

Metaphase spreads were visualized on an epifluorescence Axioimager Z2 microscope and analyzed using the metasystem ISIS software.

2D gels

DNA (5 µg) extracted from HeLa cells treated with or without doxycycline as described above and transduced with Empty, TRF2, or Top-less expressing vectors was migrated on an 0.5% agarose in 1× TBE (15-cm gel at 130 V) until the xylene dye was 2 cm from the bottom of

the gel. Bands were cut and placed horizontally for a second-dimension electrophoresis performed in 0.5 µg/ml ethidium bromide and 1× TBE (both in the gel and the running buffer). Markers were run beside each sample band. Migration was performed at 50 V for 14 hours. After migration, DNA was transferred onto a membrane, telomeric DNA was revealed and data were analyzed as above (Trioxsalen experiments).

Overhang assay

The overhang assay was adapted from van Steensel *et al.*, 1998 (van Steensel et al., 1998). Briefly, 10 µg of genomic DNA from HT1080 cells expressing sh*TERF2* and transduced with either the Empty vector or vectors expressing the TRF2 or Top-less proteins (see above) were digested with 125 and 175 units of HinfI and RsaI (Promega), respectively, overnight at 37°C. After ethanol precipitation, the samples were divided in two; half was digested with 100 units of *E. coli* Exonuclease I (New England Biolabs) for 5 hours at 37°C. All samples were hybridized with 0.2 pmoles of a ^{32}P end-labeled single-stranded $(CCCTAA)_3$ probe overnight at 50°C. Hybridized samples were loaded on a 10-cm-long, 0.9% 1× TBE agarose gel and migrated at 6 V/cm for 75 min at room temperature. The gel was then dried on 3 MM paper for 4 hours at 40°C and exposed on a phosphorimager screen. Analysis was performed as described above on a Typhoon 9500. For denaturing conditions, an in-gel denaturing hybridization was performed on the dried gel, as described previously (Karlseder et al., 2002).

References

Amiard, S., Doudeau, M., Pinte, S., Poulet, A., Lenain, C., Faivre-Moskalenko, C., Angelov, D., Hug, N., Vindigni, A., Bouvet, P., *et al.* (2007). A topological mechanism for TRF2-enhanced strand invasion. Nat Struct Mol Biol *14*, 147-154.

Bustamante, C., Keller, D., and Yang, G. (1993). Scanning force microscopy of nucleic acids and nucleoprotein assemblies. Current opinion in structural biology *3*, 363-372.

Chen, D., Bowater, R., Dorman, C.J., and Lilley, D.M. (1992). Activity of a plasmid-borne leu-500 promoter depends on the transcription and translation of an adjacent gene. Proceedings of the National Academy of Sciences of the United States of America *89*, 8784-8788.

Doksani, Y., Wu, J.Y., de Lange, T., and Zhuang, X. (2013). Super-resolution fluorescence imaging of telomeres reveals TRF2-dependent T-loop formation. Cell *155*, 345-356.

Karlseder, J., Smogorzewska, A., and de Lange, T. (2002). Senescence induced by altered telomere state, not telomere loss. Science *295*, 2446-2449.

Nettikadan, S., Tokumasu, F., and Takeyasu, K. (1996). Quantitative analysis of the transcription factor AP2 binding to DNA by atomic force microscopy. Biochem Biophys Res Commun *226*, 645-649.

Pipkin, M.E., and Lichtenheld, M.G. (2006). A reliable method to display authentic DNase I hypersensitive sites at long-ranges in single-copy genes from large genomes. Nucleic acids research *34*, e34.

Poulet, A., Buisson, R., Faivre-Moskalenko, C., Koelblen, M., Amiard, S., Montel, F., Cuesta-Lopez, S., Bornet, O., Guerlesquin, F., Godet, T., *et al.* (2009). TRF2 promotes, remodels and protects telomeric Holliday junctions. EMBO J *28*, 641-651.

Poulet, A., Pisano, S., Faivre-Moskalenko, C., Pei, B., Tauran, Y., Haftek-Terreau, Z., Brunet, F., Le Bihan, Y.V., Ledu, M.H., Montel, F., *et al.* (2012). The N-terminal domains of TRF1 and TRF2 regulate their ability to condense telomeric DNA. Nucleic acids research *40*, 2566-2576.

Rivetti, C., and Codeluppi, S. (2001). Accurate length determination of DNA molecules visualized by atomic force microscopy: evidence for a partial B- to A-form transition on mica. Ultramicroscopy *87*, 55-66.

Simonet, T., Zaragosi, L.E., Philippe, C., Lebrigand, K., Schouteden, C., Augereau, A., Bauwens, S., Ye, J., Santagostino, M., Giulotto, E., *et al.* (2011). The human TTAGGG repeat factors 1 and 2 bind to a subset of interstitial telomeric sequences and satellite repeats. Cell Res *21*, 1028-1038.

van Steensel, B., Smogorzewska, A., and de Lange, T. (1998). TRF2 protects human telomeres from end-to-end fusions. Cell *92*, 401-413.

Vincent, S., Marty, L., and Fort, P. (1993). S26 ribosomal protein RNA: an invariant control for gene regulation experiments in eucaryotic cells and tissues. Nucleic acids research *21*, 1498.

3. Article 2

Human RAP1 prevents telomere fusion in senescent cells

Lototska L[1], Songyang Z[2], Royle NJ[3], Jing Ye[4], Mendez-Bermudez A[1,4]*, Gilson E[1,4,5]*

1 Université Côte d'Azur, CNRS, INSERM, IRCAN, Faculty of Medicine Nice, France.
2 Verna and Marrs McLean Department of Biochemistry and Molecular Biology, Baylor College of Medicine, One Baylor Plaza, Houston, TX 77030, USA.
3 Department of Genetics, University of Leicester, Leicester, United Kingdom.
4 International Laboratory in Hematology and Cancer, Shanghai Jiao Tong University/ CNRS/INSERM/University Côte d'Azur, Shanghai, P.R. China.
5 Department of Genetics, CHU; Nice, France.
*Co-corresponding, co-senior authors

SUMMARY

RAP1 is an evolutionary conserved telomeric protein between yeast and mammals. Although yeast Rap1 is a key telomere capping protein preventing NHEJ and consequently telomere fusions (Pardo B. and Marcand S., 2005), and mammalian RAP1 protects against NHEJ *in vitro* (Bae NS. and Baumann P., 2007; Sarthy J. et al., 2009), its role at mammalian telomeres *in vivo* is still controversial (Sfeir A. et al., 2010; Kabir S. et al., 2014; Martinez P. et al., 2016). An emerging view is that RAP1 behaves as a backup anti-fusion factor in mammalian cells when its interacting partner, TRF2, is dysfunctional (Benarroch-Popivker D. et al., 2016; Rai R. et al., 2016) or upon telomerase inhibition in mice (Martinez P. et al., 2016).

Here we demonstrate that RAP1 is required to protect telomeres specifically in replicative senescent human cells. Downregulation of RAP1 in these cells, but not in young or dividing pre-senescent cells, leads to telomere uncapping and fusions. The anti-fusion effect of RAP1 was further explored in a HeLa cell line when the RAP1 gene can be invalidated by doxycycline (Kim H. et al., 2017). The invalidation of RAP1 in these cells gives rise to telomere fusions only upon telomerase inhibition by BIBR1532 treatment. We further showed that the fusions triggered by RAP1 loss are dependent upon ligase IV, indicating that they are generated through classical NHEJ between telomere ends.

Keywords: Telomeres, RAP1, NHEJ, chromosome fusions, replicative senescence

RESULTS

RAP1 is specifically required for telomere protection in senescent fibroblasts.

We passaged human primary lung fibroblasts (MRC-5) at 5% oxygen and we performed western blotting at different population doublings to determine the levels of RAP1 and TRF2 expression (Supplementary Fig.1A). While, as expected (Fujita K. et al., 2010; Lou Z. et al., 2015) the TRF2 levels greatly decreased (around 80%) in senescent cells, the levels of RAP1 remained nearly constant, suggesting an important role played by RAP1 in these cells. Thus, we asked whether RAP1 is required for telomere protection in senescent cells. The expression of an shRNA against RAP1 in young and senescent cells efficiently downregulated its expression (Supplementary Fig. 1B). In order to monitor telomere protection, we performed Telomere Dysfunction Induced Foci (TIF) assays by analyzing the colocalization of 53BP1, a DNA damage response (DDR) protein, with a telomeric PNA probe (Fig. 1A-B). The rate of TIFs augmented with increasing the number of cell divisions as previously reported (Herbig U. et al., 2004; Kaul Z. et al., 2011; Suzuki M. et al., 2012; Fumagalli M. et al., 2014). In agreement with previous studies failing to detect telomere dysfunction upon RAP1 disruption (Martinez P. et al., 2010; Sfeir A. et al., 2010; Kabir S. et al., 2014) the downregulation of RAP1 in young and pre-senescent cells does not increase the rate of TIF. However, the TIF rate significantly increased in fully senescent RAP1-compromised cells, revealing that RAP1 takes over telomere protection against DNA damage checkpoint activation specifically in senescent cells (Fig. 1A-B). Telomere length analysis does not show telomere length alterations due to RAP1 loss,; thus, the increase of TIFs is unlikely to be the consequence of an excess of telomere shortening in RAP1-compromised cells(Supplementary Fig. 1.C-D).

RAP1 prevents telomere fusions in senescent fibroblasts.

Then we investigated whether RAP1 also protects telomeres of senescent cells from telomere fusions by using a PCR-based method that relies on subtelomeric DNA primers which are used to amplify fusions between different chromosome ends (Supplementary Fig. 2A) (Capper R. et al., 2007; Letsolo BM. et al., 2010). We performed PCR reactions with a set of three different subtelomeric primers that in total bind to the ends of approximately 22 chromosomes. Nearly no chromosome fusions were detected in young fibroblasts (fusion frequency of $1.5x10^{-5}$; Fig. 2A-B and Supplementary Fig. 2B-C) with a modest increase in pre-senescent cells (frequency of $4.5x10^{-5}$). These low rates of telomere fusion were not

increased upon RAP1 downregulation. In contrast, senescent cells were characterized by nearly 10 times higher fusion frequency as compared to young cells (frequency of $1.4x10^{-4}$), a frequency further increased upon RAP1 downregulation (frequency of $2.6x10^{-4}$).

RAP1 protects critically short telomeres from fusion.

To determine whether the RAP1-dependent telomere protection observed in senescent cells is due to the appearance of critically short telomeres, we used a HeLa cell line with a doxycycline-inducible knockout allele of RAP1 (Kim H. et al., 2017). We treated cells with doxycycline for 15 days with or without the telomerase inhibitor BIBR1532 (Fig. 3A). As expected, BIBR1532 caused a notable decrease in telomere length (Fig. 3B). Similar to MRC-5 senescent cells (Supplementary Fig. 1D-E), no further length shortening was observed when RAP1 was inhibited (Fig. 3B) even when critically short telomeres were assayed by single telomere length analysis (STELA) of the XpYp telomere (Baird DM. et al., 2003) (Supplementary Fig. 3A).

The PCR-based telomere fusion assay revealed that RAP1 downregulation triggers an increase in fusion frequency only in HeLa cells treated with BIBR1532 (Fig. 3C and Supplementary Fig. 3B). Next, we ask whether the fusions were the result of the classical or alternative NHEJ pathway by depleting DNA ligase IV (*LIG4*) or DNA ligase III (*LIG3*) respectively (Fig. 3C and Supplementary Fig. 3C-E) (Oh S. et al., 2014). Only cells downregulated for *LIG4* were insensitive to RAP1 inhibition showing that, at least in part, the fusions triggered by RAP1 loss are dependent on the classical NHEJ pathway. Notably, in-gel telomere overhang assays in HeLa cells upon RAP1 invalidation did not show an obvious reduction in the 3' overhang length (Supplementary Fig. 3F-G) suggesting the telomere fusions triggered by RAP1 inhibition do not result from the appearance of blunted telomere ends.

Then, we analyzed the telomere abnormalities triggered by RAP1 inhibition in metaphase spreads of HeLa cells treated with BIBR1532 (Fig. 3D-F). Consistent with the fusion-PCR results, HeLa cells treated with BIBR1532 and doxycline exhibit an increase in the frequency of telomere fusions. Notably, RAP1 inhibition did not lead to telomere fragility (as recorded by multiple telomere signal or MTS) nor to telomere shortening.

Overall, these results indicate that RAP1 is required to protect critically short telomeres from classical NHEJ-mediated fusions, providing an explanation for the specific anti-fusion

role of RAP1 in senescent cells. A similar observation was made by Martinez and colleagues in a double RAP1/TERT knockout mice (Martinez P. et al., 2016).

Reversal of senescence is impaired in RAP1 compromised senescent fibroblasts.

Finally, we asked whether RAP1 inhibition could impair the return to growth of senescent cells in case of checkpoint failure. Since it is possible to reverse replicative senescence through p53 inactivation (Beauséjour C. et al., 2003), senescent human primary fibroblasts were infected with either an shRNA against $p21^{CIP1}$ ($shp21^{CIP1}$) or $shp21^{CIP1}$+shRAP1 (Fig. 4A). After approximately 10 days post infection, most of the $shp21^{CIP1}$ transduced cells restarted proliferation while losing their SA-β-gal staining (Fig. 4B). In contrast, the number of $shp21^{CIP1}$+shRAP1 cells decreased without losing their SA-β-gal staining (Fig. 4B). It is likely that the impaired restart of RAP1 compromised cells results from an increased rate of telomere aberrations. We conclude that senescent cells maintain a level of RAP1 expression sufficient to allow them to restart proliferation in case of checkpoint failure.

DISCUSSION

Here we demonstrate that the downregulation of RAP1 in human primary cells that have reached their replicative capacity give rise to telomeric fusions that are dependent on the classical NHEJ ligase IV repair pathway. Several studies in mouse and human cells have failed to detect a role for RAP1 in telomere protection (Martinez et al., 2010; Sfeir et al., 2010, Kabir et al., 2014). For instance, this was our case in young or pre-senescent cells where depletion of RAP1 did not have an adding effect on telomere fusions. The importance of the anti-fusion role of RAP1 was only evident when telomeres were shorter, in one case upon senescence and in another in HeLa cells treated with the telomerase inhibitor BIBR1532. Upon RAP1 depletion (Supplementary Fig. 3D-E and Fig. 3B), we observe neither telomere length shortening nor signs of telomere dysfunction apart from telomere fusions (Fig. 3D-F).

Altogether, our results unveil that during replicative senescence of human cells, the telomeres switch from a RAP1-independent to a RAP1-dependent mode of telomere protection. We propose that this switch is triggered by the appearance of short telomeres

unable to fold into t-loops, which is likely to be the main anti-DNA damage repair mechanism mediated by TRF2 in young cells (Fig. 4C).

The PCR-base method used on this study to detect fusion events relies on the use of sub-telomeric primers. We used three subtelomeric primers in the same PCR reaction to increase the probability of fusion detection. The minimum predicted size of a fusion detected using the 16p probe (e.g. Fig. 2B) is around 7kb, however the majority of the amplicons were shorter than that. This would imply that at least one of the telomeres that fused has no telomeric repeats and even more some of the sub-telomeric DNA should be eroded as reported previously (Capper R. et al., 2007).

Martinez and colleagues (2016) showed that RAP1 has a protective role on mouse telomeres but only in Terc-/- mice. In contrast to our cellular settings, telomere shortening was accelerated in double knockout mice (Terc-/-, Rap-/-) compared to Terc-/-. This accelerated telomere shortening upon RAP1 depletion gave rise to an increased number of telomere aberrations such as fusion events, signal free ends, multiple telomere signal and telomere sister chromatid exchanges. Together with our results, RAP1 appears to have the capability to protect against telomere fusions by different mechanisms: by inhibiting classical NHEJ (this study) and by preventing homologous recombination at chromosome ends resulting in fusogenic telomere-free ends (Rai R. et al., 2016; Martinez P. et al., 2016).

Interestingly, RAP1 has been shown to interact with the Sun1, a member of the LINC (Linker of Nucleoskeleton and Cytoskeleton) complex and to tether telomeres to the nuclear envelope specifically just after mitosis (Crabbe L et al., 2012). It is therefore possible that the depletion of RAP1 in arrested senescent cells, or in cells with short telomeres, released the telomeres from the nuclear periphery making them more mobile and prone to fusions.

A downregulation of RAP1 in senescent fibroblasts forced to divide due to checkpoint inhibition caused a massive cell death. One explanation could be that accumulated fused chromosomes in the double RAP1 and $p21^{CIP1}$ knockdown condition may trigger mitotic catastrophe, which has been described as a mechanism of cell death occurring during or after aberrant mitosis (Vakifahmetoglu H. et al., 2008).

Our findings reveal that RAP1 acts as a mechanism of telomere protection specifically in replicative senescent cells. Whether this telomere capping role of RAP1 drives its conservation through evolution as a constitutive telomeric protein raises the question of the physiological rationale to prevent telomere fusions in senescent cell.

Figure legends

Figure 1. DDR at telomeres in MRC-5 of different population doublings. A. TIF analysis. Bars represent SEM of 2 independent experiments of approximately 40-50 cells per condition. P-value was obtained by two-tailed Mann–Whitney U test ($p=0.0053$).
B. Representative images of IF-FISH with anti-53BP1 antibody and telomeric PNA probe in young (pd 26), pre-senescent (pd 66), senescent (pd 72 + 4 weeks) fibroblasts. RAP1 expression was abolished by shRNA (shRAP1).

Figure 2. Frequency of fusions in human primary fibroblasts. A. Fusion frequencies were measured by means of telomere fusion assay with 3 subtelomeric primers in the same reaction (21q1, XpYpM and 16p1). B. Representative membranes hybridized with the 16p probe are shown.

Figure 3. Telomere fusions in HeLa upon inducible RAP1 knockout. A. Western blotting with anti-RAP1 and tubulin antibodies to evaluate the efficiency of knockout, which was induced by doxycycline (DOX; 1ug/ul final concentration) treatment for 15 days. Cells were treated selectively with the telomerase inhibitor BIBR1532 for 25 days. B. Southern blot (teloblot) hybridized with a telomeric probe to evaluate the efficiency of BIBR1532. C. Frequency of fusions in HeLa cells. D. Percentage of end-to-end fusions observed in HeLa knockout vs control upon BIBR1532 treatment. Number of chromosomes analyzed per condition: -DOX = 1366, +DOX = 1474. E. Percentage of other chromosome aberrations obtained from the conditions described in D. F. Examples of chromosome aberrations observed in D and E.

Figure 4. Return to growth of post-senescent MRC-5 cells. A. Growth curves of MRC-5 fibroblasts. After reaching replicative senescence, cells were infected either with shp21CIP1 or shp21CIP1+shRAP1 and harvested 15 days post infection. B. SA-β-gal assay in senescent and post-senescent fibroblasts (day 0 and 15 of lentivirus infection). Approximately 300 cells were analyzed per condition. Percentage of SA-β-gal positive cells is indicated for each condition. C. Model of RAP1 telomere protection in young and senescent cells.

Supplementary Figure 1. RAP1 is associated with telomeres in young and senescent human fibroblasts. A. Expression of RAP1 and TRF2 in MRC-5 cells of different population doublings (pd) measured by western blotting with the anti-RAP1 and anti-TRF2 antibodies. Young corresponds to pd 26, pre-senescent to pd 66, senescent to pd 72. Senescent cells were left in culture for further 3 weeks (pd 72 + 3 weeks). B. Western blots of RAP and tubulin of young MRC-5 (pd 28) upon RAP1 knockdown. C. Southern blotting showing the telomere length of young (pd 26) and senescent cells (pd 72 + 3 weeks) upon shRAP1 treatment for 10 days. D. STELA at the Xp/Yp telomere of senescent cells transduced with either a control vector or an shRAP1 expressing vector.

Supplementary Figure 2. A. Location of the primers and probes used for telomere fusion pcr: red arrows indicate positions of subtelomere pcr primers, black arrows stand for the primers used to generate DNA probes for further hybridization with the southern blot membranes. B-C. Representative membranes of the telomere fusion assay as performed in Fig.2.

Supplementary Figure 3. Neither increase in critically short telomeres nor telomere overhang shortening occurs upon RAP1 knockdown. A. STELA assay with the XpYp probe in HeLa cells. Average telomere length and percentage of critically short telomeres (below 1.5 kb) are indicated for each sample on the images of the gels. B-C. Representative fusion PCR blots in HeLa hybridized with either the Xp/Yp probe (B) or with the 16p probe (C). The conditions used in the assay are indicated. D-E. Relative mRNA levels of LIG3 and LIG4 measured by qPCR (corresponding to the experiment shown in Fig.3). Error bars represent SD. P-values obtained by paired t-test (*** p=0.0001 for shLIG3 and **p=0.0061 for shLIG4). F. Quantification of normalized telomere overhang signal was done by dividing signal intensity obtained by native gel hybridization to the total signal obtained with denatured gels. G. Images of native and denatured gels that represent telomere overhang assay in HeLa cells.

Materials and methods

Cell lines and reagents. MRC-5 human primary lung fibroblasts were obtained from ATCC. MRC-5 cells were grown in DMEM supplemented with 10% fetal bovine serum penicillin (100 IU/ml), and streptomycin (100 μg/ml) at 37°C 5% CO2, 5% O2. HeLa CRISPR/Cas9

engineered cell line with the doxycycline inducible knockout of RAP1 was a gift from Dr. Songyang (Kim et al., 2017). Cells were grown in DMEM with 10% tetracycline-free serum. To induce knockout of RAP1, we treated cells for 15 days with doxycycline (2 μg/mL, Sigma). Telomere shortening was selectively induced by treatment with the telomerase inhibitor BIBR1532 (20 μM, Merck).

Lentivirus production and infection. Lentiviruses were produced by transient calcium phosphate transfection of 293T cells with the virus packaging plasmids, p8.91 and pVSVg, as well as with the lentiviral expression vector that contained the sequence of interest. Titration was performed approximately 10 days after infection by means of puromycin (1 μg/ml) selection of clones.

The following shRNA plasmids were purchased from Sigma and used for lentivirus production: pLKO-shScramble, pLKO-shTERF2IP, pLKO-shp21^{CIP1}, pLKO-shLIG3, pLKO-shLIG4. Infection with various shRNAs was performed for a minimum of 4 days, and depending on experiment cells were kept in culture for up to 10-15 days after infection (10 days for telomere fusion assay in MRC-5, 15 days – for post-senescent cells). Efficiency of each shRNA was checked routinely by RT-qPCR or western blotting.

Antibodies. The following antibodies were used for western blotting: rabbit polyclonal anti-RAP1, 1:5000 (Bethyl Laboratories, Inc., A300-306A), rabbit polyclonal anti-TRF2, 1:5000 (Novus

Biologicals, NB110-57130), mouse monoclonal anti-α-tubulin, 1:2000 (Merck, T9026), rabbit polyclonal anti-GAPDH, 1:1000 (Novus Biologicals 100-56875), mouse monoclonal anti-p21, 1 μg/ml (Abcam, ab16767), HRP goat anti-mouse IgG, 1:10 000 (Vector Laboratories, PI-2000) and HRP goat anti-rabbit IgG, 1:10 000 (Vector Laboratories, PI-1000).

For immunofluorescence we used the next antibodies: rabbit polyclonal anti-53BP1, 1:250 (Novus Biologicals, NB100-305), goat anti-rabbit Alexa 488 antibody, 1:400 (111-545-144; Jackson ImmunoResearch).

Primers. For RT-qPCR we used the following primers: TERF2IP-F: CGGGGAACCACAGAATAAGA, TERF2IP-R: CTCAGGTGTGGGTGGATCAT, 36B4-F: AACTCTGCATTCTCGCTTCCT, 36B4-R: ACTCGTTTGTACCCGTTGATG, p21^{CIP1}-F:

TGGTAGGAGACAGGAGACCT, p21^{CIP1}-R:AATACTCCCCACATAGCCCG, LIG3-F: GAT CAC GTG CCA CCT ACC TTG T, Lig3-R: GGC ATA GTC CAC ACA GAA CCG T, LIG4-F: CAC CTT GCG TTT TCC ACG AA-3, LIG4-R: CAG ATG CCT TCC CCC TAA GTT G.

Primers used for telomere fusion assay: *21q1: 5′-CTTGGTGTCGAGAGAGGTAG-3′, *16p1: 5′-TGGACTTCTCACTTCTAGGGCAG-3′, *XpYpM: 5′-ACCAG GTTTTCCAGTGTGTT-3′. Primers for generation of subtelomeric DNA probes: XpYpO: 5′-CCTGTAACGCTGT TAGGTAC-3′, XpYpG: 5′-AATTCCAGACACACTAGGACCCTGA-3′, 21qseq1: 5′-TGGTCTTATACACTGTGTTC -3′, 21qsq1rev: 5′-AGCTAGCTATCTACTCTAACAGAGC-3′, 16p2: 5′- TCACTGCTGTATCTCCCAGTG -3′, 16pseq1rev: 5′-GCTGGGTGAGCTTAGAGAGGAAAGC-3′.

Primers used for STELA: XpYpE2: TTGTCTCAGGGTCCTAGTG, telorette: TGCTCCGTGCAT CTGGCATCTAACCCT, teltail: TGCTCCGTGCATCTGGCATC.

RNA extraction RT-qPCR. Total RNA was extracted following instructions of the RNeasy Mini Kit (Qiagen), and then 1 ug of RNA was reverse transcribed into cDNA using the High-Capacity RNA-to-cDNA kit (Thermo Scientific). Each qPCR reaction contained 10x diluted cDNA, 0.2 μM primers and SYBR green master mix (Roche, 4913914 001).

DNA extraction. Genomic DNA was extracted either by proteinase K, RNase A and phenol/ chloroform followed by ethanol precipitation (Sambrook, 1989) or following instructions of DNA Blood and Tissue Kit (Qiagen).

Telomere fusion assay. We performed telomere fusion assay as described before (Capper R. et al., 2007; Letsolo BT. et al., 2010) with some modifications. Shortly, genomic DNA was digested with EcoRI (Promega), and accurate concentrations were measured using Qubit fluorometer (Thermo Fisher Scientific). For each sample at least 16 PCR reactions were performed using 50 ng of DNA per reaction, a mix of subtelomeric primers (21q1, 16p1, XpYpM) 0,2 μM each and the FailSafe™ PCR System (Lucigen) under following conditions: 26 cycles of 94 °C for 15 s, 58 °C for 30 s, and 68 °C for 10 min. PCR products were resolved on the 0,8 % agarose gel followed by southern blotting. Nylon membranes were hybridized with the corresponding radioactively labeled (αP32 dCTP) subtelomeric probes and a DNA ladder probe (SmartLadder MW-1700-10, Eurogentec), exposed and revealed on the Typhoon FLA 9500 Phoshphorimager (GE Healthcare Life Sciences). Molecular size of each of the

bands was calculated by ImageQuant TL 8.1 software (GE Healthcare Life Sciences). Fusion frequencies were estimated as the number of fused telomeres per genome (per 6pg of human diploid genome for MRC-5 or per 10 pg of DNA for HeLa cells).

STELA. We performed STELA as it was described by Baird DM and colleagues (Baird DM. et al., 2003) with some modifications. Shortly, total genomic DNA was digested with EcoRI, quantified by Qubit fluorometer (Thermo Fisher Scientific). A ligase reaction was performed with 10 ng DNA and telorette linker sequence by T4 DNA ligase. 250 pg of ligated DNA was used for PCR with telomere-adjacent (XpYpE2) and teltail primers, and the FailSafe™ PCR System (Lucigen). We cycled the reactions under the following conditions: 26 cycles of 94 °C for 15 s, 58 °C for 30 s, and 68 °C for 10 min. PCR products were resolved on 0,8% agarose gels followed by southern blotting. Hybridized membranes were exposed and the signal detected on the Typhoon FLA 9500 (GE Healthcare Life Sciences). Analysis was performed using the software designed by Lai and colleagues (Lai TP. Et al., 2017).

Teloblot. To measure telomere length we performed southern blot. Total DNA was digested with HinfI/RsaI (Promega), and 5 μg per sample were migrated on 1% agarose gels. After transfer of DNA to the N+ Hybond membrane (GE Healthcare), each membrane was hybridized with the telomeric DNA probe (purified 650-bp telomeric fragment) obtained by random priming using the Klenow large fragment enzyme and radioactively labeled (αP32) dCTP nucleotides. The signal was later revealed and analyzed using the Typhoon FLA 9500 (GE Healthcare Life Sciences).

Telomere overhang assay. The overhang assay was performed as described by Benarroch-Popivker et al., 2016 (Benarroch-Popivker et al., 2016). Briefly, 5 μg of genomic DNA from HeLa cells were
digested with HinfI and RsaI (Promega), and incubated with 0.2 pmoles of the radioactively end-labeled single-stranded (CCCTAA)3 probe overnight at 50°C. Hybridized samples were loaded into 0,9 % agarose gel and run at 6 V/cm for 75 min. The gel was then dried on 3 MM paper for 4 hours at 40°C and exposed on a phosphorimager screen. Telomere overhang signal was normalized to the total telomere signal, which was obtained by hybridization of the denatured gel with the same probe as the native gel. Analysis was performed using the Typhoon FLA 9500 (GE Healthcare Life Sciences).

Western blotting. Protein extracts were obtained by lysis in ice-cold RIPA buffer for 30 min followed by 30 min centrifugation at 4°C. 30 μg of proteins were separated on 4-20% acrylamide gradient SDS gels (BioRad), transferred on Amersham Protran 0.45 μm nitrocellulose membranes (GE Healthcare Life Sciences) for 90 min at 300 mA. Further the membranes were blocked in 5% skim milk in PBST buffer, and incubated thereafter with the primary and secondary antibodies. Membranes were developed using the Luminata Forte HRP substrate (Millipore) and exposed in the Fusion Solo apparatus (Vilbert Lourmat).

IF-FISH. Imunnofluorecence-FISH in MRC-5 cells and further analysis of the images were performed as described in Mendez-Bermudez A. et al., 2018 (Mendez-Bermudez A. et al., 2018). For FISH the following telomeric PNA probe was used: Cy3-OO-CCCTAACCCTAACCCTAA. For measuring DDR we used anti-53BP1 antibody.

Metaphase chromosome analysis. To obtain chromosome spreads, HeLa cells, treated selectively with BIBR1532 and doxycycline as described above, were arrested in metaphase using 50 ng/ml colcemid (KaryoMAX, Invitrogen) for 2 hours at 37ºC. Afterwards, trypsinized cells were incubated with hypotonic solution (75 mM KCl) for 15 minutes at 37ºC, fixed in ice-cold methanol : glacial acetic acid (3:1), and spread on slides. FISH with the telomeric PNA probe was performed as described above. Stained metaphase chromosomes were visualized on the Zeiss Axiovert Z2 epi-fluorescent microscope and analyzed using the metasystem ISIS software.

Senescence-associated β-galactosidase (SA-β-gal) assay. We measured the percentage of SA-β-B-gal positive cells to evaluate the percentage of senescent cells in culture. In order to do so, we used the Senescence Detection Kit (Abcam) following manufacturer instructions.

Statistics. Statistical analysis was performed by means of Prism 5 software (GraphPad). For comparison of two groups we used two-tailed Mann-Whitney U test, for multiple groups the Kruskal-Wallis test was used. P-values < 0.05 were considered significant (* $p < 0.01$, **$p < 0.001$, ***$p < 0.0001$).

REFERENCES

Bae, N. S. and Baumann, P. (2007) 'A RAP1/TRF2 complex inhibits nonhomologous end-joining at human telomeric DNA ends', *Mol Cell,* 26(3), pp. 323-34.

Baird, D. M., Rowson, J., Wynford-Thomas, D. and Kipling, D. (2003) 'Extensive allelic variation and ultrashort telomeres in senescent human cells', *Nat Genet,* 33(2), pp. 203-7.

Beauséjour, C. M., Krtolica, A., Galimi, F., Narita, M., Lowe, S. W., Yaswen, P. and Campisi, J. (2003) 'Reversal of human cellular senescence: roles of the p53 and p16 pathways', *EMBO J,* 22(16), pp. 4212-22.

Benarroch-Popivker, D., Pisano, S., Mendez-Bermudez, A., Lototska, L., Kaur, P., Bauwens, S., Djerbi, N., Latrick, C. M., Fraisier, V., Pei, B., Gay, A., Jaune, E., Foucher, K., Cherfils-Vicini, J., Aeby, E., Miron, S., Londoño-Vallejo, A., Ye, J., Le Du, M. H., Wang, H., Gilson, E. and Giraud-Panis, M. J. (2016) 'TRF2-Mediated Control of Telomere DNA Topology as a Mechanism for Chromosome-End Protection', *Mol Cell,* 61(2), pp. 274-86.

Capper, R., Britt-Compton, B., Tankimanova, M., Rowson, J., Letsolo, B., Man, S., Haughton, M. and Baird, D. M. (2007) 'The nature of telomere fusion and a definition of the critical telomere length in human cells', *Genes Dev,* 21(19), pp. 2495-508.

Crabbe, L., Cesare, A. J., Kasuboski, J. M., Fitzpatrick, J. A. and Karlseder, J. (2012) 'Human telomeres are tethered to the nuclear envelope during postmitotic nuclear assembly', *Cell Rep,* 2(6), pp. 1521-9.

Fujita, K., Horikawa, I., Mondal, A. M., Jenkins, L. M., Appella, E., Vojtesek, B., Bourdon, J. C., Lane, D. P. and Harris, C. C. (2010) 'Positive feedback between p53 and TRF2 during telomere-damage signalling and cellular senescence', *Nat Cell Biol,* 12(12), pp. 1205-12.

Fumagalli, M., Rossiello, F., Mondello, C. and d'Adda di Fagagna, F. (2014) 'Stable cellular senescence is associated with persistent DDR activation', *PLoS One,* 9(10), pp. e110969.

Herbig, U., Jobling, W. A., Chen, B. P., Chen, D. J. and Sedivy, J. M. (2004) 'Telomere shortening triggers senescence of human cells through a pathway involving ATM, p53, and p21(CIP1), but not p16(INK4a)', *Mol Cell,* 14(4), pp. 501-13.

Kabir, S., Hockemeyer, D. and de Lange, T. (2014) 'TALEN gene knockouts reveal no requirement for the conserved human shelterin protein Rap1 in telomere protection and length regulation', *Cell Rep,* 9(4), pp. 1273-80.

Kaul, Z., Cesare, A. J., Huschtscha, L. I., Neumann, A. A. and Reddel, R. R. (2011) 'Five dysfunctional telomeres predict onset of senescence in human cells', *EMBO Rep,* 13(1), pp. 52-9.

Kim, H., Li, F., He, Q., Deng, T., Xu, J., Jin, F., Coarfa, C., Putluri, N., Liu, D. and Songyang, Z. (2017) 'Systematic analysis of human telomeric dysfunction using inducible telosome/shelterin CRISPR/Cas9 knockout cells', *Cell Discov,* 3, pp. 17034.

Lai, T. P., Zhang, N., Noh, J., Mender, I., Tedone, E., Huang, E., Wright, W. E., Danuser, G. and Shay, J. W. (2017) 'A method for measuring the distribution of the shortest telomeres in cells and tissues', *Nat Commun,* 8(1), pp. 1356.

Letsolo, B. T., Rowson, J. and Baird, D. M. (2010) 'Fusion of short telomeres in human cells is characterized by extensive deletion and microhomology, and can result in complex rearrangements', *Nucleic Acids Res,* 38(6), pp. 1841-52.

Luo, Z., Feng, X., Wang, H., Xu, W., Zhao, Y., Ma, W., Jiang, S., Liu, D., Huang, J. and Songyang, Z. (2015) 'Mir-23a induces telomere dysfunction and cellular senescence by inhibiting TRF2 expression', *Aging Cell,* 14(3), pp. 391-9.

Martinez, P., Thanasoula, M., Carlos, A. R., Gómez-López, G., Tejera, A. M., Schoeftner, S., Dominguez, O., Pisano, D. G., Tarsounas, M. and Blasco, M. A. (2010) 'Mammalian Rap1 controls telomere function and gene expression through binding to telomeric and extratelomeric sites', *Nat Cell Biol,* 12(8), pp. 768-80.

Martínez, P., Gómez-López, G., Pisano, D. G., Flores, J. M. and Blasco, M. A. (2016) 'A genetic interaction between RAP1 and telomerase reveals an unanticipated role for RAP1 in telomere maintenance', *Aging Cell,* 15(6), pp. 1113-1125.

Mendez-Bermudez, A., Lototska, L., Bauwens, S., Giraud-Panis, M. J., Croce, O., Jamet, K., Irizar, A., Mowinckel, M., Koundrioukoff, S., Nottet, N., Almouzni, G., Teulade-Fichou, M. P., Schertzer, M., Perderiset, M., Londoño-Vallejo, A., Debatisse, M., Gilson, E. and Ye, J. (2018) 'Genome-wide Control of Heterochromatin Replication by the Telomere Capping Protein TRF2', *Mol Cell,* 70(3), pp. 449-461.e5.

Oh, S., Harvey, A., Zimbric, J., Wang, Y., Nguyen, T., Jackson, P. J. and Hendrickson, E. A. (2014) 'DNA ligase III and DNA ligase IV carry out genetically distinct forms of end joining in human somatic cells', *DNA Repair (Amst),* 21, pp. 97-110.

Pardo, B. and Marcand, S. (2005) 'Rap1 prevents telomere fusions by nonhomologous end joining', *EMBO J,* 24(17), pp. 3117-27.

Rai, R., Chen, Y., Lei, M. and Chang, S. (2016) 'TRF2-RAP1 is required to protect telomeres from engaging in homologous recombination-mediated deletions and fusions', *Nat Commun,* 7, pp. 10881.

Sambrook, J., Fritsch, E.F. and Maniatis, T. *Molecular Cloning: a Laboratory Manual* 2nd ed. (Cold Spring Harbor Laboratory Press, New York, 1989).

Sarthy, J., Bae, N. S., Scrafford, J. and Baumann, P. (2009) 'Human RAP1 inhibits non-homologous end joining at telomeres', *EMBO J,* 28(21), pp. 3390-9.

Sfeir, A., Kabir, S., van Overbeek, M., Celli, G. B. and de Lange, T. (2010) 'Loss of Rap1 induces telomere recombination in the absence of NHEJ or a DNA damage signal', *Science,* 327(5973), pp. 1657-61.

Suzuki, M., Suzuki, K., Kodama, S., Yamashita, S. and Watanabe, M. (2012) 'Persistent amplification of DNA damage signal involved in replicative senescence of normal human diploid fibroblasts', *Oxid Med Cell Longev,* 2012, pp. 310534.

Vakifahmetoglu, H., Olsson, M. and Zhivotovsky, B. (2008) 'Death through a tragedy: mitotic catastrophe', *Cell Death Differ,* 15(7), pp. 1153-62.

Figure1

A

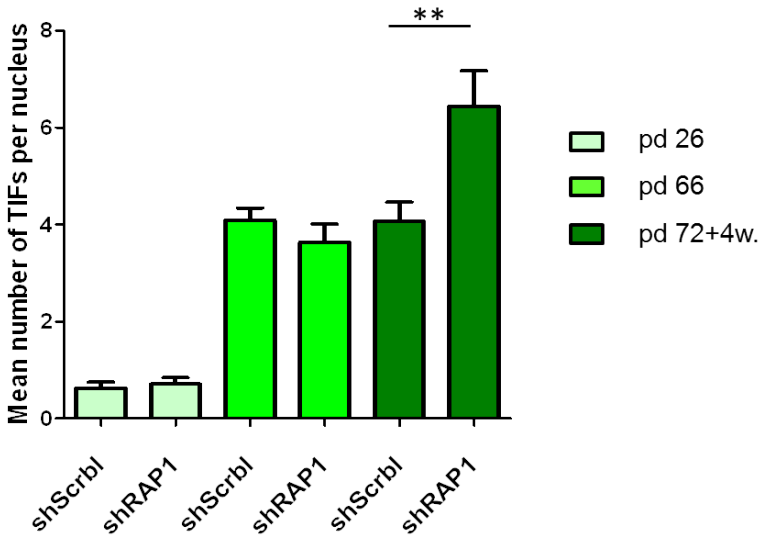
**
Mean number of TIFs per nucleus
0
2
4
6
8
shScrbl
shRAP1
shScrbl
shRAP1
shScrbl
shRAP1
pd 26
pd 66
pd 72+4w.

B

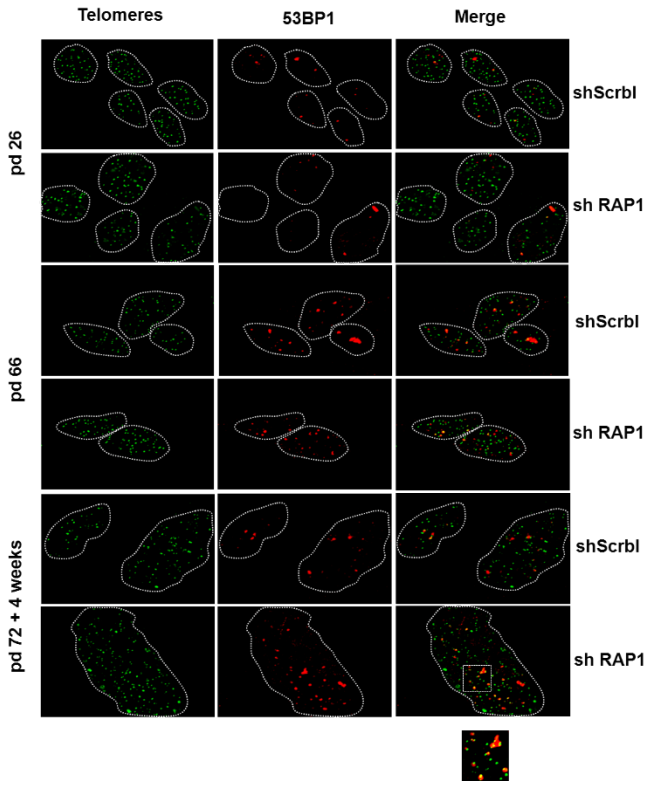
Telomeres
53BP1
Merge
pd 26
pd 66
pd 72 + 4 weeks
shScrbl
sh RAP1
shScrbl
sh RAP1
shScrbl
sh RAP1

Figure 2

A

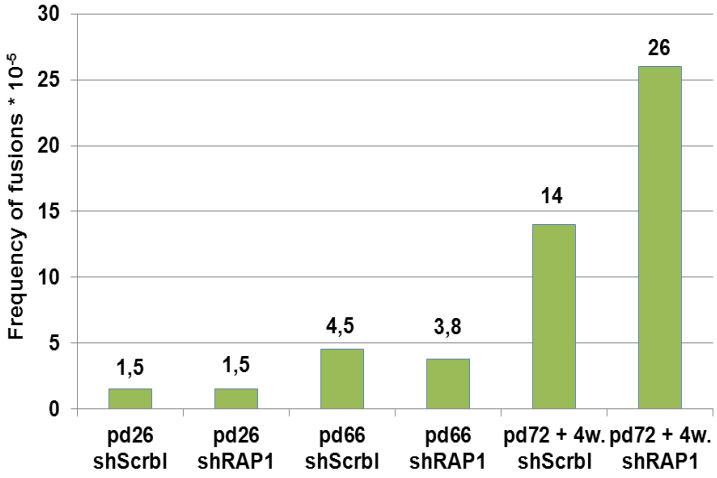
Frequency of fusions * 10-5
30
25
20
15
10
5
0
1,5
1,5
4,5
3,8
14
26
pd26 shScrbl
pd26 shRAP1
pd66 shScrbl
pd66 shRAP1
pd72 + 4w. shScrbl
pd72 + 4w. shRAP1

B

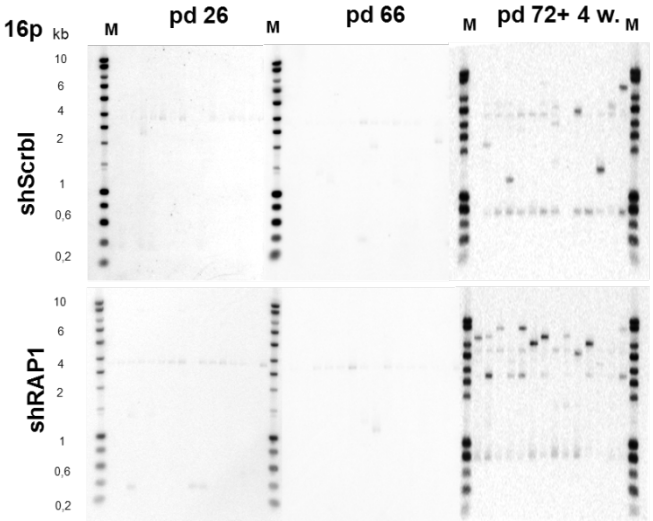
16p
kb
M
pd 26
M
pd 66
M
pd 72+ 4 w.
M
shScrbl
shRAP1
10
6
4
2
1
0,6
0,2

Figure 3

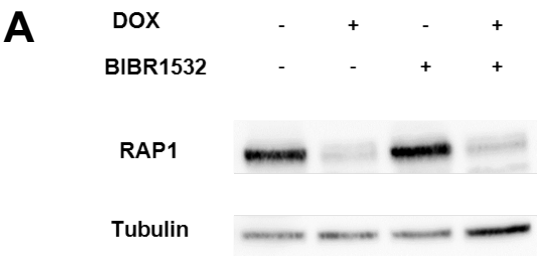
A
DOX - + - +
BIBR1532 - - + +
RAP1
Tubulin

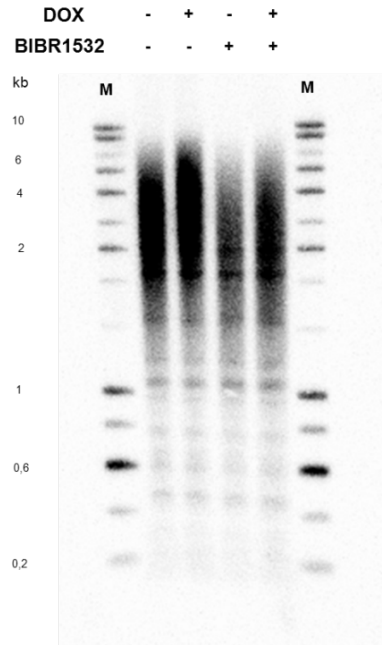
B
DOX - + - +
BIBR1532 - - + +
kb
M
M
10
6
4
2
1
0,6
0,2

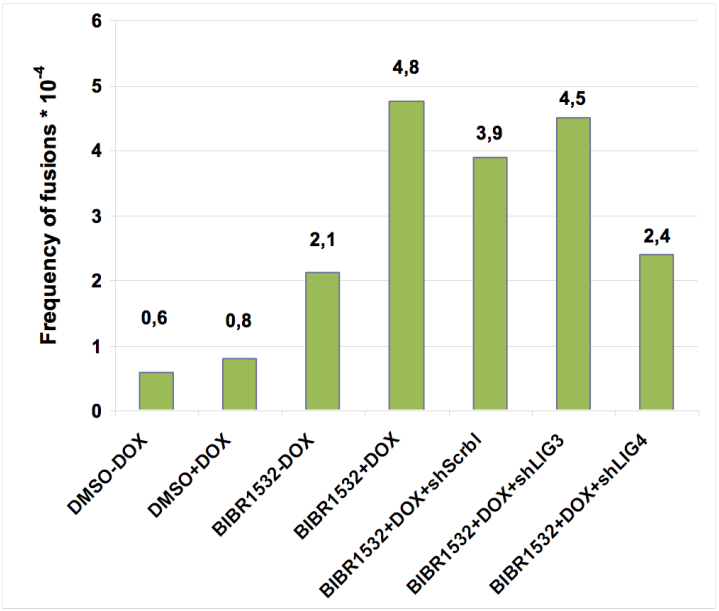
C
Frequency of fusions * 10-4
0,6
0,8
2,1
4,8
3,9
4,5
2,4
DMSO-DOX
DMSO+DOX
BIBR1532-DOX
BIBR1532+DOX
BIBR1532+DOX+shScrbl
BIBR1532+DOX+shLIG3
BIBR1532+DOX+shLIG4

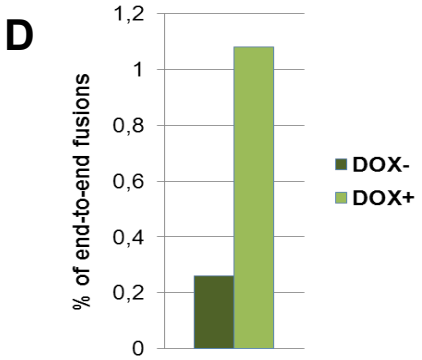
D
% of end-to-end fusions
DOX-
DOX+

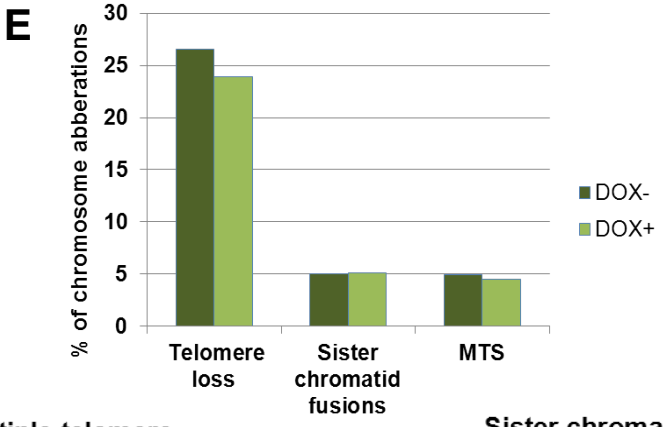
E
% of chromosome abberations
DOX-
DOX+
Telomere loss
Sister chromatid fusions
MTS

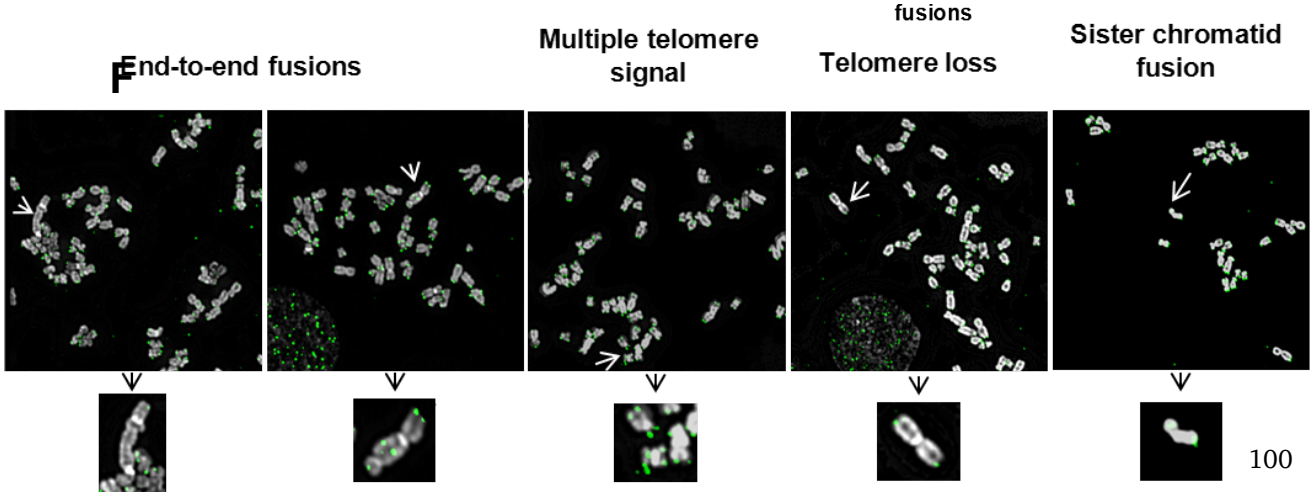
F
End-to-end fusions
Multiple telomere signal
Telomere loss
Sister chromatid fusion

Figure 4

A

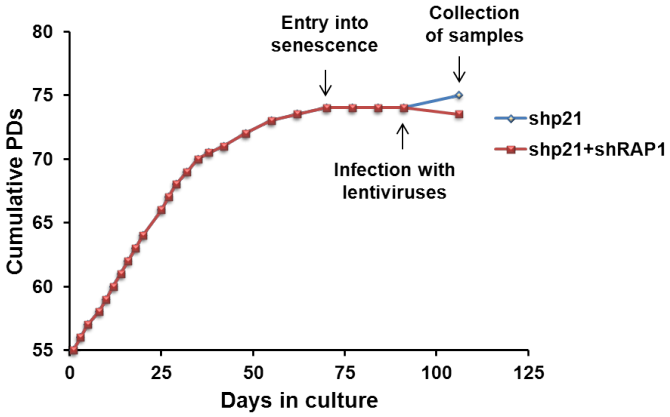
Entry into senescence
Collection of samples
Infection with lentiviruses
shp21
shp21+shRAP1
Cumulative PDs
Days in culture
80
75
70
65
60
55
0
25
50
75
100
125

B

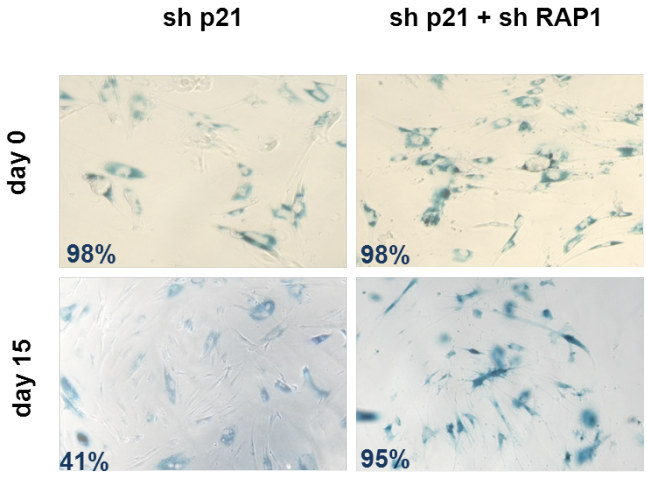
sh p21
sh p21 + sh RAP1
day 0
day 15
98%
98%
41%
95%

C

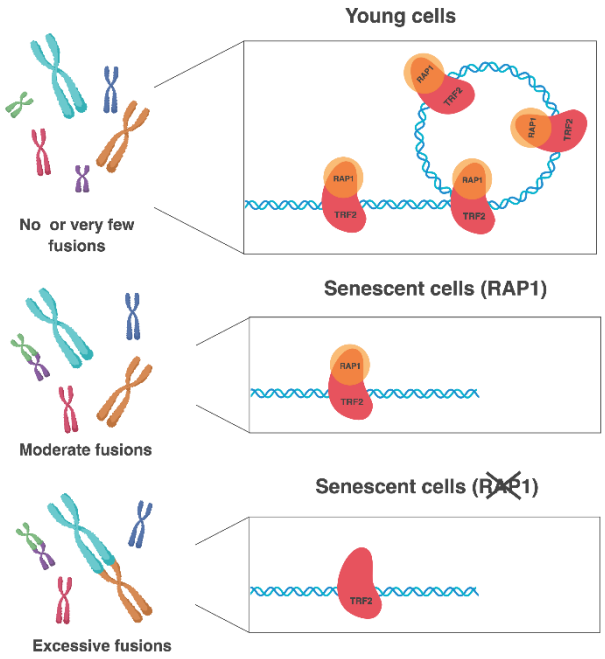
Young cells
RAP1
TRF2
No or very few fusions
Senescent cells (RAP1)
Moderate fusions
Senescent cells (RAP1)
Excessive fusions

Supplementary Figure 1

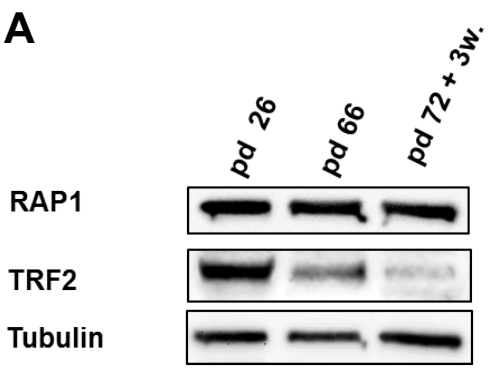

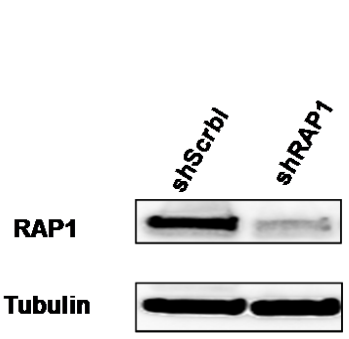

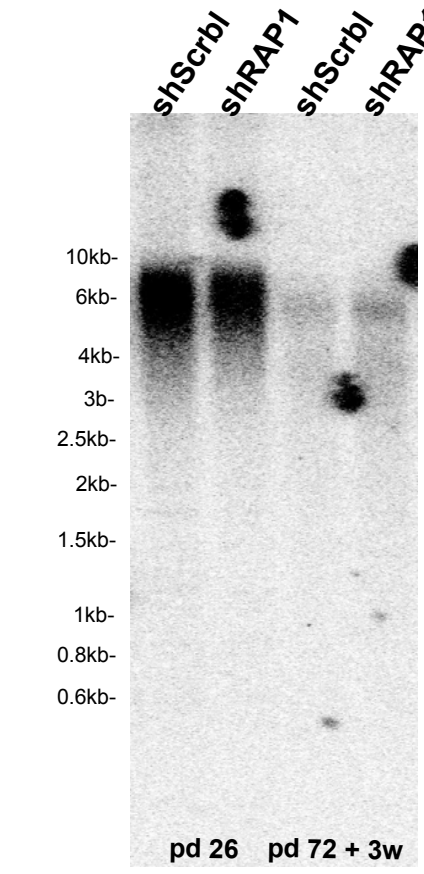

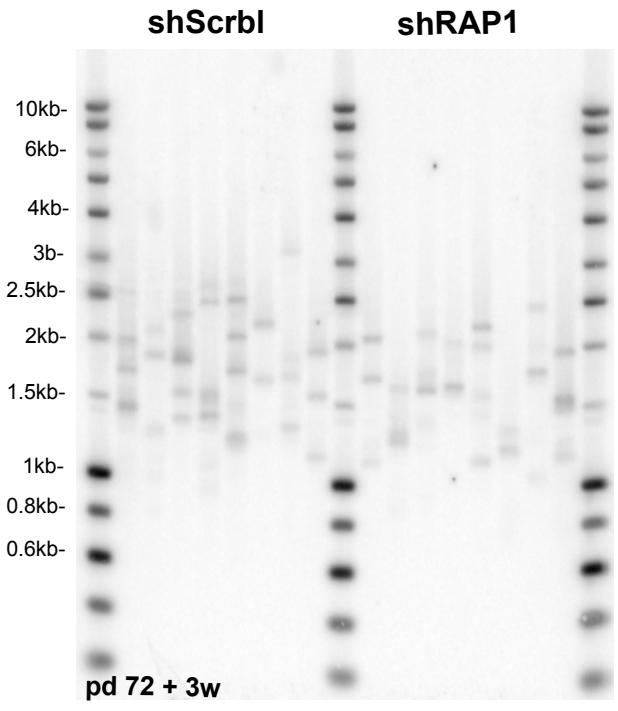

Supplementary Figure 2

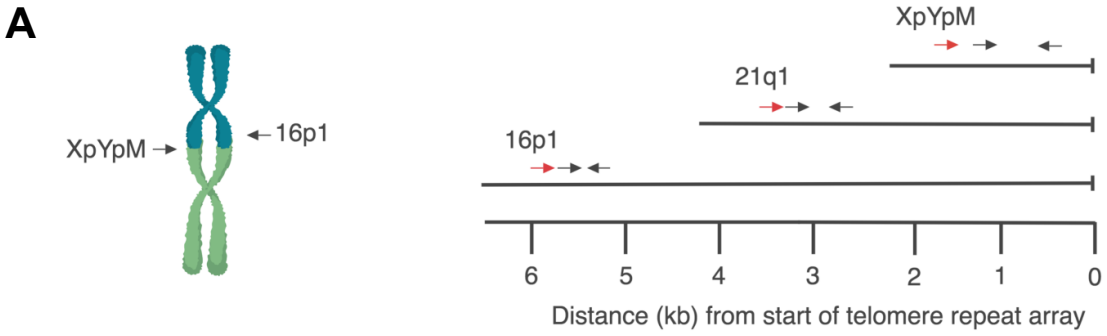

16p1: 16p, 1p, 9p, 12p, 15q, XqYq and the 2q14 interstitial locus

21q1: 21q, 1q, 2q, 5q, 6q, 6p, 8p, 10q, 13q, 17q, 19p, 19q, 22q and the 2q13 interstitial telomeric locus

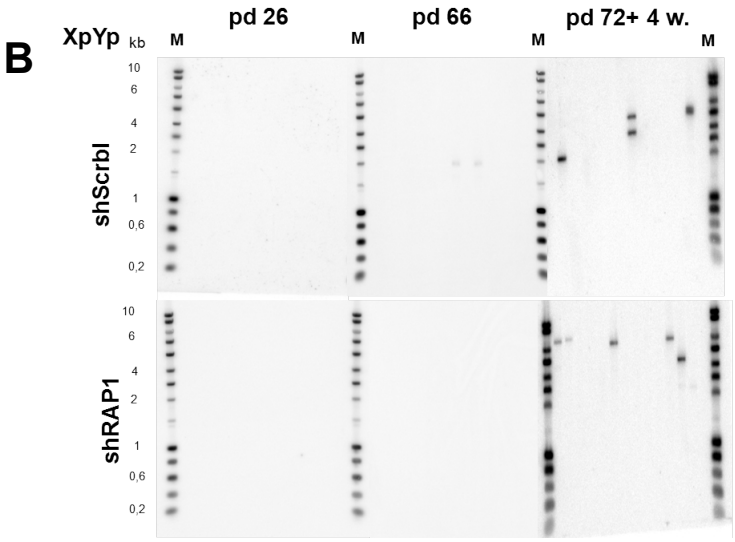

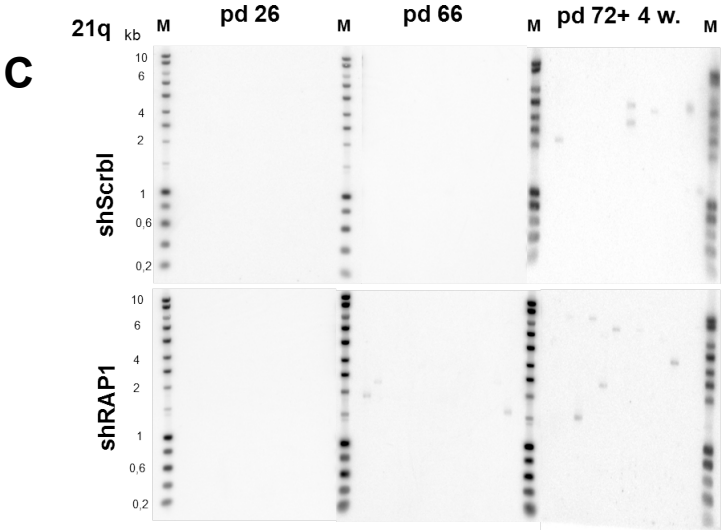

Supplementary Figure 3

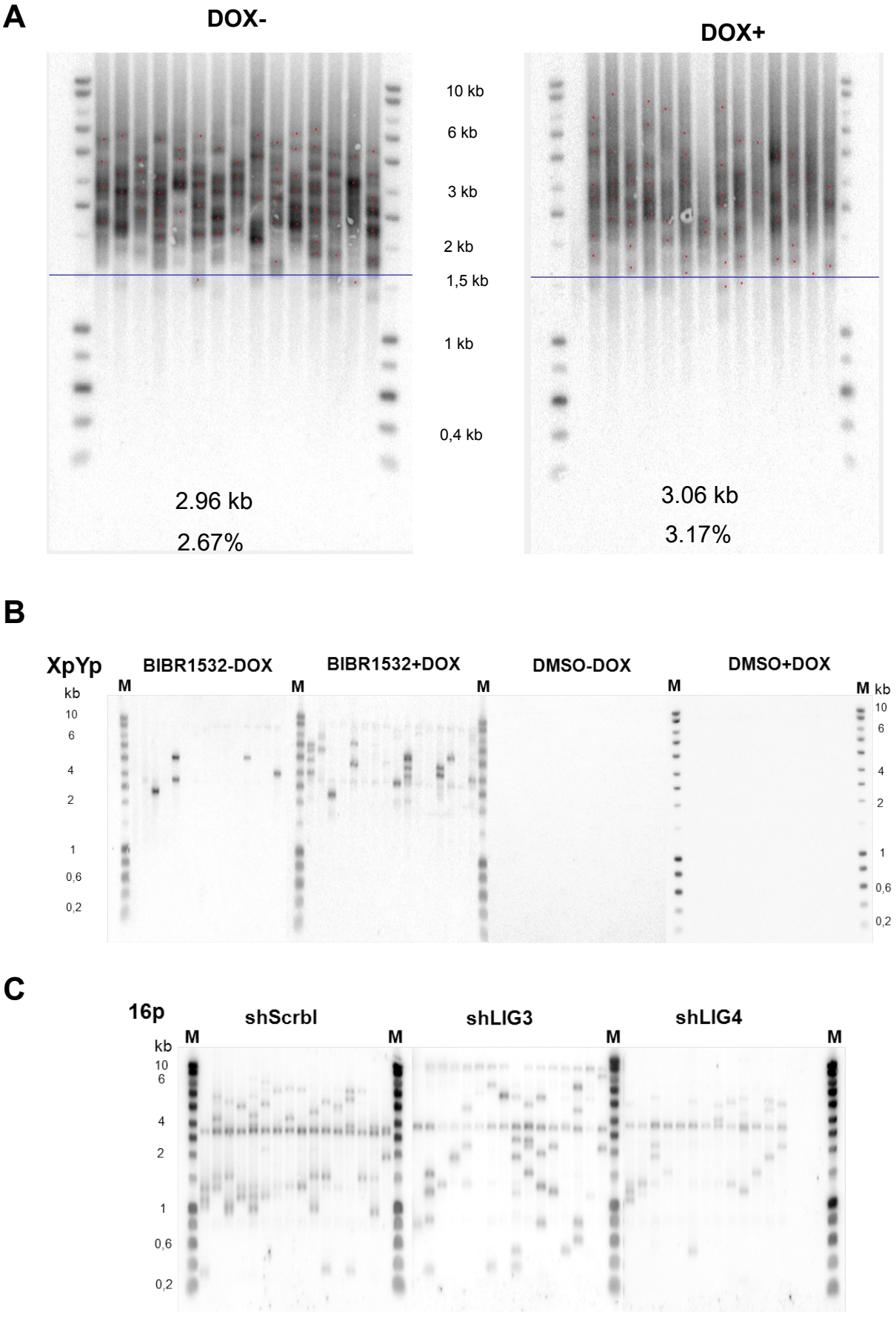

Supplementary Figure 3

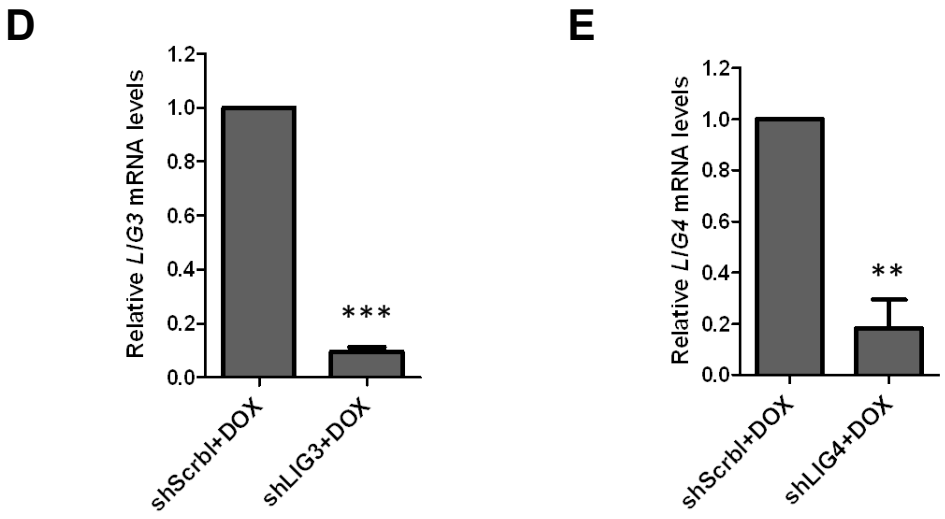

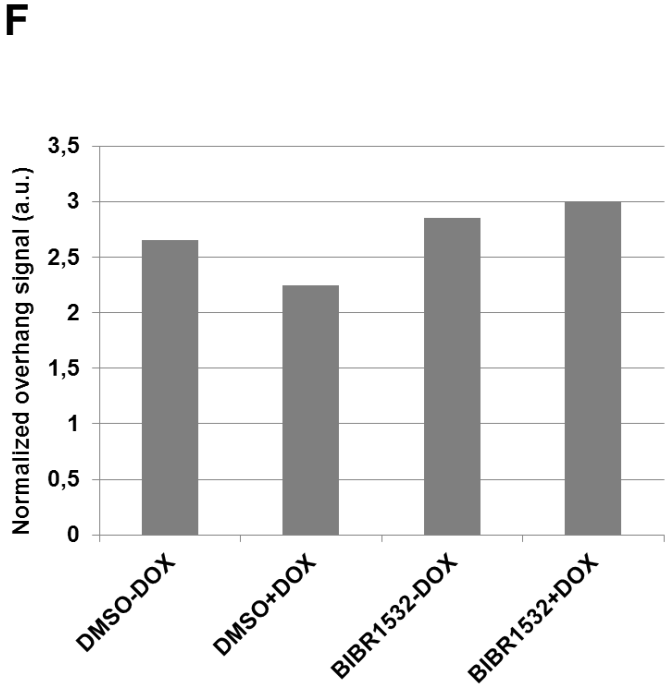

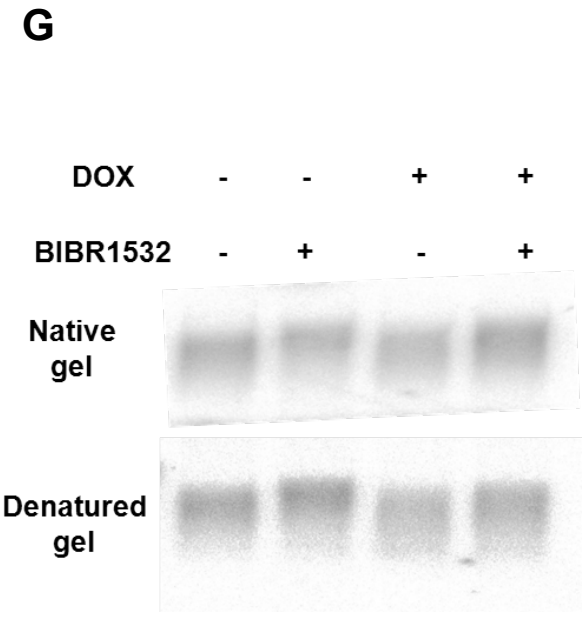

Chapter 3

General discussion and future perspectives

In this manuscript, we presented the results obtained during the Thesis project on the RAP1 role in telomere protection.

Here we report two independent scenarios where RAP1 takes over telomere protection.

First, we mutated several lysines and arginines into alanines within the TRFH domain of TRF2. This mutant, called Top-less, had impaired topological capabilities, such as DNA wrapping and also affected t-loop formation (the number of t-loops was decreased in comparison to the control). Since t-loops are natural barriers against DNA repair and DDR, we further decided to explore how partial telomere deprotection, caused by Top-less, controls NHEJ. As expected, we observed severe end-to-end fusions upon TRF2 knockdown. This fusion phenotype can be rescued by overexpression of full-length TRF2 or Top-less. The contribution of the work performed during the Thesis project was to show that Top-less in combination with RAP1 inhibition did not rescue fusions. This finding suggested that topological properties of TRF2, mediated by TRFH domain, are important in NHEJ control, and when affected, can be backed up by RAP1.

Second, as the main work of the Thesis project, we explored how RAP1 protects telomeres in senescent cells. In relation to this, the current model of different telomere states has been proposed by Cesare and Karlseder [Cesare AJ. and Karlseder J., 2012]. In this model, three different telomere states are described as an outcome either of TRF2 dysfunction or subsequent events during replicative senescence. The closed state, which can be applied to young or dividing primary cells, is based on the discovery of t-loops that are found on the chromosome extremities and serve as barriers to DNA damage [Griffith JD. et al., 1999; Doksani Y. et al, 2013; Benarroch Popivker et al., 2016]. The intermediate state exists due to the progressive telomere shortening when t-loops cannot be formed. It is characterized by partial depletion of TRF2 and accumulation of DDR markers, such as increase in TIFs. The last state is uncapped telomeres with no detectable TRF2 and excessive DDR and chromosome fusions [Cesare JA. et al., 2012]. The intermediate state can be applied to the cells that enter into replicative senescence, and the last state is an extreme case

when telomeres experience a crisis or become so critically short that it leads to fusion [Cesare JA. et al., 2013]. Importantly, telomeres in senescent cells do not fuse massively due to the presence of TRF2 [Karlseder J. et al., 2002]. In addition, a recent study shows that linear telomeres of mouse and HeLa of an average length of 20 kb, that do not form t-loops due to TRF2 downregulation, are sensitive to ATM activation, but yet can be protected from NHEJ [Van Ly D. et al., 2018] in agreement with our precedent publication [Benarroch Popivker et al., 2016]. However, in spite of all the evidence presented above, yet there is no experimental proof of t-loop dynamics in senescent cells. It may be due to the fact that there are limitations in detection and resolution of t-loops even by means of the most modern technics such as super resolution microscopy. In addition, the role of human RAP1 in human replicative senescent cells has not been addressed so far. For all these reasons, in the second project, we focus on telomere protection of cells that experience progressive telomere shortening.

To overcome the limitation of ceased cell division in senescent cells, instead of metaphase spread we decided to take advantage of the telomere fusion assay in order to detect chromosome fusions. This assay relies on PCR with different subtelomeric probes. If the fusion occurs between two different chromosome ends, it will be amplified in PCR followed by Southern blotting of the PCR products. Among the advantages, this technique is powerful enough to detect fusions originating from 22 different chromosome ends all at once [Letsolo BT. et al., 2010]. It detects sister chromatid-type fusion when there has been a deletion of at least one of the telomere repeat arrays creating an imperfect inverted repeat, as well as fusion between heterologous chromosomes containing substantial arrays of head-to-head telomere repeats [Capper R. et al., 2007]. The limitations of the assay are due to the fact that it cannot detect 1) sister chromatid-type fusions that create perfect inverted repeats; 2) fusions that have substantial deletion of DNA material enough to hamper the binding of one of the subtelomeric primers; 3) fusions involving chromosomes not covered by the subtelomeric primers that are used.

We used telomere fusion assay to detect chromosome fusions in human primary fibroblasts of different population doublings. We observed no or very few fusions in young cells, a moderate increase in fusion frequency in pre-senescent dividing cells and approximately 10-fold increase in senescence. Strikingly, senescent cells upon RAP1 knockdown demonstrated a further 2-fold increase in fusion frequency compared to the control. This was not the case either for young or pre-senescent cells, indicating that the

switch between RAP1-independent and RAP1-dependent telomere protection occurs during replicative senescence.

Furthermore, we have assayed telomere uncapping by the TIF assay in all these populations of cells. Similar to the results on fusion frequency, we observed a difference between control and RAP1 knockdown only in senescent cells. Whether this DDR activation is the cause or the consequence of the chromosome fusions that increased when RAP1 is dysfunctional, is clearly something that has to be investigated further. In mice, it was shown that RAP1 was dispensable for repression of DDR, in particular, ATM pathway; however, in the very same study, no chromosome fusions were detected when RAP1 was removed from telomeres [Sfeir A. et al., 2010]. One can speculate that RAP1 dysfunction can affect TRF2 and trigger thus DDR. In human, TRF2 expression decreases in senescent cells, whereas RAP1 level is less affected [Fujita K. et al., 2010; Swanson MJ. et al., 2016] (this Thesis). But this does not answer the question whether TRF2 or RAP1 binding to telomeres is decreased or vice versa. In senescent yeast, Rap1 re-localizes within the chromosome to modulate expression of its target genes [Platt JM. et al., 2013; Ye J. et al., 2014], as in mouse when telomeres get shorter in telomerase null cells [Martinez P. et al., 2016]. Human RAP1 binds to telomeres through interaction with TRF2, and they together form a stable complex [Li B. et al., 2000]. On the other hand, human RAP1 can bind telomeric repeats independently, but with low affinity [Arat N. and Griffith JD., 2012]. Notably, RAP1 may be necessary for more accurate and selective TRF2 recognition of telomeric DNA [Janoušková E. et al., 2015]. In the future, we aim to investigate the binding of both TRF2 and RAP1 to telomeres in young and senescent cells by means of chromatin immunoprecipitation (ChIP) or immuno-fluorescence FISH with specific antibodies and telomere probes.

To dissect the anti-fusion mechanisms of human RAP1, we used HeLa cells with doxycycline-inducible RAP1 knockout alleles [Kim H. et al., 2017]. We treated these cells with the telomerase inhibitor BIBR1532 to trigger telomere shortening and observed again increase in the fusion frequency when RAP1 expression was diminished. Later, we found that chromosome fusions upon RAP1 knockout appear through c-NHEJ. Notably, we demonstrated that RAP1 removal neither triggers a decrease of the average telomere length or increases the number of critically short telomeres or promotes telomere 3'-overhang shortening and telomere loss. Therefore, fusions cannot be simply explained by telomere changes only.

It has been shown before that many fusion events involved chromosome ends with no detectable telomere sequences [Capper R. et al., 2007]. For instance, the fusions we detected

using the PCR-based method in this work suggest that the fusions involve chromosome ends with no telomeres or even more with DNA loss extending to the subtelomeric region. In order to characterize the type of fusions and to determine the exact sequence loss at the time of the fusion, we are going to sequence them either by classical Sanger sequencing or using a novel approach to generate long read sequencing.

In search of mechanisms that drive fusion phenotype, we decided to use a genetic approach. We aim to decipher which domains of human RAP1 may be important for prevention of c-NHEJ. To do so, we designed several truncation mutants of human RAP1 (Figure 11), which lack separate domains or have a point mutation as the RAP1 mutant F336R (a mutation in the binding site of TRF2). We have done the first cell culture trial to check the expression of these mutants in HeLa (Figure 11). Therefore, in the future, we will perform the telomere fusion assay in HeLa expressing different RAP1 mutants.

Among the future work is the search for potential interactors of RAP1 that can contribute to the fusion phenotype besides TRF2. It was reported previously that human RAP1 can interact with several proteins. For instance, immunoprecipitation of endogenous RAP1 from HeLa cell nuclear extracts was able to specifically pull down TRF2, Ku86, Rad50, and RAP1[O'Connor MS. et al., 2004]. Ku86 and Rad50 are DNA repair proteins, which makes them appealing targets to test in regard to RAP1. Interestingly, the level of KU declines during replicative senescence [Seluanov A. et al., 2007].

Additionally, RAP1 has been shown to interact with Sun1, which is a member of the LINC complex (Linker of Nucleoskeleton and Cytoskeleton) that bridges inner and outer membranes of the nuclear envelope [Crabbe L. et al., 2012]. Sun domain proteins have been involved in the tethering of telomeres to the nuclear envelope in yeast [Bupp JM. et al., 2007]. Remarkably, numerous studies have demonstrated that DSBs are targeted to the nuclear periphery for the repair [Oza P. and Peterson CL., 2010]. In this regard, yeast Mps3, a member of the Sun domain protein family, plays a central role in connecting peripheral localization, DSB repair and telomeres [Schober H. et al., 2009; Oza P. et al., 2009; Oza P. and Peterson CL., 2010]. Therefore, a possible scenario is that upon inhibition of human RAP1 in senescent cells telomeres become more mobile and prone to fusions.

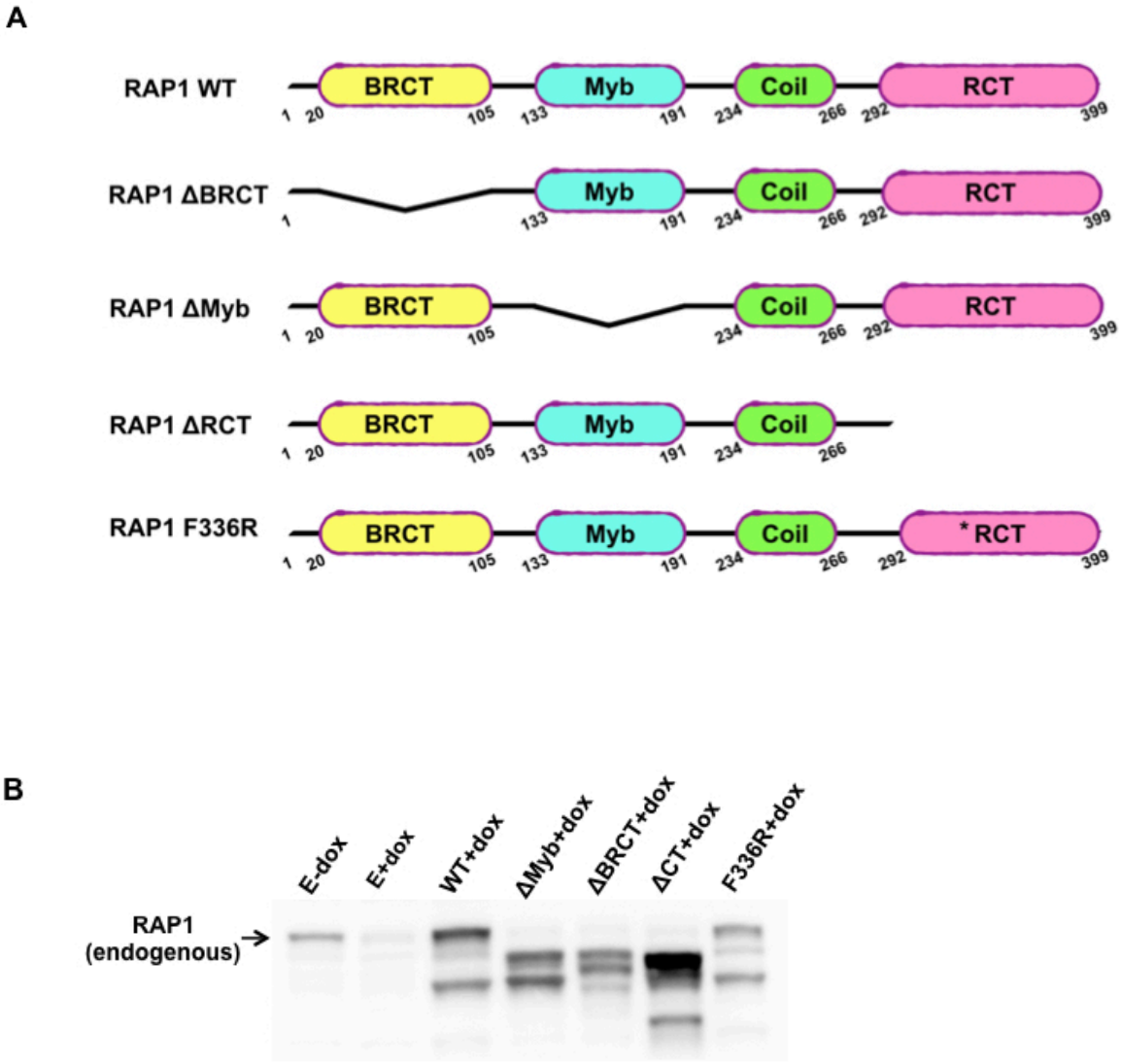

Figure 11. Human RAP1 mutants used in the study. *A. A graphical representation of the RAP1 mutant design. * corresponds to the point mutation. B. A western blot showing expression of different mutants in HeLa cells.*

Other important questions remain to be answered in the context of RAP1 and replicative senescence. Just to name a few:

1. Which chromosomes tend to fuse more often than others upon RAP1 inhibition?

2. What is the exact mechanism of cell death observed in post-senescent RAP1-deficient cells?

3. Does the observed fusion phenotype apply only to replicative senescence or is it universal for senescent cells?

Altogether, we have obtained the first evidence that senescent cells switch from RAP1-independent to RAP1-dependent mode of telomere protection.

Bibliography

Ahnesorg, P., Smith, P. and Jackson, S. P. (2006) 'XLF interacts with the XRCC4-DNA ligase IV complex to promote DNA nonhomologous end-joining', *Cell,* 124(2), pp. 301-13.

Andersen, S. L. and Sekelsky, J. (2010) 'Meiotic versus mitotic recombination: two different routes for double-strand break repair: the different functions of meiotic versus mitotic DSB repair are reflected in different pathway usage and different outcomes', *Bioessays,* 32(12), pp. 1058-66.

Andres, S. N., Vergnes, A., Ristic, D., Wyman, C., Modesti, M. and Junop, M. (2012) 'A human XRCC4-XLF complex bridges DNA', *Nucleic Acids Res,* 40(4), pp. 1868-78.

Apte, M. S. and Cooper, J. P. (2017) 'Life and cancer without telomerase: ALT and other strategies for making sure ends (don't) meet', *Crit Rev Biochem Mol Biol,* 52(1), pp. 57-73.

Arat, N. and Griffith, J. D. (2012) 'Human Rap1 interacts directly with telomeric DNA and regulates TRF2 localization at the telomere', *J Biol Chem,* 287(50), pp. 41583-94.

Arnoult, N. and Karlseder, J. (2015) 'Complex interactions between the DNA-damage response and mammalian telomeres', *Nat Struct Mol Biol,* 22(11), pp. 859-66.

Bae, N. S. and Baumann, P. (2007) 'A RAP1/TRF2 complex inhibits nonhomologous end-joining at human telomeric DNA ends', *Mol Cell,* 26(3), pp. 323-34.

Bakkenist, C. J. and Kastan, M. B. (2003) 'DNA damage activates ATM through intermolecular autophosphorylation and dimer dissociation', *Nature,* 421(6922), pp. 499-506.

Baudat, F. and de Massy, B. (2007) 'Regulating double-stranded DNA break repair towards crossover or non-crossover during mammalian meiosis', *Chromosome Res,* 15(5), pp. 565-77.

Benarroch-Popivker, D., Pisano, S., Mendez-Bermudez, A., Lototska, L., Kaur, P., Bauwens, S., Djerbi, N., Latrick, C. M., Fraisier, V., Pei, B., Gay, A., Jaune, E., Foucher, K., Cherfils-Vicini, J., Aeby, E., Miron, S., Londoño-Vallejo, A., Ye, J., Le Du, M. H., Wang, H., Gilson, E. and Giraud-Panis, M. J. (2016) 'TRF2-Mediated Control of Telomere DNA Topology as a Mechanism for Chromosome-End Protection', *Mol Cell,* 61(2), pp. 274-86.

Bennardo, N., Cheng, A., Huang, N. and Stark, J. M. (2008) 'Alternative-NHEJ is a mechanistically distinct pathway of mammalian chromosome break repair', *PLoS Genet,* 4(6), pp. e1000110.

Berman, J., Tachibana, C. Y. and Tye, B. K. (1986) 'Identification of a telomere-binding activity from yeast', *Proc Natl Acad Sci U S A,* 83(11), pp. 3713-7.

Bertuch, A. A. and Lundblad, V. (2003) 'The Ku heterodimer performs separable activities at double-strand breaks and chromosome termini', *Mol Cell Biol,* 23(22), pp. 8202-15.

Bhargava, R., Onyango, D. O. and Stark, J. M. (2016) 'Regulation of Single-Strand Annealing and its Role in Genome Maintenance', *Trends Genet,* 32(9), pp. 566-575.

Blackford, A. N. and Jackson, S. P. (2017) 'ATM, ATR, and DNA-PK: The Trinity at the Heart of the DNA Damage Response', *Mol Cell,* 66(6), pp. 801-817.

Bolderson, E., Savage, K. I., Mahen, R., Pisupati, V., Graham, M. E., Richard, D. J., Robinson, P. J., Venkitaraman, A. R. and Khanna, K. K. (2012) 'Kruppel-associated Box (KRAB)-associated co-repressor (KAP-1) Ser-473 phosphorylation regulates heterochromatin protein 1β (HP1-β) mobilization and DNA repair in heterochromatin', *J Biol Chem,* 287(33), pp. 28122-31.

Bombarde, O., Boby, C., Gomez, D., Frit, P., Giraud-Panis, M. J., Gilson, E., Salles, B. and Calsou, P. (2010) 'TRF2/RAP1 and DNA-PK mediate a double protection against joining at telomeric ends', *EMBO J,* 29(9), pp. 1573-84.

Boubakour-Azzouz, I., Bertrand, P., Claes, A., Lopez, B. S. and Rougeon, F. (2012) 'Terminal deoxynucleotidyl transferase requires KU80 and XRCC4 to promote N-addition at non-V(D)J chromosomal breaks in non-lymphoid cells', *Nucleic Acids Res,* 40(17), pp. 8381-91.

Boulton, S. J. and Jackson, S. P. (1996) 'Saccharomyces cerevisiae Ku70 potentiates illegitimate DNA double-strand break repair and serves as a barrier to error-prone DNA repair pathways', *EMBO J,* 15(18), pp. 5093-103.

Britton, S., Coates, J. and Jackson, S. P. (2013) 'A new method for high-resolution imaging of Ku foci to decipher mechanisms of DNA double-strand break repair', *J Cell Biol,* 202(3), pp. 579-95.

Bupp, J. M., Martin, A. E., Stensrud, E. S. and Jaspersen, S. L. (2007) 'Telomere anchoring at the nuclear periphery requires the budding yeast Sad1-UNC-84 domain protein Mps3', *J Cell Biol,* 179(5), pp. 845-54.

Caldecott, K. W., McKeown, C. K., Tucker, J. D., Ljungquist, S. and Thompson, L. H. (1994) 'An interaction between the mammalian DNA repair protein XRCC1 and DNA ligase III', *Mol Cell Biol,* 14(1), pp. 68-76.

Capp, J. P., Boudsocq, F., Bertrand, P., Laroche-Clary, A., Pourquier, P., Lopez, B. S., Cazaux, C., Hoffmann, J. S. and Canitrot, Y. (2006) 'The DNA polymerase lambda is required for the repair of non-compatible DNA double strand breaks by NHEJ in mammalian cells', *Nucleic Acids Res,* 34(10), pp. 2998-3007.

Capper, R., Britt-Compton, B., Tankimanova, M., Rowson, J., Letsolo, B., Man, S., Haughton, M. and Baird, D. M. (2007) 'The nature of telomere fusion and a definition of the critical telomere length in human cells', *Genes Dev,* 21(19), pp. 2495-508.

Cardoso, D. C., das Graças Pompolo, S., Cristiano, M. P. and Tavares, M. G. (2014) 'The role of fusion in ant chromosome evolution: insights from cytogenetic analysis using a molecular phylogenetic approach in the genus mycetophylax', *PLoS One,* 9(1), pp. e87473.

Celli, G. B., Denchi, E. L. and de Lange, T. (2006) 'Ku70 stimulates fusion of dysfunctional telomeres yet protects chromosome ends from homologous recombination', *Nat Cell Biol,* 8(8), pp. 885-90.

Cesare, A. J., Hayashi, M. T., Crabbe, L. and Karlseder, J. (2013) 'The telomere deprotection response is functionally distinct from the genomic DNA damage response', *Mol Cell,* 51(2), pp. 141-55.

Cesare, A. J. and Karlseder, J. (2012) 'A three-state model of telomere control over human proliferative boundaries', *Curr Opin Cell Biol,* 24(6), pp. 731-8.

Chang, H. H., Watanabe, G., Gerodimos, C. A., Ochi, T., Blundell, T. L., Jackson, S. P. and Lieber, M. R. (2016) 'Different DNA End Configurations Dictate Which NHEJ Components Are Most Important for Joining Efficiency', *J Biol Chem,* 291(47), pp. 24377-24389.

Chang, H. H. Y., Pannunzio, N. R., Adachi, N. and Lieber, M. R. (2017) 'Non-homologous DNA end joining and alternative pathways to double-strand break repair', *Nat Rev Mol Cell Biol,* 18(8), pp. 495-506.

Chapman, J. R., Taylor, M. R. and Boulton, S. J. (2012) 'Playing the end game: DNA double-strand break repair pathway choice', *Mol Cell,* 47(4), pp. 497-510.

Chayot, R., Montagne, B. and Ricchetti, M. (2012) 'DNA polymerase μ is a global player in the repair of non-homologous end-joining substrates', *DNA Repair (Amst),* 11(1), pp. 22-34.

Chen, H., Lisby, M. and Symington, L. S. (2013) 'RPA coordinates DNA end resection and prevents formation of DNA hairpins', *Mol Cell,* 50(4), pp. 589-600.

Chen, L., Huang, S., Lee, L., Davalos, A., Schiestl, R. H., Campisi, J. and Oshima, J. (2003) 'WRN, the protein deficient in Werner syndrome, plays a critical structural role in optimizing DNA repair', *Aging Cell,* 2(4), pp. 191-9.

Clouaire, T., Marnef, A. and Legube, G. (2017) 'Taming Tricky DSBs: ATM on duty', *DNA Repair (Amst),* 56, pp. 84-91.

Cong, Y. S., Wright, W. E. and Shay, J. W. (2002) 'Human telomerase and its regulation', *Microbiol Mol Biol Rev,* 66(3), pp. 407-25, table of contents.

Conrad, M. N., Wright, J. H., Wolf, A. J. and Zakian, V. A. (1990) 'RAP1 protein interacts with yeast telomeres in vivo: overproduction alters telomere structure and decreases chromosome stability', *Cell,* 63(4), pp. 739-50.

Crabbe, L., Cesare, A. J., Kasuboski, J. M., Fitzpatrick, J. A. and Karlseder, J. (2012) 'Human telomeres are tethered to the nuclear envelope during postmitotic nuclear assembly', *Cell Rep,* 2(6), pp. 1521-9.

Craxton, A., Munnur, D., Jukes-Jones, R., Skalka, G., Langlais, C., Cain, K. and Malewicz, M. (2018) 'PAXX and its paralogs synergistically direct DNA polymerase λ activity in DNA repair', *Nat Commun,* 9(1), pp. 3877.

Daley, J. M. and Sung, P. (2014) '53BP1, BRCA1, and the choice between recombination and end joining at DNA double-strand breaks', *Mol Cell Biol,* 34(8), pp. 1380-8.

de Lange, T. (2004) 'T-loops and the origin of telomeres', *Nat Rev Mol Cell Biol,* 5(4), pp. 323-9.

de Lange, T. (2005) 'Shelterin: the protein complex that shapes and safeguards human telomeres', *Genes Dev,* 19(18), pp. 2100-10.

Della-Maria, J., Zhou, Y., Tsai, M. S., Kuhnlein, J., Carney, J. P., Paull, T. T. and Tomkinson, A. E. (2011) 'Human Mre11/human Rad50/Nbs1 and DNA ligase IIIalpha/XRCC1 protein complexes act together in an alternative nonhomologous end joining pathway', *J Biol Chem,* 286(39), pp. 33845-53.

Denchi, E. L. and de Lange, T. (2007) 'Protection of telomeres through independent control of ATM and ATR by TRF2 and POT1', *Nature,* 448(7157), pp. 1068-71.

Deng, W., Wu, J., Wang, F., Kanoh, J., Dehe, P. M., Inoue, H., Chen, J. and Lei, M. (2015) 'Fission yeast telomere-binding protein Taz1 is a functional but not a structural counterpart of human TRF1 and TRF2', *Cell Res,* 25(7), pp. 881-4.

Deng, Y., Guo, X., Ferguson, D. O. and Chang, S. (2009) 'Multiple roles for MRE11 at uncapped telomeres', *Nature,* 460(7257), pp. 914-8.

Deriano, L. and Roth, D. B. (2013) 'Modernizing the nonhomologous end-joining repertoire: alternative and classical NHEJ share the stage', *Annu Rev Genet,* 47, pp. 433-55.

Dimitrova, N., Chen, Y. C., Spector, D. L. and de Lange, T. (2008) '53BP1 promotes non-homologous end joining of telomeres by increasing chromatin mobility', *Nature,* 456(7221), pp. 524-8.

Dimitrova, N. and de Lange, T. (2009) 'Cell cycle-dependent role of MRN at dysfunctional telomeres: ATM signaling-dependent induction of nonhomologous end joining (NHEJ) in G1 and resection-mediated inhibition of NHEJ in G2', *Mol Cell Biol,* 29(20), pp. 5552-63.

Doksani, Y., Wu, J. Y., de Lange, T. and Zhuang, X. (2013) 'Super-resolution fluorescence imaging of telomeres reveals TRF2-dependent T-loop formation', *Cell,* 155(2), pp. 345-356.

Dudásová, Z., Dudás, A. and Chovanec, M. (2004) 'Non-homologous end-joining factors of Saccharomyces cerevisiae', *FEMS Microbiol Rev,* 28(5), pp. 581-601.

Duursma, A. M., Driscoll, R., Elias, J. E. and Cimprich, K. A. (2013) 'A role for the MRN complex in ATR activation via TOPBP1 recruitment', *Mol Cell,* 50(1), pp. 116-22.

Emerson, C. H. and Bertuch, A. A. (2016) 'Consider the workhorse: Nonhomologous end-joining in budding yeast', *Biochem Cell Biol,* 94(5), pp. 396-406.
Falck, J., Coates, J. and Jackson, S. P. (2005) 'Conserved modes of recruitment of ATM, ATR and DNA-PKcs to sites of DNA damage', *Nature,* 434(7033), pp. 605-11.
Fell, V. L. and Schild-Poulter, C. (2015) 'The Ku heterodimer: function in DNA repair and beyond', *Mutat Res Rev Mutat Res,* 763, pp. 15-29.
Flynn, R. L. and Zou, L. (2011) 'ATR: a master conductor of cellular responses to DNA replication stress', *Trends Biochem Sci,* 36(3), pp. 133-40.
Frank-Vaillant, M. and Marcand, S. (2001) 'NHEJ regulation by mating type is exercised through a novel protein, Lif2p, essential to the ligase IV pathway', *Genes Dev,* 15(22), pp. 3005-12.
Fujita, K., Horikawa, I., Mondal, A. M., Jenkins, L. M., Appella, E., Vojtesek, B., Bourdon, J. C., Lane, D. P. and Harris, C. C. (2010) 'Positive feedback between p53 and TRF2 during telomere-damage signalling and cellular senescence', *Nat Cell Biol,* 12(12), pp. 1205-12.
Fumagalli, M., Rossiello, F., Mondello, C. and d'Adda di Fagagna, F. (2014) 'Stable cellular senescence is associated with persistent DDR activation', *PLoS One,* 9(10), pp. e110969.
Gilson, E., Roberge, M., Giraldo, R., Rhodes, D. and Gasser, S. M. (1993) 'Distortion of the DNA double helix by RAP1 at silencers and multiple telomeric binding sites', *J Mol Biol,* 231(2), pp. 293-310.
Gilson, E. and Ségal-Bendirdjian, E. (2010) 'The telomere story or the triumph of an open-minded research', *Biochimie,* 92(4), pp. 321-6.
Giraud-Panis, M. J., Pisano, S., Benarroch-Popivker, D., Pei, B., Le Du, M. H. and Gilson, E. (2013) 'One identity or more for telomeres?', *Front Oncol,* 3, pp. 48.
Giraud-Panis, M. J., Teixeira, M. T., Géli, V. and Gilson, E. (2010) 'CST meets shelterin to keep telomeres in check', *Mol Cell,* 39(5), pp. 665-76.
Goodarzi, A. A., Noon, A. T., Deckbar, D., Ziv, Y., Shiloh, Y., Löbrich, M. and Jeggo, P. A. (2008) 'ATM signaling facilitates repair of DNA double-strand breaks associated with heterochromatin', *Mol Cell,* 31(2), pp. 167-77.
Gordon, J. L., Byrne, K. P. and Wolfe, K. H. (2011) 'Mechanisms of chromosome number evolution in yeast', *PLoS Genet,* 7(7), pp. e1002190.
Grandin, N., Damon, C. and Charbonneau, M. (2000) 'Cdc13 cooperates with the yeast Ku proteins and Stn1 to regulate telomerase recruitment', *Mol Cell Biol,* 20(22), pp. 8397-408.
Greenberg, R. A. (2008) 'Recognition of DNA double strand breaks by the BRCA1 tumor suppressor network', *Chromosoma,* 117(4), pp. 305-17.
Greider, C. W. and Blackburn, E. H. (1985) 'Identification of a specific telomere terminal transferase activity in Tetrahymena extracts', *Cell,* 43(2 Pt 1), pp. 405-13.
Griffith, J. D., Comeau, L., Rosenfield, S., Stansel, R. M., Bianchi, A., Moss, H. and de Lange, T. (1999) 'Mammalian telomeres end in a large duplex loop', *Cell,* 97(4), pp. 503-14.
Grundy, G. J., Rulten, S. L., Zeng, Z., Arribas-Bosacoma, R., Iles, N., Manley, K., Oliver, A. and Caldecott, K. W. (2013) 'APLF promotes the assembly and activity of non-homologous end joining protein complexes', *EMBO J,* 32(1), pp. 112-25.
Guo, X., Deng, Y., Lin, Y., Cosme-Blanco, W., Chan, S., He, H., Yuan, G., Brown, E. J. and Chang, S. (2007) 'Dysfunctional telomeres activate an ATM-ATR-dependent DNA damage response to suppress tumorigenesis', *EMBO J,* 26(22), pp. 4709-19.

Haahr, P., Hoffmann, S., Tollenaere, M. A., Ho, T., Toledo, L. I., Mann, M., Bekker-Jensen, S., Räschle, M. and Mailand, N. (2016) 'Activation of the ATR kinase by the RPA-binding protein ETAA1', *Nat Cell Biol,* 18(11), pp. 1196-1207.

Haince, J. F., McDonald, D., Rodrigue, A., Déry, U., Masson, J. Y., Hendzel, M. J. and Poirier, G. G. (2008) 'PARP1-dependent kinetics of recruitment of MRE11 and NBS1 proteins to multiple DNA damage sites', *J Biol Chem,* 283(2), pp. 1197-208.

Hauer, M. H. and Gasser, S. M. (2017) 'Chromatin and nucleosome dynamics in DNA damage and repair', *Genes Dev,* 31(22), pp. 2204-2221.

Hayflick L. (1965) 'T he limited in vitro lifetime of human diploid cell strains', *Exp Cell Res,* 37, pp. 614-36.

Hecht, A., Laroche, T., Strahl-Bolsinger, S., Gasser, S. M. and Grunstein, M. (1995) 'Histone H3 and H4 N-termini interact with SIR3 and SIR4 proteins: a molecular model for the formation of heterochromatin in yeast', *Cell,* 80(4), pp. 583-92.

Her, J., Soo Lee, N., Kim, Y. and Kim, H. (2016) 'Factors forming the BRCA1-A complex orchestrate BRCA1 recruitment to the sites of DNA damage', *Acta Biochim Biophys Sin (Shanghai),* 48(7), pp. 658-64.

Herrmann, G., Lindahl, T. and Schär, P. (1998) 'Saccharomyces cerevisiae LIF1: a function involved in DNA double-strand break repair related to mammalian XRCC4', *EMBO J,* 17(14), pp. 4188-98.

Hewitt, G., Jurk, D., Marques, F. D., Correia-Melo, C., Hardy, T., Gackowska, A., Anderson, R., Taschuk, M., Mann, J. and Passos, J. F. (2012) 'Telomeres are favoured targets of a persistent DNA damage response in ageing and stress-induced senescence', *Nat Commun,* 3, pp. 708.

Heyer, W. D., Ehmsen, K. T. and Liu, J. (2010) 'Regulation of homologous recombination in eukaryotes', *Annu Rev Genet,* 44, pp. 113-39.

Hoa, N. N., Kobayashi, J., Omura, M., Hirakawa, M., Yang, S. H., Komatsu, K., Paull, T. T., Takeda, S. and Sasanuma, H. (2015) 'BRCA1 and CtIP Are Both Required to Recruit Dna2 at Double-Strand Breaks in Homologous Recombination', *PLoS One,* 10(4), pp. e0124495.

Huet, J., Cottrelle, P., Cool, M., Vignais, M. L., Thiele, D., Marck, C., Buhler, J. M., Sentenac, A. and Fromageot, P. (1985) 'A general upstream binding factor for genes of the yeast translational apparatus', *EMBO J,* 4(13A), pp. 3539-47.

Iijima, K., Ohara, M., Seki, R. and Tauchi, H. (2008) 'Dancing on damaged chromatin: functions of ATM and the RAD50/MRE11/NBS1 complex in cellular responses to DNA damage', *J Radiat Res,* 49(5), pp. 451-64.

IJdo, J. W., Baldini, A., Ward, D. C., Reeders, S. T. and Wells, R. A. (1991) 'Origin of human chromosome 2: an ancestral telomere-telomere fusion', *Proc Natl Acad Sci U S A,* 88(20), pp. 9051-5.

Janoušková, E., Nečasová, I., Pavloušková, J., Zimmermann, M., Hluchý, M., Marini, V., Nováková, M. and Hofr, C. (2015) 'Human Rap1 modulates TRF2 attraction to telomeric DNA', *Nucleic Acids Res,* 43(5), pp. 2691-700.

Jasin, M. and Rothstein, R. (2013) 'Repair of strand breaks by homologous recombination', *Cold Spring Harb Perspect Biol,* 5(11), pp. a012740.

Jiang, W., Crowe, J. L., Liu, X., Nakajima, S., Wang, Y., Li, C., Lee, B. J., Dubois, R. L., Liu, C., Yu, X., Lan, L. and Zha, S. (2015) 'Differential phosphorylation of DNA-PKcs regulates the interplay between end-processing and end-ligation during nonhomologous end-joining', *Mol Cell,* 58(1), pp. 172-85.

Kabir, S., Hockemeyer, D. and de Lange, T. (2014) 'TALEN gene knockouts reveal no requirement for the conserved human shelterin protein Rap1 in telomere protection and length regulation', *Cell Rep,* 9(4), pp. 1273-80.

Kadyk, L. C. and Hartwell, L. H. (1992) 'Sister chromatids are preferred over homologs as substrates for recombinational repair in Saccharomyces cerevisiae', *Genetics,* 132(2), pp. 387-402.

Kanaar, R., Troelstra, C., Swagemakers, S. M., Essers, J., Smit, B., Franssen, J. H., Pastink, A., Bezzubova, O. Y., Buerstedde, J. M., Clever, B., Heyer, W. D. and Hoeijmakers, J. H. (1996) 'Human and mouse homologs of the Saccharomyces cerevisiae RAD54 DNA repair gene: evidence for functional conservation', *Curr Biol,* 6(7), pp. 828-38.

Kaniecki, K., De Tullio, L. and Greene, E. C. (2018) 'A change of view: homologous recombination at single-molecule resolution', *Nat Rev Genet,* 19(4), pp. 191-207.

Karlseder, J., Smogorzewska, A. and de Lange, T. (2002) 'Senescence induced by altered telomere state, not telomere loss', *Science,* 295(5564), pp. 2446-9.

Kaul, Z., Cesare, A. J., Huschtscha, L. I., Neumann, A. A. and Reddel, R. R. (2011) 'Five dysfunctional telomeres predict onset of senescence in human cells', *EMBO Rep,* 13(1), pp. 52-9.

Kazda, A., Zellinger, B., Rössler, M., Derboven, E., Kusenda, B. and Riha, K. (2012) 'Chromosome end protection by blunt-ended telomeres', *Genes Dev,* 26(15), pp. 1703-13.

Kent, T., Chandramouly, G., McDevitt, S. M., Ozdemir, A. Y. and Pomerantz, R. T. (2015) 'Mechanism of microhomology-mediated end-joining promoted by human DNA polymerase θ', *Nat Struct Mol Biol,* 22(3), pp. 230-7.

Kim, H., Li, F., He, Q., Deng, T., Xu, J., Jin, F., Coarfa, C., Putluri, N., Liu, D. and Songyang, Z. (2017) 'Systematic analysis of human telomeric dysfunction using inducible telosome/shelterin CRISPR/Cas9 knockout cells', *Cell Discov,* 3, pp. 17034.

Kim, N. W., Piatyszek, M. A., Prowse, K. R., Harley, C. B., West, M. D., Ho, P. L., Coviello, G. M., Wright, W. E., Weinrich, S. L. and Shay, J. W. (1994) 'Specific association of human telomerase activity with immortal cells and cancer', *Science,* 266(5193), pp. 2011-5.

Klein, F., Laroche, T., Cardenas, M. E., Hofmann, J. F., Schweizer, D. and Gasser, S. M. (1992) 'Localization of RAP1 and topoisomerase II in nuclei and meiotic chromosomes of yeast', *J Cell Biol,* 117(5), pp. 935-48.

Kumagai, A., Lee, J., Yoo, H. Y. and Dunphy, W. G. (2006) 'TopBP1 activates the ATR-ATRIP complex', *Cell,* 124(5), pp. 943-55.

Kwei, K. A., Kung, Y., Salari, K., Holcomb, I. N. and Pollack, J. R. (2010) 'Genomic instability in breast cancer: pathogenesis and clinical implications', *Mol Oncol,* 4(3), pp. 255-66.

Lam, Y. C., Akhter, S., Gu, P., Ye, J., Poulet, A., Giraud-Panis, M. J., Bailey, S. M., Gilson, E., Legerski, R. J. and Chang, S. (2010) 'SNMIB/Apollo protects leading-strand telomeres against NHEJ-mediated repair', *EMBO J,* 29(13), pp. 2230-41.

Lamarche, B. J., Orazio, N. I. and Weitzman, M. D. (2010) 'The MRN complex in double-strand break repair and telomere maintenance', *FEBS Lett,* 584(17), pp. 3682-95.

Langerak, P., Mejia-Ramirez, E., Limbo, O. and Russell, P. (2011) 'Release of Ku and MRN from DNA ends by Mre11 nuclease activity and Ctp1 is required for homologous recombination repair of double-strand breaks', *PLoS Genet,* 7(9), pp. e1002271.

Le Guen, T., Ragu, S., Guirouilh-Barbat, J. and Lopez, B. S. (2015) 'Role of the double-strand break repair pathway in the maintenance of genomic stability', *Mol Cell Oncol,* 2(1), pp. e968020.

Lee, J. H., Goodarzi, A. A., Jeggo, P. A. and Paull, T. T. (2010) '53BP1 promotes ATM activity through direct interactions with the MRN complex', *EMBO J,* 29(3), pp. 574-85.
Lee, J. H. and Paull, T. T. (2005) 'ATM activation by DNA double-strand breaks through the Mre11-Rad50-Nbs1 complex', *Science,* 308(5721), pp. 551-4.
Lee, Y. C., Zhou, Q., Chen, J. and Yuan, J. (2016) 'RPA-Binding Protein ETAA1 Is an ATR Activator Involved in DNA Replication Stress Response', *Curr Biol,* 26(24), pp. 3257-3268.
Lenain, C., Bauwens, S., Amiard, S., Brunori, M., Giraud-Panis, M. J. and Gilson, E. (2006) 'The Apollo 5' exonuclease functions together with TRF2 to protect telomeres from DNA repair', *Curr Biol,* 16(13), pp. 1303-10.
Letsolo, B. T., Rowson, J. and Baird, D. M. (2010) 'Fusion of short telomeres in human cells is characterized by extensive deletion and microhomology, and can result in complex rearrangements', *Nucleic Acids Res,* 38(6), pp. 1841-52.
Li, B. and de Lange, T. (2003) 'Rap1 affects the length and heterogeneity of human telomeres', *Mol Biol Cell,* 14(12), pp. 5060-8.
Li, B., Oestreich, S. and de Lange, T. (2000) 'Identification of human Rap1: implications for telomere evolution', *Cell,* 101(5), pp. 471-83.
Li, X. and Heyer, W. D. (2009) 'RAD54 controls access to the invading 3'-OH end after RAD51-mediated DNA strand invasion in homologous recombination in Saccharomyces cerevisiae', *Nucleic Acids Res,* 37(2), pp. 638-46.
Lieber, M. R. (2010) 'The mechanism of double-strand DNA break repair by the nonhomologous DNA end-joining pathway', *Annu Rev Biochem,* 79, pp. 181-211.
Lingner, J., Cooper, J. P. and Cech, T. R. (1995) 'Telomerase and DNA end replication: no longer a lagging strand problem?', *Science,* 269(5230), pp. 1533-4.
Lisby, M., Mortensen, U. H. and Rothstein, R. (2003) 'Colocalization of multiple DNA double-strand breaks at a single Rad52 repair centre', *Nat Cell Biol,* 5(6), pp. 572-7.
Liti, G. (2018) 'Yeast chromosome numbers minimized using genome editing', *Nature,* 560(7718), pp. 317-318.
Liti, G. and Louis, E. J. (2003) 'NEJ1 prevents NHEJ-dependent telomere fusions in yeast without telomerase', *Mol Cell,* 11(5), pp. 1373-8.
Liu, S., Shiotani, B., Lahiri, M., Maréchal, A., Tse, A., Leung, C. C., Glover, J. N., Yang, X. H. and Zou, L. (2011) 'ATR autophosphorylation as a molecular switch for checkpoint activation', *Mol Cell,* 43(2), pp. 192-202.
Liu, X., Shao, Z., Jiang, W., Lee, B. J. and Zha, S. (2017) 'PAXX promotes KU accumulation at DNA breaks and is essential for end-joining in XLF-deficient mice', *Nat Commun,* 8, pp. 13816.
Lottersberger, F., Karssemeijer, R. A., Dimitrova, N. and de Lange, T. (2015) '53BP1 and the LINC Complex Promote Microtubule-Dependent DSB Mobility and DNA Repair', *Cell,* 163(4), pp. 880-93.
Lu, G., Duan, J., Shu, S., Wang, X., Gao, L., Guo, J. and Zhang, Y. (2016) 'Ligase I and ligase III mediate the DNA double-strand break ligation in alternative end-joining', *Proc Natl Acad Sci U S A,* 113(5), pp. 1256-60.
Luo, J., Sun, X., Cormack, B. P. and Boeke, J. D. (2018) 'Karyotype engineering by chromosome fusion leads to reproductive isolation in yeast', *Nature,* 560(7718), pp. 392-396.
Lustig, A. J., Kurtz, S. and Shore, D. (1990) 'Involvement of the silencer and UAS binding protein RAP1 in regulation of telomere length', *Science,* 250(4980), pp. 549-53.

Lysak, M. A., Berr, A., Pecinka, A., Schmidt, R., McBreen, K. and Schubert, I. (2006) 'Mechanisms of chromosome number reduction in Arabidopsis thaliana and related Brassicaceae species', *Proc Natl Acad Sci U S A,* 103(13), pp. 5224-9.

Maciejowski, J. and de Lange, T. (2017) 'Telomeres in cancer: tumour suppression and genome instability', *Nat Rev Mol Cell Biol,* 18(3), pp. 175-186.

Macrae, C. J., McCulloch, R. D., Ylanko, J., Durocher, D. and Koch, C. A. (2008) 'APLF (C2orf13) facilitates nonhomologous end-joining and undergoes ATM-dependent hyperphosphorylation following ionizing radiation', *DNA Repair (Amst),* 7(2), pp. 292-302.

Maillet, L., Boscheron, C., Gotta, M., Marcand, S., Gilson, E. and Gasser, S. M. (1996) 'Evidence for silencing compartments within the yeast nucleus: a role for telomere proximity and Sir protein concentration in silencer-mediated repression', *Genes Dev,* 10(14), pp. 1796-811.

Maloisel, L., Fabre, F. and Gangloff, S. (2008) 'DNA polymerase delta is preferentially recruited during homologous recombination to promote heteroduplex DNA extension', *Mol Cell Biol,* 28(4), pp. 1373-82.

Malu, S., Malshetty, V., Francis, D. and Cortes, P. (2012) 'Role of non-homologous end joining in V(D)J recombination', *Immunol Res,* 54(1-3), pp. 233-46.

Marcand, S. (2014) 'How do telomeres and NHEJ coexist?', *Mol Cell Oncol,* 1(3), pp. e963438.

Marcand, S., Buck, S. W., Moretti, P., Gilson, E. and Shore, D. (1996) 'Silencing of genes at nontelomeric sites in yeast is controlled by sequestration of silencing factors at telomeres by Rap 1 protein', *Genes Dev,* 10(11), pp. 1297-309.

Marcand, S., Gilson, E. and Shore, D. (1997) 'A protein-counting mechanism for telomere length regulation in yeast', *Science,* 275(5302), pp. 986-90.

Marcand, S., Pardo, B., Gratias, A., Cahun, S. and Callebaut, I. (2008) 'Multiple pathways inhibit NHEJ at telomeres', *Genes Dev,* 22(9), pp. 1153-8.

Marnef, A. and Legube, G. (2017) 'Organizing DNA repair in the nucleus: DSBs hit the road', *Curr Opin Cell Biol,* 46, pp. 1-8.

Martin, L. J. (2008) 'DNA damage and repair: relevance to mechanisms of neurodegeneration', *J Neuropathol Exp Neurol,* 67(5), pp. 377-87.

Martinez, P., Thanasoula, M., Carlos, A. R., Gómez-López, G., Tejera, A. M., Schoeftner, S., Dominguez, O., Pisano, D. G., Tarsounas, M. and Blasco, M. A. (2010) 'Mammalian Rap1 controls telomere function and gene expression through binding to telomeric and extratelomeric sites', *Nat Cell Biol,* 12(8), pp. 768-80.

Martínez, P. and Blasco, M. A. (2017) 'Telomere-driven diseases and telomere-targeting therapies', *J Cell Biol,* 216(4), pp. 875-887.

Martínez, P., Gómez-López, G., García, F., Mercken, E., Mitchell, S., Flores, J. M., de Cabo, R. and Blasco, M. A. (2013) 'RAP1 protects from obesity through its extratelomeric role regulating gene expression', *Cell Rep,* 3(6), pp. 2059-74.

Martínez, P., Gómez-López, G., Pisano, D. G., Flores, J. M. and Blasco, M. A. (2016) 'A genetic interaction between RAP1 and telomerase reveals an unanticipated role for RAP1 in telomere maintenance', *Aging Cell,* 15(6), pp. 1113-1125.

Martínez, P., Thanasoula, M., Muñoz, P., Liao, C., Tejera, A., McNees, C., Flores, J. M., Fernández-Capetillo, O., Tarsounas, M. and Blasco, M. A. (2009) 'Increased telomere fragility and fusions resulting from TRF1 deficiency lead to degenerative pathologies and increased cancer in mice', *Genes Dev,* 23(17), pp. 2060-75.

Maréchal, A. and Zou, L. (2013) 'DNA damage sensing by the ATM and ATR kinases', *Cold Spring Harb Perspect Biol,* 5(9).

Masani, S., Han, L., Meek, K. and Yu, K. (2016) 'Redundant function of DNA ligase 1 and 3 in alternative end-joining during immunoglobulin class switch recombination', *Proc Natl Acad Sci U S A,* 113(5), pp. 1261-6.

Mateos-Gomez, P. A., Gong, F., Nair, N., Miller, K. M., Lazzerini-Denchi, E. and Sfeir, A. (2015) 'Mammalian polymerase θ promotes alternative NHEJ and suppresses recombination', *Nature,* 518(7538), pp. 254-7.

Mazin, A. V., Mazina, O. M., Bugreev, D. V. and Rossi, M. J. (2010) 'Rad54, the motor of homologous recombination', *DNA Repair (Amst),* 9(3), pp. 286-302.

McClintock, B. (1939) 'The Behavior in Successive Nuclear Divisions of a Chromosome Broken at Meiosis', *Proc Natl Acad Sci U S A,* 25(8), pp. 405-16.

McClintock, B. (1941) 'The Stability of Broken Ends of Chromosomes in Zea Mays', *Genetics,* 26(2), pp. 234-82.

McVey, M., Khodaverdian, V. Y., Meyer, D., Cerqueira, P. G. and Heyer, W. D. (2016) 'Eukaryotic DNA Polymerases in Homologous Recombination', *Annu Rev Genet,* 50, pp. 393-421.

Meselson, M. and Stahl, F. W. (1958) 'THE REPLICATION OF DNA IN ESCHERICHIA COLI', *Proc Natl Acad Sci U S A,* 44(7), pp. 671-82.

Miller, K. M., Ferreira, M. G. and Cooper, J. P. (2005) 'Taz1, Rap1 and Rif1 act both interdependently and independently to maintain telomeres', *EMBO J,* 24(17), pp. 3128-35.

Mimitou, E. P. and Symington, L. S. (2009) 'Nucleases and helicases take center stage in homologous recombination', *Trends Biochem Sci,* 34(5), pp. 264-72.

Mladenov, E., Magin, S., Soni, A. and Iliakis, G. (2016) 'DNA double-strand-break repair in higher eukaryotes and its role in genomic instability and cancer: Cell cycle and proliferation-dependent regulation', *Semin Cancer Biol,* 37-38, pp. 51-64.

Mordes, D. A., Glick, G. G., Zhao, R. and Cortez, D. (2008) 'TopBP1 activates ATR through ATRIP and a PIKK regulatory domain', *Genes Dev,* 22(11), pp. 1478-89.

Moretti, P., Freeman, K., Coodly, L. and Shore, D. (1994) 'Evidence that a complex of SIR proteins interacts with the silencer and telomere-binding protein RAP1', *Genes Dev,* 8(19), pp. 2257-69.

Moynahan, M. E., Chiu, J. W., Koller, B. H. and Jasin, M. (1999) 'Brca1 controls homology-directed DNA repair', *Mol Cell,* 4(4), pp. 511-8.

Muller, H. 1938. The remaking of chromosomes. Collect.Net.

Muraki, K. and Murnane, J. P. (2018) 'The DNA damage response at dysfunctional telomeres, and at interstitial and subtelomeric DNA double-strand breaks', *Genes Genet Syst,* 92(3), pp. 135-152.

Nagai, S., Dubrana, K., Tsai-Pflugfelder, M., Davidson, M. B., Roberts, T. M., Brown, G. W., Varela, E., Hediger, F., Gasser, S. M. and Krogan, N. J. (2008) 'Functional targeting of DNA damage to a nuclear pore-associated SUMO-dependent ubiquitin ligase', *Science,* 322(5901), pp. 597-602.

Nguyen, T. H. D., Tam, J., Wu, R. A., Greber, B. J., Toso, D., Nogales, E. and Collins, K. (2018) 'Cryo-EM structure of substrate-bound human telomerase holoenzyme', *Nature,* 557(7704), pp. 190-195.

Nimonkar, A. V., Genschel, J., Kinoshita, E., Polaczek, P., Campbell, J. L., Wyman, C., Modrich, P. and Kowalczykowski, S. C. (2011) 'BLM-DNA2-RPA-MRN and EXO1-BLM-RPA-MRN constitute two DNA end resection machineries for human DNA break repair', *Genes Dev,* 25(4), pp. 350-62.

Noon, A. T., Shibata, A., Rief, N., Löbrich, M., Stewart, G. S., Jeggo, P. A. and Goodarzi, A. A. (2010) '53BP1-dependent robust localized KAP-1 phosphorylation is essential for heterochromatic DNA double-strand break repair', *Nat Cell Biol,* 12(2), pp. 177-84.

O'Connor, M. S., Safari, A., Liu, D., Qin, J. and Songyang, Z. (2004) 'The human Rap1 protein complex and modulation of telomere length', *J Biol Chem,* 279(27), pp. 28585-91.

Ochi, T., Blackford, A. N., Coates, J., Jhujh, S., Mehmood, S., Tamura, N., Travers, J., Wu, Q., Draviam, V. M., Robinson, C. V., Blundell, T. L. and Jackson, S. P. (2015) 'DNA repair. PAXX, a paralog of XRCC4 and XLF, interacts with Ku to promote DNA double-strand break repair', *Science,* 347(6218), pp. 185-188.

Okamoto, K., Bartocci, C., Ouzounov, I., Diedrich, J. K., Yates, J. R. and Denchi, E. L. (2013) 'A two-step mechanism for TRF2-mediated chromosome-end protection', *Nature,* 494(7438), pp. 502-5.

Olovnikov, A. M. (1973) 'A theory of marginotomy. The incomplete copying of template margin in enzymic synthesis of polynucleotides and biological significance of the phenomenon', *J Theor Biol,* 41(1), pp. 181-90.

Orthwein, A., Fradet-Turcotte, A., Noordermeer, S. M., Canny, M. D., Brun, C. M., Strecker, J., Escribano-Diaz, C. and Durocher, D. (2014) 'Mitosis inhibits DNA double-strand break repair to guard against telomere fusions', *Science,* 344(6180), pp. 189-93.

Ottaviani, D., LeCain, M. and Sheer, D. (2014) 'The role of microhomology in genomic structural variation', *Trends Genet,* 30(3), pp. 85-94.

Oza, P., Jaspersen, S. L., Miele, A., Dekker, J. and Peterson, C. L. (2009) 'Mechanisms that regulate localization of a DNA double-strand break to the nuclear periphery', *Genes Dev,* 23(8), pp. 912-27.

Oza, P. and Peterson, C. L. (2010) 'Opening the DNA repair toolbox: localization of DNA double strand breaks to the nuclear periphery', *Cell Cycle,* 9(1), pp. 43-9.

Pannunzio, N. R., Li, S., Watanabe, G. and Lieber, M. R. (2014) 'Non-homologous end joining often uses microhomology: implications for alternative end joining', *DNA Repair (Amst),* 17, pp. 74-80.

Pardo, B. and Marcand, S. (2005) 'Rap1 prevents telomere fusions by nonhomologous end joining', *EMBO J,* 24(17), pp. 3117-27.

Park, S., Kang, J. M., Kim, S. J., Kim, H., Hong, S. and Lee, Y. J. (2015) 'Smad7 enhances ATM activity by facilitating the interaction between ATM and Mre11-Rad50-Nbs1 complex in DNA double-strand break repair', *Cell Mol Life Sci,* 72(3), pp. 583-596.

Phan, A. T. and Mergny, J. L. (2002) 'Human telomeric DNA: G-quadruplex, i-motif and Watson-Crick double helix', *Nucleic Acids Res,* 30(21), pp. 4618-25.

Plate, I., Hallwyl, S. C., Shi, I., Krejci, L., Müller, C., Albertsen, L., Sung, P. and Mortensen, U. H. (2008) 'Interaction with RPA is necessary for Rad52 repair center formation and for its mediator activity', *J Biol Chem,* 283(43), pp. 29077-85.

Platt, J. M., Ryvkin, P., Wanat, J. J., Donahue, G., Ricketts, M. D., Barrett, S. P., Waters, H. J., Song, S., Chavez, A., Abdallah, K. O., Master, S. R., Wang, L. S. and Johnson, F. B. (2013) 'Rap1 relocalization contributes to the chromatin-mediated gene expression profile and pace of cell senescence', *Genes Dev,* 27(12), pp. 1406-20.

Podhorecka, M., Skladanowski, A. and Bozko, P. (2010) 'H2AX Phosphorylation: Its Role in DNA Damage Response and Cancer Therapy', *J Nucleic Acids,* 2010.

Polo, S. E. and Jackson, S. P. (2011) 'Dynamics of DNA damage response proteins at DNA breaks: a focus on protein modifications', *Genes Dev,* 25(5), pp. 409-33.

Poschke, H., Dees, M., Chang, M., Amberkar, S., Kaderali, L., Rothstein, R. and Luke, B. (2012) 'Rif2 promotes a telomere fold-back structure through Rpd3L recruitment in budding yeast', *PLoS Genet,* 8(9), pp. e1002960.

Poulet, A., Buisson, R., Faivre-Moskalenko, C., Koelblen, M., Amiard, S., Montel, F., Cuesta-Lopez, S., Bornet, O., Guerlesquin, F., Godet, T., Moukhtar, J., Argoul, F., Déclais, A. C., Lilley, D. M., Ip, S. C., West, S. C., Gilson, E. and Giraud-Panis, M. J. (2009) 'TRF2 promotes, remodels and protects telomeric Holliday junctions', *EMBO J,* 28(6), pp. 641-51.

Rai, R., Chen, Y., Lei, M. and Chang, S. (2016) 'TRF2-RAP1 is required to protect telomeres from engaging in homologous recombination-mediated deletions and fusions', *Nat Commun,* 7, pp. 10881.

Rai, R., Hu, C., Broton, C., Chen, Y., Lei, M. and Chang, S. (2017) 'NBS1 Phosphorylation Status Dictates Repair Choice of Dysfunctional Telomeres', *Mol Cell,* 65(5), pp. 801-817.e4.

Ramsden, D. A. (2011) 'Polymerases in nonhomologous end joining: building a bridge over broken chromosomes', *Antioxid Redox Signal,* 14(12), pp. 2509-19.

Ray Chaudhuri, A. and Nussenzweig, A. (2017) 'The multifaceted roles of PARP1 in DNA repair and chromatin remodelling', *Nat Rev Mol Cell Biol,* 18(10), pp. 610-621.

Ray, S., Breuer, G., DeVeaux, M., Zelterman, D., Bindra, R. and Sweasy, J. B. (2018) 'DNA polymerase beta participates in DNA End-joining', *Nucleic Acids Res,* 46(1), pp. 242-255.

Riballo, E., Kühne, M., Rief, N., Doherty, A., Smith, G. C., Recio, M. J., Reis, C., Dahm, K., Fricke, A., Krempler, A., Parker, A. R., Jackson, S. P., Gennery, A., Jeggo, P. A. and Löbrich, M. (2004) 'A pathway of double-strand break rejoining dependent upon ATM, Artemis, and proteins locating to gamma-H2AX foci', *Mol Cell,* 16(5), pp. 715-24.

Ribes-Zamora, A., Indiviglio, S. M., Mihalek, I., Williams, C. L. and Bertuch, A. A. (2013) 'TRF2 interaction with Ku heterotetramerization interface gives insight into c-NHEJ prevention at human telomeres', *Cell Rep,* 5(1), pp. 194-206.

Roberts, S. A. and Ramsden, D. A. (2007) 'Loading of the nonhomologous end joining factor, Ku, on protein-occluded DNA ends', *J Biol Chem,* 282(14), pp. 10605-13.

Rossiello, F., Aguado, J., Sepe, S., Iannelli, F., Nguyen, Q., Pitchiaya, S., Carninci, P. and d'Adda di Fagagna, F. (2017) 'DNA damage response inhibition at dysfunctional telomeres by modulation of telomeric DNA damage response RNAs', *Nat Commun,* 8, pp. 13980.

Rudd, M. K., Friedman, C., Parghi, S. S., Linardopoulou, E. V., Hsu, L. and Trask, B. J. (2007) 'Elevated rates of sister chromatid exchange at chromosome ends', *PLoS Genet,* 3(2), pp. e32.

Saint-Léger, A., Koelblen, M., Civitelli, L., Bah, A., Djerbi, N., Giraud-Panis, M. J., Londoño-Vallejo, A., Ascenzioni, F. and Gilson, E. (2014) 'The basic N-terminal domain of TRF2 limits recombination endonuclease action at human telomeres', *Cell Cycle,* 13(15), pp. 2469-74.

Sallmyr, A. and Tomkinson, A. E. (2018) 'Repair of DNA double-strand breaks by mammalian alternative end-joining pathways', *J Biol Chem,* 293(27), pp. 10536-10546.

Sarthy, J., Bae, N. S., Scrafford, J. and Baumann, P. (2009) 'Human RAP1 inhibits non-homologous end joining at telomeres', *EMBO J,* 28(21), pp. 3390-9.

Sartori, A. A., Lukas, C., Coates, J., Mistrik, M., Fu, S., Bartek, J., Baer, R., Lukas, J. and Jackson, S. P. (2007) 'Human CtIP promotes DNA end resection', *Nature,* 450(7169), pp. 509-14.

Schmidt, J. C. and Cech, T. R. (2015) 'Human telomerase: biogenesis, trafficking, recruitment, and activation', *Genes Dev,* 29(11), pp. 1095-105.

Schmutz, I., Timashev, L., Xie, W., Patel, D. J. and de Lange, T. (2017) 'TRF2 binds branched DNA to safeguard telomere integrity', *Nat Struct Mol Biol,* 24(9), pp. 734-742.

Schober, H., Ferreira, H., Kalck, V., Gehlen, L. R. and Gasser, S. M. (2009) 'Yeast telomerase and the SUN domain protein Mps3 anchor telomeres and repress subtelomeric recombination', *Genes Dev,* 23(8), pp. 928-38.

Schubert, I. (2007) 'Chromosome evolution', *Curr Opin Plant Biol,* 10(2), pp. 109-15.

Seluanov, A., Danek, J., Hause, N. and Gorbunova, V. (2007) 'Changes in the level and distribution of Ku proteins during cellular senescence', *DNA Repair (Amst),* 6(12), pp. 1740-8.

Selvarajah, S., Yoshimoto, M., Park, P. C., Maire, G., Paderova, J., Bayani, J., Lim, G., Al-Romaih, K., Squire, J. A. and Zielenska, M. (2006) 'The breakage-fusion-bridge (BFB) cycle as a mechanism for generating genetic heterogeneity in osteosarcoma', *Chromosoma,* 115(6), pp. 459-67.

Sfeir, A. and de Lange, T. (2012) 'Removal of shelterin reveals the telomere end-protection problem', *Science,* 336(6081), pp. 593-7.

Sfeir, A., Kabir, S., van Overbeek, M., Celli, G. B. and de Lange, T. (2010) 'Loss of Rap1 induces telomere recombination in the absence of NHEJ or a DNA damage signal', *Science,* 327(5973), pp. 1657-61.

Sfeir, A., Kosiyatrakul, S. T., Hockemeyer, D., MacRae, S. L., Karlseder, J., Schildkraut, C. L. and de Lange, T. (2009) 'Mammalian telomeres resemble fragile sites and require TRF1 for efficient replication', *Cell,* 138(1), pp. 90-103.

Shamanna, R. A., Lu, H., de Freitas, J. K., Tian, J., Croteau, D. L. and Bohr, V. A. (2016) 'WRN regulates pathway choice between classical and alternative non-homologous end joining', *Nat Commun,* 7, pp. 13785.

Shao, Y., Lu, N., Wu, Z., Cai, C., Wang, S., Zhang, L. L., Zhou, F., Xiao, S., Liu, L., Zeng, X., Zheng, H., Yang, C., Zhao, Z., Zhao, G., Zhou, J. Q., Xue, X. and Qin, Z. (2018) 'Creating a functional single-chromosome yeast', *Nature,* 560(7718), pp. 331-335.

Sharif, H., Li, Y., Dong, Y., Dong, L., Wang, W. L., Mao, Y. and Wu, H. (2017) 'Cryo-EM structure of the DNA-PK holoenzyme', *Proc Natl Acad Sci U S A,* 114(28), pp. 7367-7372.

Sharma, V., Khurana, S., Kubben, N., Abdelmohsen, K., Oberdoerffer, P., Gorospe, M. and Misteli, T. (2015) 'A BRCA1-interacting lncRNA regulates homologous recombination', *EMBO Rep,* 16(11), pp. 1520-34.

Shay, J. W. and Wright, W. E. (2004) 'Telomeres are double-strand DNA breaks hidden from DNA damage responses', *Mol Cell,* 14(4), pp. 420-1.

Shimada, M., Dumitrache, L. C., Russell, H. R. and McKinnon, P. J. (2015) 'Polynucleotide kinase-phosphatase enables neurogenesis via multiple DNA repair pathways to maintain genome stability', *EMBO J,* 34(19), pp. 2465-80.

Shiotani, B., Nguyen, H. D., Håkansson, P., Maréchal, A., Tse, A., Tahara, H. and Zou, L. (2013) 'Two distinct modes of ATR activation orchestrated by Rad17 and Nbs1', *Cell Rep,* 3(5), pp. 1651-62.

Shiotani, B. and Zou, L. (2009) 'Single-stranded DNA orchestrates an ATM-to-ATR switch at DNA breaks', *Mol Cell,* 33(5), pp. 547-58.

Shore, D. and Nasmyth, K. (1987) 'Purification and cloning of a DNA binding protein from yeast that binds to both silencer and activator elements', *Cell,* 51(5), pp. 721-32.

Simsek, D., Brunet, E., Wong, S. Y., Katyal, S., Gao, Y., McKinnon, P. J., Lou, J., Zhang, L., Li, J., Rebar, E. J., Gregory, P. D., Holmes, M. C. and Jasin, M. (2011) 'DNA ligase III promotes alternative nonhomologous end-joining during chromosomal translocation formation', *PLoS Genet,* 7(6), pp. e1002080.

Sishc, B. J. and Davis, A. J. (2017) 'The Role of the Core Non-Homologous End Joining Factors in Carcinogenesis and Cancer', *Cancers (Basel),* 9(7).

Smith, M. J. and Rothstein, R. (2017) 'Poetry in motion: Increased chromosomal mobility after DNA damage', *DNA Repair (Amst),* 56, pp. 102-108.

Smogorzewska, A., Karlseder, J., Holtgreve-Grez, H., Jauch, A. and de Lange, T. (2002) 'DNA ligase IV-dependent NHEJ of deprotected mammalian telomeres in G1 and G2', *Curr Biol,* 12(19), pp. 1635-44.

Spagnolo, L., Rivera-Calzada, A., Pearl, L. H. and Llorca, O. (2006) 'Three-dimensional structure of the human DNA-PKcs/Ku70/Ku80 complex assembled on DNA and its implications for DNA DSB repair', *Mol Cell,* 22(4), pp. 511-9.

Stark, J. M., Pierce, A. J., Oh, J., Pastink, A. and Jasin, M. (2004) 'Genetic steps of mammalian homologous repair with distinct mutagenic consequences', *Mol Cell Biol,* 24(21), pp. 9305-16.

Stewart, G. S., Wang, B., Bignell, C. R., Taylor, A. M. and Elledge, S. J. (2003) 'MDC1 is a mediator of the mammalian DNA damage checkpoint', *Nature,* 421(6926), pp. 961-6.

Stucki, M., Clapperton, J. A., Mohammad, D., Yaffe, M. B., Smerdon, S. J. and Jackson, S. P. (2005) 'MDC1 directly binds phosphorylated histone H2AX to regulate cellular responses to DNA double-strand breaks', *Cell,* 123(7), pp. 1213-26.

Sturzenegger, A., Burdova, K., Kanagaraj, R., Levikova, M., Pinto, C., Cejka, P. and Janscak, P. (2014) 'DNA2 cooperates with the WRN and BLM RecQ helicases to mediate long-range DNA end resection in human cells', *J Biol Chem,* 289(39), pp. 27314-26.

Sugiyama, T. and Kowalczykowski, S. C. (2002) 'Rad52 protein associates with replication protein A (RPA)-single-stranded DNA to accelerate Rad51-mediated displacement of RPA and presynaptic complex formation', *J Biol Chem,* 277(35), pp. 31663-72.

Suzuki, M., Suzuki, K., Kodama, S., Yamashita, S. and Watanabe, M. (2012) 'Persistent amplification of DNA damage signal involved in replicative senescence of normal human diploid fibroblasts', *Oxid Med Cell Longev,* 2012, pp. 310534.

Swanson, M. J., Baribault, M. E., Israel, J. N. and Bae, N. S. (2016) 'Telomere protein RAP1 levels are affected by cellular aging and oxidative stress', *Biomed Rep,* 5(2), pp. 181-187.

Tadi, S. K., Tellier-Lebègue, C., Nemoz, C., Drevet, P., Audebert, S., Roy, S., Meek, K., Charbonnier, J. B. and Modesti, M. (2016) 'PAXX Is an Accessory c-NHEJ Factor that Associates with Ku70 and Has Overlapping Functions with XLF', *Cell Rep,* 17(2), pp. 541-555.

Temime-Smaali, N., Guittat, L., Wenner, T., Bayart, E., Douarre, C., Gomez, D., Giraud-Panis, M. J., Londono-Vallejo, A., Gilson, E., Amor-Guéret, M. and Riou, J. F. (2008) 'Topoisomerase IIIalpha is required for normal proliferation and telomere stability in alternative lengthening of telomeres', *EMBO J,* 27(10), pp. 1513-24.

Teo, H., Ghosh, S., Luesch, H., Ghosh, A., Wong, E. T., Malik, N., Orth, A., de Jesus, P., Perry, A. S., Oliver, J. D., Tran, N. L., Speiser, L. J., Wong, M., Saez, E., Schultz, P., Chanda, S. K., Verma, I. M. and Tergaonkar, V. (2010) 'Telomere-independent Rap1 is an IKK adaptor and regulates NF-kappaB-dependent gene expression', *Nat Cell Biol,* 12(8), pp. 758-67.

Truong, L. N., Li, Y., Shi, L. Z., Hwang, P. Y., He, J., Wang, H., Razavian, N., Berns, M. W. and Wu, X. (2013) 'Microhomology-mediated End Joining and Homologous Recombination share the initial end resection step to repair DNA double-strand breaks in mammalian cells', *Proc Natl Acad Sci U S A,* 110(19), pp. 7720-5.

Tsipouri, V., Schueler, M. G., Hu, S., Dutra, A., Pak, E., Riethman, H., Green, E. D. and Program, N. C. S. (2008) 'Comparative sequence analyses reveal sites of ancestral chromosomal fusions in the Indian muntjac genome', *Genome Biol,* 9(10), pp. R155.

Uematsu, N., Weterings, E., Yano, K., Morotomi-Yano, K., Jakob, B., Taucher-Scholz, G., Mari, P. O., van Gent, D. C., Chen, B. P. and Chen, D. J. (2007) 'Autophosphorylation of DNA-PKCS regulates its dynamics at DNA double-strand breaks', *J Cell Biol,* 177(2), pp. 219-29.

Uziel, T., Lerenthal, Y., Moyal, L., Andegeko, Y., Mittelman, L. and Shiloh, Y. (2003) 'Requirement of the MRN complex for ATM activation by DNA damage', *EMBO J,* 22(20), pp. 5612-21.

Van Ly, D., Low, R. R. J., Frölich, S., Bartolec, T. K., Kafer, G. R., Pickett, H. A., Gaus, K. and Cesare, A. J. (2018) 'Telomere Loop Dynamics in Chromosome End Protection', *Mol Cell,* 71(4), pp. 510-525.e6.

van Overbeek, M. and de Lange, T. (2006) 'Apollo, an Artemis-related nuclease, interacts with TRF2 and protects human telomeres in S phase', *Curr Biol,* 16(13), pp. 1295-302.

van Steensel, B., Smogorzewska, A. and de Lange, T. (1998) 'TRF2 protects human telomeres from end-to-end fusions', *Cell,* 92(3), pp. 401-13.

Verdun, R. E., Crabbe, L., Haggblom, C. and Karlseder, J. (2005) 'Functional human telomeres are recognized as DNA damage in G2 of the cell cycle', *Mol Cell,* 20(4), pp. 551-61.

Verma, P. and Greenberg, R. A. (2016) 'Noncanonical views of homology-directed DNA repair', *Genes Dev,* 30(10), pp. 1138-54.

Wang, H., Rosidi, B., Perrault, R., Wang, M., Zhang, L., Windhofer, F. and Iliakis, G. (2005) 'DNA ligase III as a candidate component of backup pathways of nonhomologous end joining', *Cancer Res,* 65(10), pp. 4020-30.

Wang, H., Zeng, Z. C., Perrault, A. R., Cheng, X., Qin, W. and Iliakis, G. (2001) 'Genetic evidence for the involvement of DNA ligase IV in the DNA-PK-dependent pathway of non-homologous end joining in mammalian cells', *Nucleic Acids Res,* 29(8), pp. 1653-60.

Wang, J., Gong, Z. and Chen, J. (2011) 'MDC1 collaborates with TopBP1 in DNA replication checkpoint control', *J Cell Biol,* 193(2), pp. 267-73.

Wang, M., Wu, W., Rosidi, B., Zhang, L., Wang, H. and Iliakis, G. (2006) 'PARP-1 and Ku compete for repair of DNA double strand breaks by distinct NHEJ pathways', *Nucleic Acids Res,* 34(21), pp. 6170-82.

Wang, Q., Goldstein, M., Alexander, P., Wakeman, T. P., Sun, T., Feng, J., Lou, Z., Kastan, M. B. and Wang, X. F. (2014) 'Rad17 recruits the MRE11-RAD50-NBS1 complex to regulate the cellular response to DNA double-strand breaks', *EMBO J,* 33(8), pp. 862-77.

Wang, W. and Lan, H. (2000) 'Rapid and parallel chromosomal number reductions in muntjac deer inferred from mitochondrial DNA phylogeny', *Mol Biol Evol,* 17(9), pp. 1326-33.

Wang, Y., Ghosh, G. and Hendrickson, E. A. (2009) 'Ku86 represses lethal telomere deletion events in human somatic cells', *Proc Natl Acad Sci U S A,* 106(30), pp. 12430-5.

Waters, C. A., Strande, N. T., Wyatt, D. W., Pryor, J. M. and Ramsden, D. A. (2014) 'Nonhomologous end joining: a good solution for bad ends', *DNA Repair (Amst),* 17, pp. 39-51.

Watson, J. D. (1972) 'Origin of concatemeric T7 DNA', *Nat New Biol,* 239(94), pp. 197-201.

Williams, R. S., Williams, J. S. and Tainer, J. A. (2007) 'Mre11-Rad50-Nbs1 is a keystone complex connecting DNA repair machinery, double-strand break signaling, and the chromatin template', *Biochem Cell Biol,* 85(4), pp. 509-20.

Wright, W. D., Shah, S. S. and Heyer, W. D. (2018) 'Homologous recombination and the repair of DNA double-strand breaks', *J Biol Chem,* 293(27), pp. 10524-10535.

Wu, L. and Hickson, I. D. (2003) 'The Bloom's syndrome helicase suppresses crossing over during homologous recombination', *Nature,* 426(6968), pp. 870-4.

Wurster, D. H. and Benirschke, K. (1970) 'Indian muntjac, Muntiacus muntjak: a deer with a low diploid chromosome number', *Science,* 168(3937), pp. 1364-6.

Xing, M., Yang, M., Huo, W., Feng, F., Wei, L., Jiang, W., Ning, S., Yan, Z., Li, W., Wang, Q., Hou, M., Dong, C., Guo, R., Gao, G., Ji, J., Zha, S., Lan, L., Liang, H. and Xu, D. (2015) 'Interactome analysis identifies a new paralogue of XRCC4 in non-homologous end joining DNA repair pathway', *Nat Commun,* 6, pp. 6233.

Yang, D., Xiong, Y., Kim, H., He, Q., Li, Y., Chen, R. and Songyang, Z. (2011) 'Human telomeric proteins occupy selective interstitial sites', *Cell Res,* 21(7), pp. 1013-27.

Yang, G., Liu, C., Chen, S. H., Kassab, M. A., Hoff, J. D., Walter, N. G. and Yu, X. (2018) 'Super-resolution imaging identifies PARP1 and the Ku complex acting as DNA double-strand break sensors', *Nucleic Acids Res,* 46(7), pp. 3446-3457.

Yang, K., Guo, R. and Xu, D. (2016) 'Non-homologous end joining: advances and frontiers', *Acta Biochim Biophys Sin (Shanghai),* 48(7), pp. 632-40.

Ye, J., Lenain, C., Bauwens, S., Rizzo, A., Saint-Léger, A., Poulet, A., Benarroch, D., Magdinier, F., Morere, J., Amiard, S., Verhoeyen, E., Britton, S., Calsou, P., Salles, B., Bizard, A., Nadal, M., Salvati, E., Sabatier, L., Wu, Y., Biroccio, A., Londoño-Vallejo, A., Giraud-Panis, M. J. and Gilson, E. (2010) 'TRF2 and apollo cooperate with topoisomerase 2alpha to protect human telomeres from replicative damage', *Cell,* 142(2), pp. 230-42.

Ye, J., Renault, V. M., Jamet, K. and Gilson, E. (2014) 'Transcriptional outcome of telomere signalling', *Nat Rev Genet,* 15(7), pp. 491-503.

Yeung, F., Ramírez, C. M., Mateos-Gomez, P. A., Pinzaru, A., Ceccarini, G., Kabir, S., Fernández-Hernando, C. and Sfeir, A. (2013) 'Nontelomeric role for Rap1 in regulating metabolism and protecting against obesity', *Cell Rep,* 3(6), pp. 1847-56.

Yin, X., Liu, M., Tian, Y., Wang, J. and Xu, Y. (2017) 'Cryo-EM structure of human DNA-PK holoenzyme', *Cell Res,* 27(11), pp. 1341-1350.

Yoo, H. Y., Kumagai, A., Shevchenko, A. and Dunphy, W. G. (2007) 'Ataxia-telangiectasia mutated (ATM)-dependent activation of ATR occurs through phosphorylation of TopBP1 by ATM', *J Biol Chem,* 282(24), pp. 17501-6.

Yu, X., Wu, L. C., Bowcock, A. M., Aronheim, A. and Baer, R. (1998) 'The C-terminal (BRCT) domains of BRCA1 interact in vivo with CtIP, a protein implicated in the CtBP pathway of transcriptional repression', *J Biol Chem,* 273(39), pp. 25388-92.

Zhong, Q., Chen, C. F., Li, S., Chen, Y., Wang, C. C., Xiao, J., Chen, P. L., Sharp, Z. D. and Lee, W. H. (1999) 'Association of BRCA1 with the hRad50-hMre11-p95 complex and the DNA damage response', *Science,* 285(5428), pp. 747-50.

Zhu, C., Mills, K. D., Ferguson, D. O., Lee, C., Manis, J., Fleming, J., Gao, Y., Morton, C. C. and Alt, F. W. (2002) 'Unrepaired DNA breaks in p53-deficient cells lead to oncogenic gene amplification subsequent to translocations', *Cell,* 109(7), pp. 811-21.

Zhu, X. D., Niedernhofer, L., Kuster, B., Mann, M., Hoeijmakers, J. H. and de Lange, T. (2003) 'ERCC1/XPF removes the 3' overhang from uncapped telomeres and represses formation of telomeric DNA-containing double minute chromosomes', *Mol Cell,* 12(6), pp. 1489-98.

Zimmermann, M. and de Lange, T. (2014) '53BP1: pro choice in DNA repair', *Trends Cell Biol,* 24(2), pp. 108-17.

Zou, L. and Elledge, S. J. (2003) 'Sensing DNA damage through ATRIP recognition of RPA-ssDNA complexes', *Science,* 300(5625), pp. 1542-8.

Appendix I. Article 3

Molecular Cell
Article

Genome-wide Control of Heterochromatin Replication by the Telomere Capping Protein TRF2

Aaron Mendez-Bermudez,[1,2] Liudmyla Lototska,[2] Serge Bauwens,[2] Marie-Jose` phe Giraud-Panis,[2] Olivier Croce,[2] Karine Jamet,[2] Agurtzane Irizar,[2] Macarena Mowinckel,[2] Stephane Koundrioukoff,[3,4] Nicolas Nottet,[5] Genevieve Almouzni,[6] Mare-Paule Teulade-Fichou,[7] Michael Schertzer,[8] Mylène Perderiset,[8] Arturo Londoño-Vallejo,[8] Michelle Debatisse,[3] Eric Gilson,[1,2,9,10,11,*] and Jing Ye[1,10,*]

[1]Shanghai Ruijin Hospital, Shanghai Ruijin Hospital North, Shanghai Jiao Tong University School of Medicine, Université Cć te d'Azur, CNRS, Inserm, "Laboratoire International Associé" (LIA) Hematology and Cancer, State Key Laboratory of Medical Genomics, "Pć le Sino-Franç ais de Recherche en Sciences du Vivant et Gé nomique," Shanghai, P.R. China
[2]Université Cć te d'Azur, CNRS, Inserm, IRCAN, Faculty of Medicine Nice, France
[3]Institut Gustave Roussy, Sorbonne Université s, UPMC University, Paris, France
[4]CNRS, UMR 8200, Villejuif, France
[5]Université Cć te d'Azur, CNRS, IPMC, France
[6]Institut Curie, PSL University, Sorbonne Universités, UPMC University, CNRS, UMR3664, Paris, France
[7]Institut Curie, PSL University, Sorbonne Universités, UPMC, CNRS, Inserm, UMR9187/U1196, Orsay, France
[8]Institut Curie, PSL Research University, Sorbonne Universités, CNRS UMR3244 Telomere and Cancer Lab, Paris, France
[9]Department of Genetics, CHU, Nice, France
[10]These authors contributed equally
[11]Lead Contact
*Correspondence: eric.gilson@unice.fr (E.G.), yj11254@rjh.com.cn (J.Y.)
https://doi.org/10.1016/j.molcel.2018.03.036

SUMMARY

Hard-to-replicate regions of chromosomes (e.g., pericentromeres, centromeres, and telomeres) impede replication fork progression, eventually leading, in the event of replication stress, to chromosome fragility, aging, and cancer. Our knowledge of the mechanisms controlling the stability of these regions is essentially limited to telomeres, where fragility is counteracted by the shelterin proteins. Here we show that the shelterin subunit TRF2 ensures progression of the replication fork through pericentromeric heterochromatin, but not centromeric chromatin. In a process involving its N-terminal basic domain, TRF2 binds to pericentromeric Satellite III sequences during S phase, allowing the recruitment of the G-quadruplex-resolving helicase RTEL1 to facilitate fork progression. We also show that TRF2 is required for the stability of other heterochromatic regions localized throughout the genome, paving the way for future research on heterochromatic replication and its relationship with aging and cancer.

INTRODUCTION

Certain regions of our genome are particularly hard to replicate and, therefore, impede replication fork progression, generating chromosome fragility under conditions of replication stress (Cortez, 2015; Nikolov and Taddei, 2016). Such regions include telomeres (Mart´nez et al., 2009; Miller et al., 2006; Sfeir et al., 2009), heterochromatin, centromeres (Aze et al., 2016; Deng et al., 2012; Sullivan and Karpen, 2004), an heterogeneous group of chromosomal loci comprising common fragile sites (Le Tallec et al., 2014), and various repetitive sequences (Usdin et al., 2015). Our knowledge of the molecular mechanisms underlying the instability of hard-to-replicate regions remains limited. The prevailing view is that their compaction triggers fork stalling (Aze et al., 2016; Nikolov and Taddei, 2016). Composed of G-rich repetitive DNA repeats, telomeres are bound to the end-protective protein complex shelterin (de Lange, 2005) and packaged into a particular type of chromatin that can fold into unusual structures (Gilson and Gć li, 2007). Of the various shelterin subunits, telomeric repeat-binding factor 1 (TRF1) and TRF2 bind to telomeric DNA duplexes whereas POT1 binds to single-stranded regions (Giraud-Panis et al., 2013).

Interestingly, TRF1 and TRF2 play distinct roles in counteracting telomere fragility. TRF1 prevents replication fork stalling, ATR activation, and telomere fragility by recruiting the Bloom helicase (BLM), most likely to remove secondary structures formed by the G-rich strand of telomeres (Zimmermann et al., 2014). TRF1 also protects the interstitial telomeric sequence (ITS) at 2q14 from instability generated by replicative stress (Bosco and de Lange, 2012). However, the stability of other ITSs is not controlled by TRF1, suggesting that the effect of TRF1 on 2q14 is probably due to its particularly long telomeric DNA sequence resulting from an ancestral telomere fusion that gave rise to chromosome 2. On the other hand, TRF2 is involved in the resolution of topological problems caused by replication fork progression through telomeric chromatin (Ye et al., 2010). Data suggest

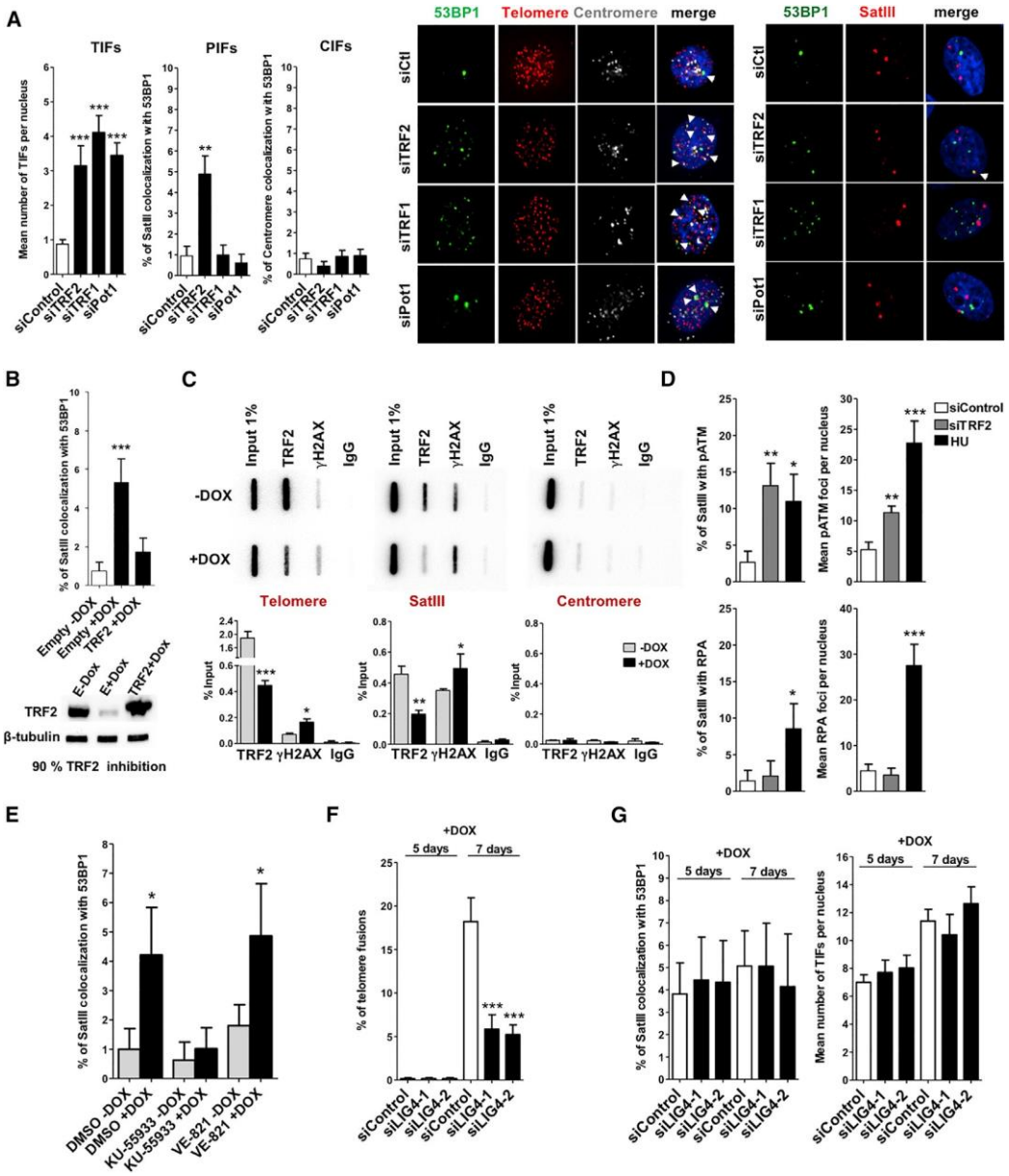

Figure 1. TRF2 Protects Pericentromeres against DNA Damage

(A) Immunofluorescence detection of 53BP1 (green) combined with FISH probes staining telomeres (TIFs), SatIII (PIFs), or centromeres (CIFs) (red) in BJ-HELT cells transfected with the indicated siRNAs for 72 hr. The percentage of mRNA inhibition, estimated by RT-qPCR of three biological replicates, was *TERF2* = 85%; *TERF1* = 78%, and *POT1* = 86%. Error bars indicate SEM of three biological replicates.

(B) PIFs of HeLa cells incubated with doxycycline (DOX) for 5 days to induce shTRF2 expression. Cells were transduced for 6 days with either an empty vector control or the full-length TRF2 protein.

(C) ChIP analysis of HeLa cells with TRF2 downregulation. Cells were incubated with DOX for 5 days to induce shTRF2 expression. The immunoprecipitate obtained with TRF2, gH2AX antibodies, and IgG control were spotted onto slot blots and hybridized with either telomeric, SatIII (composed of 106 bp TTCCA repeated sequence), or centromeric probes. Quantification of three independent experiments is shown. Statistical analyses were performed using unpaired two-tailed t test (*p < 0.05, **p < 0.001, ***p < 0.0001).

(D) Graphs showing the percentage of SatIII FISH signal staining with phospho-ATM (ser1981) or the replication protein A (RPA) antibodies in MRC5 primary cell line. The mean number of pATM and RPA per nucleus is shown on the right panel. siRNAs were incubated for 72 hr while hydroxyurea (HU; 1.5 mM) was added to the culture for 24 hr.

(legend continued on next page)

that TRF2 may act as a topological stress sensor, recognizing positive DNA supercoiling generated during telomeric replication (Amiard et al., 2007; Benarroch-Popivker et al., 2016; Gilson and Géli, 2007; Poulet et al., 2012; Ye et al., 2010). Moreover, TRF2 specifically binds to several structural features of stalled forks, particularly three- and four-way DNA junctions (Fouché et al., 2006; Poulet et al., 2009; Saint-Léger et al., 2014). Overall, TRF1 and TRF2 seem to work independently when dealing with replication problems caused by the peculiarities of telomeric chromatin: TRF1 prevents "classical" fork stalling and ATR signaling, and TRF2 manages specific topological problems caused by telomeric replication.

In this study, we explore whether shelterin proteins execute general functions outside telomeres to stabilize hard-to-replicate regions. We studied the effects of TRF1, TRF2, and POT1 downregulation on pericentromeric and centromeric stability. We found that TRF2 is specifically required for replication fork progression through pericentromeres and to ensure genome-wide heterochromatic stability.

RESULTS

TRF2 Is Required for Pericentromeric Stability

To investigate the putative role played by shelterins in the stability of pericentromeres and centromeres, we knocked down the expression levels of three key shelterin subunits (TRF1, TRF2, and POT1) in a human immortalized fibroblast cell line (BJ-HELT). We then scored the co-localizations of p53-binding protein 1 (53BP1), a DNA damage response (DDR) protein, and three PNA probes hybridizing, respectively, to the DNA of telomeric repeats (5′-TTAGGG), pericentromeric Satellite III (SatIII) repeats (5′-TGGAA; see Figure S1A), and centromeric alphoid repeats. The co-localization events were termed TIFs, PIFs, or CIFs (telomere, pericentromere, or centromere dysfunction-induced foci, respectively). As expected (Takai et al., 2003), downregulation of TRF1, TRF2, and POT1 upon specific small interfering RNA (siRNA) transfection increased the frequency of TIFs (Figure 1A), and downregulation of TRF1 increased the number of multiple telomeric signals (MTSs) (Figure S1B). However, only TRF2 downregulation (70% protein inhibition; Figure S1C) increased the frequency of PIFs, and none of the genetic downregulations mentioned above changed CIF numbers (Figure 1A). Increases in PIF frequency were also evident in TRF2-compromised primary fibroblasts (Figure S1D) and in HeLa cells, in which an shRNA targeting *TERF2* mRNA was induced by doxycycline (DOX) (Grolimund et al., 2013), leading to 90% reduction in TRF2 protein expression (Figure 1B) without overt alteration of the cell cycle (Figure S1E). Notably, the increase in the number of pericentromeric damages caused by DOX was rescued by ectopic expression of TRF2, ruling out an off-target effect of the interfering RNA (Figure 1B). The pericentromeric damages caused by TRF2 downregulation can also be observed in chromatin immunoprecipitation (ChIP) experiments using γH2AX antibodies and performed in HeLa cells treated with DOX (Figure 1C). Although weaker than telomeric damage, pericentromeric damage was specific to these regions since a centromeric probe yielded no signal above background level (Figure 1C). Overall, these results unequivocally show that TRF2, but not TRF1 or POT1, knockdown specifically triggers pericentromeric damage.

Next, we identified the pericentromeric DDR pathway inhibited by TRF2 by scoring co-localizations of the SatIII repeat PNA probe, the activated (phosphorylated) form of the ataxia telangiectasia mutated kinase (pATM), and the replication protein A (RPA) (a marker of the ATR signaling pathway). Primary fibroblast cells, transfected with a siRNA targeting *TERF2*, exhibited an increased association of pATM (but not RPA) with pericentromeres (monitored as SatIII foci) (Figure 1D; Figure S1F). Control hydroxyurea-treated cells exhibited increased levels of pATM and RPA both at pericentromeres and throughout the genome (Figure 1D). Next, we asked whether ATM was responsible for the pericentromeric damages triggered by TRF2 downregulation. Inhibition of ATM expression (either by treating cells with KU-55933, a specific inhibitor of ATM, or by downregulating ATM expression using specific siRNAs) suppressed PIF formation in TRF2-compromised cells (Figure 1E; Figures S1G and S1H). In agreement with the observed absence of ATR pathway activation at pericentromeres in these conditions, ATR inhibition (using the specific ATR inhibitor VE-821 or specific siRNAs) did not abolish PIF formation in TRF2-compromised cells (Figure 1E; Figures S1G and S1H). We conclude that TRF2 downregulation triggers an ATM-dependent DDR pathway at pericentromeres.

Since ATM is activated at double-stranded DNA breaks, we asked whether the pericentromeric damages were caused by breakage of dicentric chromosomes formed via telomeric fusions, even though the PIF assays were performed 5 days after DOX induction, at a time where no fusions were detectable (Figure 1F). We found that prevention of telomere fusions by downregulating DNA ligase 4 (Smogorzewska and de Lange, 2002; van Steensel et al., 1998) (Figure 1F; Figure S1I) did not inhibit PIF formation (Figure 1G). We conclude that the pericentromeric damages caused by TRF2 downregulation cannot be merely explained by telomere fusion and dicentric chromosome breakage.

In summary, TRF2 prevents ATM activation at pericentromeres, encouraging us to explore how TRF2 impacted pericentromeric stability.

Unconventional Binding of TRF2 to Pericentromeres

TRF2 associated specifically with pericentromeric chromatin, as revealed by ChIP experiments followed by slot blotting

(E) PIFs from HeLa cells with (+DOX) or without (−DOX) TRF2 depletion for 5 days. One day before harvesting, ATM or ATR was inhibited using either KU-55933 (10 mM for 24 hr) or VE-821 (10 mM for 24 hr), respectively.

(F) Percentage of telomere fusions after 5 or 7 days of TRF2 downregulation in HeLa cells. Cells were transfected with two different siRNAs against LIG4 or an siControl (***$p < 0.0001$; Mann-Whitney U test).

(G) PIFs (left) and TIFs (right) analysis of the conditions described in (F).

For all IF-FISH experiments in this figure, approximately 40 nuclei were analyzed per replicate. SEMs of three biological replicates are shown. Statistical analyses were performed using Mann-Whitney U test (*$p < 0.05$, **$p < 0.001$, ***$p < 0.0001$).

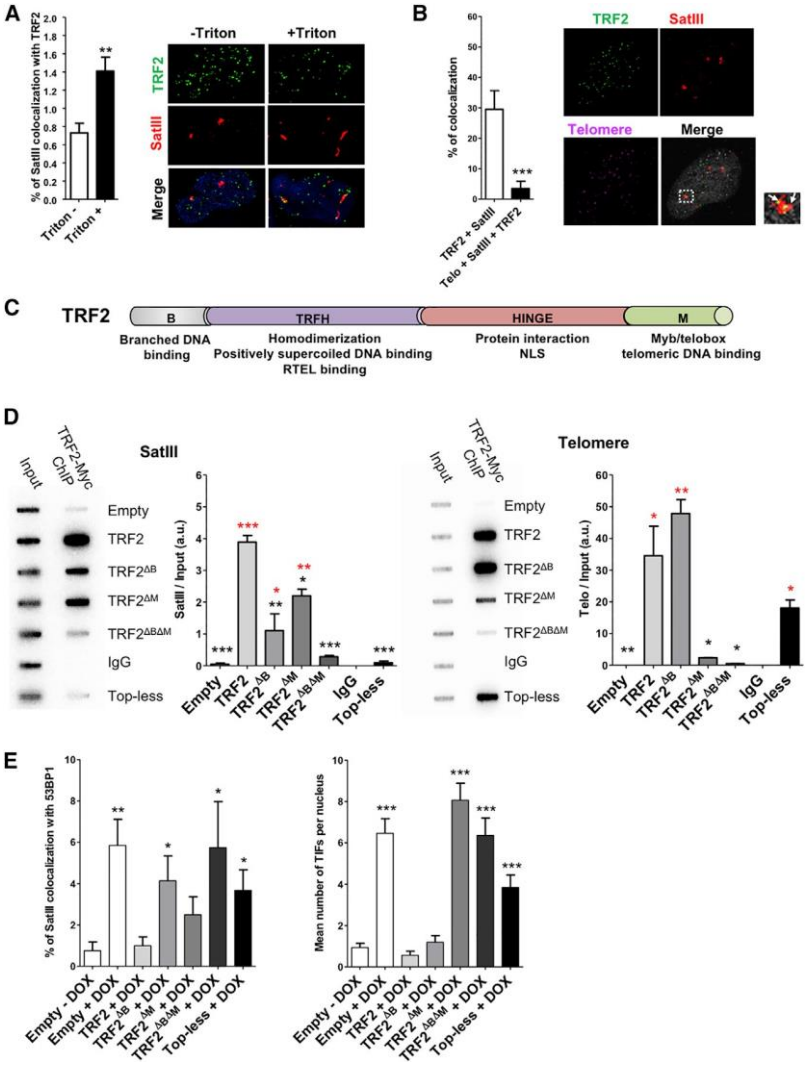

Figure 2. TRF2 Binds Pericentromeres in a Non-classical Way

(A) Binding of TRF2-SatIII–of Triton X-100-treated cells.

(B) Quantification and representative IF-FISH images of associations between TRF2 (green), SatIII (red), and telomeres (purple) in BJ-HELT cells.

(C) Relevant TRF2 domains. TRF2 contains a NH_2-terminal basic domain that recognizes branched DNA structures (B domain). Within the homodimerization domain (TRFH), the DNA wrapping property of TRF2 is found. The nuclear localization signal (NLS) and the platform for shelterin protein-protein interactions are found in the hinge domain. The Myb/telobox domain found at the C-terminal end (M domain) is required for telomere-specific binding.

(D) ChIP analysis of BJ-HELT cells transduced for 5 days with lentiviruses containing the full-length Myc-tag TRF2 protein or truncated mutant forms. ChIP was performed with an anti-Myc antibody, and the IP enrichment was visualized with a SatIII probe (left) or a telomeric probe (right). Error bars represent SEM of two biological replicates. Black stars show the significance as compared to the TRF2 condition while red stars are in relation to the empty condition (*p <0.05, **p <0.001, ***p < 0.0001; one-way ANOVA).

(E) PIFs (left) and TIFs (right) of HeLa cells transduced with TRF2 mutant lentivirus for 5 days. Endogenous TRF2 was downregulated by the addition of doxycycline (+DOX) 3 days before cell fixation.

For all microscopy analysis displayed in this figure, error bars show SEMs of n = 3. Statistical analyses were performed using Mann-Whitney U test (*p <0.05, **p <0.001, ***p <0.0001).

with a SatIII probe (Figure 1C), qPCR of pericentromeric DNA sequences (Figures S2A and S2B), and microscopy assays monitoring the co-localization of TRF2 with SatIII PNA foci (Figure 2A). The association of TRF2 to pericentromeres was weaker than that at telomeres; however, we could not detect any TRF2 association at centromeres (Figure 1C; see also Figure S2A), showing that TRF2-pericentromere interaction is specific. When Triton X-100 was used to remove soluble and weakly bound chromatin proteins (Martini et al., 1998), TRF2 signal at SatIII foci increased, indicating that TRF2 was tightly bound to pericentromeric chromatin (Figure 2A). We ruled out the possibility that the TRF2-SatIII associations were dependent on TRF2 binding to telomeres because 90% of TRF2-SatIII co-localized foci exhibited no obvious telomeric signals (Figure 2B).

The association of TRF2 with pericentromeres was distinct from that of telomeric binding since purified TRF2 did not bind to SatIII DNA in a DNA sequence-specific manner (Figure S2C).

Next, we set to identify the TRF2 domains (schematically summarized in Figure 2C) required for pericentromeric binding. In agreement with an unconventional binding of TRF2 to pericentromeres, the absence of the Myb/telobox DNA-binding domain ($TRF2^{DM}$) only moderately affected TRF2-SatIII associations as revealed by ChIP while, as expected, it totally abolished telomeric DNA binding (Figure 2D; Figures S2D and S2E). Conversely, two TRF2 alleles that normally bind telomeric DNA sequences, one lacking the basic N-terminal domain ($TRF2^{DB}$; Figure 2C) and one that is impaired in the amino acid of the TRFH domain required for positively supercoiled DNA binding (the ''Top-less'' allele) (Benarroch-Popivker et al., 2016), were more defective in SatIII than in telomeric association (Figure 2D; Figures S2D and S2E). From comparisons between the effects of $TRF2^{DB}$, i.e., an impaired binding and damages at pericentromeres, but not at telomeres, and $TRF2^{DM}$, i.e., an impaired binding and damage at telomeres, but not at pericentromeres, one can deduce that the telomeric and pericentromeric functions of TRF2 are genetically separated in the $TRF2^{DB}$ and $TRF2^{DM}$ alleles (compare both panels of Figures 2D and 2E).

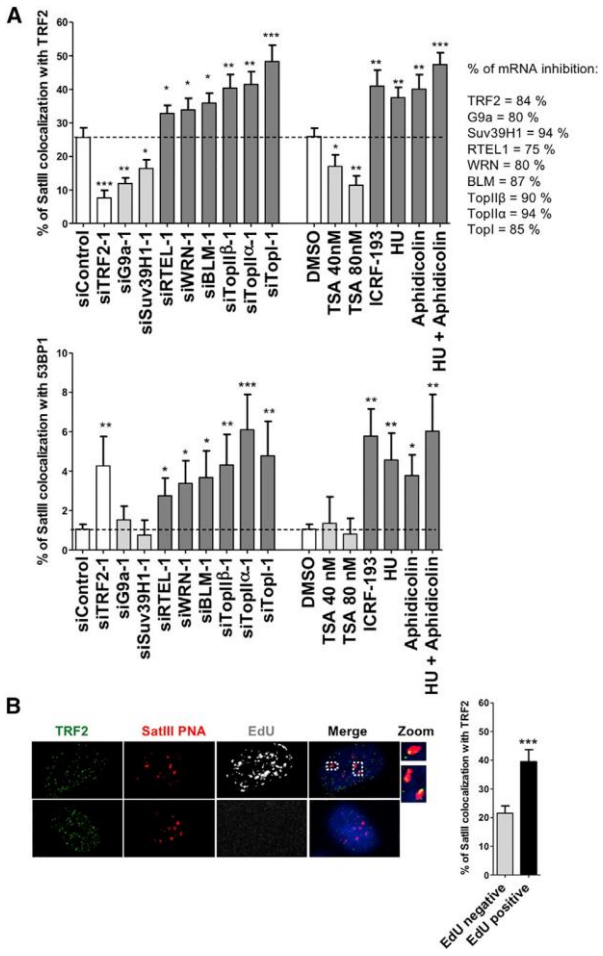

Figure 3. TRF2 Binding to Pericentromeres Increases upon Replication and Topological Stress

(A) BJ-HELT cells were transfected with three different RNAi sequences per target gene for 72 hr. In this figure, downregulation of one RNAi target sequence (see Figure S3A for other 2 target sequences) and cells treated with sub-lethal doses of TSA, ICRF-193 (3 mg/mL), hydroxyurea (HU; 1.5 mM), and aphidicolin (300 nM) for 24 hr are shown. Graphs represent the percentage of SatIII PNA signal associations with TRF2 (top) or 53BP1 (PIFs; bottom). Only transfections resulting in >75% inhibition verified by qPCR were used. Approximately 40 nuclei were analyzed per replicate. Error bars indicate SEM of n =3.

(B) Quantification and representative IF-FISH images of TRF2 (green) and SatIII (red) co-localization in the presence of 5-ethynyl-2′-deoxyuridine (EdU; 10 mM for 2 hr) in BJ-HELT cells.

Statistical analyses were performed using Mann-Whitney U test (*p <0.05, **p < 0.001, ***p < 0.0001).

TRF2-Pericentromere Association Requires Heterochromatin

As pericentromeres constitute the largest part of constitutive heterochromatin, we explored whether the TRF2-SatIII association was modulated by key genes involved in heterochromatin formation. We found that downregulation of the histone methyltransferases SUV39H1 and G9a, responsible for the methylation of Lys-9 of histone H3, promoted TRF2 dissociation from pericentromeres but not from telomeres (Figure 3A; Figures S3A and S3B). The same effect was observed after treatment with trichostatin A (TSA), an inhibitor of histone deacetylases I and II that reduces H3K9me3 formation (Figure 3A). Conversely, reduced TRF2 expression did not change the number of H3K9me3 marks on pericentromeric or telomeric chromatin (Figure S3C), indicating that TRF2 was not involved in heterochromatin formation. When the level of heterochromatin was reduced, the decreased binding of TRF2 to pericentromeres did not trigger pericentromeric damages (Figure 3A), suggesting that TRF2 binds to and protects pericentromeres from DNA damage caused by the presence of heterochromatin.

TRF2 Associates with Pericentromeres during S Phase

The extent of association of TRF2 with pericentromeres, but not telomeres, increased in EdU-positive cells (Figure 3B) and at the late S/G2 phase (when pericentromeric DNA replicates) (Figure S3D), suggesting that TRF2 was involved in pericentromeric replication. Indeed, sub-lethal doses of hydroxyurea (HU)/aphidicolin leading to replication alteration increased TRF2 recruitment by pericentromeres and PIF number (Figure 3A). Notably, the latter effect was rescued by TRF2 overexpression (Figure S3E).

Further evidence of a role for TRF2 in pericentromeric replication was provided by the observation that downregulation of genes encoding topoisomerases and helicases (TOP1, TOPIIa, TOPIIb, BLM, WRN, and RTEL1), or treatment with the topoisomerase II inhibitor ICRF-193, increased the numbers of TRF2-SatIII foci and PIFs (Figure 3A; Figure S3A). Under such conditions, no obvious change in the number of TRF2-telomeric foci (Figure S3B) was observed, and only TOPIIa, BLM, and RTEL1 protected telomeres from damage (Figure S3F), confirming the distinct roles played by TRF2 at telomeres and pericentromeres.

TRF2 Assists Replication Fork Progression through Pericentromeres

Next, we explored how TRF2 prevents pericentromeric replicative damage. We first found that BrdU incorporation in S phase was delayed after TRF2 downregulation at SatIII DNA but not at other DNA repeat-containing regions, such as alphoid or Alu repeats (Figures S4A and S4B). Second, DNA combing experiments coupled with PNA hybridization were used to specifically analyze pericentromeric and centromeric fibers separately from bulk fibers. We found that TRF2 depletion reduced the replication speed of pericentromeric fibers, identified as large regions of SatIII PNA hybridization (from 0.78 kilobase pairs [kb]/min to 0.66 kb/min) but not those of centromeric or bulk DNA fibers (Figure 4A; Figure S4C). Notably, in control cells, the replication speed of the pericentromeric and centromeric fibers was approximately 20% slower than those of bulk DNA fibers, confirming that the former regions are hard to replicate (Figure 4A). In agreement with the absence of any role for TRF1 in pericentromeric stability (Figure 1A), TRF1 downregulation did not slow the replication speed of pericentromeric fibers (Figure S5A).

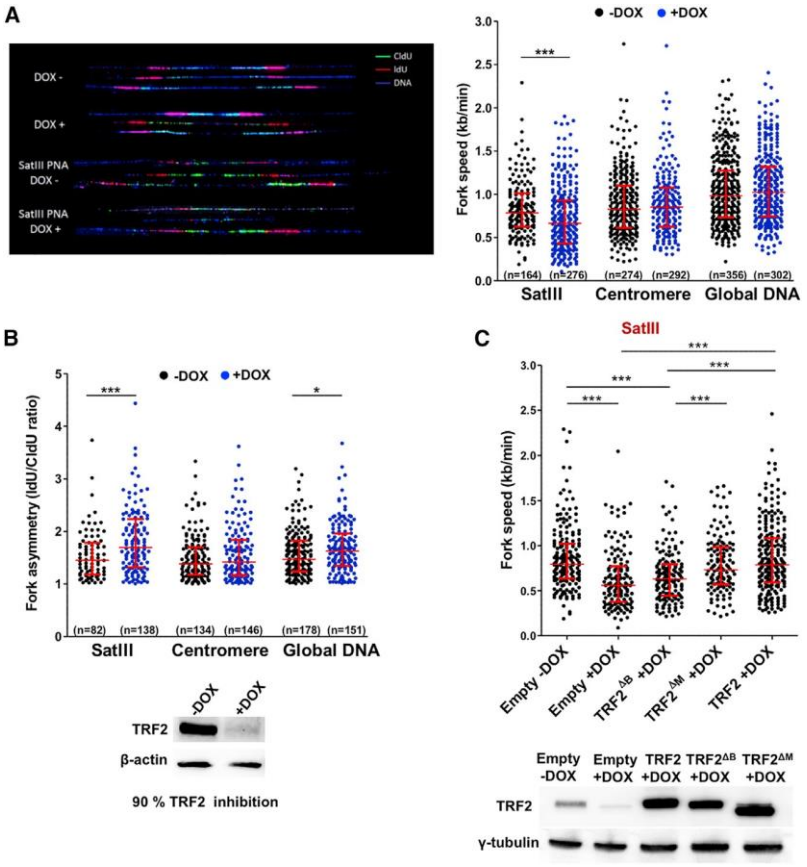

Figure 4. TRF2 Facilitates Pericentromere Replication

(A) Representative fibers of newlysynthesized DNA labeled with iododeoxyuridine (green) and chlorodeoxyuridine (red) for 30 min in HeLa cells with (+DOX) or without (DOX) TRF2 depletion. DNA staining and SatIII PNA probe signals are shown in blue for better visualization (left). Quantification of fork speed is shown for SatIII, centromere, and global DNA replication (right). The number of fibers analyzed is indicated in parentheses. Raw image data can be accessed through https://doi.org/10.17632/zjvptr88c2.1.

(B) Fork asymmetry of the conditions described above.

(C) Fork speed quantification of SatIII and global DNA fibers of HeLa cells transduced with lentivirus expressing truncated forms of TRF2 or the full-length version for 6 days. Four days before cell harvesting, doxycycline (DOX) was added to the cells to inhibit TRF2.

Bars represent the median ± interquartile range of n = 2 (*p <0.05, ***p <0.0001; Mann-Whitney U test). Immunoblots showing TRF2 and mutants expression for the experiment are presented.

We also calculated the level of fork asymmetry reflecting the extent of fork stalling (Figure S4C). After TRF2 downregulation, fork asymmetry increased in pericentromeric fibers but not in either centromeric fibers or TRF1-depleted cells (Figure 4B; Figure S5B). Notably, a slight but significant increase in fork asymmetry in terms of bulk replication was evident upon TRF2 depletion, suggesting that TRF2 might prevent fork stalling at regions other than pericentromeres (Figure 4B). These results, together with the preferred TRF2-pericentromere association in S phase (Figure 3B), indicate that TRF2 acts at a subset of forks that are experiencing difficulties in progression through pericentromeric heterochromatin, a hypothesis consistent with the significant enrichment of TRF2 in newly replicated DNA (Alabert et al., 2014) and at HU-arrested replication forks (Dungrawala et al., 2015). The normal pericentromeric replication speed was restored upon expression of wild-type TRF2, ruling out an off-target effect of the shRNA against *TERF2* (Figure 4C).

We next explored whether the two separation-of-function TRF2 mutants TRF2^{DM} and TRF2^{DB} protected pericentromeres from replication defects. We found that TRF2^{DM}, but not TRF2^{DB}, rescued the pericentromeric replication defects of TRF2-compromised cells. Such behavior is in complete agreement with the distinct abilities of the two mutants to bind to and protect pericentromeres from damage (Figure 2E), again emphasizing that different TRF2 functions are in play during pericentromeric and telomeric protection. As expected, replication speed of bulk DNA was not affected by TRF2^{DM} or TRF2^{DB} (Figure S5C).

Overall, these results show that TRF2 specifically assists replication fork progression through pericentromeres and that the abilities of TRF2 to bind to and protect pericentromeres, and to facilitate their replication, are mechanistically linked.

TRF2-Mediated ATM Inhibition Partially Assists Pericentromere Replication

We next explored how TRF2 facilitated replication fork progression through pericentromeres. As ATR signaling is required for replication fork progression throughout the genome (Técher et al., 2016), we investigated the putative contribution of this kinase to TRF2-dependent pericentromeric replication control. As expected (Técher et al., 2016), ATR inhibition by VE-821 decreased the global replication speed, and this effect was accentuated at pericentromeres when TRF2 was depleted (Figure S5D), indicating that ATR and TRF2 played independent roles during pericentromeric replication, in agreement with the absence of ATR signaling at pericentromeres after TRF2 depletion (Figure 1D).

Since TRF2 prevents ATM activation at both telomeres (Denchi and de Lange, 2007) and pericentromeres (Figure 1D), we next asked whether such TRF2-dependent ATM attenuation facilitated pericentromeric replication. We observed no change in the speed of global replication after addition of the ATM inhibitor KU-55933 (Figure S5D). The pericentromeric replication speed was partially rescued upon ATM inhibition in

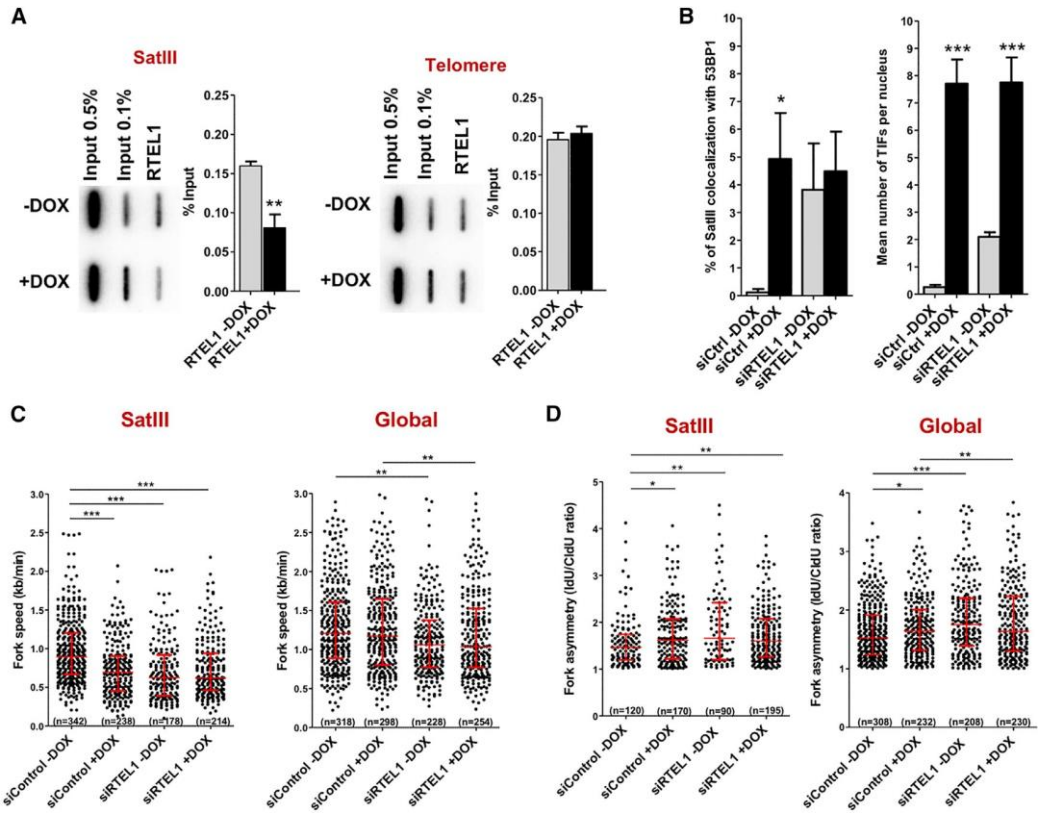

Figure 5. TRF2 Recruits RTEL1 to Pericentromeres

(A) RTEL1 ChIP experiments in HeLa cells with (+DOX) or without (DOX) TRF2 knockdown. Slot blot membranes were hybridized with SatIII radioactive probe, stripped, and re-hybridized with a telomeric probe. Error bars represent SEMs of three independent experiments (**p <0.001, two-tailed Student's t test).

(B) PIF (left) and TIF (right) quantification performed in HeLa cells with TRF2 inhibition (+DOX) for 4 days. Transfection with siRTEL1 or control was performed for 3 days. Error bars show SEM of n = 3 (*p <0.05, ***p <0.0001, using Mann-Whitney U test).

(C and D) Replication fork speed (C) and fork asymmetry (D) assessed by DNA combing in HeLa cells transfected with siRTEL1 for 72 hr and TRF2 depletion as indicated above. The number of fibers analyzed for SatIII and global DNA replication are indicated in parentheses. Bars show the median ± interquartile range of n = 2. Statistical analyses were performed using Mann-Whitney U test (**p <0.001, ***p <0.0001).

TRF2-compromised cells (Figure S5D). This indicates that, even if the ATM inhibition plays a role in pericentromeric replication, other TRF2 functions are required to assist fork progression through pericentromeric chromatin.

TRF2 Assists Pericentromeric Replication by Recruiting RTEL1

The fact that both TRF2 recruitment and the number of PIFs increased upon downregulation of the helicase RTEL1 (Figure 3A), which is known to interact with TRF2 (Sarek et al., 2015) and to be involved in fork progression (Vannier et al., 2012), suggested that TRF2 played a role in pericentromeric replication by recruiting this helicase to stalled forks. ChIP experiments revealed that RTEL1 binding to pericentromeres was TRF2 dependent (Figure 5A). On the other hand, localization of RTEL1 to telomeres was TRF2 independent, which appeared to contradict data of a previous study (Sarek et al., 2015). However, TRF2 at telomeres binds to RTEL1 only transiently during the cell cycle (Sarek et al., 2015); the interaction may thus be undetectable in unsynchronized cells. Pericentromeric damages increased upon RTEL1 downregulation at a similar extent than in TRF2-compromised cells (Figure 5B). In contrast, telomeric damages were much higher after TRF2 depletion than after RTEL1 downregulation (Figure 5B), emphasizing again the different roles played by TRF2 at telomeres and pericentromeres.

We used DNA combing to directly assess the contribution of RTEL1 to pericentromeric replication. We found that RTEL1 downregulation reduced pericentromeric fork speed (to 0.63 kb/min versus the 0.90 kb/min of the control) (Figure 5C). Importantly, this reduction was similar to that observed when TRF2 was depleted (0.69 kb/min) or upon TRF2 and RTEL1 double downregulation (0.62 kb/min). Similarly, the extent of fork asymmetry after RTEL1 depletion increased to the level detected after TRF2 knockdown or in the double RTEL1 and TRF2 downregulations (Figure 5D). As expected, RTEL1 reduction slowed the

global replication fork speed and increased fork asymmetry (Vannier et al., 2012) (Figures 5C and 5D).

Overall, our results showed that TRF2 and RTEL1 acted together to protect pericentromeres from damages and impairment of fork progression.

G-Quadruplexes Impair Replication Fork Progression at Pericentromeres

Given that G-quadruplexes (G4s) are enriched in the pericentromeric area of chromosome 9 (Henderson et al., 2014), that SatIII DNA repeats can pair to form stable purine-rich duplexes similar to G4 structures (Zhu et al., 1996), and that RTEL1 can unfold G4 structures (Vannier et al., 2012), we hypothesized that pericentromeres formed arrays of G4 or G4-like structures that impaired replication fork progression.

We first asked whether stabilization of G4 formation would increase the binding of TRF2 to pericentromeres. Indeed, treatment of cells with the G4 ligands Phen-DC3 and Phen-DC6, two bisquinoliniums exhibiting strong G4 selectivity and stabilization (De Cian et al., 2007), increased TRF2 recruitment at pericentromeres. No further increase was evident upon RTEL1 downregulation (Figure 6A), suggesting that G4 ligands and RTEL1 depletion act similarly when mediating TRF2-pericentromere association.

Both G4 ligands increased pericentromeric damage when added to control, TRF2-, or RTEL1-compromised cells (Figure 6B), indicating that G4s constitute a threat to pericentromeric integrity. We next treated cells with Phen-DC3 and measured the replication speed via DNA combing. Pericentromeric fork speed decreased specifically in cells treated with Phen-DC3, and this was slightly accentuated by TRF2 downregulation (Figure 6C). Similarly, fork asymmetry increased specifically at pericentromeres in Phen-DC3-treated cells (Figure 6D). Therefore, pericentromeric G4s opposed normal fork progression, triggering fork stalling. In the hypothesis that TRF2 and RTEL1 are required to resolve pericentromeric G4s, thus allowing forks to progress, one would expect that the G4 signal increased after TRF2 or RTEL1 depletion. To assay G4 formation at pericentromeres, we used the monoclonal 1H6 antibody that was previously shown to bind abundantly to pericentromeres of chromosome 9 and that recognizes G4 and G4-like structures (Henderson et al., 2014). As expected, we observed that the antibody labeled pericentromeres (Figure 6E). Importantly, such labeling was accentuated after TRF2 or RTEL1 downregulation (Figure 6E), showing that TRF2 and RTEL1 negatively regulated the levels of G4 or G4-like structures at pericentromeres.

TRF2 Can Be Recruited to an Artificial Fork Block

We next asked whether TRF2 could be recruited to stalled forks in another hard-to-replicate chromatin region featuring a strong interaction between LacI-GFP and a LacO DNA repeat array (Beuzer et al., 2014) (Figure 7A). We found that TRF2 co-localized with LacI-GFP in 20% of replicating cells but only in 5% of non-replicating cells. To closely mimic the heterochromatic environment, we created a LacI-GFP construct fused to heterochromatin protein 1a (LacI-HP1a-GFP). Recruitment of TRF2 to LacI-HP1a-GFP foci increased to 32% in EdU-positive cells, but the extent of co-localization was only 9% in non-replicating cells (Figure 7A). As expected, DDR activation was evident at the LacO array of cells transfected with LacI-GFP– or LacI-HP1a-GFP-expressing plasmids (Figures S6A and S6B). Similar to the association of TRF2 with SatIII, the recruitment of TRF2 to LacI-GFP foci was telomere independent (Figure S6C). We conclude that TRF2 can be recruited to an artificial replication fork block that is not at pericentromeres.

TRF2 Is Required for Genome-wide Heterochromatin Replication

The above results, as well as the genome-wide increase in fork asymmetry triggered by TRF2 downregulation (Figure 4B), suggested that TRF2 might be active at hard-to-replicate regions other than pericentromeres. Thus, we asked whether TRF2 played a more general role in genomic stability. ChIP-seq experiments performed on BJ-HELT cells revealed that reduced TRF2 expression triggered γH2AX enrichment at both telomeric and SatIII repeats (Figure 7B; Figures S7A and S7B), thus confirming the results shown in Figure 1. In addition, several chromosomal arm regions, damaged upon TRF2 knockdown, correlated with H3K9me3-enriched regions as revealed by ChIP-seq experiments performed in the same cell line ($p = 0.72$; Pearson's analysis) (Figure 7B; Figure S7B). The heterochromatin nature of the regions protected by TRF2 was confirmed by ENCODE data (Figures S7C and S7D). We conclude that TRF2 is required to protect heterochromatin not only at pericentromeres, but also at heterochromatin area throughout the genome.

DISCUSSION

This work unveils a direct and specific role of the telomeric protein TRF2 in replication fork progression through pericentromeres and therefore in their protection. Indeed, TRF2 binds pericentromeres during S phase, and TRF2-compomised cells exhibited a reduced fork progression and damages at pericentromeres but neither at centromeres nor globally throughout the genome. The other telomeric protein, TRF1, part of the same shelterin complex than TRF2 at telomeres, had no apparent effect on pericentromeric replication.

An intriguing aspect of this study is the specific binding of TRF2 to pericentromeres (e.g., Figure 1C), which cannot be merely explained by telomere-pericentromere interactions (Figure 2B), a SatIII DNA sequence-specific binding, or a loose association of TRF2 with chromatin, as it is resistant to Triton X-100 extraction (Figure 1A). The fact that TRF2 binding to pericentromeres is lower than to telomeres (see Figure 1C) has to be interpreted in the light of the different binding modes of TRF2 to these two DNA regions. Indeed, TRF2-pericentromere association (1) does not require the Myb/telobox domain; (2) requires the TRF2 domains known to recognize particular DNA structures in a sequence-independent manner, i.e., the basic domain that binds branched DNA structures, such as those at stalled forks (Fouché et al., 2006; Poulet et al., 2009; Schmutz et al., 2017) or G4s (Pedroso et al., 2009), and the DNA wrapping domain of TRFH that binds positive supercoils, such as those formed during replication (Benarroch-Popivker et al., 2016; Ye et al., 2010); (3) increases during S phase and upon topological stress, replication stress, and G4 stabilization; and

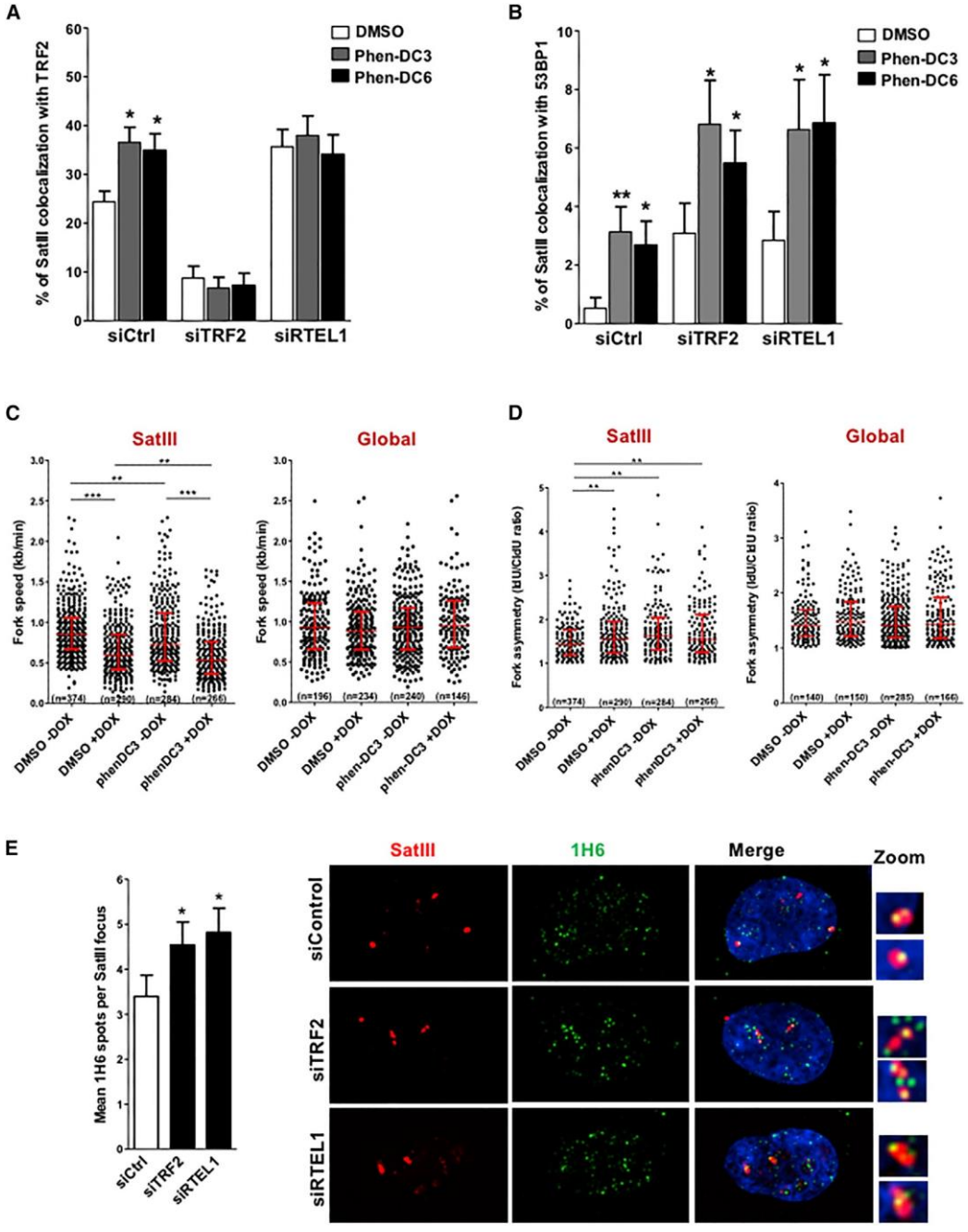

Figure 6. TRF2 Prevents Accumulation of G4-like Structures at Pericentromeres

(A and B) TRF2 association to SatIII regions (A) and PIFs (B) in HeLa cells transfected with siRNA against TRF2, RTEL, and control for 72 hr. Phen-DC3 or Phen-DC6 was added (final concentration 10 mM) 4 hr before cell fixation. Graphs show the mean ± SE of three biological replicates. Statistical analyses were performed using Mann-Whitney U test (*$p < 0.05$).

(C and D) Fork speed quantification (C) and asymmetry (D) of SatIII and global DNA fibers after Phen-DC3 treatment (4 hr at 10 mM) in HeLa cells. TRF2 was knocked down by the addition of doxycycline (DOX). **$p < 0.001$, ***$p < 0.0001$; Mann-Whitney U test.

(E) Associations of G4-like structures identified with the 1H6 antibody (green) and SatIII (red). Error bars represent SEM of n = 3. Mann-Whitney U test (*$p < 0.05$) was used to estimate statistical significance.

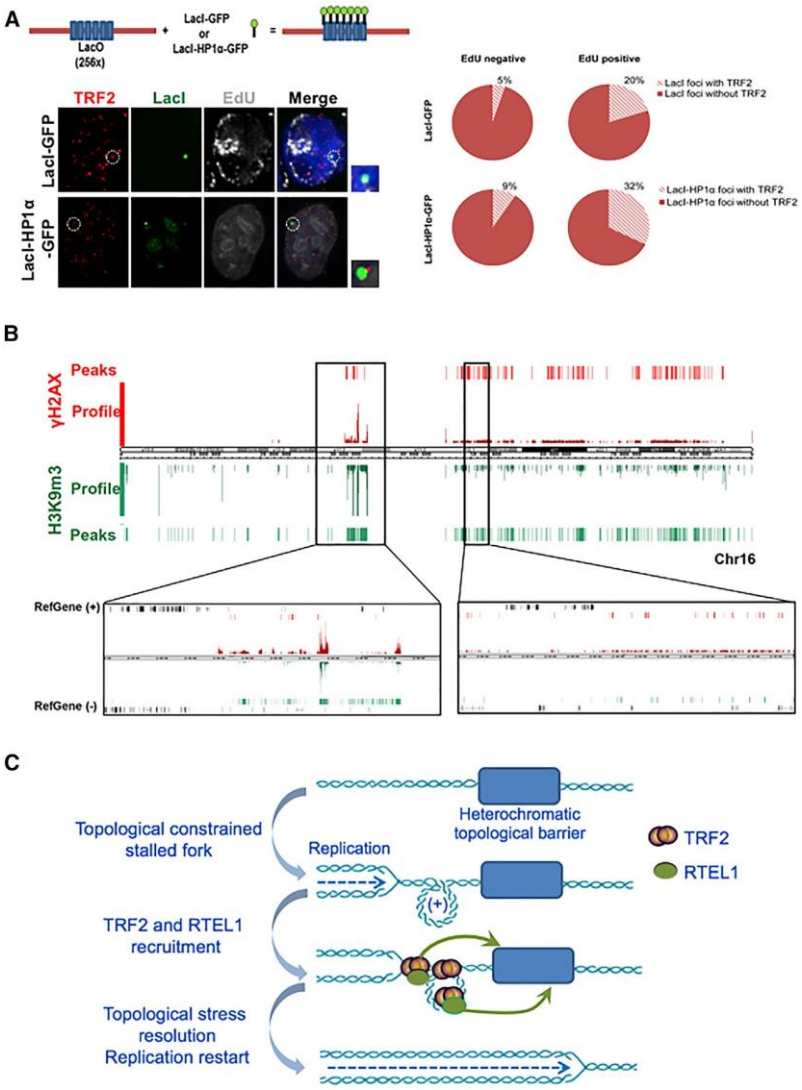

Figure 7. TRF2 Protects Genome-wide Heterochromatic Regions against DNA Damage

(A) Scheme of the experiment (top). Representative IF images (bottom) of HeLa-3 8 cells transfected with LacI-GFP or LacI-HP1a-GFP for 24 hr. EdU (1 mM) was added to the cells for 14 hr. Pie charts (right) show the percentage of LacI-GFP or LacI-HP1a-GFP foci co-localizing with TRF2 in dividing and non-dividing cells.

(B) Profile of gH2AX reads and peaks of siTRF2 versus siControl after normalization with its corresponding input DNA on chromosome 16 of BJ-HELT cell line. TRF2 knockdown was performed for 72 hr, achieving 85% *TERF2* mRNA inhibition. Profile of reads and peaks of H3K9me3 in BJ-HELT without treatment are shown. Zoom of two regions (black boxes) showing the density of genes (black lines) in both strands of the DNA are presented. Note the lack of gene-rich regions in areas where gH2AX (upon TRF2 downregulation) and H3K9me3 are present. The full set of chromosomes is presented in Figure S7B.

(C) Model of pericentromeric replication assisted by TRF2. Our results point toward a specific role of TRF2 to remove topological barriers during the replication of pericentromeres and other heterochromatin regions throughout the genome. We propose that the formation of topologically constrained stalled forks in these regions both prevents the formation of large, single-strand regions and ATR activation and triggers the formation of DNA conformations such as positive DNA supercoils (+) and branched DNA localized at regressed forks that constitute known substrates for direct TRF2 binding. The role of recruited TRF2 to topologically constrained stalled forks can be seen in two ways: (1) to prevent ATM signaling that could be activated upon fork collapse and (2) to recruit RTEL1 and possibly other enzymes to remove G4s and the topological barrier. Whether RTEL1 is recruited directly as a complex with TRF2 or sequentially after the binding of TRF2 to or around the stalled fork is unknown.

(4) decreases upon heterochromatin reduction. Moreover, TRF2 can be recruited to an artificial fork-stalling site (LacI-GFP/LacI-HP1a-GFP). Combined, these results point toward a model in which TRF2 binds in a sequence-independent, but structure-dependent, manner to DNA conformations formed during replication of pericentromeric heterochromatin, such as positive supercoils, branched DNA, and G4 DNA (see model in Figure 7C).

Importantly, this unconventional binding of TRF2 to pericentromeres is required for appropriate progression of pericentromeric forks during unchallenged replication, as demonstrated by the differential behavior of the two separation-of-function alleles TRF2^{DB} and TRF2^{DM} (Figures 2D and 2E). Indeed, TRF2^{DB} expression causes a decrease in pericentromeric binding as compared to TRF2, as well as pericentromeric DNA damage and impaired replication, but had little effect on telomere binding and protection, while TRF2^{DM} was defective in telomere binding and protection but was binding to pericentromeres, protected them efficiently against DNA damage, and allowed fork progression. Of note, even though TRF2^{DM} and TRF2^{DB} have clearly different pericentromeric phenotypes (Figure 4C), they both bind SatIII (Figure 2). A likely explanation is that TRF2^{DB} lacks an important property to assist in pericentromeric replication, which is preserved in TRF2^{DM}. This could be the ability to recognize specific DNA conformations (e.g., stalled forks or G4s) or to recruit factors involved in fork progression (e.g., FEN1; Muftuoglu et al., 2006).

The pericentromeric replicative impairment induced by TRF2 downregulation activated the ATM, but not the ATR, pathway of DNA damage response. In fact, the pericentromeric replication was partially relying on this TRF2-dependent ATM inhibition, implying that ATM activation can impair pericentromeric

replication. One possibility is that ATM activation reduces the availability of deoxyribonucleoside triphosphates at the arrested fork (Técher et al., 2016). Another non-exclusive possibility is that TRF2 regulates ATM-dependent processing of DNA breaks that may form if pericentromeric forks collapse (Bradshaw et al., 2005).

How does one explain that ATR is not activated by the pericentromeric stalled forks formed upon TRF2 downregulation? One possibility is that pericentromeric heterochromatin forms potent topological barriers impeding DNA polymerase progression and the dissipation of superhelical strain, thus preventing replicative helicases to form large, single-stranded regions and subsequent ATR activation. These topological barriers could result from higher-order heterochromatin structures, tight protein/RNA-DNA interactions, or even long-range chromatin association or interactions with subnuclear structures. Whether the formation of pericentromeric G4s, which we demonstrate here to impair fork progression through pericentromeres, constitutes per se a topological barrier or is a consequence of the topological blockade, further impeding fork progression, is an interesting question that would deserve further studies. In any case, such topologically constrained forks are expected to regress, resulting in four-way DNA structure formation (Postow et al., 2001). Thus, we propose that TRF2 is specifically required to assist topologically constrained pericentromeric forks, first by binding to the various DNA conformations that can be formed at or around these forks, such as branched DNA, positive DNA supercoils, and G4s, and then by suppressing ATM activation as well as by recruiting the RTEL1 helicase and possibly other enzymes to remove the blockades (see model in Figure 7C).

Interestingly, it was recently reported that the ATR checkpoint is also suppressed during centromere replication (Aze et al., 2016), suggesting that topologically constrained forks are also formed at centromeres. In this hypothesis, their resolution would not require TRF2 since we failed to detect centromeric damage and replication defect in TRF2-compromised cells. Since human centromeres are not formed of classical heterochromatin (Guenatri et al., 2004; Sullivan and Karpen, 2004), one might speculate that TRF2 required specific heterochromatin features to be recruited and to act at topologically constrained stalled forks. This hypothesis is further supported by the enhanced recruitment of TRF2 to a fork block generated by LacI-GFP when HP1a is added to the fusion protein (Figure 7A) and the genome-wide protection by TRF2 of heterochromatin regions (Figure 7B).

Overall, our findings highlight a broader role for TRF2 than what was initially expected from a telomere-specific factor. Intriguingly, our data put forward a close link between the mechanisms ensuring stability of telomeres and of genome-wide heterochromatin via TRF2, suggesting unexpected crosstalk between these chromosomal regions during aging and cancer. Moreover, our findings provide a rationale for many puzzling observations linking heterochromatin to telomeres (Jain et al., 2010; Perrini et al., 2004; Smogorzewska et al., 2000) and raise the interesting possibility that the two chromosomal elements share an evolutionary mechanism involved in the stabilization of ancestral linear chromosomes.

STAR+METHODS

Detailed methods are provided in the online version of this paper and include the following:

- KEY RESOURCES TABLE
- CONTACT FOR REAGENT AND RESOURE SHARING
- EXPERIMENTAL MODEL AND SUBJECT DETAILS
- METHOD DETAILS
  - Transient Transfections
  - Real-Time qPCR
  - Immunofluorescence-FISH
  - Image Acquisition and Analysis
  - Metaphase Analysis
  - Band-Shift Competition Assay
  - Chromatin Immunoprecipitation
  - ChIP Sequencing and Analysis
  - BrdU-IP Replication Assay
  - Slot Blotting
  - Western Blotting
  - DNA Combing: Cells, Slide Preparation, and FISH-IF Detection
  - DNA Combing: Analysis
- QUANTIFICATION AND STATISTICAL ANALYSIS
  - Statistics
- DATA AND SOFTWARE AVAILABILITY

SUPPLEMENTAL INFORMATION

Supplemental Information includes seven figures and two tables and can be found with this article online at https://doi.org/10.1016/j.molcel.2018.03.036.

ACKNOWLEDGMENTS

We greatly thank Yiming Lu for his continued support and advice, Claire Vourc'h and Patrick Heun for helpful discussions, Joachim Lingner for the HeLa cell line, and Peter Lansdorp for the IH6 antibody used in this study. This work was performed using the genomic, PICMI, and CYTOMED facilities of IRCAN (supported by FEDER, ARC, le Ministère de l'Enseignement Supérieur, la région Provence Alpes-Côte d'Azur and Inserm). The exchanges between the E.G. and J.Y. labs were supported by the PHC Cai Yuanpei program of the Ministry of Foreign Affair (36721YM). The work in the E.G. lab was supported by grants from the Fondation ARC (2016-2019 –PGA1*20160203873), Ligue Contre le Cancer (E.G., "Equipes Labellisées," LIGUE 2014), ANR ("Teloloop," ANR-1582-30020690), Institut Nationale du Cancer (INCa) (TELOCHROM and REPLITOP), "Investments for the Future" LABEX SIGNALIFE (reference ANR-11-LABX-0028-01), and the cross-cutting program of Inserm on aging (AGEMED, PTVieillissement). The work in the J.Y. lab was supported by the National Natural Science Foundation of China (grant numbers 81270433, 81471400, 81522017, and 91749126), the Shanghai Municipal Education Commission (Oriental Scholars Program; 2012-67), and the Foundation of Shanghai Jiaotong University School of Medicine for Translational Medicine Innovation project (grant number 15ZH4005). Work in G.A.'s lab is supported by la Ligue Nationale contre le Cancer (Equipe labellisée Ligue) and ERC-2015-ADG-694694 ChromADICT.

AUTHOR CONTRIBUTIONS

A.M.-B. conducted and coordinated most of the experiments, interpreted the results, and wrote the manuscript. L.L. performed western blotting and different cell biology experiments. S.B., S.K., and M.D. performed and interpreted DNA combing experiments. M.-J.G.-P. conducted EMSA experiments and wrote the manuscript. O.C., K.J., and N.N. processed and analyzed ChIP-seq data. A.I. performed different immunofluorescence experiments. M.M.

helped with ATM experiments. G.A., M.-P.T.-F., M.S., M.P., and A.L.-V. provided different reagents and cellular constructs. E.G. designed all experiments, interpreted the results, and wrote the manuscript. J.Y. coordinated all experiments, interpreted the results, and wrote the manuscript.

DECLARATION OF INTERESTS

The authors declare no competing interests.

Received: October 9, 2017
Revised: February 20, 2018
Accepted: March 29, 2018
Published: May 3, 2018

SUPPORTING CITATIONS

The following reference appears in the Supplemental Information: Hansen et al. (2010).

REFERENCES

Alabert, C., Bukowski-Wills, J.C., Lee, S.B., Kustatscher, G., Nakamura, K., de Lima Alves, F., Menard, P., Mejlvang, J., Rappsilber, J., and Groth, A. (2014). Nascent chromatin capture proteomics determines chromatin dynamics during DNA replication and identifies unknown fork components. Nat. Cell Biol. *16*, 281–293.

Amiard, S., Doudeau, M., Pinte, S., Poulet, A., Lenain, C., Faivre-Moskalenko, C., Angelov, D., Hug, N., Vindigni, A., Bouvet, P., et al. (2007). A topological mechanism for TRF2-enhanced strand invasion. Nat. Struct. Mol. Biol. *14*, 147–154.

Aze, A., Sannino, V., Soffientini, P., Bachi, A., and Costanzo, V. (2016). Centromeric DNA replication reconstitution reveals DNA loops and ATR checkpoint suppression. Nat. Cell Biol. *18*, 684–691.

Benarroch-Popivker, D., Pisano, S., Mendez-Bermudez, A., Lototska, L., Kaur, P., Bauwens, S., Djerbi, N., Latrick, C.M., Fraisier, V., Pei, B., et al. (2016). TRF2-mediated control of telomere DNA topology as a mechanism for chromosome-end protection. Mol. Cell *61*, 274–286.

Beuzer, P., Quivy, J.P., and Almouzni, G. (2014). Establishment of a replication fork barrier following induction of DNA binding in mammalian cells. Cell Cycle *13*, 1607–1616.

Biroccio, A., Cherfils-Vicini, J., Augereau, A., Pinte, S., Bauwens, S., Ye, J., Simonet, T., Horard, B., Jamet, K., Cervera, L., et al. (2013). TRF2 inhibits a cell-extrinsic pathway through which natural killer cells eliminate cancer cells. Nat. Cell Biol. *15*, 818–828.

Bosco, N., and de Lange, T. (2012). A TRF1-controlled common fragile site containing interstitial telomeric sequences. Chromosoma *121*, 465–474.

Bradshaw, P.S., Stavropoulos, D.J., and Meyn, M.S. (2005). Human telomeric protein TRF2 associates with genomic double-strand breaks as an early response to DNA damage. Nat. Genet. *37*, 193–197.

Cortez, D. (2015). Preventing replication fork collapse to maintain genome integrity. DNA Repair (Amst.) *32*, 149–157.

De Cian, A., Delemos, E., Mergny, J.L., Teulade-Fichou, M.P., and Monchaud, D. (2007). Highly efficient G-quadruplex recognition by bisquinolinium compounds. J. Am. Chem. Soc. *129*, 1856–1857.

de Lange, T. (2005). Shelterin: the protein complex that shapes and safeguards human telomeres. Genes Dev. *19*, 2100–2110.

Denchi, E.L., and de Lange, T. (2007). Protection of telomeres through independent control of ATM and ATR by TRF2 and POT1. Nature *448*, 1068–1071.

Deng, W., Tsao, S.W., Guan, X.Y., and Cheung, A.L. (2012). Pericentromeric regions are refractory to prompt repair after replication stress-induced breakage in HPV16E6E7-expressing epithelial cells. PLoS ONE *7*, e48576.

Dungrawala, H., Rose, K.L., Bhat, K.P., Mohni, K.N., Glick, G.G., Couch, F.B., and Cortez, D. (2015). The replication checkpoint prevents two types of fork collapse without regulating replisome stability. Mol. Cell *59*, 998–1010.

Fouché, N., Cesare, A.J., Willcox, S., Ozgür, S., Compton, S.A., and Griffith, J.D. (2006). The basic domain of TRF2 directs binding to DNA junctions irrespective of the presence of TTAGGG repeats. J. Biol. Chem. *281*, 37486–37495.

Gilson, E., and Géli, V. (2007). How telomeres are replicated. Nat. Rev. Mol. Cell Biol. *8*, 825–838.

Giraud-Panis, M.J., Pisano, S., Benarroch-Popivker, D., Pei, B., Le Du, M.H., and Gilson, E. (2013). One identity or more for telomeres? Front. Oncol. *3*, 48.

Grolimund, L., Aeby, E., Hamelin, R., Armand, F., Chiappe, D., Moniatte, M., and Lingner, J. (2013). A quantitative telomeric chromatin isolation protocol identifies different telomeric states. Nat. Commun. *4*, 2848.

Guenatri, M., Bailly, D., Maison, C., and Almouzni, G. (2004). Mouse centric and pericentric satellite repeats form distinct functional heterochromatin. J. Cell Biol. *166*, 493–505.

Hansen, R.S., Thomas, S., Sandstrom, R., Canfield, T.K., Thurman, R.E., Weaver, M., Dorschner, M.O., Gartler, S.M., and Stamatoyannopoulos, J.A. (2010). Sequencing newly replicated DNA reveals widespread plasticity in human replication timing. Proc. Natl. Acad. Sci. USA *107*, 139–144.

Henderson, A., Wu, Y., Huang, Y.C., Chavez, E.A., Platt, J., Johnson, F.B., Brosh, R.M., Jr., Sen, D., and Lansdorp, P.M. (2014). Detection of G-quadruplex DNA in mammalian cells. Nucleic Acids Res. *42*, 860–869.

Jain, D., Hebden, A.K., Nakamura, T.M., Miller, K.M., and Cooper, J.P. (2010). HAATI survivors replace canonical telomeres with blocks of generic heterochromatin. Nature *467*, 223–227.

Langmead, B., Trapnell, C., Pop, M., and Salzberg, S.L. (2009). Ultrafast and memory-efficient alignment of short DNA sequences to the human genome. Genome Biol. *10*, R25.

Le Tallec, B., Koundrioukoff, S., Wilhelm, T., Letessier, A., Brison, O., and Debatisse, M. (2014). Updating the mechanisms of common fragile site instability: how to reconcile the different views? Cell. Mol. Life Sci. *71*, 4489–4494.

Li, H., Handsaker, B., Wysoker, A., Fennell, T., Ruan, J., Homer, N., Marth, G., Abecasis, G., and Durbin, R.; 1000 Genome Project Data Processing Subgroup (2009). The Sequence Alignment/Map format and SAMtools. Bioinformatics *25*, 2078–2079.

Martínez, P., Thanasoula, M., Muñoz, P., Liao, C., Tejera, A., McNees, C., Flores, J.M., Fernández-Capetillo, O., Tarsounas, M., and Blasco, M.A. (2009). Increased telomere fragility and fusions resulting from TRF1 deficiency lead to degenerative pathologies and increased cancer in mice. Genes Dev. *23*, 2060–2075.

Martini, E., Roche, D.M., Marheineke, K., Verreault, A., and Almouzni, G. (1998). Recruitment of phosphorylated chromatin assembly factor 1 to chromatin after UV irradiation of human cells. J. Cell Biol. *143*, 563–575.

Michalet, X., Ekong, R., Fougerousse, F., Rousseaux, S., Schurra, C., Hornigold, N., van Slegtenhorst, M., Wolfe, J., Povey, S., Beckmann, J.S., and Bensimon, A. (1997). Dynamic molecular combing: stretching the whole human genome for high-resolution studies. Science *277*, 1518–1523.

Miller, K.M., Rog, O., and Cooper, J.P. (2006). Semi-conservative DNA replication through telomeres requires Taz1. Nature *440*, 824–828.

Muftuoglu, M., Wong, H.K., Imam, S.Z., Wilson, D.M., 3rd, Bohr, V.A., and Opresko, P.L. (2006). Telomere repeat binding factor 2 interacts with base excision repair proteins and stimulates DNA synthesis by DNA polymerase beta. Cancer Res. *66*, 113–124.

Nikolov, I., and Taddei, A. (2016). Linking replication stress with heterochromatin formation. Chromosoma *125*, 523–533.

Pedroso, I.M., Hayward, W., and Fletcher, T.M. (2009). The effect of the TRF2 N-terminal and TRFH regions on telomeric G-quadruplex structures. Nucleic Acids Res. *37*, 1541–1554.

Perrini, B., Piacentini, L., Fanti, L., Altieri, F., Chichiarelli, S., Berloco, M., Turano, C., Ferraro, A., and Pimpinelli, S. (2004). HP1 controls telomere capping, telomere elongation, and telomere silencing by two different mechanisms in Drosophila. Mol. Cell *15*, 467–476.

Postow, L., Crisona, N.J., Peter, B.J., Hardy, C.D., and Cozzarelli, N.R. (2001). Topological challenges to DNA replication: conformations at the fork. Proc. Natl. Acad. Sci. USA *98*, 8219–8226.

Poulet, A., Buisson, R., Faivre-Moskalenko, C., Koelblen, M., Amiard, S., Montel, F., Cuesta-Lopez, S., Bornet, O., Guerlesquin, F., Godet, T., et al. (2009). TRF2 promotes, remodels and protects telomeric Holliday junctions. EMBO J. *28*, 641–651.

Poulet, A., Pisano, S., Faivre-Moskalenko, C., Pei, B., Tauran, Y., Haftek-Terreau, Z., Brunet, F., Le Bihan, Y.V., Ledu, M.H., Montel, F., et al. (2012). The N-terminal domains of TRF1 and TRF2 regulate their ability to condense telomeric DNA. Nucleic Acids Res. *40*, 2566–2576.

Saint-Léger, A., Koelblen, M., Civitelli, L., Bah, A., Djerbi, N., Giraud-Panis, M.J., Londoño-Vallejo, A., Ascenzioni, F., and Gilson, E. (2014). The basic N-terminal domain of TRF2 limits recombination endonuclease action at human telomeres. Cell Cycle *13*, 2469–2474.

Sarek, G., Vannier, J.B., Panier, S., Petrini, J.H., and Boulton, S.J. (2015). TRF2 recruits RTEL1 to telomeres in S phase to promote t-loop unwinding. Mol. Cell *57*, 622–635.

Schindelin, J., Arganda-Carreras, I., Frise, E., Kaynig, V., Longair, M., Pietzsch, T., Preibisch, S., Rueden, C., Saalfeld, S., Schmid, B., et al. (2012). Fiji: an open-source platform for biological-image analysis. Nat. Methods *9*, 676–682.

Schmutz, I., Timashev, L., Xie, W., Patel, D.J., and de Lange, T. (2017). TRF2 binds branched DNA to safeguard telomere integrity. Nat. Struct. Mol. Biol. *24*, 734–742.

Sfeir, A., Kosiyatrakul, S.T., Hockemeyer, D., MacRae, S.L., Karlseder, J., Schildkraut, C.L., and de Lange, T. (2009). Mammalian telomeres resemble fragile sites and require TRF1 for efficient replication. Cell *138*, 90–103.

Smogorzewska, A., and de Lange, T. (2002). Different telomere damage signaling pathways in human and mouse cells. EMBO J. *21*, 4338–4348.

Smogorzewska, A., van Steensel, B., Bianchi, A., Oelmann, S., Schaefer, M.R., Schnapp, G., and de Lange, T. (2000). Control of human telomere length by TRF1 and TRF2. Mol. Cell. Biol. *20*, 1659–1668.

Sullivan, B.A., and Karpen, G.H. (2004). Centromeric chromatin exhibits a histone modification pattern that is distinct from both euchromatin and heterochromatin. Nat. Struct. Mol. Biol. *11*, 1076–1083.

Takai, H., Smogorzewska, A., and de Lange, T. (2003). DNA damage foci at dysfunctional telomeres. Curr. Biol. *13*, 1549–1556.

Técher, H., Koundrioukoff, S., Carignon, S., Wilhelm, T., Millot, G.A., Lopez, B.S., Brison, O., and Debatisse, M. (2016). Signaling from Mus81-Eme2-dependent DNA damage elicited by Chk1 deficiency modulates replication fork speed and origin usage. Cell Rep. *14*, 1114–1127.

Usdin, K., House, N.C., and Freudenreich, C.H. (2015). Repeat instability during DNA repair: insights from model systems. Crit. Rev. Biochem. Mol. Biol. *50*, 142–167.

van Steensel, B., Smogorzewska, A., and de Lange, T. (1998). TRF2 protects human telomeres from end-to-end fusions. Cell *92*, 401–413.

Vannier, J.B., Pavicic-Kaltenbrunner, V., Petalcorin, M.I., Ding, H., and Boulton, S.J. (2012). RTEL1 dismantles T loops and counteracts telomeric G4-DNA to maintain telomere integrity. Cell *149*, 795–806.

Ye, J., Lenain, C., Bauwens, S., Rizzo, A., Saint-Léger, A., Poulet, A., Benarroch, D., Magdinier, F., Morere, J., Amiard, S., et al. (2010). TRF2 and apollo cooperate with topoisomerase 2alpha to protect human telomeres from replicative damage. Cell *142*, 230–242.

Zang, C., Schones, D.E., Zeng, C., Cui, K., Zhao, K., and Peng, W. (2009). A clustering approach for identification of enriched domains from histone modification ChIP-seq data. Bioinformatics *25*, 1952–1958.

Zhu, L., Chou, S.H., and Reid, B.R. (1996). A single G-to-C change causes human centromere TGGAA repeats to fold back into hairpins. Proc. Natl. Acad. Sci. USA *93*, 12159–12164.

Zimmermann, M., Kibe, T., Kabir, S., and de Lange, T. (2014). TRF1 negotiates TTAGGG repeat-associated replication problems by recruiting the BLM helicase and the TPP1/POT1 repressor of ATR signaling. Genes Dev. *28*, 2477–2491.

STAR+METHODS

KEY RESOURCES TABLE

REAGENT or RESOURCE	SOURCE	IDENTIFIER
Antibodies		
Rabbit polyclonal anti-53BP1	Novus Biologicals	NB100-305; RRID: AB_10001695
Mouse monoclonal anti-TRF2	Novus Biologicals	NB100-56506; RRID: AB_839054
Rabbit polyclonal anti-TRF2	Novus Biologicals	NB110-57130; RRID: AB_844199
Anti-PCNA	Santa Cruz Biotechnology	sc-25280; RRID: AB_628109
Anti-pATM (ser1981)	Cell Signaling Technology	4526; RRID: AB_2062663
Anti-RTEL1	Londono-Vallejo Lab	N/A
IH6	P. Lansdorp Lab	Henderson et al., 2014
Anti-pChK1 (ser317)	Cell Signaling Technology	2344; RRID: AB_331488
Anti-pChK2	Abcam	ab32148; RRID: AB_726828
Anti-beta-actin	Abcam	ab8227; RRID: AB_2305186
Anti-BrdU	Abcam	ab2284; RRID: AB_302944
H3	Abcam	ab1791; RRID: AB_302613
Anti-gH2AX	Abcam	ab2893; RRID: AB_303388
Anti-H3K9me3	Upstate	07-442; RRID: AB_310620
Anti-H4K4me3	Upstate	07-473; RRID: AB_1977252
Anti-rabbit Alexa 488 antibody	Jackson ImmunoResearch	111-545-144; RRID: AB_2338052
Goat anti-mouse Alexa 488 antibody	Jackson ImmunoResearch	115-545-146; RRID: AB_2307324
HRP goat anti-mouse IgG	Vector Laboratories	PI-2000; RRID: AB_2336177
HRP goat anti-rabbit IgG	Vector Laboratories	PI-1000; RRID: AB_2336198
Anti-BrdU-FITC	BD Biosciences	347583; RRID: AB_400327
Rat anti-BrdU	AbD Serotec	OBT0030; RRID: AB_609568
Goat anti-mouse Alexa Fluor 488	Invitrogen	A11029; RRID: AB_138404
Goat anti-rat Alexa Fluor 594	Invitrogen	A11007; RRID: AB_141374
Goat anti-rat Alexa Fluor 555	Invitrogen	A21434; RRID: AB_141733
Mouse anti-ssDNA	Millipore	MAB3034; RRID: AB_94645
Anti-mouse Cy5.5	Abcam	ab6947; RRID: AB_955087
Anti-goat Cy5.5	Abcam	ab6951; RRID: AB_955084
Alexa Fluor 488 streptavidin	Thermo Scientific	S32354; RRID: AB_2315383
Mouse anti-BrdU	BD Biosciences	347580; RRID: AB_400326
Anti-goat Cy5.5	Abcam	ab6951; RRID: AB_955084
Chemicals, Peptides, and Recombinant Proteins		
VE-193	Sigma	SML1109
KU-55933	Sigma	SML1415
Hydroxyurea	Sigma	H8627
BrdU	Sigma	B-5002
IdU	Sigma	17125
CldU	MP Biomedicals	105478
Thymidine	Sigma	T9250
ICRF-193	Sigma	I4659
TSA	Sigma	T1952
Aphidicoline	Calbiochem	178273
Phen-DC3	Teulade-Fichoulab	N/A
Phen-DC6	Teulade-Fichoulab	N/A

(*Continued on next page*)

Continued

REAGENT or RESOURCE	SOURCE	IDENTIFIER
Critical Commercial Assays		
Dharmafect 1 transfection reagent	Dharmacon	T-2001
Lipofectamine-2000	Thermo Fisher Scientific	11668019
High-Capacity RNA-to-cDNA kit	Thermo Fisher Scientific	4387406
FastStart SYBR Green Master	Roche	05673484001
Deposited Data		
gH2AX ChIP-seq data	This paper	GEO: GSE95221
H3K9me3 ChIP-seq data	This paper	GEO: GSE102278
Raw image data	This paper	https://doi.org/10.17632/zjvptr88c2.1
Experimental Models: Cell Lines		
shTERF2-inducible HeLa cell line	Grolimund et al., 2013	N/A
BJ-HELT	Biroccio et al., 2013	N/A
HeLa-38	Beuzer et al., 2014	N/A
MRC5 primary cell line	ATCC	CCL-171
Oligonucleotides		
SatIII PNA probe: TTCCATTCCATTCCATTCCA	This work	N/A
Centro PNA probe: AAACTAGACAGAAGCATT	This work	N/A
Temere PNA probe: CCCTAACCCTAACCCTAA	This work	N/A
Primers for qPCR	This work	See Table S1
siRNA sequences	Dharmacon	See Table S2
Recombinant DNA		
LacI-GFP plasmid	Beuzer et al., 2014	N/A
LacI-HP1a plasmid	This work	N/A
Software and Algorithms		
ImageQuant Software	GE Healthcare	N/A
ImageJ-FIJI	Schindelin et al., 2012	N/A
GraphPad Prism 5	GraphPad	https://www.graphpad.com/
Sicer	Zang et al., 2009	N/A
Bowtie2	Langmead et al., 2009	N/A
Samtools	Li et al., 2009	N/A

CONTACT FOR REAGENT AND RESOURE SHARING

Further information and requests for resources and reagents should be directed to and will be fulfilled by the Lead Contact, Eric Gilson (eric.gilson@unice.fr).

EXPERIMENTAL MODEL AND SUBJECT DETAILS

Human primary MRC-5 cells were obtained from the ATCC. The shTERF2-inducible HeLa cell line was a gift from the Joachim Lingner lab (Grolimund et al., 2013). HeLa-38 was a gift from Evi Soutoglou lab (Beuzer et al., 2014). BJ-HELT was immortalized by transduction of hTERT and SV40 ER genes (Biroccio et al., 2013). All cell lines used in this study were grown in DMEM supplemented with 10% fetal calf serum. All cell lines were routinely tested for mycoplasma contamination.

METHOD DETAILS

Transient Transfections

siRNA (On-TargetPlus SMARTpool, Dharmacon) transfections were performed with Dharmafect 1 transfection reagent (Dharmacon) for 72 hr. Transfections of LacI-GFP or LacI-HP1a-GFP were carried out for 24 hr using Lipofectamine-2000 following the manufacturer's instructions. For siRNA reference and sequences, see Table S2.

Real-Time qPCR

QPCR was used to determine the efficiency of siRNA downregulation and for ChIP validation. For siRNA inhibition, total RNA (RNeasy Mini Kit, QIAGEN) was reverse transcribed using the High-Capacity RNA-to-cDNA kit (Thermo Scientific). qPCR was performed using an Applied StepOnePlus system (Life Technologies) with SYBR green master mix (Roche, 4913914 001). Only siRNA transfections giving rise to a reduction of R 75% were used in this study. For primer sequences used in qPCR, see Table S1.

Immunofluorescence-FISH

Cells were grown onto glass coverslips and fixed for 12 min with 3.7% formaldehyde. Cells were then permeabilized with 0.5% Triton X-100 for 5 min and dehydrated in increasing concentrations of ethanol for 3 min (50%, 70% and 100%). Hybridization of PNA probes was performed for at least 2 hr at RT after a 3-min denaturation in 70% formamide, 10 mM Tris pH 7.2 and 1% blocking solution (Roche) at 80C. After that, the cells were washed in a 70% formamide, 10 mM Tris pH 7.2 solution for 30 min, followed by a solution containing 150 mM NaCl and 50 mM Tris pH 7.5 for 15 min. Next, the cells were incubated with blocking buffer (1% Triton X-100, 1% BSA and 5% goat serum) and incubated overnight at 4C with the desired antibody. Cells were then washed with 1X PBS and incubated for 1 hr with the corresponding secondary antibody. Finally, the cells were preserved in a mounting solution with DAPI (Vectashield, Vector Laboratories).

Cells treated with Triton X-100 before cell fixation were washed in CSK buffer (10mM Pipes pH 7, 100 mM NaCl, 300 mM sucrose, 3mM MgCl2 supplemented with protease inhibitors) and incubated for 5 min at RT with 0.5% Triton X-100.

Image Acquisition and Analysis

Imaging was performed with a Zeiss LSM 5 Exciter confocal laser scanning microscope. A minimum of 15 z-planes were acquired (736 X 512 pixels per frame using a 8-bit pixel depth for each channel) with a 63X oil immersion objective (Plan-Apochromat 63x/1.4 Oil DIC). Images were analyzed with the ZEN 2009 (Zeiss). To determine the association between PNA and IF signals, the profile of the signal intensity was generated with ImageJ software (Schindelin et al., 2012). Positive associations were score when both profiles overlap.

Metaphase Analysis

Cells were arrested at metaphase stage using colcemid (final concentration 0.05 mg/ml) for 1 2 hr or 4 5 hr for primary pre-senescent cells. Trypsinized cells were incubated with 0.075 M KCl for 12 min at 37C followed by methanol/glacial acetic acid (3:1) fixation. Telomeres and pericentromeres were visualized with PNA probes hybridized for 2 hr in 70% formamide, 10 mM Tris pH 7.2 and 1% blocking solution (Roche) buffer. Images were obtained with a Zeiss Axiovert Z2 epi-fluorescent microscope.

Band-Shift Competition Assay

The double-stranded DNA probe and competitors for the competition assays were obtained by hybridization of 106-base synthetic oligonucleotides (Eurogentec). DsSat3 was $5^{0\ 32}$P-labeled on the top strand using T4 polynucleotide kinase (Promega) and gamma-^{32}P ATP in conditions recommended by the manufacturer. Non-incorporated ATP was removed by ethanol precipitation. DNA concentration was measured by absorbance after hybridization. His-TRF2 was purified as previously described (Poulet et al., 2012).

Five nM $5^{0\ 32}$P labeled dsSat3 probe was mixed with increasing amounts of competitor and incubated with His-TRF2 (20 nM final concentration) in 10 ml of 20 mM HEPES pH 8, 150 mM KCl, 1 mM DTT, 500 mg/ml acetylated BSA, and 5% Glycerol solution for 15 min on ice. After incubation, 2 ml of 15% ficoll was added and the samples were loaded on a 1% 0.5X TBE agarose gel with 7.5 V/cm current. Electrophoresis was performed in the same buffer at the same voltage for 30 min, then the gel was dried on DE81 paper and exposed overnight on a phosphorimager screen. The screen was scanned using a Typhoon FLA 9000 laser scanner (GE Healthcare) and the bands quantified using Image Quant TL software (GE Healthcare). Experiments were repeated at least three times for each competitor.

Chromatin Immunoprecipitation

Cells were cross-linked for 12 min with 1% formaldehyde and washed with cold PBS. The cells were centrifuged and the pellet re-suspended in cell lysis buffer (5 mM PIPES pH 8, 85 mM KCl, 0.5% NP40 and protease inhibitors). The cells were pelleted at 4C and re-suspended in nucleus lysis buffer (50 mM Tris pH 8, 10 mM EDTA, 1% SDS, protease inhibitors) and the cells were sonicated using a Bioruptor to get an average fragment size of 400 bp. IPs were set up with 40 mg of DNA and incubated overnight with the desired antibody. Magnetic beads (Dynabeads, Life Technologies) were added for 2 hr. The beads were washed with a low salt buffer (150 mM NaCl, 1% Triton X-100, 0.1% SDS), a high salt buffer (500 mM NaCl, 1% Triton X-100, 0.1% SDS), followed by a lithium salt buffer (0.25 M LiCl, 1% NP40, 1% deoxycholic acid). Chromatin was eluted with a 1% SDS, 0.1 M NaHCO3 solution and the cross-link reversed at 65 C overnight. The DNA was treated with RNaseA (10 mg/ml for 20 min), proteinase K (10 mg/ml for 1 hr at 50C) followed by phenol-chloroform purification and ethanol precipitation. Quantification of immunoprecipitated DNA was performed with the Qubit HS kit (Thermo Scientific).

ChIP Sequencing and Analysis

gH2AX ChIP-seq, library preparation and sequencing was performed at the BGI Tech Solutions (China) using the Illumina system while H3K9me3 ChIP-seq was performed using a SOLiD 5 sequencer (Roche) according to the manufacturer's instructions. Two biological replicates were performed per condition, the reads (30-40 million per sample) were merged and the alignment of short reads to the human genome (hg19, UCSC) was performed using the default parameters from the Bowtie2 program (Langmead et al., 2009). Output files (SAM format) were converted into BAM files and indexed using the SAMTools program (Li et al., 2009). Peak calling was perform using the Sicer program (Zang et al., 2009) with the following settings: window size 200; gap size 600; cut off 10-3 for gH2AX and 10-4 for H3K9me3.

To calculate the total number of reads containing repetitive sequences (Figure S7B), we counted for each dataset the total number of reads containing 49 bp of continuous repeat elements (without mismatches) and divided by the total number of reads. IP samples were normalized to their corresponding input.

BrdU-IP Replication Assay

Cells were synchronized using the double-thymidine block method. Briefly, 2 mM final concentration of thymidine was added to the cells for 19 hr. The cells were released from the block by adding fresh media for 9 hr followed by a second thymidine incubation for 15 hr. After the second block, the cells were released and harvested every 2 hr. BrdU (final concentration 20 uM) was added to the media 1 hr before cell harvesting. Next, the DNA was extracted using standard methods and sonicated to an average size of 800 bp. The DNA was denatured at 95 C for 10 min and incubated with a BrdU antibody overnight at 4 C in IP buffer (0.1 M sodium phosphate pH 7.0, 1.4 M NaCl, 0.5% Triton X-100). Magnetic beads (Dynabeads Protein G, Life technologies) were used for immunoprecipitation. Beads were re-suspended in proteinase K buffer (50 mM Tris pH 8.0, 10 mM EDTA, 0.5% SDS) and treated with RNase A (10 mg/mL) and proteinase K (10 mg/ml) for 2 hr at 55C. Next, the beads were incubated at 80C for 3 min followed by phenol/chloroform extraction and ethanol precipitation.

Slot Blotting

The DNA obtained from ChIP and BrdU-IP experiments was denatured (0.5 M NaOH, 2 M NaCl and 25 mM EDTA) and blotted onto nylon membranes using a slot blot apparatus, crosslinked, and hybridized with different radioactively labeled probes. The membranes were exposed onto phosphorimager screens and the signal intensity was quantified with ImageQuant software.

Western Blotting

Total protein extracts were obtained using ice-cold RIPA buffer for 30 min. Samples were separated by SDS-PAGE electrophoresis using NuPAGE Mini gels (Life Technologies). Proteins were transferred onto Protran BA 85 nitrocellulose membranes (Whatman, GE Healthcare) followed by at least 1h blocking with PBST in 5% skim milk. Hybridization with primary antibodies was performed overnight at 4C followed by 1 hr incubation with secondary horseradish peroxidase conjugated antibodies. Membranes were developed using the Luminata Forte HRP substrate (Millipore) and exposed in the Fusion Solo apparatus (Vilbert Lourmat).

DNA Combing: Cells, Slide Preparation, and FISH-IF Detection

HeLa cells were pulse-labeled for 30 min with 20 mM final concentration IdU followed by 30 min CldU (100 mM final concentration), and a final 5 min incubation of 1 mM thymidine. The cells were collected and embedded in 2% low melting agarose plugs. DNA plugs were incubated for 48 hr at 42 C in PK buffer (1% SDS, 0.25 EDTA and 1 mg/ml Proteinase K). Next, agarose plugs were heated at 68 C for 15 min in 1X TE containing b-Agarase I buffer (NEB, M0392). The melted agarose was cooled down to 42 C and incubated for 48 hr in the presence of b-Agarase I (NEB, M0392) and 30 min with 0.25 M MES pH 5.5. DNA present in the melted b-Agarase-digested agarose was stretched onto in-house silanized coverslips.

Next, slides were denatured in 1 N NaOH for 5 min at RT, rinsed in 1X PBS at 4C for 5 min and dehydrated in increasing concentrations of ethanol for 5 min each (50%, 70% and 100%) at RT. The slides were then incubated with blocking solution (1.5% blocking reagent Roche 11096176001 and 0.05% Tween 20) for 30 min at 37 C followed by incubation with mouse anti-BrdU-FITC (347583, BD Biosciences) together with rat anti-BrdU (OBT0030, AbD Serotec) antibody. Next, the samples were washed in NaCl 0.5M, Tris 20 mM pH 7.8, Tween-20 0.5%, for 6 min at RT. Samples were then incubated for 30 min at 37 C with secondary antibodies goat anti-mouse AlexaFluor 488 (Invitrogen, A11029) together with a goat anti-rat AlexaFluor 594 (Invitrogen, A11007) or goat anti-rat Alexa Fluor 555 (Invitrogen, A21434). In the case of global replication studies, the slides were washed 3 times for 5 min each in 1X PBS and incubated for 30 min at 37C with a mouse anti-ssDNA (Millipore, MAB3034) antibody followed by incubation with an anti-mouse Cy5.5 (Abcam, ab6947) antibody. After washes in 1X PBS, the slides were incubated for 30 min at 37C with a donkey anti-goat Cy5.5 (Abcam, ab6951) antibody, washed, and mounted with VectaShield (Vector Laboratories, H-1000).

In the case of SatIII hybridization, the DNA was denatured for 8 min in 1 N NaOH and dehydrated in 70% ethanol for 5 min at 20C followed by dehydration with 85% and 100% ethanol for 5 min each at RT. The PNA probe (SatIII: Biotin-O-TTCCATTCCATTC CATTCCA; Centromere: Biotin-O-AAACTAGACAGAAGCATT) was denatured for 5 min at 95 C and diluted in hybridization mix (10% dextrane sulfate, 50% formamide, 2 x SSC, 1% Tween 20) to a final concentration of 1 mM. Hybridization took place overnight at 37C, followed by washes with 50% formamide and 2XSSC pH 7 solution at RT. The slides were washed in 2XSSC and incubated in blocking solution as described above. Then, the following antibodies were added, in this order: Alexa Fluor 488 streptavidin

(ThermoScientific, S32354), rabbit anti-streptavidin-biotin, AlexaFluor 488 streptavidin (ThermoFisherScientific, S32354), mouse anti-BrdU (BDBiosciences, 347580) together with anti-BrdU (AbDSerotec, OBT0030) followed by a donkey anti-goat Cy5.5 (Abcam, ab6951). All antibody incubations were 30 min at 37 C, with 1X PBS washes between antibodies.

Finally, an epifluorescence microscope (Axio Imager.Z2, Carl Zeiss) equipped with a 63X objective lens (PL APO, NA 1.4 Oil DIC M27) connected to a charge-coupled device camera (Cool-SNAP HQ2; Roper Scientific), and MetaMorph software (Roper Scientific) was used for image acquisition.

DNA Combing: Analysis

The DNA molecules were stretched at a constant speed (300 mm/sec) on silanized coverslips with an automated combing device (FiberComb, GENOMIC VISION). This procedure gives a uniform stretching factor of 2 kb/mm across the surface (Michalet et al., 1997).

To calculate replication speed, only IdU tracks flanked by a CldU tracks present in intact fibers, established by DNA counter-staining, were measured. Tracks ending at the same point as the DNA counterstained fiber were omitted. To determine the length in kb/min, the ratio between the lengths of the IdU + CldU tracks divided by the labeling time in minutes was calculated using the ImageJ (FIJI) software. Fork asymmetry (presented as IdU/CldU in the graphs) was calculated as the ratio of the longest track over the shortest; therefore, the IdU/CldU ratio is R1. Statistical analysis of the median distributions was calculated with the nonparametric Mann-Whitney rank sum test using GraphPad Prism 5 software.

QUANTIFICATION AND STATISTICAL ANALYSIS

Statistics

GraphPad Prism 5 software was used to generate graphs and to perform statistical analysis. p values were obtained using either the two-tailed Student's t test or Mann-Whitney U test. The test used is indicated in figure legends. Differences were considered statistically significant when $p < 0.05$ (* $p < 0.01$, ** $p < 0.001$, *** $p < 0.0001$). Absence of statistical annotation indicates non-significance.

DATA AND SOFTWARE AVAILABILITY

ChIP-seq raw data, profile of reads, and peak analysis were deposited in the Gene Expression Omnibus database under accession number GEO: GSE95221 (gH2AX data) and GEO: GSE102278 (H3K9me3 data).

Raw image data have been deposited to Mendeley Data and are available at: https://doi.org/10.17632/zjvptr88c2.1.

Molecular Cell, Volume *70*

Supplemental Information

Genome-wide Control of Heterochromatin Replication by the Telomere Capping Protein TRF2

Aaron Mendez-Bermudez, Liudmyla Lototska, Serge Bauwens, Marie-Josèphe Giraud-Panis, Olivier Croce, Karine Jamet, Agurtzane Irizar, Macarena Mowinckel, Stephane Koundrioukoff, Nicolas Nottet, Genevieve Almouzni, Mare-Paule Teulade-Fichou, Michael Schertzer, Mylène Perderiset, Arturo Londoño-Vallejo, Michelle Debatisse, Eric Gilson, and Jing Ye

Figure S1. Related to Figure 1.

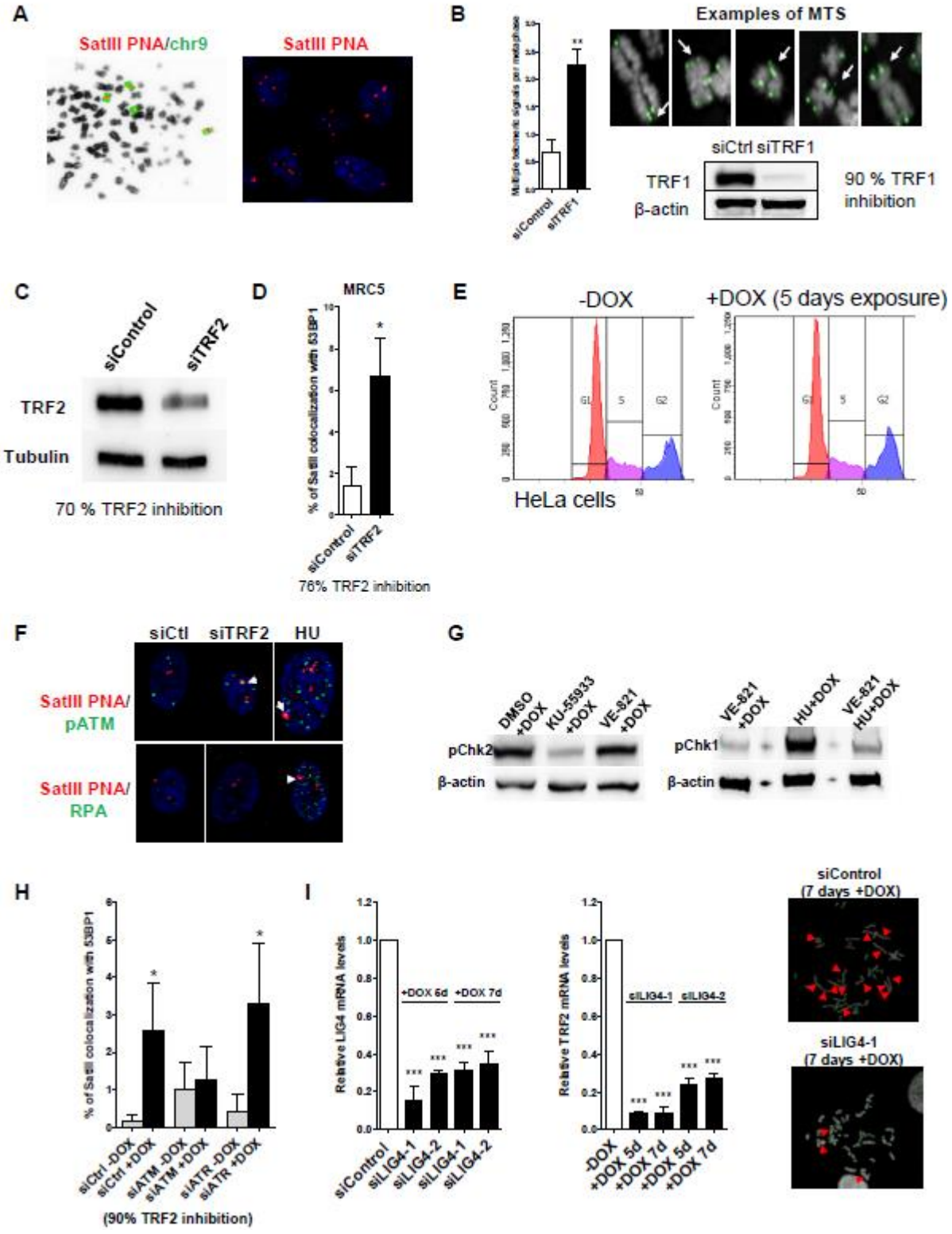

Figure S2. Related to Figure 2.

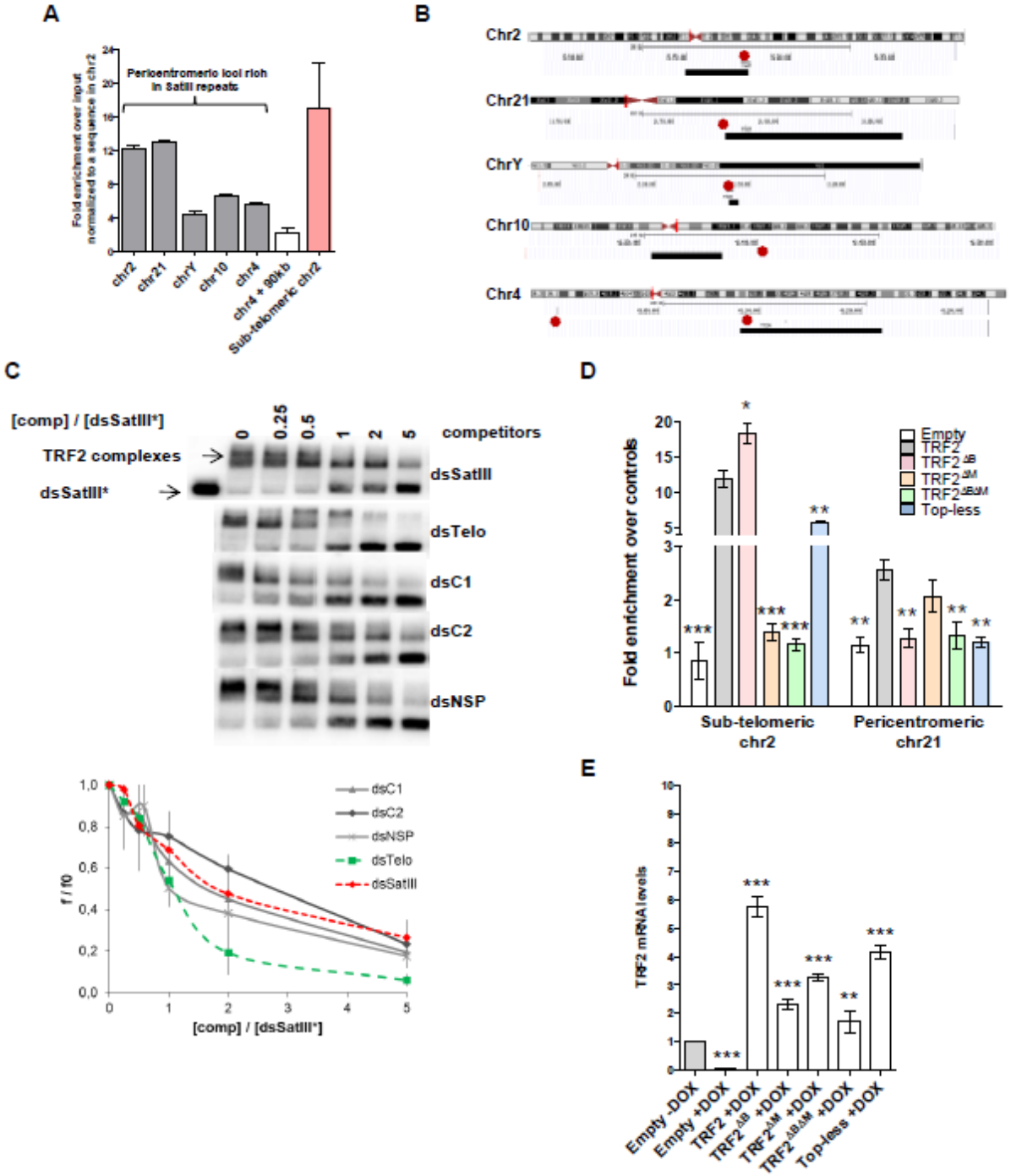

Figure S3. Related to Figure 3.

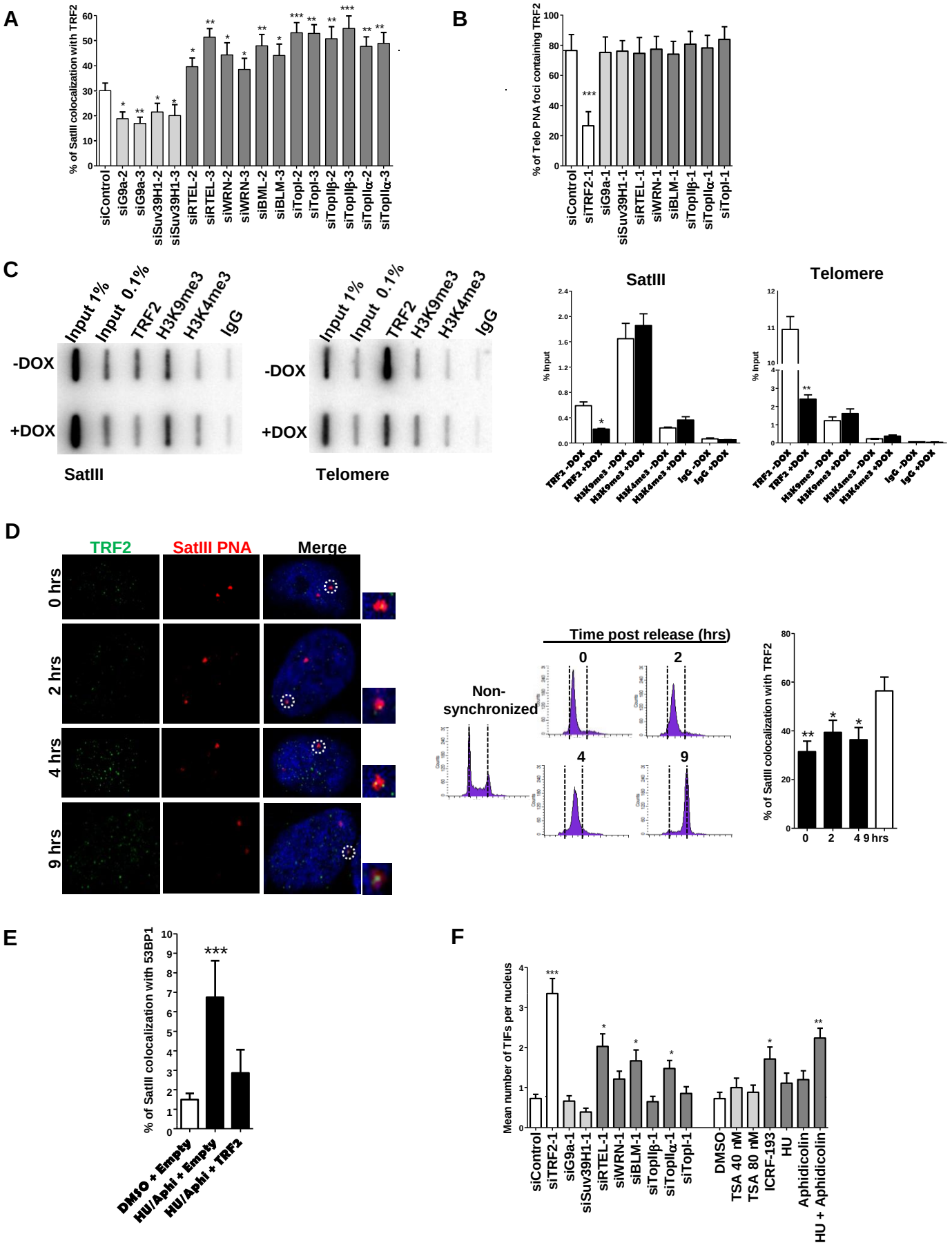

Figure S4. Related to Figure 4.

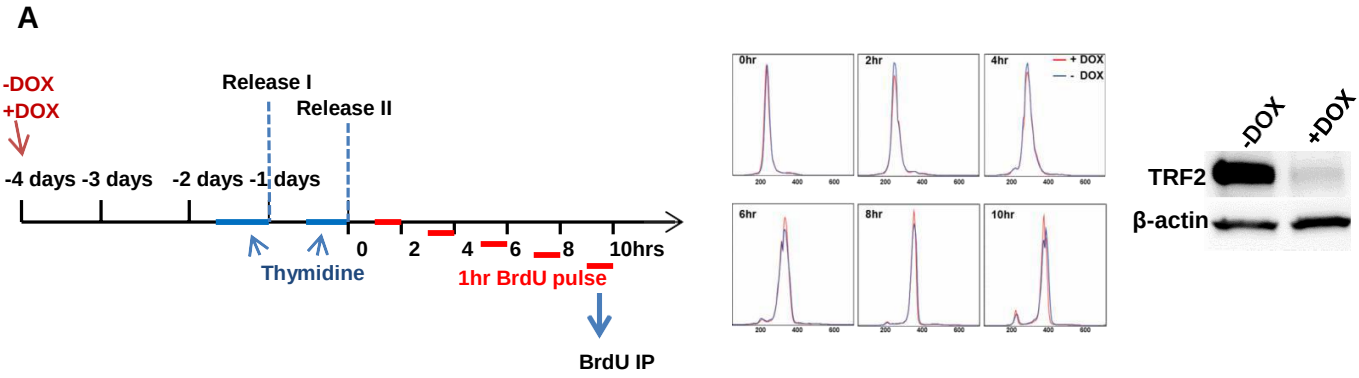

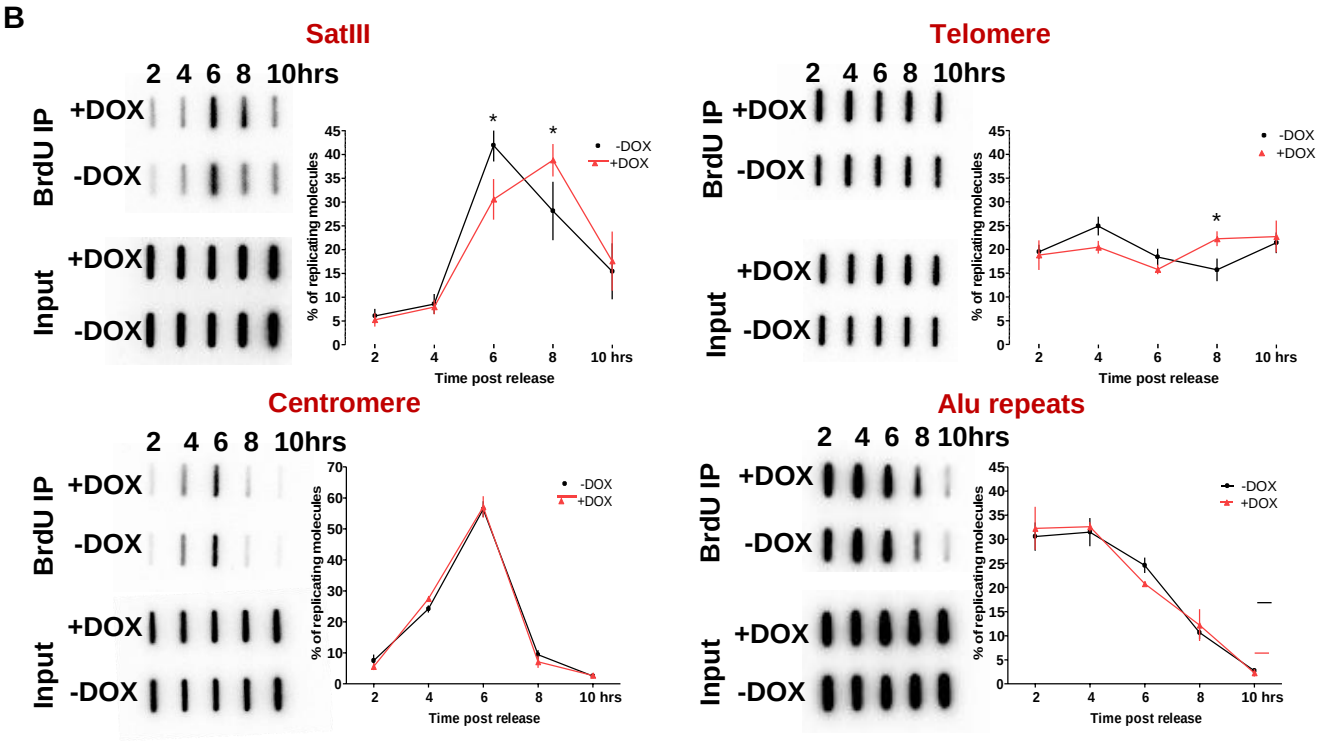

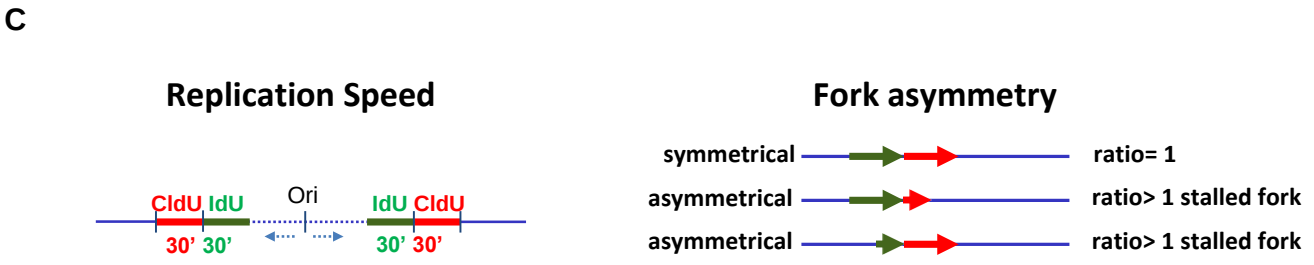

Figure S5. Related to Figure 4 and 5.

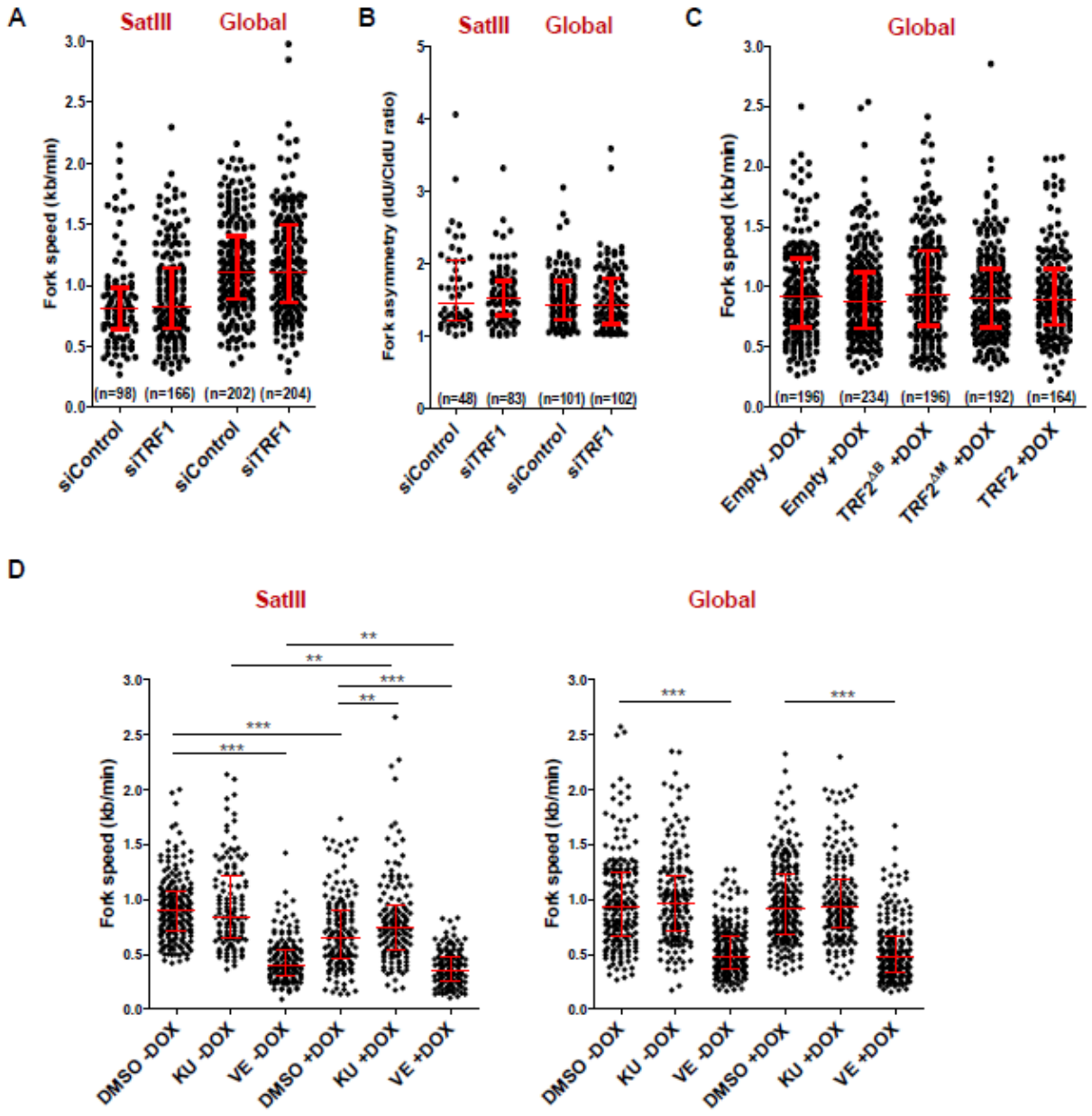

Figure S6. Related to Figure 7

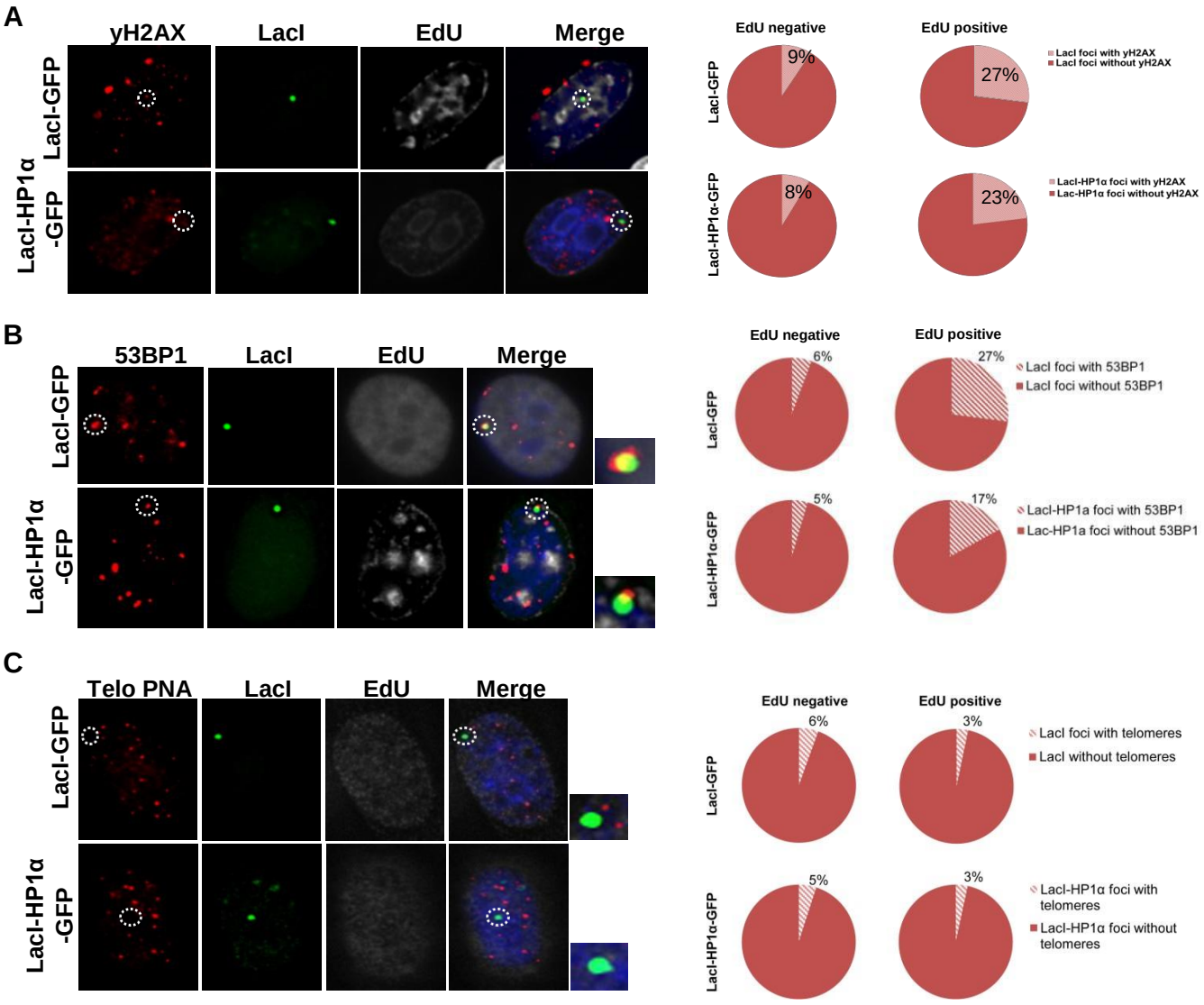

Figure S7. Related to Figure 7.

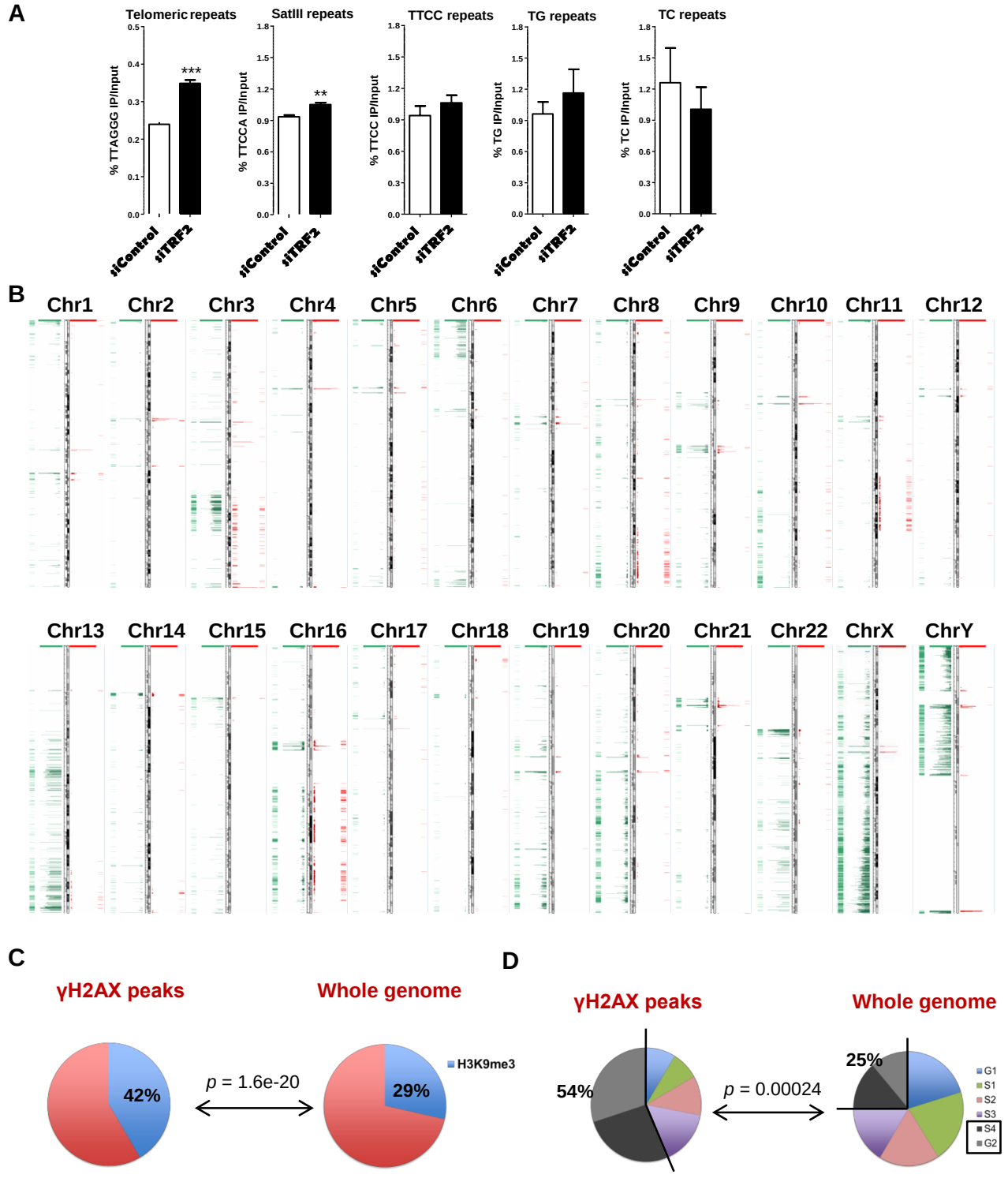

Supplementary Figures

Figure S1. Pericentromeric DNA protection by TRF2

(A) Metaphase chromosome spread of BJ-HELT cells labelled with a SatIII PNA probe together with a whole chromosome 9 paint probe. The pattern of hybridization of the PNA SatIII probe is consistent with the largest number of SatIII repeats in pericentromeres of this chromosome. Hybridization of the SatIII PNA probe on interphase BJ-HELT cells (right panel).

(B) Quantification of Multiple Telomere Signals (MTS) in metaphase chromosome spreads of TRF1 depleted cells. Telomere staining is shown in green. Approximately 1000 chromosomes were quantified per condition. Downregulation of TRF1 is shown by immunobloting. Error bars indicate standard deviation of n=3, $**p < 0.001$; two-tailed Student's *t* test.

(C) Downregulation of TRF2 in BJ-HELT cells.

(D) Quantification of PIFs upon TRF2 downregulation MRC5 primary cells. Down-regulation of TRF2 was assessed by RT-qPCR. *P* values of n = 3 were obtained using the Mann-Whitney U test ($* p < 0.05$).

(E) FACS analysis HeLa cells containing an inducible shTRF2 sequence and incubated with doxycycline (DOX) for 5 days.

(F) Representative IF images of associations between SatIII (red) and phospho-ATM or RPA (green) in MRC5 cell line. Quantification is shown in Figure 1D.

(G) Expression of phospho checkpoint 1 or 2 (pChK1 or pChK2) in HeLa cells treated with doxycycline to downregulate TRF2 expression. Cells were treated with KU-55933 (10 μM for 24 h), VE-821 (10 μM for 24 h) or hydroxyurea (HU; 1.5 μM for 24 hrs).

(H) PIFs of HeLa cells after 5 day doxycycline and 72 h siRNA incubation against ATM or ATR. *TERF2* (90%), *ATM* (75%) and *ATR* (72%) inhibition was estimated by RT-qPCR. SEM of n=3; * $p < 0.05$; Mann-Whitney U test.

(I) Relative *LIG4* (left) and *TERF2* (right) mRNA levels of HeLa cells from the experiment presented in Figure 1F and G, (*** $p < 0.0001$; One-way ANOVA). Examples of metaphase spreads of cells transfected with siLig4 and controls are shown (right panel). Telomeres were stained in green while fusions are marked with arrow heads.

Figure S2. TRF2 binding to pericentromeres rich in SatIII repeats

(A) Fold enrichment (obtained by qPCR) of loci close or being part of SatIII-rich repeats in BJ-HELT. The white bar shows enrichment of a site located 90 kb away from a SatIII-rich repeat block at chromosome 4. qPCR from a sub-telomeric locus rich in telomeric-variant repeats is shown (red bar).

(B) Location of the amplicons generated by qPCR described in *A* (red star) in relation to continuous arrays of SatIII repeats (black thick lines). Bars represent SD of n = 3.

(C) EMSA performed with 5 nM of the dsSatIII labelled probe (dsSatIII*), 20 nM of His-TRF2 and increasing amounts of competitors being either SatIII repeats (dsSatIII), telomeric repeats (dsTelo), SatIII scrambled repeats (dsC1 and dsC2) or an unrelated sequence (dsNSP). Quantification of the EMSA shows the variations of the normalized fraction of DNA bound (f) in each condition. Normalization was performed using the fraction of DNA bound in the absence of competitor (f0). Error bars represent standard deviation of n = 3.

(D) qPCR from the conditions presented in Figure 2D showing the enrichment of different TRF2 mutants normalized to two different sequences where TRF2 does not bind. Fold enrichment of a subtelomere region containing TTAGGG repeats and a pericentromeric region containing TGGAA SatIII repeats is shown. Error bars represent SD of n = 3 (*p* values in relation to TRF2 condition; *$p < 0.05$; **$p < 0.001$; *** $p < 0.0001$. One-way ANOVA).

(E) *TERF2* mRNA levels of the experiment shown in Figure 2d. Error bars represent SD of n = 3; *** $p < 0.0001$; One-way ANOVA.

Figure S3. TRF2 binding to SatIII regions is cell cycle regulated

(A) Quantification of TRF2-SatIII associations of BJ-HELT cells transfected for 72 h with 2 different RNAi sequences per target gene. Only transfections resulting in > 75% inhibition verified by RT-qPCR were used.

(B) Percentage of telomeric PNA signal containing TRF2 in BJ-HELT cells transfected for 72 h.

(C) Slot blots showing ChIP experiments performed in TRF2-depleted HeLa cells (+DOX) for 4 days and control (-DOX). The membrane was initially hybridrized with a SatIII probe followed by a telomeric DNA probe. Errors bars represent SEM of n = 2.

(D) Quantification of TRF2-SatIII associations in HeLa cells synchronized by two pulses of thymidine. The cells were collected 0, 2, 4 and 9 h after releasing of the replication block. FACS analysis of the progression of the cell cycle is shown. Bars represent SEM of n = 2.

(E) PIF quantification of BJ-HELT cells transduced for 6 days with lentivirus containing the full-length TRF2 protein or an empty vector control and treated with hydroxyurea (HU; 1.5 µM) and aphidicolin (aphi- 300 nM) for 24 h. Mean ±SE of n = 3 is shown.

(F) TIFs quantification in BJ-HELT cells transfected for 72 h with one RNAi sequence. Only transfections resulting in > 75% inhibition verified by qPCR were used.

In all the panels from this figure, statistical analyses were performed using Mann-Whitney U test (* $p < 0.05$, ** $p < 0.001$, *** $p < 0.0001$).

Figure S4. TRF2 modulates SatIII replication

(A) Schematic view of the replication experiment performed in HeLa cells using BrdU. DOX was added to the cells 4 days before the releasing of the thymidine block. Cells were collected

every 2 h, with the addition of BrdU 1 h before cell collection. Finally, BrdU IP was performed and the product spot on membranes for subsequent probe hybridization. Synchronization of the cells with or without TRF2 depletion (+ or –DOX) was assessed by FACS, while the expression of TRF2 by immunoblotting (right side).

(B) BrdU immunoprecipitated DNA was spotted on nylon membranes, which were hybridized with a SatIII radioactively labelled probe. The membrane was stripped and sequentially hybridized with telomere, centromere and Alu probes. Each BrdU-IP sample was normalized to its corresponding input. The graphs represent the signal of each condition as a percentage of all BrdU incorporated across the 5 time points collected from three biological replicates (* $p < 0.05$; Mann-Whitney U test performed at each time point between + and - DOX).

(C) HeLa cells were pulse-labeled for 30 min with 20 µM final concentration IdU followed by 30 min CldU (100 µM final concentration). Replication speed was estimated by measuring the length of the IdU + CldU tracks divided by the time in minutes of complete fibers. Fork asymmetry represents the ratio of the longest track over the shorter.

Figure S5. TRF2, but not TRF1, controls replication speed at SatIII

(A-B) Fork speed (A) and asymmetry (B) of SatIII and total DNA labelled tracks in HeLa cells with TRF1 downregulation and control.

(C) Fork speed quantification of global DNA fibers from the experiment described in Figure 4C.

(D) Fork speed of SatIII (left) and total DNA (right) fibers in HeLa cells. Cells were treated with the ATM inhibitor (KU-55933; 10 uM for 24 h) or the ATR inhibitor (VE-821; 10 uM for 24 h), with (+DOX) or without (-DOX) five-day TRF2 depletion.

Bars show the median ± interquartile range or n = 2. Statistical analyses were performed using Mann-Whitney U test (** $p < 0.001$, *** $p < 0.0001$).

Figure S6. LacO replication blockade leads to DDR activation

(A-C) Representative IF images of HeLa-38 cells transfected with LacI-GFP or LacI-HP1α-GFP for 24 h and stained with γH2AX antibody (A), 53BP1 (B) or a telomeric PNA probe (C). EdU (1 μM) was added to the cells for 14 h. Percentage of LacI-GFP or LacI-HP1α-GFP foci colocalizing with either γH2AX, 53BP1 or telomeric PNA signal in dividing and non-dividing cells is shown. At least 50 nuclei containing the LacI-GFP or LacI-HP1α-GFP were analysed per condition.

Figure S7. TRF2 protects genome-wide heterochromatic regions against DNA damages

(A) Quantification of γH2AX ChIP-seq reads composed of pure repeated sequences (indicated at the top of each graph) from BJ-HELT cells after siControl or siTRF2 for 72 h incubation. The number of repetitive-sequence reads obtained in the immunoprecipitated samples was normalized to the total number of reads in the input. Error bars show the SD of n = 2 (**$p < 0.001$, **$p < 0.0001$; two-tailed Student's *t* test).

(B) Profile of γH2AX reads and peaks (red, right side) of siTRF2 vs. siControl after normalization with its corresponding input DNA on each chromosome of BJ-HELT cell line. TRF2 knockdown was performed for 72 h achieving 85% *TERF2* mRNA inhibition. Profile of reads and peaks of H3K9me3 in BJ-HELT without cell treatment (green, left side) are shown.

(C) Pie charts showing the percentage of γH2AX peaks (siTRF2 vs siControl as described above) overlapping H3K9me3 peaks from HeLa-S3 cells deposited in the ENCODE database. Positive overlap was considered when at least one nucleotide was shared between the two conditions using BEDtool intersect algorithms. The *p* value (McNemar's test) represents the probability that the γH2AX peaks are enriched in H3K9me3 marks compared to H3K9me3 of the whole genome.

(D) Comparison between the replication timing pattern (Repli-seq; (Hansen et al., 2010)) of BJ cells (whole genome) and the γH2AX peaks obtained in this work (see Figure S7B). The percentage shows the replication of either γH2AX peaks or overall regions occurring in the S4 and G2 cell cycle stages. The distribution of the overlap was calculated using BEDtools. *P* values were obtained using the McNemar's test.

Table S1 Oligonucleotides used in this study, Related to STAR Methods section: Real time qPCR.

Oligo	Sequence (5' – 3')
LigaseIV-F	GAACGTATGCAAATGCACAAAGA
LigaseIV-R	ACCTTCAGTAGGAGAAGCACC
Suv39-F	ATTCGCAAGAACAGCTTCGT
Suv39-R	ACACGTCCTCCACGTAGTCC
TOPIIa-F	TTAATGCTGCGGACAACAAACA
TOPIIa-R	CGACCACCTGTCACTTTCTTTT
BLM-F	CGGATTTTGTTCCACCTTCT
BLM-R	AGCAGTTCGTTCCCACAATC
WRN-F	TGAAGATGACCTCCCCTTCTT
WRN-R	TGGCAACATCTGTCAACTCC
TopIIB-F	GGTTCGTGTAGAGGGGTCAA
TopIIB-R	GCTGATTTGCTGGAATCCTT
TopI-F	ATCCTGAAGGCATCAAGTGG
TopI-R	TTCATGGTCGAGCATTTTTG
TRF2-F	GTTGGAGGATTCCGTAGCTG
TRF2-R	GACCTTCCAGCAGAAGATGCT
ATM-F	TTGATCTTGTGCCTTGGCTAC
ATM-R	TATGGTGTACGTTCCCCATGT
ATR-F	ACCTCAGCAGTAATAGTGATGGA
ATR-R	GGCCACTGTATTCAAGGGAAAT
G9a-F	GGGCGGGAAAATCACCTCC
G9a-R	CACTCATGCGGAAATGCTGTAT
RTEL1-F	TCTCCAGAGCAAAGGAGGAC
RTEL1-R	CCATCCTGATGCTGGTCAC
POT1-F	TGGGTATTGTACCCCTCCAA
POT1-R	GATGAAGCATTCCAACCACGG

Table S2 siRNA used in this study, Related to STAR Methods section: Transient transfection

siRNA	Reference	Sequence
TRF2	L-003546-00-0005	
TRF1	L-010542-00-0005	
POT1	L-004205-00-0005	
WRN-1	L-010378-00-0005	
WRN-2	J-010378-05	GAUCCAUUGUGUAUAGUUA
WRN-3	J-010378-06	GCACCAAAGAGCAUUGUUA
BLM-1	L-007287-00-0005	
BLM-2	J-007287-06	CUAAAUCUGUGGAGGGUUA
BLM-3	J-007287-07	GAUCAAUGCUGCACUGCUU
RTEL1-1	L-013379-00-0005	
RTEL1-2	J-013379-05	CCGCAGAGCACACAACAUU
RTEL1-3	J-013379-06	UAUUCAUGCCGUACAAUUA
TOP1-1	L-005278-00-0005	
TOP1-2	J-005278-05	GAAAAUGGCUUCUCUAGUC
TOP1-3	J-005278-06	GAUUUCCGAUUGAAUGAUU
TOP2A-1	L-004239-00-0005	

TOP2A-2	J-004239-06	CGAAAGGAAUGGUUAACUA
TOP2A-3	J-004239-07	GAUGAACUCUGCAGGCUAA
TOP2B-1	L-004240-00-0005	
TOP2B-2	J-004240-07	GAAGUUGUCUGUUGAGAGA
TOP2B-3	J-004240-08	CGAAAGACCUAAAUACACA
SUV39H1-1	L-009604-00-0005	
SUV39H1-2	J-009604-07	CUAAGAAGCGGGUCCGUAU
SUV39H1-3	J-009604-08	GGUGAAAUGGCGUGGAUAU
LIG4-1	J-004254-09	GCACAAAGAUGGAGAUGUA
LIG4-2	J-004254-10	GGGAGUGUCUCAUGUAAUA
G9a-1	L-006937-00-0005	
G9a-2	J-006937-05	GGACCUUCAUCUGCGAGUA
G9a-3	J-006937-06	GAACAUCGAUCGCAACAUC
CONTROL	D-001810-01	UGGUUUACAUGUCGACUAA

Note : All siRNAs were purchased from Dharmacon. Reference starting with “L” (On-Target Plus SMARTpool) is a mixture or 4 siRNAs against the gene of interest.